Biochemical properties and physiological functions of extracellular iron-binding proteins

by

Jacob Jean Weber

B.A., Bethel College, 2014

AN ABSTRACT OF A DISSERTATION

submitted in partial fulfillment of the requirements for the degree

DOCTOR OF PHILOSOPHY

Biochemistry and Molecular Biophysics Graduate Group
College of Arts and Sciences

KANSAS STATE UNIVERSITY
Manhattan, Kansas

2021

Abstract

Iron is an essential micronutrient to all animals, but it is highly toxic if it is not properly managed. Insects have processes to maintain iron homeostasis through iron absorption, transport, and storage; moreover, as part of their innate immunity, insects produce iron sequestering proteins to protect against iron-scavenging pathogens. Transferrins are a family of iron-binding proteins found in animals. In mammals, secreted transferrins reversibly bind two ferric ions and function in iron transport and immune-related iron sequestration. Insect iron homeostasis is poorly understood, and the role of insect transferrin in iron homeostasis is not well-studied. This dissertation explores the biochemical and structural characteristics and *in vivo* localization of secreted insect transferrin-1 (Tsf1) using two model insect species, *Drosophila melanogaster* and *Manduca sexta*.

Biochemical characterization of Tsf1 was performed to test the hypotheses that the protein binds iron with high affinity and releases the iron as a function of pH decrease. Experiments revealed that Tsf1 binds a single ferric ion with high affinity at neutral pH (log K' = 18), and releases iron over a moderately acidic pH range (6.2 to 5.0). These results indicated that Tsf1 may have physiological functions similar to some mammalian transferrins: binding and sequestering iron in extracellular fluids and releasing iron in the acidic environment of endosomes for uptake into cells. Structural characterization of Tsf1 revealed a novel mechanism of iron coordination, where iron was ligated by two tyrosine residues and two carbonate anions. Mutational analysis of Tsf1 explored the importance of the two tyrosines and a highly conserved carbonate-binding asparagine to the properties of high-affinity iron binding and pH-mediated iron release. *In vivo* studies of Tsf1 localization in *D. melanogaster* tissues were performed to test the hypothesis that Tsf1 is endocytosed into cells as a possible mechanism for iron transport.

Except for two specialized cell types, Tsf1 did not localize in the endosomes of insect cells, which indicated that uptake of Tsf1 is not an essential mechanism for iron transport in healthy insects. This work furthers our understanding of Tsf1 function in iron sequestration and transport in insects, and it provides insight regarding the similarities and differences in iron homeostasis between insects and humans.

Biochemical properties and physiological functions of extracellular iron-binding proteins

by

Jacob Jean Weber

B.A., Bethel College, 2014

A DISSERTATION

submitted in partial fulfillment of the requirements for the degree

DOCTOR OF PHILOSOPHY

Biochemistry and Molecular Biophysics Graduate Group
College of Arts and Sciences

KANSAS STATE UNIVERSITY
Manhattan, Kansas

2021

Approved by:

Major Professor
Maureen Gorman

Copyright

Abstract

Iron is an essential micronutrient to all animals, but it is highly toxic if it is not properly managed. Insects have processes to maintain iron homeostasis through iron absorption, transport, and storage; moreover, as part of their innate immunity, insects produce iron sequestering proteins to protect against iron-scavenging pathogens. Transferrins are a family of iron-binding proteins found in animals. In mammals, secreted transferrins reversibly bind two ferric ions and function in iron transport and immune-related iron sequestration. Insect iron homeostasis is poorly understood, and the role of insect transferrin in iron homeostasis is not well-studied. This dissertation explores the biochemical and structural characteristics and *in vivo* localization of secreted insect transferrin-1 (Tsf1) using two model insect species, *Drosophila melanogaster* and *Manduca sexta*.

Biochemical characterization of Tsf1 was performed to test the hypotheses that the protein binds iron with high affinity and releases the iron as a function of pH decrease. Experiments revealed that Tsf1 binds a single ferric ion with high affinity at neutral pH (log $K' = 18$), and releases iron over a moderately acidic pH range (6.2 to 5.0). These results indicated that Tsf1 may have physiological functions similar to some mammalian transferrins: binding and sequestering iron in extracellular fluids and releasing iron in the acidic environment of endosomes for uptake into cells. Structural characterization of Tsf1 revealed a novel mechanism of iron coordination, where iron was ligated by two tyrosine residues and two carbonate anions. Mutational analysis of Tsf1 explored the importance of the two tyrosines and a highly conserved carbonate-binding asparagine to the properties of high-affinity iron binding and pH-mediated iron release. *In vivo* studies of Tsf1 localization in *D. melanogaster* tissues were performed to test the hypothesis that Tsf1 is endocytosed into cells as a possible mechanism for iron transport.

Except for two specialized cell types, Tsf1 did not localize in the endosomes of insect cells, which indicated that uptake of Tsf1 is not an essential mechanism for iron transport in healthy insects. This work furthers our understanding of Tsf1 function in iron sequestration and transport in insects, and it provides insight regarding the similarities and differences in iron homeostasis between insects and humans.

Table of Contents

List of Figures

List of Tables

Acknowledgements

I must first express my utmost appreciation to my advisor, Dr. Maureen Gorman, for her leadership, patience, and support through the years of my studies and research. Her diligent application of scientific knowledge and practices have been a great example for me to look up to. I will be forever grateful for the opportunity to learn from her and work with her.

I would also like to thank my committee members: Dr. Michael Kanost for his knowledge and support on many aspects of my projects, Dr. Yoonseong Park for his knowledge and time spent guiding me with microscopy and dissection techniques, and Dr. Brian Geisbrecht for his suggestions and resources regarding my protein structure projects. I also thank Dr. Tom Platt for serving as my outside chairperson.

I would like to thank my current and former lab members. I thank Dr. Neal Dittmer for his detailed and useful suggestions, as well as his humor, which always brought enjoyment to the lab. I thank Lisa Brummett for her positive attitude and all the important things she maintained in the lab. I thank Dr. Miao Li for her support and for being a great example of a graduate student for me to work alongside. I thank Michelle Coco Mora for her support and work in the lab.

Many others also supported and assisted me during my time at K-State. I thank my collaborator, Dr. Scott Lovell and his group, at Kansas University for the opportunity of working on a project together and being able to learn from his team. I thank Susan Whitaker at K-State's Biotechnology/Proteomics Core Lab and Joel Sanneman at K-State's CVM Confocal Facility for their time put into training me. Much thanks to Dr. Erika Geisbrecht for her patience and guidance in my first semester during my first rotational research course.

Finally, I would like to thank my family and friends for their support and for keeping me balanced through my time perusing my degree.

Dedication

To my parents, David and Sarah Weber, for your loving support and instilling in me the art of perseverance and the practice of hard work, which were all necessary to complete this journey.

To my wife, Kylie Weber, for your unending support, love, and encouragement throughout this journey.

To my son, Watson Weber, may you always have an inquisitive spirit and discerning mind.

Chapter 1 - Literature Review

Introduction to Iron Homeostasis

Iron is an essential micronutrient for nearly all organisms. It is involved in several critical cellular processes, such as electron transport, cell differentiation, DNA and RNA synthesis, enzymatic cofactors, and gene expression (Lieu et al., 2001). Iron is an abundant element on earth, but it is problematic for organisms to absorb (Frey and Reed, 2012). The difficulty of iron absorption comes from its tendency to form insoluble precipitates in its ferric form (Fe^{3+}) (Spiro and Saltman, 1969). Its soluble form, ferrous iron (Fe^{2+}), will readily react with oxygen species to create toxic free radicals (Meneghini, 1997). These free radicals can damage DNA, proteins, carbohydrates, and lipids, leading to a condition known as oxidative stress (Meneghini, 1997). Animals primarily obtain iron through dietary intake and subsequent intestinal absorption, while prokaryotic organisms obtain iron from their surrounding environment using various scavenging techniques (Anderson and Frazer, 2017; Cassat and Skaar, 2013). Consequently, an animal's ability to sequester iron in extracellular fluids and withhold it from invading pathogens is a major part of their innate immunity (Cassat and Skaar, 2013).

Iron's involvement in biological processes, its potential toxicity, and its role in immunity have led animals to evolve efficient and regulated processes to maintain iron homeostasis. The major processes of iron homeostasis are iron absorption, transport, storage, and sequestration (Anderson and Frazer, 2017; Cassat and Skaar, 2013; Kosman, 2020, 2010). The mechanisms underlying these homeostatic processes have been well-studied only in mammals.

Due to their success as the largest group of animals on earth, it is obvious that insects have evolved effective processes for managing iron; however, very little is understood about insect iron homeostasis. Our interest in studying insect iron homeostasis resides in the following

reasons: (1) insects are used as model organisms for studying human disease and biology (Adamski et al., 2019; Calap-Quintana et al., 2017; Cheng et al., 2018; Kanost et al., 2016; Pandey and Nichols, 2011), thus understanding the similarities and differences of fundamental processes between the organisms is important; (2) insects may elucidate evolutionarily ancient or poorly understood mechanisms of iron homeostasis (Tang and Zhou, 2013); and, (3) the mechanisms underlying iron homeostasis in insect biology may be targets of insect control strategies that could target insects that are pests or vectors of disease (Nichol et al., 2002; Pham and Winzerling, 2010; Tang and Zhou, 2013).

This literature review will first compare what is known about the processes of iron homeostasis in mammals and insects, followed by an in-depth look at the involvement of the transferrin family of proteins in iron homeostasis.

Overview of mammalian iron homeostasis

In the mammalian intestine, iron absorption occurs when duodenal cytochrome b (Dcytb) reduces Fe^{3+} to Fe^{2+}, followed by transport of Fe^{2+} across the apical membrane by divalent metal transporter-1 (DMT1) (Han, 2011). Once inside the enterocyte, Fe^{2+} can either be utilized by the cell, stored as Fe^{3+} in ferritin, or exported into the serum. Export of Fe^{2+} occurs via a ferrous permease, ferroportin, followed by oxidation of Fe^{2+} to Fe^{3+} by a multi-copper oxidase (Donovan et al., 2005; Vulpe et al., 1999). Fe^{3+} in the serum is rapidly bound by transferrin for transport. Transferrin can bind two Fe^{3+} ions. The process of iron uptake from the serum is initiated when transferrin binds to its receptor, transferrin receptor-1 (TfR1), on the surface of a cell (Kawabata, 2019). Iron release from the transferrin-TfR1 complex occurs via two possible paths: 1) the transferrin-TfR1 complex is endocytosed, the acidification of the endosome leads to iron release,

followed by reduction by a ferric reductase (STEAP2 or STEAP3), and transport from the endosome into the cytoplasm by DMT1; or, 2) the iron in the transferrin-TfR1 complex is reduced by a ferric reductase at the cell surface, and the iron is transported across the cellular membrane by Zip8 or Zip14 (Kosman, 2020). The pathways of iron absorption, export, transport, and delivery described in this paragraph are modeled in Figure 1-1A.

Iron is stored throughout the body's organs, but the primary location is in the hepatocytes of the liver (Anderson and Frazer, 2017; Garrick and Garrick, 2009). The iron storage protein, ferritin, is primarily found in the cytoplasm and can store thousands of iron atoms (Theil, 2004). Some iron-poor ferritin is in the serum; moreover, extracellular ferritin receptors have been identified (Chen et al., 2005; Li et al., 2009). Thus, ferritin may also have a role in iron transport (Hentze et al., 2010).

Iron homeostasis is regulated systemically and at the cellular level. Systemic regulation of iron levels is primarily controlled by a peptide, hepcidin, which is produced and secreted by the liver (Anderson and Frazer, 2017; Ganz, 2013). Hepcidin binds to ferroportin, leading to its internalization and subsequent degradation (Anderson and Frazer, 2017). Expression of hepcidin is dependent on the levels iron-saturated (holo) transferrin and its interaction with a low-affinity receptor, transferrin receptor-2 (TfR2) (Kawabata, 2019). High levels of holo-transferrin bound to TfR2 induces signals that lead to an increase in the expression of hepcidin. Thus, when iron is fully supplied in the body and serum levels of holo-transferrin are high, hepcidin expression will increase and lead to a decrease of iron export into the serum; conversely, when iron is in demand and holo-transferrin levels in the serum are low, hepcidin levels decrease to promote iron export into the serum.

Regulation of iron uptake and storage in the cell occurs at the mRNA level to modulate the expression of various proteins. Two of these regulated proteins are ferritin and TfR1 (Anderson and Frazer, 2017). The mRNAs of these proteins have iron-responsive elements (IREs) in their untranslated region, and these IREs can be bound by iron regulatory proteins (IRPs) (Volz, 2008). IRPs change their conformation depending on the amount of available iron in the cytoplasm, and in low iron environments the IRPs will bind to the IREs of ferritin and TfR1 (Anderson and Frazer, 2017; Volz, 2008). In the case of ferritin mRNA, the binding of an IRP will inhibit its translation, leading to a decrease in expression and less storage of iron (Wilkinson and Pantopoulos, 2014). In the case of TfR1 mRNA, the binding of an IRP will inhibit its degradation, leading to an increase in the level of the receptor and more iron transport into the cell (Wilkinson and Pantopoulos, 2014).

Despite the tightly regulated pathways for absorbing, trafficking, and storing iron in mammals, infectious pathogens have developed several ways to scavenge iron from intracellular and extracellular locations within their hosts (Cassat and Skaar, 2013). To defend against these pathogens, the mammalian innate immune system responds in part with an iron sequestration process that involves the modulation of iron regulatory proteins and expression of high-affinity iron-binding proteins. An immune response that decreases the amount of circulating iron is called a hypoferremic response. Once a pathogen has infected the host, Toll-like receptor activation and proinflammatory cytokines elicit the immune system to respond by modulating iron distribution through increased levels of hepcidin systemically and locally (Armitage et al., 2011; Drakesmith and Prentice, 2012; Peyssonnaux et al., 2006). Iron availability during infections is also modulated by several cytokines that act independently of hepcidin expression to modulate levels of proteins involved in iron homeostasis (Weiss, 2005). One of the first lines

of defense against iron-scavenging pathogens, is the protein lactoferrin (Cassat and Skaar, 2013; Legrand et al., 2005). Even in the absence of infection, lactoferrin is secreted into bodily fluids and mucosal layers at high concentrations and binds iron with high affinity (Baker and Baker, 2012; Legrand et al., 2005). Lactoferrin is also released by neutrophils at areas of infection (Cassat and Skaar, 2013).

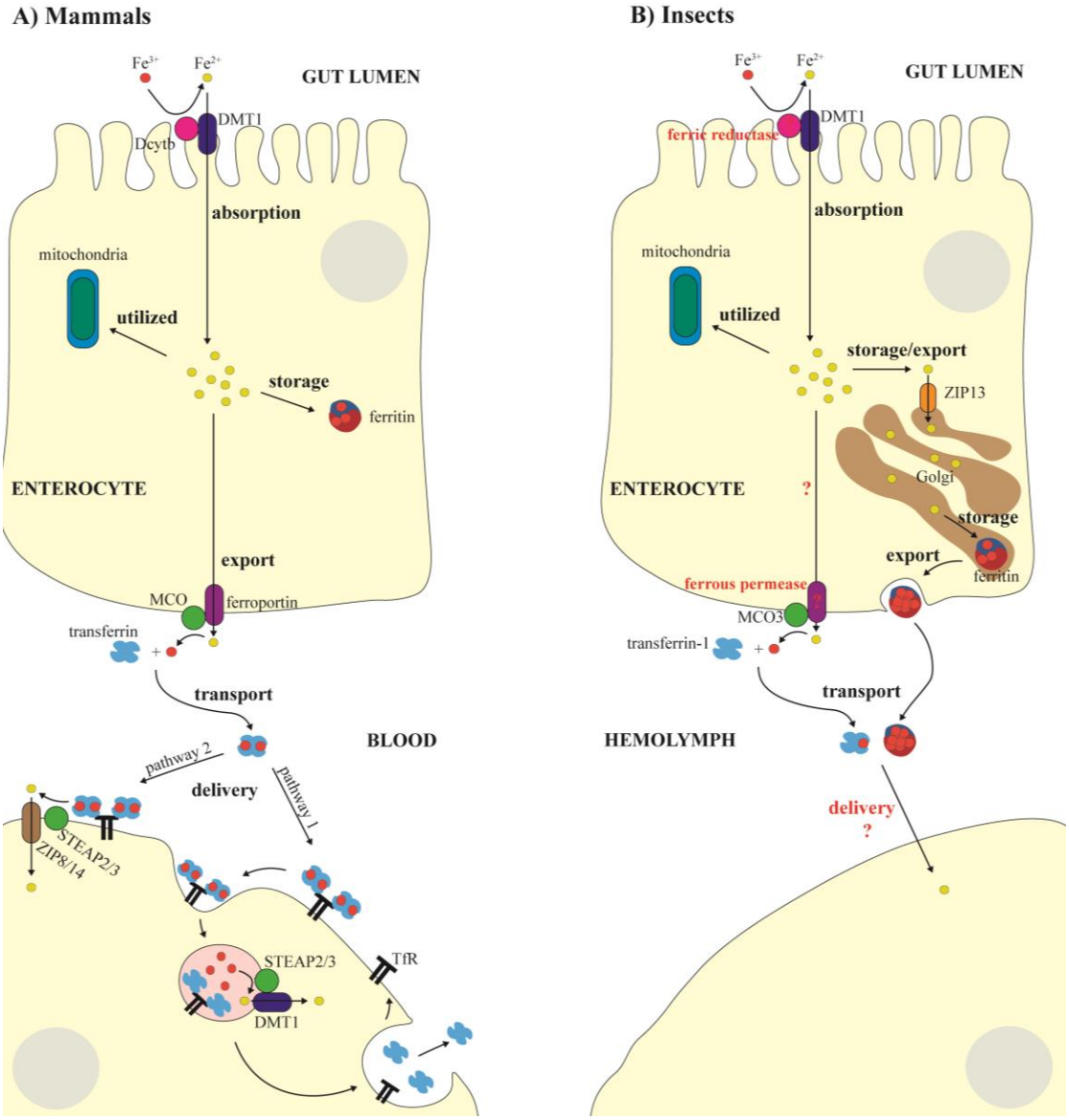

Figure 1-1. Comparison of the main pathways of iron homeostasis in (A) mammals and (B) insects (unknown mechanisms in insects are shown in red).

Overview of insect iron homeostasis

Iron absorption from the insect gut is thought to involve a similar mechanism as the one in mammals (Figure 1-1B) (Folwell et al., 2006; Tang and Zhou, 2013). A DMT1 orthologue has been identified and studied for metal transport properties in *Drosophila melanogaster* and *Anopheles albimanus* (Bettedi et al., 2011; Martínez-Barnetche et al., 2007). In *D. melanogaster*, this divalent metal transporter gene is known as *Malvolio*, and its expression occurs highly in the anterior and posterior midgut, Malpighian tubules, nervous system, and testis. Malvolio mutants show iron-depleted midguts and whole body iron deficiencies, but under a high iron diet, the whole body iron levels are restored (Bettedi et al., 2011). After a blood feeding in *A. albimanus*, DMT1 expression is down regulated in the midgut and upregulated in the Malpighian tubules, indicating that DMT1 may be involved in regulating iron absorption in these insects (Martínez-Barnetche et al., 2007). There is no verified insect DcytB protein involved in reducing Fe^{3+} to Fe^{2+} during iron absorption, but two predicted ferric reductase genes have been identified in *D. melanogaster* (Mandilaras et al., 2013), and one in *Anopheles gambiae* (Winzerling and Pham, 2006). The salivary glands of *D. melanogster* have also been implicated in the uptake of iron via basal endosomal trafficking during the prepupal development stage (Farkaš et al., 2018).

Intracellular trafficking and export of iron in the insect enterocytes seems to differ from that of mammals. Unlike mammalian ferritin, which is typically cytosolic, insect ferritin is predominantly a secreted form of ferritin, and its subcellular localization is mostly in the ER and Golgi apparatus (Figure 1-1B) (Geiser et al., 2006; Mehta et al., 2009; Missirlis et al., 2007; Pham and Winzerling, 2010; Winzerling et al., 1995). In *D. melanogaster*, it has been shown that a zinc/iron permease, dZIP13, transports iron from the cytosol to the secretory pathway, where the iron is loaded onto ferritin (Xiao et al., 2014). Because insect ferritin is secreted and there is

no identified ferroportin homologue in insects, the export of iron from the enterocytes is believed to occur primarily through the secretion of iron-loaded ferritin into the hemolymph (Geiser et al., 2006; Missirlis et al., 2007; Pham and Winzerling, 2010; Tang and Zhou, 2013). RNAi of ferritin in the midgut of *D. melanogaster* on a normal diet led to iron accumulation in the gut, a decrease in systemic iron levels, and a decreased survival (Tang and Zhou, 2012). Aside from secreted ferritin, the following models have also been proposed for iron export from insect enterocytes: (1) an unidentified ferrous iron permease coupled with a multicopper oxidase (MCO) with ferroxidase activity; and, (2) the export of iron-bound transferrin through the secretory pathway (Xiao et al., 2019).

Trafficking of iron in insect hemolymph (circulatory fluid) is most likely occurring through the secreted iron-binding proteins, ferritin and transferrin-1 (Figure 1-1B). The majority of iron in the hemolymph is bound to ferritin, with a smaller amount bound to transferrin-1, which is opposite of protein-bound iron in the serum of mammals (Huebers et al., 1988). In *D. melanogaster*, ferritin has been clearly linked to systemic iron distribution and is an essential gene, whereas transferrin-1 has only been clearly linked to trafficking iron from the midgut to the fat body and is not an essential gene (Iatsenko et al., 2020; Pham and Winzerling, 2010; Xiao et al., 2019). When radioactively labeled iron is loaded onto ferritin and transferrin-1 and injected into the hemolymph of *Manduca sexta* larvae, the radioactive iron is transported and delivered into tissues (Huebers et al., 1988). While it is clear ferritin and transferrin-1 are involved in transporting iron in hemolymph and delivering it to tissues, neither protein has an identified receptor in insects and their delivery mechanism is unknown (Figure 1-1B) (Tang and Zhou, 2013).

Insects do not have a single organ equivalent to the liver of mammals, but instead the functions of the mammalian liver are found in separate tissues in insects: oenocytes, fat body, and iron cells (Mehta et al., 2009). In *D. melanogaster*, a large amount of the stored iron in insects is found in ferritin accumulated in specialized midgut enterocytes called "iron cells" (Mandilaras et al., 2013; Mehta et al., 2009).

The mechanisms underlying systemic regulation of iron in insects are not known and no homologue of hepcidin, ferroportin, or TfR have been reported. However, some aspects of iron regulation at the cellular level in insects have been discovered. IRP homologues with IRE binding ability have been identified in *D. melanogaster*, *M. sexta*, *Aedes aegypti*, and *A. gambiae* (Lind et al., 2006; Zhang et al., 2001a; Zhang et al., 2001b; Zhang et al., 2002). Only three genes containing IREs have been identified in insects: two genes that encode *ferritin* (ferritin 1 and ferritin 2) and one that encodes *succinate dehydrogenase B*. Succinate dehydrogenase is a key enzyme in the citric acid cycle and is therefore intrinsically tied to oxidative phosphorylation. It has been hypothesized that regulating these genes with the IRE/IRP system during iron deficient conditions in insects would lead to the following: suppression of *ferritin 1* and *ferritin 2* expression, resulting in decreased iron storage and increased availability of iron; and suppression of *succinate dehydrogenase B* expression, which would slow down the citric acid cycle and lead to less iron needed for the numerous iron-sulfur containing proteins in the electron transport chain (Kohler et al., 1995; Mandilaras et al., 2013). Interestingly, ferritin expression in the midgut "iron cells" of *D. melanogaster* is not affected by a decrease in iron concentration (Mehta et al., 2009). The lack of ferritin regulation in the "iron cells" could be due to tissue-specific alternative splicing of ferritin-1 pre-mRNA that removes the IRE, or a tissue-specific lack of IRP expression (Mehta et al., 2009; Nichol et al., 2002).

Intracellular regulation of iron in insects also occurs independently of the IRP/IRE system through the direct interaction of iron with dZIP13 (Xu et al., 2019). When iron binds to dZIP13, the protein is stabilized and protected from degradation; therefore, when iron levels are high in the enterocyte, more dZIP13 is available to transport iron from the cytosol to the secretory pathway where it can be loaded into ferritin and secreted (Xu et al., 2019).

Like mammals, insects limit the availability of free iron to reduce oxidative stress and to protect against invading pathogens using secreted iron-binding proteins. In insects this process of iron sequestration is believed to be primarily performed by ferritin and transferrin-1 (Geiser and Winzerling, 2012; Pham and Winzerling, 2010).

A further detailed review of transferrin-1's function in insect iron homeostasis will be discussed in a later section of this review (see section entitiled: Insect Transferrins)

Transferrins

The transferrin family of proteins are monomeric glycoproteins that were originally identified in vertebrates and characterized based on their iron binding properties and their functional role in transporting and sequestering iron (Johansson, 1958; Masson et al., 1966; Surgenor et al., 1949). Today, however, it is known that the transferrin family members are found in nearly all metazoans and have evolved various functions, not all of which are related to binding iron (Lambert, 2012). This review will focus on the iron-binding transferrins with identified functions in iron homeostasis.

Biological functions of transferrins

The well-studied vertebrate transferrins involved in iron homeostasis are serum transferrin (STf), lactoferrin (LTf), and ovotransferrin (OTf). These secreted bilobal proteins are typically 70-80 kDa. Their function in iron homeostasis is dependent on their expression patterns and ability to reversibly bind two ferric ions.

STf is largely expressed and secreted into the blood by the liver, where it functions by binding two ferric ions with high affinity in the serum and delivering the iron into cells. The method of iron delivery by STf is a regulated process and involves binding to its receptors, release of iron and recycling back into the serum (Kosman, 2020). In fact, STf has been shown to complete over 100 cycles of iron binding, transport and delivery to cells during its time in circulation (Dhungana et al., 2004). Mutations of STf in mice and humans can lead to anemia, iron overload in tissues, and can be lethal unless treated (Anderson and Vulpe, 2009; Trenor et al., 2000). Mice with a severe deficiency of STf die shortly after birth (Anderson and Vulpe, 2009; Bernstein, 1987). Under normal conditions, STf is only ~30% saturated with iron, thus any "free" iron is quickly bound up by unsaturated (apo) STf, which makes the risk of iron-induced free radical formation and oxidative stress low (Anderson and Frazer, 2017).

LTf has high affinity for two ferric ions and the unique ability amongst its transferrin family members to retain its bound ferric ions in highly acidic conditions (Baker and Baker, 2012). LTf is secreted into bodily fluids and at sites of infection as a potent iron-withholding immune protein to defend against fungal, bacterial, viral, and parasitic pathogens (Fernandes and Carter, 2017; Jenssen and Hancock, 2009). Expression of LTf occurs early in development and continues into adulthood, with highest protein level expression occurring in respiratory epithelial cells, tonsil epithelial cells, and several types of glandular cells (salivary, stomach, epididymis,

prostate, and mammary) (Teng, 2002). LTf is also expressed and stored in the secondary granules of neutrophils until it is secreted during times of infection (Gutteberg et al., 1989; Zarember et al., 2007). Mutations of LTf in mice and humans have led to increased susceptibility to several types of pathogenic infections (Fujihara and Hayashi, 1995; Keijser et al., 2008; Mohamed et al., 2007; Velusamy et al., 2013). During times of infection and the resulting inflammation, LTf is critical to sequestering free iron, alleviating the inflammatory response, and restoring iron homeostasis (Cutone et al., 2017; Rosa et al., 2017); moreover, during infection the concentration of LTf in the blood can rise 200 fold (Farnaud and Evans, 2003). Unlike STf, LTf is not essential to regulated iron transport, as mice with a null mutation in LTf have apparently normal iron homeostasis (Ward et al., 2003); however, LTf has been implicated in absorbing iron from the gut through receptor mediated endocytosis, internalization, and subsequent degradation (Akiyama et al., 2013; Ashida et al., 2004; Mikogami et al., 1994). While LTf's iron-withholding properties are well established, several alternative functions have been investigated: iron absorption, bacteriocidal, anti-inflammatory, anti-oxidant, anti-tumor, immunomodulator, protease, protease inhibitor, ribonuclease, procoagulant, promicrobial, and transcription factor (Actor et al., 2009; Akiyama et al., 2013; Conneely, 2001; Farnaud and Evans, 2003; Ogasawara et al., 2014).

OTf is a transferrin family member found in birds, and it makes up 12% of the protein content of bird egg white (Superti et al., 2007). Like STf and LTf in mammals, OTf is secreted, binds two ferric ions, and is expressed in the liver and glandular cells of several tissues, most notably the oviduct (Giansanti et al., 2012; Lambert et al., 2005a; Rathnapala et al., 2021). With its similarities to STf and LTf, it is no surprise that OTf has both an iron transport and immune role in birds (Giansanti et al., 2012). OTf that is expressed by the liver and secreted into the

blood, also referred to as serum OTf, functions in iron transport, while OTf that is expressed by the oviduct and other glandular cells has antimicrobial and anti-inflammatory functions (Cooper et al., 2019; Giansanti et al., 2012; Shimazaki and Takahashi, 2018; Superti et al., 2007; Valenti et al., 1982, 1981, 1980; Wellman-Labadie et al., 2008; Xie et al., 2002; Zhu et al., 2019). When comparing OTf expressed for iron transport to the OTf expressed for immune purposes, the only difference is their glycosylation pattern at a single residue (Iwase and Hotta, 1977; Williams, 1968).

Structure and iron coordination of transferrins

The first crystal structures of STf, LTf, and OTf revealed that these transferrins have similar structures (Anderson et al., 1989; Bailey et al., 1988; Kurokawa et al., 1995), which was not surprising given their high (~50 to 80%) amino acid sequence similarities (Baker, 1994). Since these initial structures were solved, several structures of each transferrin have been solved in various species and in various conformational states (Mizutani et al., 2012). All three transferrins adopt a bilobal fold, with a globular amino-terminal lobe (N-lobe) and a globular carboxyl-terminal lobe (C-lobe) (Figure 1-2A – F). The N- and C-lobes are homologous and are thought to have arisen from a gene duplication event more than 580 million years ago (Lambert et al., 2005a). The two lobes are connected by a short linker peptide of 10 to 12 residues. Each lobe is divided into two domains: the N1 and N2 domains of the N-lobe and the C1 and C2 domains of the C-lobe (Figure 1-2A – F). The two domains of each lobe are separated by a cleft, and only come together at a hinge-like region (Mizutani et al., 2012). The cleft formed between the domains of each lobe is where the iron binding sites are found.

When the transferrins are in their iron-bound (holo) form, their lobes are typically found in a closed conformation (Figure 1-2D – F), while in their unbound (apo) form, their lobes are found in an open conformation (Figure 1-2A – C). The conformational change from an open to closed state arises when the proteins bind iron and the domains of each lobe rotate to clamp down on the iron. The degree of rotational change appears to be highest in the N-lobe, with values around 50˚ of rotation reported for LTf and OTf, whereas the C-lobe only rotates 35˚ in OTf (Mizutani et al., 2001).

The folding pattern of the N- and C-lobes are nearly superimposable; an RMSD of 1.2 Å was reported for a structural alignment of the N- and C-lobes of LTf. Moreover, each domain is composed of a β-sheet surrounded by α-helices on both sides (Baker, 1994). The hinge-like region connecting the two domains is composed of two β-strands. The overall structure is stabilized by several disulfide bonds in each lobe. These structural aspects allow each domain to act as single rigid unit as conformational changes occur during the iron binding and release process (Mizutani et al., 2012).

The crystal structures of the holo-form of STf, LTf, and OTf have demonstrated that not only do these proteins have remarkably similar overall structures, but they also have similar methods of iron coordination (Anderson et al., 1989; Bailey et al., 1988; Kurokawa et al., 1995). At each lobe's iron binding site, the ferric (Fe^{3+}) ion is in a distorted octahedral coordination sphere with six ligating atoms. Four residues provide iron-coordinating bonds, one from aspartate, one from histidine, and one bond from each of two tyrosines, and the remaining two iron coordinating bonds are provided by a synergistically bound bidentate anion (Figure 1-2G – I). The anion in physiological conditions is typically carbonate (CO_3^{2-}) (Harris, 2012; Masson and Heremans, 1968; Schade et al., 1949; Warner and Weber, 1953). The iron coordinating

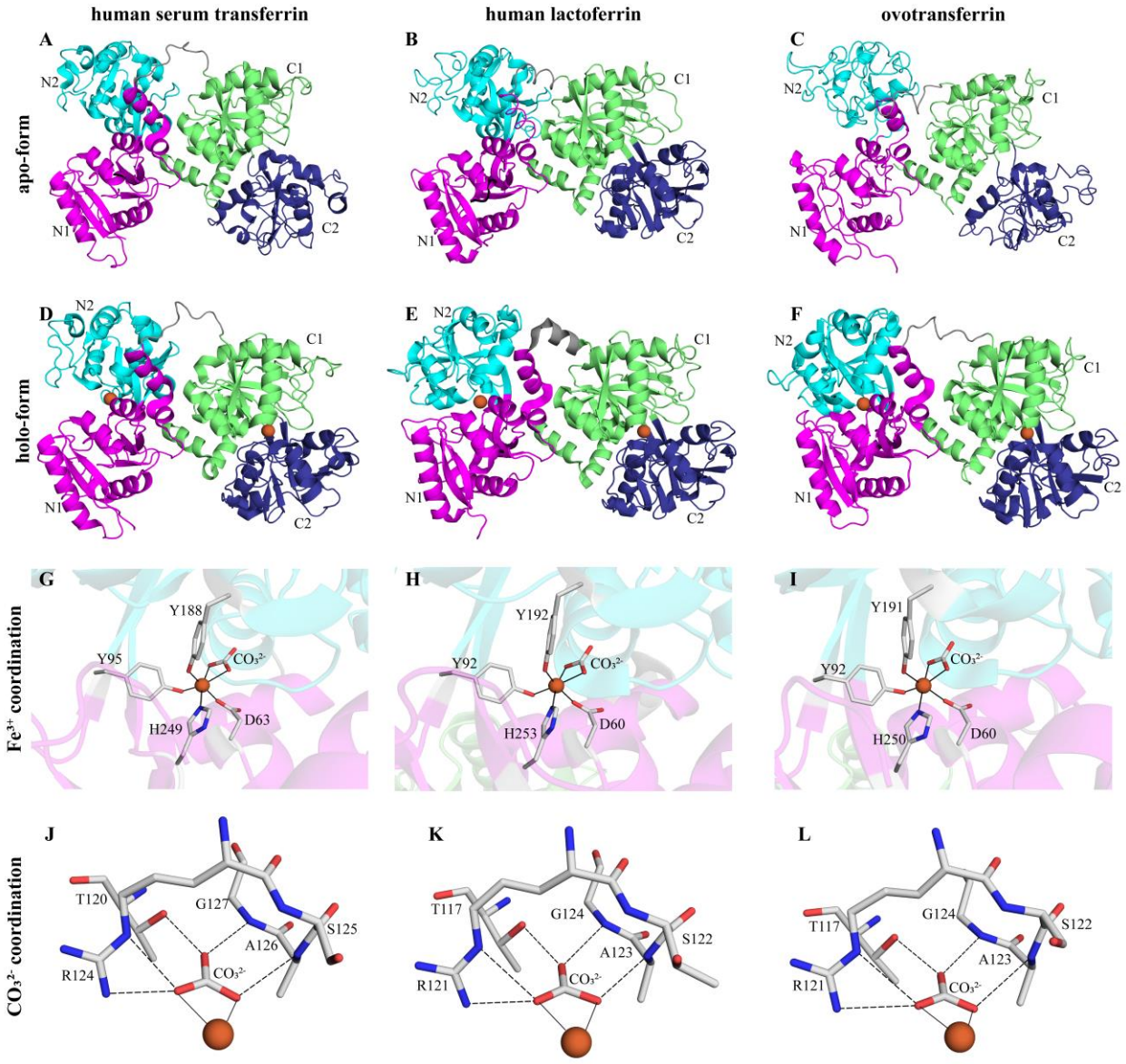

Figure 1-2. Common structural aspects of vertebrate transferrins.

(A – C) Overall apo-structures of human STf (PDB: 2HAV), human LTf (PDB: 1CB6), and chicken OTf (PDB: 1AIV). (D – F) Overall holo-structures of human STf (PDB: 3QYT), human LTf (PDB: 1LFG), and chicken OTf (PDB: 1OVT). (A – F) The domains are colored as follows: N1 domain as magenta, N2 domain as Cyan, C1 domain as green, and C2 as blue. The linker peptide between the N- and C-lobe is colored in grey. (D – F) The iron ion is represented as an orange sphere in each lobe. (G – I) Iron coordination and (J – L) CO_3^{2-} binding in human STf (PDB: 1D3K), human LTf (PDB: 1LFG), and chicken OTf (PDB: 1OVT). The coordinating amino acid residues and CO_3^{2-} are shown in grey stick models. The iron coordinating bonds are shown as solid lines and the hydrogen bonds with CO_3^{2-} are shown as dashed lines.

aspartate and histidine are found in domain 1 (N1 and C1), while the two tyrosines are found in domain 2 (N2 and C2). The four iron-coordinating residues are completely conserved in both lobes of STf, LTf, and OTf sequences (Baker, 1994; Lambert et al., 2005a; Mizutani et al., 2012); moreover, their importance to iron coordination has been extensively studied through mutational analysis (H. R. Faber et al., 1996; R. H. Faber et al., 1996; Grady et al., 1995; Grossmann et al., 1998, 1993; He et al., 2000a, 2000b, 1998; Q Y He et al., 1997; Q. Y. He et al., 1997b, 1997a; Lin et al., 1993; MacGillivray et al., 2000; Mason and He, 2002; Mason et al., 2005; Mecklenburg et al., 1997; Nicholson et al., 1997; Ward et al., 1996; Woodworth et al., 1991; Zak et al., 1995). While mutations of any of the four residues do cause perturbations of iron coordination, only mutations of the tyrosines cause complete loss of iron binding (Q. Y. He et al., 1997a; Mason and He, 2002; Mason et al., 2005; Ward et al., 1996).

Binding of the synergistic CO_3^{2-} at the iron binding site occurs in domain 2 of each lobe through the side chains of a threonine and an arginine, and the backbone amide groups of two N-terminal helix residues (Figure 1-2J – L) (Anderson et al., 1989; Bailey et al., 1988; Kurokawa et al., 1995). The binding of CO_3^{2-} at the site is considered synergistic because it is crucial for the formation of a stable Fe^{3+}- CO_3^{2-}-transferrin complex (Harris, 2012). Mutagenesis studies of the CO_3^{2-} binding residues, arginine and threonine, found that mutating either of these residues diminishes the iron binding affinity (H. R. Faber et al., 1996; Grossmann et al., 1998; Harris et al., 1999; He et al., 2000a; Li et al., 1998; Mason and He, 2002; Zak et al., 2002, 1995); moreover, a double mutation of both residues causes a complete loss of iron binding (Zak et al., 2002).

Mechanism of iron binding

The first step in the mechanism of iron binding was elucidated when NMR and kinetic studies of apo-STf provided evidence that the carbonate binds to the protein first to form a CO_3^{2-}-transferrin binary complex, followed by the iron binding to form the Fe^{3+}- CO_3^{2-}-transferrin complex (Kojima and Bates, 1981; Zweier et al., 1981). Since these findings, the remaining steps of the process have been explored, but are not fully understood (Mizutani et al., 2012).

Structures of the apo-transferrins show that the cleft between domain 1 and 2 is in an open conformation, and the iron binding site and anion coordinating residues are exposed. The one exception is the C-lobe of apo-LTf, which is in the closed conformation (Anderson et al., 1989). It is likely that an electrostatic attraction of the negatively charged CO_3^{2-} to the positively charged ligating arginine is what promotes CO_3^{2-} binding before the positively charged iron ion (Baker, 1994). Once the carbonate is bound in place, a ferric-chelator complex (a chelator is likely present *in vivo* to prevent precipitation of the iron) binds to the two tyrosines in domain 2 and the chelator is replaced by the carbonate. This intermediate step in the iron-binding process has been supported by two OTf crystal structures (Kuser et al., 2002; Mizutani et al., 1999); however, it not clear if this intermediated Fe^{3+}- CO_3^{2-}-transferrin complex is in the open or closed conformation prior to replacement of the chelator (Mizutani et al., 1999). The last step includes the rotation of the domains so that the last two coordinating residues in domain 1, aspartate and histidine, can close down on the iron and complete the iron binding process with the lobe in the closed conformation (Baker, 1994; Mizutani et al., 2012).

The iron binding mechanism of these transferrins results in an extremely high iron affinity measurements. The association constant of LTf for iron is measured in the range of 10^{22}

– 10^{24}, and for STf it is in the range of 10^{20} – 10^{21} (Aisen et al., 1978; Aisen and Leibman, 1972; Pakdaman et al., 1998).

Mechanism of iron release

The difference in physiological function between STf, OTf, and LTf is facilitated in part by how these proteins release iron. Many *in vitro* studies of iron release remove the iron by simply using iron chelators while simultaneously decreasing the pH of solution, which leads to protonation of residues involved in iron coordination. STf and OTf release iron in buffers over the pH range of 6.0 to 4.0 (Day et al., 1992; Dewan et al., 1993). In contrast, LTf is much more acid-stable and retains iron until the pH drops to 4.0 to 2.5 (Day et al., 1992). In vivo studies have discovered that STf and OTf release iron for delivery into the cell through a series of events which involves their receptor, while the only mechanism of releasing iron from LTf is believed to be through degradation (Akiyama et al., 2013; Baker and Baker, 2012). The difficulty of removing of iron from LTf is part of what gives the protein its potent bacteriostatic function.

TfR1 is a homodimer that binds two STfs on the cell surface, and it has a higher affinity for iron saturated holo-STf than it does for apo-STf (Aisen, 2001; Eckenroth et al., 2011; Kawabata, 2019). When holo-STf binds to TfR1, STf undergoes a conformational change that weakens iron binding and increases the ferric ion's reduction potential to a point where physiological molecules could readily reduce it to Fe^{2+} (Dhungana et al., 2004; Kosman, 2020). At this point, the iron in the STf-TfR1 complex can be reduced at the surface by a ferric reductase and transported in the cytosol by a ferrous iron transporter, or the STf-TfR1 complex can be endocytosed (Kosman, 2020). When the STf-TfR1 complex is endocytosed, the

acidification of the endosome, conformational changes, and iron chelators are likely to all play a part in the release of iron from STf (Baker, 1994).

One factor in the release of iron from STf is a conformational change in the position of the CO_3^{2-} binding arginine (Adams et al., 2003; Harris, 2012; MacGillivray et al., 1998). This change is believed to occur because of the protonation of the synergistic CO_3^{2-} and is the initial step toward larger domain movements as iron is released (Adams et al., 2003).

Another major structural change that occurs in STf and OTf as the pH decreases, is the protonation of two basic amino acid residues that are found in the cleft between the N1 and N2 domains. At neutral pH, the side chains of these residues form a hydrogen bond and help to hold the protein in the closed conformation; however, in acidic conditions, these basic residues are readily protonated, leading to a charge repulsion. This repulsion helps to drive the domains apart and into the open conformation, leading to iron release (Baker and Lindley, 1992; Dewan et al., 1993; MacGillivray et al., 1998; Mizutani et al., 2012). Such a mechanism for iron release does not exist between the domains 1 and 2 of LTf (Anderson et al., 1989; Peterson et al., 2000); moreover, in LTf, there are cooperative interactions between the N- and C-lobes that help to stabilize the protein's iron binding sites (Peterson et al., 2000).

Insect Transferrins

Compared to LTf, STf, and OTf, much less is understood about insect transferrin structure, iron binding properties, and function. Phylogenic studies of insect transferrins have shown there are four orthologous groups: transferrin-1 (Tsf1), transferrin-2 (Tsf2), transferrin-3 (Tsf3), and transferrin-4 (Tsf4) (Bai et al., 2016; Najera et al., 2021). Tsf2 is a membrane-associated protein that has been studied in *D. melanogaster*, where it was shown to bind one iron

ion and function in the formation of septate junctions (Hall et al., 2014; Tiklová et al., 2010). The function of Tsf3 and Tsf4 have not been studied, but their sequences indicate that they are membrane bound and are not predicted to bind iron (Najera et al., 2021). Tsf1 is the only group thought to have an important role in insect iron homeostasis because Tsf1 sequences and experimental evidence consistently indicate the protein is both secreted and binds iron (Bonilla et al., 2015; Brummett et al., 2017; Geiser and Winzerling, 2012; Hattori et al., 2015; Iatsenko et al., 2020; Najera et al., 2021; Qu et al., 2014; Simmons et al., 2013; Xiao et al., 2019; Zhang et al., 2014). While Tsf1 may have a role in iron homeostasis, it is not orthologous to serum transferrin (Bai et al., 2016). This section on insect transferrins will focus primarily on Tsf1 and the evidence linking it to iron homeostasis in insects.

Tsf1 structure and biochemical reactivity

Most Tsf1 sequences are only 20 to 30% identical to human STf and human LTf; moreover, low percent identity is seen even amongst Tsf1 sequences from different orders of insects (Table 1-1). Further analysis of Tsf1 sequences show they contain a N-terminal signal peptide, which is typical for secreted proteins, and typically range in size from 70 to 80 KDa (Geiser and Winzerling, 2012; Najera et al., 2021).

As previously discussed, vertebrate transferrins utilize four highly conserved residues, two tyrosines, one aspartate, and one histidine, to bind and release iron in both the N-lobe and the C-lobe; moreover, the iron-coordinating synergistic anion is held in place by a conserved arginine and threonine. The two tyrosines and two anion-binding residues are essential to iron binding (Ward et al., 1996; Zak et al., 2002). While the histidine and aspartate are important to iron affinity and the iron release mechanism in vertebrate transferrins, they are not essential to

the binding of iron. Several sequence-based studies of Tsf1 from more than 20 insect species have found that only the two iron-coordinating tyrosines and the two anion-binding residues are fully conserved, and there is a complete of lack conservation of the histidine and in some cases the aspartate (Baker, 1994; Geiser and Winzerling, 2012; Lambert et al., 2005a; Najera et al., 2021). Moreover, in most Tsf1 sequences, these essential residues are only conserved in the N-lobe, and the C-lobe is believed to lack iron-binding capabilities. Of the sequences analyzed in published studies, only sequences from *Blaberus discoidalis*, *Mastotermes darwiniensis*, *Apriona.germari*, *Protaetia brevitarsis*, and *Romalea microptera* show conservation of the iron coordinating residues in both the N-lobe and C-lobe (Geiser and Winzerling, 2012; Lambert et al., 2005a; Najera et al., 2021).

Table 1-1. Percent identity matrix of vertebrate transferrins and insect transferrin-1s

Protein[a]	STf	LTf	OTf	Bdsf1	TcTsf1	AaTsf1	DmTsf1	RpTsf1	BiTsf1	MsTsf1	RmTsf1
STf	-										
LTf	62	-									
OTf	52	52	-								
BdTsf1	32	32	31	-							
TcTsf1	35	33	32	59	-						
AaTsf1	23	22	22	40	39	-					
DmTsf1	25	25	23	35	38	45	-				
RpTsf1	28	26	25	49	49	38	37	-			
BiTsf1	27	27	27	47	46	38	35	45	-		
MsTsf1	28	26	25	46	49	38	36	43	44	-	
RmTsf1	33	32	32	59	58	38	35	50	48	45	-

[a]Percent identity values were obtained using Clustal Omega and the output format "ClustalW" (https://www.ebi.ac.uk/Tools/msa/clustalo/). The protein sequences (not including signal peptides) were gathered from UniprotKB. Protein abbreviation information is as follows: STf, *Homo sapien*, P02787 (abbreviation, species, accession number); LTf, *Homo sapien*, P02788; OTf, *Gallus gallus*, P02789; BdTsf1, *Blaberus discoidalis*, Q02942; TcTsf1, *Tribolium castaneum*, A0A139WAX1; AaTsf1, *Aedes aegypti*, Q16894; DmTsf1, *Drosophila melanogaster*, Q9VWV6; RpTsf1, *Rhodnius prolixus*, B8LJ43; BiTsf1, *Bombus ignitus*, A8D919; MsTsf1, *Manduca sexta*, P22297; RmTsf1, *Romalea microptera*, Q6USR2.

The capability to bind iron has been experimentally demonstrated in Tsf1 from three species: *M. sexta* (MsTsf1), *B. discoidalis* (BdTsf1), and *Sarcophaga peregrina* (SpTsf1) (Bartfeld and Law, 1990; Brummett et al., 2017; Gasdaska et al., 1996; Kurama et al., 1995). BdTsf1 is one of the few Tsf1 sequences that has predicted iron binding in both lobes, while MsTsf1 and SpTsf1 are predicted to bind iron only in the N-lobe (Geiser and Winzerling, 2012). Biochemical analysis of BdTsf1 verified that it does bind two iron ions, and it has spectral and pH-mediated iron release properties that are similar to those of serum transferrin (Gasdaska et al., 1996). Biochemical analysis of MsTsf1 and SpTsf1 verified they bind only one iron ion, and MsTsf1 displayed similar spectral properties to vertebrate transferrins (Bartfeld and Law, 1990; Brummett et al., 2017; Kurama et al., 1995).

Unlike the glycosylated vertebrate transferrins, some Tsf1s are not glycosylated. The lack of glycosylation in *A. aegypti* Tsf1 was proven through digestion experiments (Yoshiga et al., 1997). In a study of 34 Tsf1 sequences from seven orders of insects, it was found that putative O- and N-linked glycosylation sites were lacking from a number of species: *A. aegypti*, *Culex quinuefasciatus*, *Glossina morsitans morsitans*, *Sarcophaga peregrina*, and *Rhodinius prolixu* (Geiser and Winzerling, 2012). Interestingly, the Tsf1s that appear to lack glycosylation are all from insects that are blood feeding disease vectors. It has been hypothesized that these Tsf1s evolved, under selective pressure from pathogens, to lack glycosylation as a method to prevent targeting and scavenging of the insect's iron (Geiser and Winzerling, 2012).

Tsf1 in iron transport

Evidence from studies of Tsf1 suggest it has a role in iron transport, but the information and importance of the findings are limited. Similar to serum transferrin in the blood, Tsf1 is

secreted into the hemolymph where it can be distributed throughout the open circulatory system of insects (Brummett et al., 2017; Huebers et al., 1988; Winzerling et al., 1995). The fat body, which has similar functions to the mammalian liver, is a major source of Tsf1 expression in several insects: *A. aegypti*, *Apriona germari*, *Bombus ignites*, *Choristoneura fumiferana*, *D. melanogaster*, *M. sexta*, and *Romelea microptera* (Ampasala et al., 2004; Ding et al. et al., 2004; Harizanova et al., 2005; He et al., 2015; Kim et al., 2009; Lee et al., 2006; Xiao et al., 2019; Zhou et al., 2009). Tissue specific knockdown of Tsf1 in the *D. melanogaster* larval fat body resulted in iron accumulation in the gut, and decreased iron levels in the fat body (Xiao et al., 2019). The functional importance behind Tsf1 trafficking iron from the gut to the fat body is not clear because iron-loaded ferritin is believed to be the major source of iron export from enterocytes, but it is possible that Tsf1 and ferritin both have a part in iron transport (Geiser and Winzerling, 2012; Xiao et al., 2019).

Radioactive iron loaded onto Tsf1 (^{59}Fe-Tsf1) and injected into the hemolymph of *M. sexta* larvae was found to be transported from the hemolymph into the fat body, and *S. peregrina* adult females inject with ^{59}Fe-Tsf1 delivered the iron to eggs (Bartfeld and Law, 1990; Kurama et al., 1995). In both studies, the radioactive iron ended up bound to ferritin. There is no identified Tsf1 receptor, so the mechanism of iron delivery to these tissues in unknown.

Tsf1 in immunity

Evidence from studies of Tsf1 show a clear role as an immune protein, with iron sequestration and iron relocation being the likely mechanism of defense against pathogens.

Similar to LTf, Tsf1 is secreted into saliva, molting fluid, seminal fluid and several other bodily fluids (Bonilla et al., 2015; Brummett et al., 2017; Geiser and Winzerling, 2012; Hattori et

al., 2015; Qu et al., 2014; Simmons et al., 2013; Zhang et al., 2014). Studies from several species of insects at many different stages of development, have shown that challenging the insect to various bacteria, parasites, and fungi results in an up-regulation of Tsf1. Moreover, the dsRNA mediated suppression of Tsf1 in *Plutella xylostella* larvae resulted in increased susceptibility to the bacteria *Bacillus thuringiensis* (Kim and Kim, 2010).

Aside from being found in secreted fluids and hemolymph, Tsf1 has also been shown to be loaded into developing oocytes (Hirai et al., 2000; Kurama et al., 1995; Nichol et al., 2002). Moreover, the Tsf1 in the developing eggs transferred their iron to ferritin and the apo-Tsf1 was retained in the egg (Kurama et al., 1995). Like OTf in birds, it has been hypothesized that this apo-Tsf1 may function as an iron with-holding agent for the egg's defense from pathogens (Geiser and Winzerling, 2012; Nichol et al., 2002). Purified Tsf1 from *S. bullata* showed an ability to inhibit cultured bacteria, *Staphylococcus aureus* and *Escherichia coli*, in a dose responsive manner (Ciencialová et al., 2008). Purified holo-Tsf1 from *M. sexta* did not inhibit *E. coli* growth, while the apo-MsTsf1 did inhibit (Brummett et al., 2017). These studies strongly suggest that Tsf1 has a bacteriostatic function, likely mediated by its ability to withhold iron from pathogens.

While sequestering iron through high-affinity iron binding is one mechanism Tsf1 can defend insects from pathogens, another immune response that Tsf1 functions in is the hypoferremic response (Iatsenko et al., 2020). A study of *D. melanogaster* Tsf1 showed that in response to several bacterial and fungal challenges, Tsf1 is upregulated by the Imd and Toll pathways and is essential to relocating iron from hemolymph to the fat body (Iatsenko et al., 2020). The 5' upstream region of many *Tsf1* genes has one or more Nuclear factor κB (NF-kB) binding sites (Geiser and Winzerling, 2012). NF-kB plays a major role in the insect and

mammalian immune response to pathogens, and it is activated by the IMD and Toll pathways (Hetru and Hoffmann, 2009).

Tsf1 in reducing oxidative stress

In animals, free iron can lead to oxidative stress through the formation of free radicals via the Fenton reaction (Meneghini, 1997). Because insects have an open circulatory system, which bathes the tissues in hemolymph, it would be essential to keep free iron levels low in the hemolymph to limit potential damage to tissues. Analysis of hemolymph from healthy *M. sexta* larvae showed no measurable amount of non-protein bound iron (Adamo et al., 2007).

Tsf1 appears to function in the process of limiting oxidative stress through its ability to sequester iron in the hemolymph. A study of the beetle *P. brevitarsis* found that challenging the beetle with various stressors (wounding, pathogenic infection, and iron injection) caused an increase in PbTsf1 mRNA levels (Kim et al., 2008a). In a follow-up study, the same group found that reducing PbTsf1 mRNA levels through RNAi followed by challenging the beetle with stressors (heat shock, fungal infection, and H_2O_2 injection) caused an increase of iron and reactive oxygen species in the hemolymph and ultimately increased the amounts of apoptosis in tissues (Kim et al., 2008b).

Inducing iron overload in hemolymph through iron injections also causes an up-regulation of Tsf1 mRNA in *B. ignitus* worker bees and *A. germari* (Lee et al., 2006; Wang et al., 2009). In contrast, when insects are fed an iron rich diet, the whole-body Tsf1 mRNA levels tend to decrease (Ampasala et al., 2004; Bartfeld and Law, 1990; Harizanova et al., 2005; Huebers et al., 1988; Lee et al., 2006; Yoshiga et al., 1999). Taken together, these studies indicate that in order to reduce oxidative stress, Tsf1 responds to free iron levels in different locations by being

differentially expressed. For example: a decrease in Tsf1 and its trafficking of iron from the gut to other tissues would be beneficial during times of high dietary iron intake so that other tissues would not be iron-overloaded, whereas an increase in Tsf1 presence during high levels of free iron in the hemolymph would also help to protect tissues from free radical-induced oxidative stress.

Goals of Current Research

The mechanisms behind Tsf1's role in iron transport, immunity, and reducing oxidative stress is tied to its presumed ability to bind iron with high affinity in hemolymph and secreted fluids and to release the iron for delivery into cells. However, sequence analysis studies of putative iron binding residues in Tsf1s have highlighted the possibility that iron coordination of many Tsf1s may differ from vertebrate transferrins. These predicted changes at the iron binding site could greatly affect Tsf1's iron affinity and iron release. The contradiction between Tsf1's biological functions and predicted biochemical properties had not been adequately addressed. Also, the importance of the non-iron-binding C-lobe in many Tsf1s had not been adequately studied. Therefore, my first project aimed to address these issues by biochemically characterizing Tsf1 from two model insects, *M. sexta* (MsTsf1) and *D. melanogaster* (DmTsf1). My specific aims were as follows:

(1) Evaluate the putative iron-coordinating and anion-binding residues in an updated collection of Tsf1 sequences by performing sequence alignments.

(2) Purify recombinantly expressed full-length DmTsf1 and native MsTsf1.

(3) Characterize MsTsf1 and DmTsf1's iron coordination, affinity for iron, and iron release.

(4) Purify an N-lobe mutant of recombinant DmTsf1 and compare its biochemical properties to full-length DmTsf1.

When beginning my research, no structure of an insect transferrin had been solved. Similar to the reasoning behind my first project, the Tsf1 structural information and mechanism of iron coordination was based mostly on predictions from sequence-based analysis comparing Tsf1 to vertebrate transferrins. With the low percent identity of Tsf1s to vertebrate transferrin sequences (20-30%) and the putative iron coordinating residues of Tsf1s being different from vertebrate transferrins, I wanted to determine more information on the overall structure and the residues involved in iron coordination of Tsf1. Therefore, my second project focused on determining the crystal structure of holo-MsTsf1. My specific aims for this project were as follows:

(1) Purify native MsTsf1 from the hemolymph of larvae.

(2) Determine if the purified MsTsf1 is saturated with iron.

(3) Through collaboration with the Protein Structure Laboratory at Kansas University, solve the crystal structure of holo-MsTsf1.

(4) Analyze the overall crystal structure and iron coordination of MsTsf1.

(5) Use computational docking to predict whether alternative anions found in insect hemolymph could participate in the iron coordination of MsTsf1.

The structural results of MsTsf1 from my second project elucidated a number of novel characteristics. One finding was that the iron at the MsTsf1 binding site was coordinated by two tyrosines (Tyr90 and Tyr204) and two carbonate anions. One carbonate is in a position similar to

the position of the synergistic carbonate in vertebrate transferrin iron coordination sites, while the second carbonate was in a novel position. Binding of this second carbonate occurred through a single amino acid residue, Asn121, which is highly conserved in insect sequences. Therefore, for my third project I wanted to probe the importance of specific amino acid residues involved in iron coordination and anion binding in MsTsf1. My specific aims were as follows:

(1) Produce several MsTsf1 mutant forms of Asn121 through site-directed mutagenesis.

(2) Produce a MsTsf1 double mutant of both Tyr90 and Tyr204 through multisite-directed mutagenesis.

(3) Express and purify the wild-type and mutant forms of recombinant MsTsf1.

(4) Characterize the WT and mutant MsTsf1s' iron coordination, affinity for iron, and iron release.

(5) Determine if the mutations cause any secondary structural changes by using circular dichroism.

(6) Determine if iron binding causes any secondary structural changes by using circular dichroism.

Tsf1's role in iron transport is not clear. While Tsf1 is involved in trafficking iron from the gut and hemolymph into the fat body (Iatsenko et al., 2020; Xiao et al., 2019), the mechanism of iron delivery into cells is not known. In mammals, one pathway for iron delivery into cells occurs when holo-STf binds to its receptors, the transferrin-receptor complex is endocytosed, and iron release from STf occurs in the endosome. Despite the lack of an identified receptor of Tsf1, I was interested in testing whether insect cells take up Tsf1 via endocytosis as a possible iron delivery pathway. Thus, my fourth project involved the following specific aims:

(1) Dissect tissues from *D. melanogaster* larvae and adult flies and perform immunostaining for Tsf1.

(2) Determine which tissues, if any, show uptake of Tsf1 through confocal imaging.

(3) For tissues that show staining and uptake of Tsf1, determine if Tsf1 colocalizes with the early endosomal marker, Rab5, by using immunostaining and confocal imaging.

References

Actor, J.K., Hwang, S.-A., Kruzel, M.L., 2009. Lactoferrin as a Natural Immune Modulator. Curr Pharm Des 15, 1956–1973.

Adamo, S.A., Fidler, T.L., Forestell, C.A., 2007. Illness-induced anorexia and its possible function in the caterpillar, Manduca sexta. Brain, Behavior, and Immunity 21, 292–300. https://doi.org/10.1016/j.bbi.2006.10.006

Adams, T.E., Mason, A.B., He, Q.-Y., Halbrooks, P.J., Briggs, S.K., Smith, V.C., MacGillivray, R.T.A., Everse, S.J., 2003. The Position of Arginine 124 Controls the Rate of Iron Release from the N-lobe of Human Serum Transferrin: A STRUCTURAL STUDY *. Journal of Biological Chemistry 278, 6027–6033. https://doi.org/10.1074/jbc.M210349200

Adamski, Z., Bufo, S.A., Chowański, S., Falabella, P., Lubawy, J., Marciniak, P., Pacholska-Bogalska, J., Salvia, R., Scrano, L., Słocińska, M., Spochacz, M., Szymczak, M., Urbański, A., Walkowiak-Nowicka, K., Rosiński, G., 2019. Beetles as Model Organisms in Physiological, Biomedical and Environmental Studies – A Review. Front Physiol 10, 319. https://doi.org/10.3389/fphys.2019.00319

Aisen, P., 2001. Chemistry and biology of eukaryotic iron metabolism. The International Journal of Biochemistry & Cell Biology 33, 940–959. https://doi.org/10.1016/S1357-2725(01)00063-2

Aisen, P., Leibman, A., 1972. Lactoferrin and transferrin: A comparative study. Biochimica et Biophysica Acta (BBA) - Protein Structure 257, 314–323. https://doi.org/10.1016/0005-2795(72)90283-8

Aisen, P., Leibman, A., Zweier, J., 1978. Stoichiometric and site characteristics of the binding of iron to human transferrin. J. Biol. Chem. 253, 1930–1937.

Akiyama, Y., Oshima, K., Kuhara, T., Shin, K., Abe, F., Iwatsuki, K., Nadano, D., Matsuda, T., 2013. A lactoferrin-receptor, intelectin 1, affects uptake, sub-cellular localization and

release of immunochemically detectable lactoferrin by intestinal epithelial Caco-2 cells. Journal of Biochemistry 154, 437–448. https://doi.org/10.1093/jb/mvt073

Ampasala, D.R., Zheng, S.-C., Retnakaran, A., Krell, P.J., Arif, B.M., Feng, Q.-L., 2004. Cloning and expression of a putative transferrin cDNA of the spruce budworm, Choristoneura fumiferana. Insect Biochemistry and Molecular Biology 34, 493–500. https://doi.org/10.1016/j.ibmb.2004.03.002

Anderson, B.F., Baker, H.M., Norris, G.E., Rice, D.W., Baker, E.N., 1989. Structure of human lactoferrin: crystallographic structure analysis and refinement at 2.8 A resolution. J. Mol. Biol. 209, 711–734. https://doi.org/10.1016/0022-2836(89)90602-5

Anderson, G.J., Frazer, D.M., 2017. Current understanding of iron homeostasis. Am J Clin Nutr 106, 1559S-1566S. https://doi.org/10.3945/ajcn.117.155804

Anderson, G.J., Vulpe, C.D., 2009. Mammalian iron transport. Cell. Mol. Life Sci. 66, 3241–3261. https://doi.org/10.1007/s00018-009-0051-1

Armitage, A.E., Eddowes, L.A., Gileadi, U., Cole, S., Spottiswoode, N., Selvakumar, T.A., Ho, L.-P., Townsend, A.R.M., Drakesmith, H., 2011. Hepcidin regulation by innate immune and infectious stimuli. Blood 118, 4129–4139. https://doi.org/10.1182/blood-2011-04-351957

Ashida, K., Sasaki, H., Suzuki, Y.A., Lönnerdal, B., 2004. Cellular internalization of lactoferrin in intestinal epithelial cells. Biometals 17, 311–315. https://doi.org/10.1023/B:BIOM.0000027710.13543.3f

Bai, L., Qiao, M., Zheng, R., Deng, C., Mei, S., Chen, W., 2016. Phylogenomic analysis of transferrin family from animals and plants. Comp. Biochem. Physiol. Part D Genomics Proteomics 17, 1–8. https://doi.org/10.1016/j.cbd.2015.11.002

Bailey, S., Evans, R.W., Garratt, R.C., Gorinsky, B., Hasnain, S., Horsburgh, C., Jhoti, H., Lindley, P.F., Mydin, A., Sarra, R., 1988. Molecular structure of serum transferrin at 3.3-A resolution. Biochemistry 27, 5804–5812. https://doi.org/10.1021/bi00415a061

Baker, E.N., 1994. Structure and Reactivity of Transferrins, in: Sykes, A.G. (Ed.), Advances in Inorganic Chemistry. Academic Press, pp. 389–463. https://doi.org/10.1016/S0898-8838(08)60176-2

Baker, E.N., Lindley, P.F., 1992. New perspectives on the structure and function of transferrins. J. Inorg. Biochem. 47, 147–160. https://doi.org/10.1016/0162-0134(92)84061-q

Baker, H.M., Baker, E.N., 2012. A structural perspective on lactoferrin function. Biochemistry and Cell Biology 90, 320–328.

Bartfeld, N.S., Law, J.H., 1990. Biochemical and Molecular Characterization of Transferrin from Manduca sexta, in: Hagedorn, H.H., Hildebrand, J.G., Kidwell, M.G., Law, J. H. (Eds.),

Molecular Insect Science. Springer US, Boston, MA, pp. 125–130. https://doi.org/10.1007/978-1-4899-3668-4_15

Bernstein, S.E., 1987. Hereditary hypotransferrinemia with hemosiderosis, a murine disorder resembling human atransferrinemia. J Lab Clin Med 110, 690–705. https://doi.org/10.5555/uri:pii:0022214387904677

Bettedi, L., Aslam, M.F., Szular, J., Mandilaras, K., Missirlis, F., 2011. Iron depletion in the intestines of Malvolio mutant flies does not occur in the absence of a multicopper oxidase. Journal of Experimental Biology 214, 971–978. https://doi.org/10.1242/jeb.051664

Bonilla, M.L., Todd, C., Erlandson, M., Andres, J., 2015. Combining RNA-seq and proteomic profiling to identify seminal fluid proteins in the migratory grasshopper Melanoplus sanguinipes (F). BMC Genomics 16, 1096. https://doi.org/10.1186/s12864-015-2327-1

Brummett, L.M., Kanost, M.R., Gorman, M.J., 2017. The immune properties of Manduca sexta transferrin. Insect Biochem. Mol. Biol. 81, 1–9. https://doi.org/10.1016/j.ibmb.2016.12.006

Calap-Quintana, P., González-Fernández, J., Sebastiá-Ortega, N., Llorens, J.V., Moltó, M.D., 2017. Drosophila melanogaster Models of Metal-Related Human Diseases and Metal Toxicity. Int J Mol Sci 18. https://doi.org/10.3390/ijms18071456

Cassat, J.E., Skaar, E.P., 2013. Iron in Infection and Immunity. Cell Host & Microbe 13, 509–519. https://doi.org/10.1016/j.chom.2013.04.010

Chen, T.T., Li, L., Chung, D.-H., Allen, C.D.C., Torti, S.V., Torti, F.M., Cyster, J.G., Chen, C.-Y., Brodsky, F.M., Niemi, E.C., Nakamura, M.C., Seaman, W.E., Daws, M.R., 2005. TIM-2 is expressed on B cells and in liver and kidney and is a receptor for H-ferritin endocytosis. Journal of Experimental Medicine 202, 955–965. https://doi.org/10.1084/jem.20042433

Cheng, L., Baonza, A., Grifoni, D., 2018. Drosophila Models of Human Disease. Biomed Res Int 2018, 7214974. https://doi.org/10.1155/2018/7214974

Ciencialová, A., Neubauerová, T., Šanda, M., Šindelka, R., Cvačka, J., Voburka, Z., Buděšínský, M., Kašička, V., Sázelová, P., Šolínová, V., Macková, M., Koutek, B., Jiráček, J., 2008. Mapping the peptide and protein immune response in the larvae of the fleshfly Sarcophaga bullata. Journal of Peptide Science 14, 670–682. https://doi.org/10.1002/psc.967

Conneely, O.M., 2001. Antiinflammatory activities of lactoferrin. J Am Coll Nutr 20, 389S-395S; discussion 396S-397S. https://doi.org/10.1080/07315724.2001.10719173

Cooper, C.A., Tizard, M.L., Stanborough, T., Moore, S.C., Chandry, P.S., Jenkins, K.A., Wise, T.G., O'Neil, T.E., Layton, D.S., Morris, K.R., Moore, R.J., Fegan, N., Doran, T.J., 2019. Overexpressing ovotransferrin and avian β-defensin-3 improves antimicrobial capacity of

chickens and poultry products. Transgenic Res 28, 51–76. https://doi.org/10.1007/s11248-018-0101-2

Cutone, A., Rosa, L., Lepanto, M.S., Scotti, M.J., Berlutti, F., Bonaccorsi di Patti, M.C., Musci, G., Valenti, P., 2017. Lactoferrin Efficiently Counteracts the Inflammation-Induced Changes of the Iron Homeostasis System in Macrophages. Front. Immunol. 8, 705. https://doi.org/10.3389/fimmu.2017.00705

Day, C.L., Stowell, K.M., Baker, E.N., Tweedie, J.W., 1992. Studies of the N-terminal half of human lactoferrin produced from the cloned cDNA demonstrate that interlobe interactions modulate iron release. J. Biol. Chem. 267, 13857–13862.

Dewan, J.C., Mikami, B., Hirose, M., Sacchettini, J.C., 1993. Structural evidence for a pH-sensitive dilysine trigger in the hen ovotransferrin N-lobe: implications for transferrin iron release. Biochemistry 32, 11963–11968. https://doi.org/10.1021/bi00096a004

Dhungana, S., Taboy, C.H., Zak, O., Larvie, M., Crumbliss, A.L., Aisen, P., 2004. Redox Properties of Human Transferrin Bound to Its Receptor †. Biochemistry 43, 205–209. https://doi.org/10.1021/bi0353631

Ding et al., X., Li, S., Borst, D.W., 2004. Identification and cDNA cloning of transferrin, a major fat body protein in the lubber grasshopper [WWW Document]. URL https://sicb.burkclients.com/meetings/2004/schedule/abstractdetails.php3?id=177 (accessed 6.28.21).

Donovan, A., Lima, C.A., Pinkus, J.L., Pinkus, G.S., Zon, L.I., Robine, S., Andrews, N.C., 2005. The iron exporter ferroportin/Slc40a1 is essential for iron homeostasis. Cell Metabolism 1, 191–200. https://doi.org/10.1016/j.cmet.2005.01.003

Drakesmith, H., Prentice, A.M., 2012. Hepcidin and the Iron-Infection Axis. Science 338, 768–772. https://doi.org/10.1126/science.1224577

Eckenroth, B.E., Steere, A.N., Chasteen, N.D., Everse, S.J., Mason, A.B., 2011. How the binding of human transferrin primes the transferrin receptor potentiating iron release at endosomal pH. Proc Natl Acad Sci USA 108, 13089–13094. https://doi.org/10.1073/pnas.1105786108

Faber, H.R., Baker, C.J., Day, C.L., Tweedie, J.W., Baker, E.N., 1996. Mutation of Arginine 121 in Lactoferrin Destabilizes Iron Binding by Disruption of Anion Binding: Crystal Structures of R121S and R121E Mutants † , ‡. Biochemistry 35, 14473–14479. https://doi.org/10.1021/bi961729g

Faber, R.H., Bland, T., Day, C.L., Norris, G.E., Tweedie, J.W., Baker, E.N., 1996. Altered Domain Closure and Iron Binding in Transferrins: The Crystal Structure of the Asp60Ser Mutant of the Amino-terminal Half-molecule of Human Lactoferrin. Journal of Molecular Biology 256, 352–363. https://doi.org/10.1006/jmbi.1996.0091

Farkaš, R., Beňová-Liszeková, D., Mentelová, L., Beňo, M., Babišová, K., Trusinová-Pečeňová, L., Raška, O., Chase, B.A., Raška, I., 2018. Endosomal vacuoles of the prepupal salivary glands of Drosophila play an essential role in the metabolic reallocation of iron. Develop. Growth Differ. 60, 411–430. https://doi.org/10.1111/dgd.12562

Farnaud, S., Evans, R.W., 2003. Lactoferrin--a multifunctional protein with antimicrobial properties. Mol. Immunol. 40, 395–405. https://doi.org/10.1016/s0161-5890(03)00152-4

Fernandes, K.E., Carter, D.A., 2017. The Antifungal Activity of Lactoferrin and Its Derived Peptides: Mechanisms of Action and Synergy with Drugs against Fungal Pathogens. Front Microbiol 8. https://doi.org/10.3389/fmicb.2017.00002

Folwell, J.L., Barton, C.H., Shepherd, D., 2006. Immunolocalisation of the D. melanogaster Nramp homologue Malvolio to gut and Malpighian tubules provides evidence that Malvolio and Nramp2 are orthologous. Journal of Experimental Biology 209, 1988–1995. https://doi.org/10.1242/jeb.02193

Frey, P.A., Reed, G.H., 2012. The Ubiquity of Iron. ACS Chem. Biol. 7, 1477–1481. https://doi.org/10.1021/cb300323q

Fujihara, T., Hayashi, K., 1995. Lactoferrin inhibits herpes simplex virus type-1 (HSV-1) infection to mouse cornea. Archives of Virology 140, 1469–1472. https://doi.org/10.1007/BF01322673

Ganz, T., 2013. Systemic iron homeostasis. Physiol Rev 93, 1721–1741. https://doi.org/10.1152/physrev.00008.2013

Garrick, M.D., Garrick, L.M., 2009. Cellular iron transport. Biochimica et Biophysica Acta (BBA) - General Subjects 1790, 309–325. https://doi.org/10.1016/j.bbagen.2009.03.018

Gasdaska, J.R., Law, J.H., Bender, C.J., Aisen, P., 1996. Cockroach transferrin closely resembles vertebrate transferrins in its metal ion-binding properties: a spectroscopic study. J. Inorg. Biochem. 64, 247–258. https://doi.org/10.1016/s0162-0134(96)00052-9

Geiser, D.L., Winzerling, J.J., 2012. Insect transferrins: multifunctional proteins. Biochim. Biophys. Acta 1820, 437–451. https://doi.org/10.1016/j.bbagen.2011.07.011

Geiser, D.L., Zhang, D., Winzerling, J.J., 2006. Secreted ferritin: Mosquito defense against iron overload? Insect Biochemistry and Molecular Biology 36, 177–187. https://doi.org/10.1016/j.ibmb.2005.12.001

Giansanti, F., Leboffe, L., Pitari, G., Ippoliti, R., Antonini, G., 2012. Physiological roles of ovotransferrin. Biochim. Biophys. Acta 1820, 218–225. https://doi.org/10.1016/j.bbagen.2011.08.004

Grady, J.K., Mason, A.B., Woodworth, R.C., Chasteen, N.D., 1995. The effect of salt and site-directed mutations on the iron(III)-binding site of human serum transferrin as probed by EPR spectroscopy. Biochem. J. 309 (Pt 2), 403–410. https://doi.org/10.1042/bj3090403

Grossmann, J.G., Crawley, J.B., Strange, R.W., Patel, K.J., Murphy, L.M., Neu, M., Evans, R.W., Hasnain, S.S., 1998. The nature of ligand-induced conformational change in transferrin in solution. An investigation using X-ray scattering, XAFS and site-directed mutants. J Mol Biol 279, 461–472. https://doi.org/10.1006/jmbi.1998.1787

Grossmann, J.G., Mason, A.B., Woodworth, R.C., Neu, M., Lindley, P.F., Hasnain, S.S., 1993. Asp ligand provides the trigger for closure of transferrin molecules. Direct evidence from X-ray scattering studies of site-specific mutants of the N-terminal half-molecule of human transferrin. J Mol Biol 231, 554–558. https://doi.org/10.1006/jmbi.1993.1308

Gutteberg, T.J., Røkke, O., Andersen, O., Jørgensen, T., 1989. Early Fall of Circulating Iron and Rapid Rise of Lactoferrin in Septicemia and Endotoxemia: An Early Defence Mechanism. Scandinavian Journal of Infectious Diseases 21, 709–715. https://doi.org/10.3109/00365548909021701

Hall, S., Bone, C., Oshima, K., Zhang, L., McGraw, M., Lucas, B., Fehon, R.G., Ward, R.E., 2014. Macroglobulin complement-related encodes a protein required for septate junction organization and paracellular barrier function in Drosophila. Development 141, 889–898. https://doi.org/10.1242/dev.102152

Han, O., 2011. Molecular mechanism of intestinal iron absorption. Metallomics 3, 103. https://doi.org/10.1039/c0mt00043d

Harizanova, N., Georgieva, T., Dunkov, B.C., Yoshiga, T., Law, J.H., 2005. Aedes aegypti transferrin. Gene structure, expression pattern, and regulation. Insect Mol Biol 14, 79–88. https://doi.org/10.1111/j.1365-2583.2004.00533.x

Harris, W.R., 2012. Anion binding properties of the transferrins. Implications for function. Biochimica et Biophysica Acta (BBA) - General Subjects 1820, 348–361. https://doi.org/10.1016/j.bbagen.2011.07.017

Harris, W.R., Cafferty, A.M., Trankler, K., Maxwell, A., MacGillivray, R.T.A., 1999. Thermodynamic studies on anion binding to apotransferrin and to recombinant transferrin N-lobe half molecules. Biochimica et Biophysica Acta (BBA) - Protein Structure and Molecular Enzymology 1430, 269–280. https://doi.org/10.1016/S0167-4838(99)00007-2

Hattori, M., Komatsu, S., Noda, H., Matsumoto, Y., 2015. Proteome Analysis of Watery Saliva Secreted by Green Rice Leafhopper, Nephotettix cincticeps. PLOS ONE 10, e0123671. https://doi.org/10.1371/journal.pone.0123671

He, Q.Y., Mason, A.B., Nguyen, V., MacGillivray, R.T., Woodworth, R.C., 2000a. The chloride effect is related to anion binding in determining the rate of iron release from the human transferrin N-lobe. Biochem. J. 350 Pt 3, 909–915.

He, Q.Y., Mason, A.B., Pakdaman, R., Chasteen, N.D., Dixon, B.K., Tam, B.M., Nguyen, V., MacGillivray, R.T., Woodworth, R.C., 2000b. Mutations at the histidine 249 ligand profoundly alter the spectral and iron-binding properties of human serum transferrin N-lobe. Biochemistry 39, 1205–1210. https://doi.org/10.1021/bi9915216

He, Q Y, Mason, A.B., Woodworth, R.C., 1997. Iron release from recombinant N-lobe and single point Asp63 mutants of human transferrin by EDTA. Biochem J 328, 439–445.

He, Q. Y., Mason, A.B., Woodworth, R.C., Tam, B.M., MacGillivray, R.T., Grady, J.K., Chasteen, N.D., 1997a. Inequivalence of the two tyrosine ligands in the N-lobe of human serum transferrin. Biochemistry 36, 14853–14860. https://doi.org/10.1021/bi9719556

He, Q.-Y., Mason, A.B., Woodworth, R.C., Tam, B.M., MacGillivray, R.T.A., Grady, J.K., Chasteen, N.D., 1998. Mutations at Nonliganding Residues Tyr-85 and Glu-83 in the N-Lobe of Human Serum Transferrin. Journal of Biological Chemistry 273, 17018–17024. https://doi.org/10.1074/jbc.273.27.17018

He, Q. Y., Mason, A.B., Woodworth, R.C., Tam, B.M., Wadsworth, T., MacGillivray, R.T., 1997b. Effects of mutations of aspartic acid 63 on the metal-binding properties of the recombinant N-lobe of human serum transferrin. Biochemistry 36, 5522–5528. https://doi.org/10.1021/bi963028p

He, Y., Cao, X., Li, K., Hu, Y., Chen, Y., Blissard, G., Kanost, M.R., Jiang, H., 2015. A genome-wide analysis of antimicrobial effector genes and their transcription patterns in Manduca sexta. Insect Biochemistry and Molecular Biology 62, 23–37. https://doi.org/10.1016/j.ibmb.2015.01.015

Hentze, M.W., Muckenthaler, M.U., Galy, B., Camaschella, C., 2010. Two to Tango: Regulation of Mammalian Iron Metabolism. Cell 142, 24–38. https://doi.org/10.1016/j.cell.2010.06.028

Hetru, C., Hoffmann, J.A., 2009. NF-κB in the Immune Response of Drosophila. Cold Spring Harb Perspect Biol 1, a000232. https://doi.org/10.1101/cshperspect.a000232

Hirai, M., Watanabe, D., Chinzei, Y., 2000. A juvenile hormone-repressible transferrin-like protein from the bean bug, Riptortus clavatus: cDNA sequence analysis and protein identification during diapause and vitellogenesis. Arch Insect Biochem Physiol 44, 17–26. https://doi.org/10.1002/(SICI)1520-6327(200005)44:1<17::AID-ARCH3>3.0.CO;2-O

Huebers, H.A., Huebers, E., Finch, C.A., Webb, B.A., Truman, J.W., Riddiford, L.M., Martin, A.W., Massover, W.H., 1988. Iron binding proteins and their roles in the tobacco hornworm, Manduca sexta (L.). J. Comp. Physiol. B, Biochem. Syst. Environ. Physiol. 158, 291–300. https://doi.org/10.1007/bf00695327

Iatsenko, I., Marra, A., Boquete, J.-P., Peña, J., Lemaitre, B., 2020. Iron sequestration by transferrin 1 mediates nutritional immunity in Drosophila melanogaster. PNAS 117, 7317–7325. https://doi.org/10.1073/pnas.1914830117

Iwase, H., Hotta, K., 1977. Ovotransferrin subfractionation dependent upon carbohydrate chain differences. Journal of Biological Chemistry 252, 5437–5443. https://doi.org/10.1016/S0021-9258(19)63369-7

Jenssen, H., Hancock, R.E.W., 2009. Antimicrobial properties of lactoferrin. Biochimie 91, 19–29. https://doi.org/10.1016/j.biochi.2008.05.015

Johansson, B., 1958. Chromatographic Separation of Lactalbumin from Human Milk Whey on Calcium Phosphate Columns. Nature 181, 996–997. https://doi.org/10.1038/181996b0

Kanost, M.R., Arrese, E.L., Cao, X., Chen, Y.-R., Chellapilla, S., Goldsmith, M.R., Grosse-Wilde, E., Heckel, D.G., Herndon, N., Jiang, Haobo, Papanicolaou, A., Qu, J., Soulages, J.L., Vogel, H., Walters, J., Waterhouse, R.M., Ahn, S.-J., Almeida, F.C., An, C., Aqrawi, P., Bretschneider, A., Bryant, W.B., Bucks, S., Chao, H., Chevignon, G., Christen, J.M., Clarke, D.F., Dittmer, N.T., Ferguson, L.C.F., Garavelou, S., Gordon, K.H.J., Gunaratna, R.T., Han, Y., Hauser, F., He, Y., Heidel-Fischer, H., Hirsh, A., Hu, Y., Jiang, Hongbo, Kalra, D., Klinner, C., König, C., Kovar, C., Kroll, A.R., Kuwar, S.S., Lee, S.L., Lehman, R., Li, K., Li, Z., Liang, H., Lovelace, S., Lu, Z., Mansfield, J.H., McCulloch, K.J., Mathew, T., Morton, B., Muzny, D.M., Neunemann, D., Ongeri, F., Pauchet, Y., Pu, L.-L., Pyrousis, I., Rao, X.-J., Redding, A., Roesel, C., Sanchez-Gracia, A., Schaack, S., Shukla, A., Tetreau, G., Wang, Y., Xiong, G.-H., Traut, W., Walsh, T.K., Worley, K.C., Wu, D., Wu, W., Wu, Y.-Q., Zhang, X., Zou, Z., Zucker, H., Briscoe, A.D., Burmester, T., Clem, R.J., Feyereisen, R., Grimmelikhuijzen, C.J.P., Hamodrakas, S.J., Hansson, B.S., Huguet, E., Jermiin, L.S., Lan, Q., Lehman, H.K., Lorenzen, M., Merzendorfer, H., Michalopoulos, I., Morton, D.B., Muthukrishnan, S., Oakeshott, J.G., Palmer, W., Park, Y., Passarelli, A.L., Rozas, J., Schwartz, L.M., Smith, W., Southgate, A., Vilcinskas, A., Vogt, R., Wang, P., Werren, J., Yu, X.-Q., Zhou, J.-J., Brown, S.J., Scherer, S.E., Richards, S., Blissard, G.W., 2016. Multifaceted biological insights from a draft genome sequence of the tobacco hornworm moth, Manduca sexta. Insect Biochemistry and Molecular Biology 76, 118–147. https://doi.org/10.1016/j.ibmb.2016.07.005

Kawabata, H., 2019. Transferrin and transferrin receptors update. Free Radical Biology and Medicine 133, 46–54. https://doi.org/10.1016/j.freeradbiomed.2018.06.037

Keijser, S., Jager, M.J., Dogterom-Ballering, H.C.M., Schoonderwoerd, D.T., de Keizer, R.J.W., Krose, C.J.M., Houwing-Duistermaat, J.J., van der Plas, M.J.A., van Dissel, J.T., Nibbering, P.H., 2008. Lactoferrin Glu561Asp polymorphism is associated with susceptibility to herpes simplex keratitis. Experimental Eye Research 86, 105–109. https://doi.org/10.1016/j.exer.2007.09.013

Kim, B.Y., Lee, K.S., Choo, Y.M., Kim, I., Hwang, J.S., Sohn, H.D., Jin, B.R., 2008a. Molecular cloning and characterization of a transferrin cDNA from the white-spotted flower chafer, Protaetia brevitarsis: Short Communication. DNA Sequence 19, 146–150. https://doi.org/10.1080/10425170701461854

Kim, B.Y., Lee, K.S., Choo, Y.M., Kim, I., Je, Y.H., Woo, S.D., Lee, S.M., Park, H.C., Sohn, H.D., Jin, B.R., 2008b. Insect transferrin functions as an antioxidant protein in a beetle larva. Comp. Biochem. Physiol. B, Biochem. Mol. Biol. 150, 161–169. https://doi.org/10.1016/j.cbpb.2008.02.009

Kim, B.Y., Lee, K.S., Yoon, H.J., Kim, I., Li, J., Sohn, H.D., Jin, B.R., 2009. Expression profile of the iron-binding proteins transferrin and ferritin heavy chain subunit in the bumblebee Bombus ignitus. Comparative Biochemistry and Physiology Part B: Biochemistry and Molecular Biology 153, 165–170. https://doi.org/10.1016/j.cbpb.2009.02.014

Kim, J., Kim, Y., 2010. A viral histone H4 suppresses expression of a transferrin that plays a role in the immune response of the diamondback moth, Plutella xylostella: A viral histone H4 against transferrin expression. Insect Molecular Biology no-no. https://doi.org/10.1111/j.1365-2583.2010.01014.x

Kohler, S.A., Henderson, B.R., Kühn, L.C., 1995. Succinate Dehydrogenase b mRNA of Drosophila melanogaster Has a Functional Iron-responsive Element in Its 5′-Untranslated Region. Journal of Biological Chemistry 270, 30781–30786. https://doi.org/10.1074/jbc.270.51.30781

Kojima, N., Bates, G.W., 1981. The formation of Fe3+-transferrin-CO3(2-) via the binding and oxidation of Fe2+. Journal of Biological Chemistry 256, 12034–12039. https://doi.org/10.1016/S0021-9258(18)43229-2

Kosman, D.J., 2020. A holistic view of mammalian (vertebrate) cellular iron uptake. Metallomics 12, 1323–1334. https://doi.org/10.1039/D0MT00065E

Kosman, D.J., 2010. Redox cycling in iron uptake, efflux, and trafficking. J. Biol. Chem. 285, 26729–26735. https://doi.org/10.1074/jbc.R110.113217

Kurama, T., Kurata, S., Natori, S., 1995. Molecular Characterization of an Insect Transferrin and its Selective Incorporation into Eggs During Oogenesis. European Journal of Biochemistry 228, 229–235. https://doi.org/10.1111/j.1432-1033.1995.0229n.x

Kurokawa, H., Mikami, B., Hirose, M., 1995. Crystal Structure of Diferric Hen Ovotransferrin at 2.4 Å Resolution. Journal of Molecular Biology 254, 196–207. https://doi.org/10.1006/jmbi.1995.0611

Kuser, P., Hall, D.R., Haw, M.L., Neu, M., Evans, R.W., Lindley, P.F., 2002. The mechanism of iron uptake by transferrins: the X-ray structures of the 18 kDa NII domain fragment of duck ovotransferrin and its nitrilotriacetate complex. Acta Crystallogr D Biol Crystallogr 58, 777–783. https://doi.org/10.1107/S0907444902003724

Lambert, L.A., 2012. Molecular evolution of the transferrin family and associated receptors. Biochim. Biophys. Acta 1820, 244–255. https://doi.org/10.1016/j.bbagen.2011.06.002

Lambert, L.A., Perri, H., Halbrooks, P.J., Mason, A.B., 2005a. Evolution of the transferrin family: conservation of residues associated with iron and anion binding. Comp. Biochem. Physiol. B, Biochem. Mol. Biol. 142, 129–141. https://doi.org/10.1016/j.cbpb.2005.07.007

Lambert, L.A., Perri, H., Meehan, T.J., 2005b. Evolution of duplications in the transferrin family of proteins. Comparative Biochemistry and Physiology Part B: Biochemistry and Molecular Biology 140, 11–25. https://doi.org/10.1016/j.cbpc.2004.09.012

Lee, K.S., Kim, B.Y., Kim, H.J., Seo, S.J., Yoon, H.J., Choi, Y.S., Kim, I., Han, Y.S., Je, Y.H., Lee, S.M., Kim, D.H., Sohn, H.D., Jin, B.R., 2006. Transferrin inhibits stress-induced apoptosis in a beetle. Free Radic. Biol. Med. 41, 1151–1161. https://doi.org/10.1016/j.freeradbiomed.2006.07.001

Legrand, D., Elass, E., Carpentier, M., Mazurier, J., 2005. Lactoferrin: Lactoferrin: a modulator of immune and inflammatory responses. Cell. Mol. Life Sci. 62, 2549. https://doi.org/10.1007/s00018-005-5370-2

Li, J.Y., Paragas, N., Ned, R.M., Qiu, A., Viltard, M., Leete, T., Drexler, I.R., Chen, X., Sanna-Cherchi, S., Mohammed, F., Williams, D., Lin, C.S., Schmidt-Ott, K.M., Andrews, N.C., Barasch, J., 2009. Scara5 Is a Ferritin Receptor Mediating Non-Transferrin Iron Delivery. Developmental Cell 16, 35–46. https://doi.org/10.1016/j.devcel.2008.12.002

Li, Y., Harris, W.R., Maxwell, A., MacGillivray, R.T.A., Brown, T., 1998. Kinetic Studies on the Removal of Iron and Aluminum from Recombinant and Site-Directed Mutant N-Lobe Half Transferrins †. Biochemistry 37, 14157–14166. https://doi.org/10.1021/bi9810454

Lieu, P.T., Heiskala, M., Peterson, P.A., Yang, Y., 2001. The roles of iron in health and disease. Molecular Aspects of Medicine 22, 1–87. https://doi.org/10.1016/S0098-2997(00)00006-6

Lin, L.N., Mason, A.B., Woodworth, R.C., Brandts, J.F., 1993. Calorimetric studies of the N-terminal half-molecule of transferrin and mutant forms modified near the Fe3+-binding site. Biochemical Journal 293, 517–522. https://doi.org/10.1042/bj2930517

Lind, M.I., Missirlis, F., Melefors, Ö., Uhrigshardt, H., Kirby, K., Phillips, J.P., Söderhäll, K., Rouault, T.A., 2006. Of Two Cytosolic Aconitases Expressed in Drosophila, Only One Functions as an Iron-regulatory Protein. Journal of Biological Chemistry 281, 18707–18714. https://doi.org/10.1074/jbc.M603354200

MacGillivray, R.T., Bewley, M.C., Smith, C.A., He, Q.Y., Mason, A.B., Woodworth, R.C., Baker, E.N., 2000. Mutation of the iron ligand His 249 to Glu in the N-lobe of human transferrin abolishes the dilysine “trigger” but does not significantly affect iron release. Biochemistry 39, 1211–1216. https://doi.org/10.1021/bi991522y

MacGillivray, R.T., Moore, S.A., Chen, J., Anderson, B.F., Baker, H., Luo, Y., Bewley, M., Smith, C.A., Murphy, M.E., Wang, Y., Mason, A.B., Woodworth, R.C., Brayer, G.D., Baker, E.N., 1998. Two high-resolution crystal structures of the recombinant N-lobe of human transferrin reveal a structural change implicated in iron release. Biochemistry 37, 7919–7928. https://doi.org/10.1021/bi980355j

Mandilaras, K., Pathmanathan, T., Missirlis, F., 2013. Iron Absorption in Drosophila melanogaster. Nutrients 5, 1622–1647. https://doi.org/10.3390/nu5051622

Martínez-Barnetche, J., García Solache, M., Neri Lecona, A., Tello López, Á.T., del Carmen Rodríguez, M., Gamba, G., Vázquez, N., Rodríguez, M.H., Lanz-Mendoza, H., 2007. Cloning and functional characterization of the Anopheles albimanus DMT1/NRAMP homolog: Implications in iron metabolism in mosquitoes. Insect Biochemistry and Molecular Biology 37, 532–539. https://doi.org/10.1016/j.ibmb.2007.02.009

Mason, A., He, Q.-Y., 2002. Molecular Aspects of Release of Iron from Transferrin. https://doi.org/10.1201/9780824744175.ch4

Mason, A.B., Halbrooks, P.J., James, N.G., Connolly, S.A., Larouche, J.R., Smith, V.C., MacGillivray, R.T.A., Chasteen, N.D., 2005. Mutational Analysis of C-Lobe Ligands of Human Serum Transferrin: Insights into the Mechanism of Iron Release. Biochemistry 44, 8013–8021. https://doi.org/10.1021/bi050015f

Masson, P.L., Heremans, J.F., 1968. Metal-combining properties of human lactoferrin (red milk protein). 1. The involvement of bicarbonate in the reaction. Eur J Biochem 6, 579–584. https://doi.org/10.1111/j.1432-1033.1968.tb00484.x

Masson, P.L., Heremans, J.F., Dive, C.H., 1966. An iron-binding protein common to many external secretions. Clinica Chimica Acta 14, 735–739. https://doi.org/10.1016/0009-8981(66)90004-0

Mecklenburg, S.L., Mason, A.B., Woodworth, R.C., Donohoe, R.J., 1997. Distinction of the two binding sites of serum transferrin by resonance Raman spectroscopy. Biospectroscopy 3, 435–444. https://doi.org/10.1002/(SICI)1520-6343(1997)3:6<435::AID-BSPY2>3.0.CO;2-#

Mehta, A., Deshpande, A., Bettedi, L., Missirlis, F., 2009. Ferritin accumulation under iron scarcity in Drosophila iron cells. Biochimie 91, 1331–1334. https://doi.org/10.1016/j.biochi.2009.05.003

Meneghini, R., 1997. Iron Homeostasis, Oxidative Stress, and DNA Damage. Free Radical Biology and Medicine 23, 783–792. https://doi.org/10.1016/S0891-5849(97)00016-6

Mikogami, T., Heyman, M., Spik, G., Desjeux, J.F., 1994. Apical-to-basolateral transepithelial transport of human lactoferrin in the intestinal cell line HT-29cl.19A. American Journal of Physiology-Gastrointestinal and Liver Physiology 267, G308–G315. https://doi.org/10.1152/ajpgi.1994.267.2.G308

Missirlis, F., Kosmidis, S., Brody, T., Mavrakis, M., Holmberg, S., Odenwald, W.F., Skoulakis, E.M.C., Rouault, T.A., 2007. Homeostatic Mechanisms for Iron Storage Revealed by Genetic Manipulations and Live Imaging of Drosophila Ferritin. Genetics 177, 89–100. https://doi.org/10.1534/genetics.107.075150

Mizutani, K., Mikami, B., Hirose, M., 2001. Domain closure mechanism in transferrins: new viewpoints about the hinge structure and motion as deduced from high resolution crystal structures of ovotransferrin N-lobe. Journal of Molecular Biology 309, 937–947. https://doi.org/10.1006/jmbi.2001.4719

Mizutani, K., Toyoda, M., Mikami, B., 2012. X-ray structures of transferrins and related proteins. Biochimica et Biophysica Acta (BBA) - General Subjects, Transferrins: Molecular mechanisms of iron transport and disorders 1820, 203–211. https://doi.org/10.1016/j.bbagen.2011.08.003

Mizutani, K., Yamashita, H., Kurokawa, H., Mikami, B., Hirose, M., 1999. Alternative Structural State of Transferrin. Journal of Biological Chemistry 274, 10190–10194. https://doi.org/10.1074/jbc.274.15.10190

Mohamed, J.A., DuPont, H.L., Jiang, Z.D., Belkind-Gerson, J., Figueroa, J.F., Armitige, L.Y., Tsai, A., Nair, P., Martinez-Sandoval, F.J., Guo, D., Hayes, P., Okhuysen, P.C., 2007. A Novel Single-Nucleotide Polymorphism in the Lactoferrin Gene Is Associated with Susceptibility to Diarrhea in North American Travelers to Mexico. Clinical Infectious Diseases 44, 945–952. https://doi.org/10.1086/512199

Najera, D.G., Dittmer, N.T., Weber, J.J., Kanost, M.R., Gorman, M.J., 2021. Phylogenetic and sequence analyses of insect transferrins suggest that only transferrin 1 has a role in iron homeostasis. Insect Science 28, 495–508. https://doi.org/10.1111/1744-7917.12783

Nichol, H., Law, J.H., Winzerling, J.J., 2002. Iron Metabolism in Insects. Annu. Rev. Entomol. 47, 535–559. https://doi.org/10.1146/annurev.ento.47.091201.145237

Nicholson, H., Anderson, B.F., Bland, T., Shewry, S.C., Tweedie, J.W., Baker, E.N., 1997. Mutagenesis of the Histidine Ligand in Human Lactoferrin: Iron Binding Properties and Crystal Structure of the Histidine-253 → Methionine Mutant,. Biochemistry 36, 341–346. https://doi.org/10.1021/bi961908y

Ogasawara, Y., Imase, M., Oda, H., Wakabayashi, H., Ishii, K., 2014. Lactoferrin Directly Scavenges Hydroxyl Radicals and Undergoes Oxidative Self-Degradation: A Possible Role in Protection against Oxidative DNA Damage. IJMS 15, 1003–1013. https://doi.org/10.3390/ijms15011003

Pakdaman, R., Petitjean, M., El Hage Chahine, J.-M., 1998. Transferrins. A mechanism for iron uptake by lactoferrin. Eur J Biochem 254, 144–153. https://doi.org/10.1046/j.1432-1327.1998.2540144.x

Pandey, U.B., Nichols, C.D., 2011. Human Disease Models in Drosophila melanogaster and the Role of the Fly in Therapeutic Drug Discovery. Pharmacol Rev 63, 411–436. https://doi.org/10.1124/pr.110.003293

Peterson, N.A., Anderson, B.F., Jameson, G.B., Tweedie, J.W., Baker, E.N., 2000. Crystal structure and iron-binding properties of the R210K mutant of the N-lobe of human lactoferrin: implications for iron release from transferrins. Biochemistry 39, 6625–6633. https://doi.org/10.1021/bi0001224

Peyssonnaux, C., Zinkernagel, A.S., Datta, V., Lauth, X., Johnson, R.S., Nizet, V., 2006. TLR4-dependent hepcidin expression by myeloid cells in response to bacterial pathogens. Blood 107, 3727–3732. https://doi.org/10.1182/blood-2005-06-2259

Pham, D.Q.D., Winzerling, J.J., 2010. Insect ferritins: Typical or atypical? Biochimica et Biophysica Acta (BBA) - General Subjects 1800, 824–833. https://doi.org/10.1016/j.bbagen.2010.03.004

Qu, M., Ma, L., Chen, P., Yang, Q., 2014. Proteomic Analysis of Insect Molting Fluid with a Focus on Enzymes Involved in Chitin Degradation. J. Proteome Res. 13, 2931–2940. https://doi.org/10.1021/pr5000957

Rathnapala, E.C.N., Ahn, D.U., Abeyrathne, S., 2021. Functional properties of ovotransferrin from chicken egg white and its derived peptides: a review. Food Sci Biotechnol 30, 619–630. https://doi.org/10.1007/s10068-021-00901-3

Rosa, L., Cutone, A., Lepanto, M.S., Paesano, R., Valenti, P., 2017. Lactoferrin: A Natural Glycoprotein Involved in Iron and Inflammatory Homeostasis. Int J Mol Sci 18, 1985. https://doi.org/10.3390/ijms18091985

Schade, A.L., Reinhart, R.W., Levy, H., 1949. Carbon dioxide and oxygen in complex formation with iron and siderophilin, the iron-binding component of human plasma. Arch Biochem 20, 170–172.

Shimazaki, Y., Takahashi, A., 2018. Antibacterial activity of lysozyme-binding proteins from chicken egg white. Journal of Microbiological Methods 154, 19–24. https://doi.org/10.1016/j.mimet.2018.10.001

Simmons, L.W., Tan, Y.-F., Millar, A.H., 2013. Sperm and seminal fluid proteomes of the field cricket Teleogryllus oceanicus: identification of novel proteins transferred to females at mating. Insect Mol. Biol. 22, 115–130. https://doi.org/10.1111/imb.12007

Spiro, Th.G., Saltman, P., 1969. Polynuclear complexes of iron and their biological implications, in: Jørgensen, C.K., Neilands, J.B., Nyholm, R.S., Reinen, D., Williams, R.J.P. (Eds.), Structure and Bonding, Structure and Bonding. Springer Berlin Heidelberg, Berlin, Heidelberg, pp. 116–156. https://doi.org/10.1007/BFb0118856

Superti, F., Ammendolia, M.G., Berlutti, F., Valenti, P., 2007. Ovotransferrin, in: Huopalahti, R., López-Fandiño, R., Anton, M., Schade, R. (Eds.), Bioactive Egg Compounds. Springer Berlin Heidelberg, Berlin, Heidelberg, pp. 43–50. https://doi.org/10.1007/978-3-540-37885-3_7

Surgenor, D.M., Koechlin, B.A., Strong, L.E., 1949. CHEMICAL, CLINICAL, AND IMMUNOLOGICAL STUDIES ON THE PRODUCTS OF HUMAN PLASMA FRACTIONATION. XXXVII. THE METAL-COMBINING GLOBULIN OF HUMAN PLASMA [WWW Document]. https://doi.org/10.1172/JCI102056

Tang, X., Zhou, B., 2013. Iron homeostasis in insects: Insights from Drosophila studies. IUBMB Life 65, 863–872. https://doi.org/10.1002/iub.1211

Tang, X., Zhou, B., 2012. Ferritin is the key to dietary iron absorption and tissue iron detoxification in Drosophila melanogaster. FASEB J 27, 288–298. https://doi.org/10.1096/fj.12-213595

Teng, C.T., 2002. Lactoferrin gene expression and regulation: an overview. Biochem. Cell Biol. 80, 7–16. https://doi.org/10.1139/o01-215

Theil, E.C., 2004. IRON, FERRITIN, AND NUTRITION. Annu. Rev. Nutr. 24, 327–343. https://doi.org/10.1146/annurev.nutr.24.012003.132212

Tiklová, K., Senti, K.-A., Wang, S., Gräslund, A., Samakovlis, C., 2010. Epithelial septate junction assembly relies on melanotransferrin iron binding and endocytosis in Drosophila. Nat Cell Biol 12, 1071–1077. https://doi.org/10.1038/ncb2111

Trenor, C.C., Campagna, D.R., Sellers, V.M., Andrews, N.C., Fleming, M.D., 2000. The molecular defect in hypotransferrinemic mice. Blood 96, 1113–1118. https://doi.org/10.1182/blood.V96.3.1113

Valenti, P., Antonini, G., Fanelli, M.R., Orsi, N., Antonini, E., 1982. Antibacterial activity of matrix-bound ovotransferrin. Antimicrob Agents Chemother 21, 840–841. https://doi.org/10.1128/AAC.21.5.840

Valenti, P., De Stasio, A., Seganti, L., Mastromarino, P., Sinibaldi, L., Orsi, N., 1980. Capacity of staphylococci to grow in the presence of ovotransferrin or CrCl3 as a character of potential pathogenicity. J Clin Microbiol 11, 445–447.

Valenti, P., Stasio, A., Mastromerino, P., Seganti, L., Sinibaldi, L., Orsi, N., 1981. Influence of bicarbonate and citrate on the bacteriostatic action of ovotransferrin towards staphylococci. FEMS Microbiology Letters 10, 77–79. https://doi.org/10.1111/j.1574-6968.1981.tb06210.x

Velusamy, S.K., Ganeshnarayan, K., Markowitz, K., Schreiner, H., Furgang, D., Fine, D.H., Velliyagounder, K., 2013. Lactoferrin Knockout Mice Demonstrates Greater Susceptibility to Aggregatibacter actinomycetemcomitans–Induced Periodontal Disease. Journal of Periodontology 84, 1690–1701. https://doi.org/10.1902/jop.2013.120587

Volz, K., 2008. The functional duality of iron regulatory protein 1. Curr Opin Struct Biol 18, 106–111. https://doi.org/10.1016/j.sbi.2007.12.010

Vulpe, C.D., Kuo, Y.-M., Murphy, T.L., Cowley, L., Askwith, C., Libina, N., Gitschier, J., Anderson, G.J., 1999. Hephaestin, a ceruloplasmin homologue implicated in intestinal iron transport, is defective in the sla mouse. Nat Genet 21, 195–199. https://doi.org/10.1038/5979

Wang, D., Kim, B.Y., Lee, K.S., Yoon, H.J., Cui, Z., Lu, W., Jia, J.M., Kim, D.H., Sohn, H.D., Jin, B.R., 2009. Molecular characterization of iron binding proteins, transferrin and ferritin heavy chain subunit, from the bumblebee Bombus ignitus. Comparative

Biochemistry and Physiology Part B: Biochemistry and Molecular Biology 152, 20–27. https://doi.org/10.1016/j.cbpb.2008.09.082

Ward, P.P., Mendoza-Meneses, M., Cunningham, G.A., Conneely, O.M., 2003. Iron Status in Mice Carrying a Targeted Disruption of Lactoferrin. Mol Cell Biol 23, 178–185. https://doi.org/10.1128/MCB.23.1.178-185.2003

Ward, P.P., Zhou, X., Conneely, O.M., 1996. Cooperative interactions between the amino- and carboxyl-terminal lobes contribute to the unique iron-binding stability of lactoferrin. J. Biol. Chem. 271, 12790–12794. https://doi.org/10.1074/jbc.271.22.12790

Warner, R.C., Weber, I., 1953. The Metal Combining Properties of Conalbumin 1. J. Am. Chem. Soc. 75, 5094–5101. https://doi.org/10.1021/ja01116a056

Weiss, G., 2005. Modification of iron regulation by the inflammatory response. Best Practice & Research Clinical Haematology 18, 183–201. https://doi.org/10.1016/j.beha.2004.09.001

Wellman-Labadie, O., Picman, J., Hincke, M.T., 2008. Comparative antibacterial activity of avian egg white protein extracts. British Poultry Science 49, 125–132. https://doi.org/10.1080/00071660801938825

Wilkinson, N., Pantopoulos, K., 2014. The IRP/IRE system in vivo: insights from mouse models. Front. Pharmacol. 5. https://doi.org/10.3389/fphar.2014.00176

Williams, J., 1968. A comparison of glycopeptides from the ovotransferrin and serum transferrin of the hen. Biochemical Journal 108, 57–67. https://doi.org/10.1042/bj1080057

Winzerling, J., Pham, D., 2006. Iron metabolism in insect disease vectors: Mining the Anopheles gambiae translated protein database. Insect Biochemistry and Molecular Biology 36, 310–321. https://doi.org/10.1016/j.ibmb.2006.01.006

Winzerling, J.J., Nez, P., Porath, J., Law, J.H., 1995. Rapid and efficient isolation of transferrin and ferritin from Manduca sexta. Insect Biochemistry and Molecular Biology 25, 217–224. https://doi.org/10.1016/0965-1748(94)00058-P

Woodworth, R.C., Mason, A.B., Funk, W.D., MacGillivray, R.T.A., 1991. Expression and initial characterization of five site-directed mutants of the N-terminal half-molecule of human transferrin. Biochemistry 30, 10824–10829. https://doi.org/10.1021/bi00109a002

Xiao, G., Liu, Z.-H., Zhao, M., Wang, H.-L., Zhou, B., 2019. Transferrin 1 Functions in Iron Trafficking and Genetically Interacts with Ferritin in Drosophila melanogaster. Cell Rep 26, 748-758.e5. https://doi.org/10.1016/j.celrep.2018.12.053

Xiao, G., Wan, Z., Fan, Q., Tang, X., Zhou, B., 2014. The metal transporter ZIP13 supplies iron into the secretory pathway in Drosophila melanogaster. Elife 3, e03191. https://doi.org/10.7554/eLife.03191

Xie, H., Newberry, L., Clark, F.D., Huff, W.E., Huff, G.R., Balog, J.M., Rath, N.C., 2002. Changes in serum ovotransferrin levels in chickens with experimentally induced inflammation and diseases. Avian Dis 46, 122–131. https://doi.org/10.1637/0005-2086(2002)046[0122:CISOLI]2.0.CO;2

Xu, J., Wan, Z., Zhou, B., 2019. Drosophila ZIP13 is posttranslationally regulated by iron-mediated stabilization. Biochimica et Biophysica Acta (BBA) - Molecular Cell Research 1866, 1487–1497. https://doi.org/10.1016/j.bbamcr.2019.06.009

Yoshiga, T., Georgieva, T., Dunkov, B.C., Harizanova, N., Ralchev, K., Law, J.H., 1999. Drosophila melanogaster transferrin. Cloning, deduced protein sequence, expression during the life cycle, gene localization and up-regulation on bacterial infection. Eur J Biochem 260, 414–420. https://doi.org/10.1046/j.1432-1327.1999.00173.x

Yoshiga, T., Hernandez, V.P., Fallon, A.M., Law, J.H., 1997. Mosquito transferrin, an acute-phase protein that is up-regulated upon infection. Proc. Natl. Acad. Sci. U.S.A. 94, 12337–12342. https://doi.org/10.1073/pnas.94.23.12337

Zak, O., Aisen, P., Crawley, J.B., Joannou, C.L., Patel, K.J., Rafiq, M., Evans, R.W., 1995. Iron Release from Recombinant N-lobe and Mutants of Human Transferrin. Biochemistry 34, 14428–14434. https://doi.org/10.1021/bi00044a020

Zak, O., Ikuta, K., Aisen, P., 2002. The synergistic anion-binding sites of human transferrin: chemical and physiological effects of site-directed mutagenesis. Biochemistry 41, 7416–7423. https://doi.org/10.1021/bi0160258

Zarember, K.A., Sugui, J.A., Chang, Y.C., Kwon-Chung, K.J., Gallin, J.I., 2007. Human Polymorphonuclear Leukocytes Inhibit Aspergillus fumigatus Conidial Growth by Lactoferrin-Mediated Iron Depletion. J Immunol 178, 6367–6373. https://doi.org/10.4049/jimmunol.178.10.6367

Zhang, D., Albert, D.W., Kohlhepp, P., D.-Pham, D.Q., Winzerling, J.J., 2001a. Repression of Manduca sexta ferritin synthesis by IRP1/IRE interaction: IRP1 represses M. sexta ferritin translation. Insect Molecular Biology 10, 531–539. https://doi.org/10.1046/j.0962-1075.2001.00293.x

Zhang, D., Dimopoulos, G., Wolf, A., Miñana, B., Kafatos, F.C., Winzerling, J.J., 2002. Cloning and molecular characterization of two mosquito iron regulatory proteins. Insect Biochemistry and Molecular Biology 32, 579–589. https://doi.org/10.1016/S0965-1748(01)00138-2

Zhang, D., Ferris, C., Gailer, J., Kohlhepp, P., Winzerling, J.J., 2001b. Manduca sexta IRP1: molecular characterization and in vivo response to iron. Insect Biochemistry and Molecular Biology 32, 85–96. https://doi.org/10.1016/S0965-1748(01)00083-2

Zhang, J., Lu, A., Kong, L., Zhang, Q., Ling, E., 2014. Functional analysis of insect molting fluid proteins on the protection and regulation of ecdysis. J. Biol. Chem. 289, 35891–35906. https://doi.org/10.1074/jbc.M114.599597

Zhou, G., Velasquez, L.S., Geiser, D.L., Mayo, J.J., Winzerling, J.J., 2009. Differential regulation of transferrin 1 and 2 in Aedes aegypti. Insect Biochemistry and Molecular Biology 39, 234–244. https://doi.org/10.1016/j.ibmb.2008.12.004

Zhu, G., Jiang, Y., Yao, Y., Wu, N., Luo, J., Hu, M., Tu, Y., Xu, M., 2019. Ovotransferrin ameliorates the dysbiosis of immunomodulatory function and intestinal microbiota induced by cyclophosphamide. Food Funct. 10, 1109–1122. https://doi.org/10.1039/C8FO02312C

Zweier, J.L., Wooten, J.B., Cohen, J.S., 1981. Studies of anion binding by transferrin using carbon-13 nuclear magnetic resonance spectroscopy. Biochemistry 20, 3505–3510. https://doi.org/10.1021/bi00515a031

Chapter 2 - Iron binding and release properties of transferrin-1 from *Drosophila melanogaster* and *Manduca sexta*: implications for insect iron homeostasis[1]

Abstract

Transferrins belong to an ancient family of extracellular proteins. The best-characterized transferrins are mammalian proteins that function in iron sequestration or iron transport; they accomplish these functions by having a high-affinity Fe^{3+}-binding site in each of their two homologous lobes. Insect hemolymph transferrins (Tsf1s) also function in iron sequestration and transport; however, sequence-based predictions of their Fe^{3+}-binding residues have suggested that most Tsf1s have a single, lower-affinity Fe^{3+}-binding site. To reconcile the apparent contradiction between the known physiological functions and predicted biochemical properties of Tsf1s, we purified and characterized the iron-binding properties of Drosophila melanogaster Tsf1 (DmTsf1), Manduca sexta Tsf1 (MsTsf1), and the N-lobe of DmTsf1 ($DmTsf1_N$). Using UV-Vis spectroscopy, we found that these proteins bind Fe^{3+}, but they exhibit shifts in their spectra compared to mammalian transferrins. Through equilibrium dialysis experiments, we determined that DmTsf1 and MsTsf1 bind only one Fe^{3+}; their affinity for Fe^{3+} is high (log K' = 18), but less than that of the well-characterized mammalian transferrins (log K' ~ 20); and they release Fe^{3+} under moderately acidic conditions (pH_{50} = 5.5). Fe^{3+} release analysis of $DmTsf1_N$ suggested that Fe^{3+} binding in the N-lobe is stabilized by the C-lobe. Our findings will be critical for elucidating the mechanisms of Tsf1 function in iron sequestration and transport in insects.

[1] This chapter was published as follows: Weber, J.J., Kanost, M.R., Gorman, M.J., 2020. Iron binding and release properties of transferrin-1 from *Drosophila melanogaster* and *Manduca*

sexta: implications for insect iron homeostasis. *Insect Biochemistry and Molecular Biology* 125, 103438.

Key words: transferrin, insect, iron binding, iron homeostasis, insect immunity, hemolymph

Abbreviations: BdTsf1, Tsf1 from Blaberus discoidalis; cDNA; complementary DNA; CO32-, carbonate; DEAE, diethylaminoethyl; DmTsf1, Tsf1 from Drosophila melanogaster; DmTsf1N, recombinant amino-lobe of DmTsf1; HCO3-, bicarbonate; LfN, lactoferrin amino-lobe mutant; LMCT, ligand-to-metal charge transfer; MOI, multiplicity of infection; MsTsf1, Tsf1 from Manduca sexta; pH50, pH at 50% iron saturation; r, specific binding constant; Sf9, cell line from Spodoptera frugiperda; sTfN, serum transferrin amino-lobe mutant; Tsf1, insect transferrin-1; UV-Vis, ultraviolet-visible

Introduction

Iron in animals is a double-edged sword: it is essential to critical cellular processes, yet dangerous due to potential interactions that create reactive oxygen species (Kosman, 2010). Iron is also an important factor in the immune system, as it is often the sought-after prize between a host and invading pathogens (Barber and Elde, 2015). Therefore, animals have a set of proteins that are involved in regulation, storage, transport, and sequestration of iron. Members of the transferrin superfamily are involved in carrying out a number of these functions (Baker, 1994). These secreted proteins are typically 70-80 kDa and structurally comprise two homologous lobes, an amino- and carboxyl-lobe, connected by a short linker sequence. Many have a high affinity ferric (Fe^{3+}) ion binding site in each lobe, thus, these proteins can protect cells by keeping free iron levels extremely low in extracellular environments (Aisen et al., 1978; Baldwin

et al., 1984). The best-understood transferrins are those in mammals, including serum transferrin and lactoferrin. Serum transferrin binds and transports iron in the serum and delivers it into cells through a receptor-mediated endocytic pathway (Octave et al., 1983). Lactoferrin functions as an innate immune protein by sequestering iron in secreted fluids and blood (Farnaud and Evans, 2003; Jenssen and Hancock, 2009). A transferrin found in birds, ovotransferrin, has dual functions; it binds iron in the serum like serum transferrin and it sequesters iron in eggs like lactoferrin (Giansanti et al., 2012).

Crystal structures of serum transferrin, lactoferrin, and ovotransferrin have provided evidence for three common features of the Fe^{3+} binding sites: 1) four highly conserved amino acid ligands (an aspartate, a histidine and two tyrosines) whose side chains directly interact with the Fe^{3+} at the binding sites, 2) a synergistic anion cofactor, typically carbonate (CO_3^{2-}), and 3) two amino acid residues (threonine and arginine) that coordinate and hold the anion cofactor at the site (Anderson et al., 1989; Bailey et al., 1988; Kurokawa et al., 1995). A mutation of any of these six residues leads to accelerated release of iron, and mutations of the tyrosines can lead to a loss of iron binding (He et al., 1997b; Lambert et al., 2005; Mason and He, 2002; Mason et al., 2005; Ward et al., 1996).

The difference in physiological function between serum transferrin and lactoferrin is facilitated by a difference in iron binding ability at low pH. Serum transferrin binds to iron at neutral pH in serum, and, after it delivers iron into cells via endocytosis, the acidification of the endosome leads to release of iron over the pH range of 6.0 to 4.0 (Day et al., 1992). In contrast, lactoferrin retains iron unless the pH drops to 4.0 to 2.5 (Day et al., 1992). The difference in pH-mediated release comes from two factors: 1) in lactoferrin, cooperative interactions between the amino- and carboxyl-lobes help to stabilize the protein's iron binding sites, and 2) in serum

transferrin, two lysine residues in the amino-lobe form a hydrogen-bond, but, upon acidification in the endosome, the lysines are protonated, leading to a charge repulsion that opens the lobe and releases the iron (Baker and Lindley, 1992; Day et al., 1992; Jameson et al., 1998; MacGillivray et al., 1998; Peterson et al., 2000; Ward et al., 1996).

Compared with the well-studied vertebrate transferrins, little is known about the biochemical properties of insect transferrins. The focus of this study is insect transferrin-1 (Tsf1). Similar to serum transferrin, Tsf1 is found in high concentrations in hemolymph; and, similar to lactoferrin, it is found in many secreted fluids (Bonilla et al., 2015; Brummett et al., 2017; Geiser and Winzerling, 2012; Hattori et al., 2015; Qu et al., 2014; Simmons et al., 2013; Zhang et al., 2014). Tsf1 appears to have a non-essential role in iron transport (Huebers et al., 1988; Kurama et al., 1995; Xiao et al., 2019), and it also protects insects from infection and oxidative stress by sequestering iron (Brummett et al., 2017; Geiser and Winzerling, 2012; Kim et al., 2008; Lee et al., 2006; Yoshiga et al., 1997). A puzzling aspect of Tsf1 comes from bioinformatic analyses. All Tsf1 amino-lobes have a predicted substitution, relative to the well-studied vertebrate transferrins, of at least one of the four iron-binding residues; moreover, carboxyl-lobe substitutions in many Tsf1 sequences indicate that those lobes do not bind iron (Geiser and Winzerling, 2012; Lambert et al., 2005). These observations suggest that most Tsf1s have a single lower-affinity iron binding site, but this prediction seems to be at odds with the known physiological functions of Tsf1s, which are all thought to involve high affinity iron binding.

Previous biochemical analyses of Tsf1 have not addressed this apparent contradiction between predicted biochemical properties and known biological functions. To date, biochemical analyses of Tsf1s have been limited to Tsf1 from the cockroach *Blaberus discoidalis* (BdTsf1)

and Tsf1 from the moth *Manduca sexta* (MsTsf1). BdTsf1 has spectral and pH-mediated release properties that are similar to those of serum transferrin, but its affinity for iron is unknown (Gasdaska et al., 1996). It is not a very representative Tsf1 because, unlike most Tsf1s, it has residues for iron binding in both the amino- and carboxyl-lobes (Gasdaska et al., 1996; Lambert, 2012; Lambert et al., 2005). MsTsf1, which has a more representative sequence, also has spectral properties similar to those of the mammalian transferrins, but it binds only one ferric ion with unknown affinity (Bartfeld and Law, 1990; Huebers et al., 1988). No analyses of Tsf1 structure have been reported.

The goals of this study were to evaluate the iron binding and release properties of Tsf1s and to assess the functional role of a non-iron binding carboxyl-lobe. After evaluating the putative iron binding residues of 98 Tsf1 sequences, we decided to focus our biochemical studies on two representative Tsf1s: *Drosophila melanogaster* Tsf1 (DmTsf1) and MsTsf1. By using spectroscopic characterization and equilibrium dialysis, we analyzed the iron binding and release properties of purified DmTsf1 and MsTsf1, and the amino-lobe of DmTsf1 ($DmTsf1_N$). We found that DmTsf1 and MsTsf1 have one metal binding site and a high affinity for Fe^{3+}, and that they released their iron in a pH-mediated manner that is comparable to serum transferrin's release of iron in the endosome. We also found that $DmTsf1_N$ coordinates and releases iron differently than the full-length DmTsf1, indicating that the carboxyl-lobe influences iron binding in the amino-lobe. This work furthers our understanding of the underlying mechanisms of iron homeostasis in insects.

Materials and Methods

Sequence alignment for binding residue determination

Serum transferrin, lactoferrin, ovotransferrin and Tsf1 sequences were collected through the UniProt data base (UniProt Consortium, 2019). Redundant or partial sequences were removed. The orthology of the putative Tsf1 sequences was verified by phylogenetic analysis (not shown). A sequence alignment was created with Clustal Omega using the EMBL-EBI server (Madeira et al., 2019) and can be found in Appendix A. Information (including order, species, and accession number) about each sequence used in the alignment is listed in supplementary Table 2-3.

Recombinant baculovirus production

A full length DmTsf1 cDNA (LP08340) was obtained from the Drosophila Genomics Resource Center. For full-length DmTsf1 expression, the cDNA was amplified by PCR with the use of forward (5'-GGATCCATGATGTCGCCGCAT-3') and reverse (5'-GCGGCCGCTCACT GCTTGGCAATC-3') primers, digested with *Bam*HI and *Not*I, and inserted into the pOET3 transfer plasmid. The flashBAC Gold system (Oxford Expression Technologies) was used to generate a recombinant baculovirus. For the $DmTsf1_N$ mutant, the amino-lobe amino acid sequence was predicted by analyzing alignments with structurally known transferrins using Clustal Omega at the EMBL-EBI server (Madeira et al., 2019). We used forward (5'-GTTGTTGGATCCATGAT GTCGCCGCAT-3') and reverse (5'-GAGCGTGATGGCAGTTGAGCGGCCGCGTTGTTT-3') primers to amplify the $DmTsf1_N$ cDNA, which encodes amino acid residues 1-379 followed by a stop codon, and then generated a recombinant baculovirus with the procedure we used for full-length DmTsf1.

Protein expression and purification

For DmTsf1 and DmTsf1$_N$, recombinant baculovirus was used to infect ~3 liters of Sf9 cells (at 2 x 10^6 cells/ml in Sf900III serum free medium) using an MOI of 1. After 48 h, cells were separated from the culture medium by centrifugation at 500 × g. Ammonium sulfate was added to the culture medium to 100% saturation, and protein precipitation was allowed to occur at 4°C for two days. The floating precipitate was collected with a pipet and dialyzed three times against 20 mM Tris, pH 8.3 (4°C). The dialyzed sample was applied to a Q-Sepharose Fast Flow column (1.5 x 10 cm), and proteins were eluted with a linear gradient of 0-1 M NaCl in 20 mM Tris, pH 8.4 (4°C). Fractions containing transferrin were pooled and concentrated with Amicon Ultracel centrifugal filters with a 30 kDa molecular weight cut-off and then applied to a HiLoad 16/60 Superdex 200 column (GE Healthcare) equilibrated in 20 mM Tris, 150 mM NaCl, pH 7.4. DmTsf1$_N$ required an extra purification step. After the Superdex 200 column, fractions containing DmTsf1$_N$ were pooled and concentrated as described above. The sample was applied to an UnoQ column (Bio-Rad), and proteins were eluted using a linear gradient of 10-500 mM NaCl in 20 mM Tris, pH 8.3. Following this method, 35.0 mg of DmTsf1 was purified from 3.2 liters of infected cells, and 22.3 mg of DmTsf1$_N$ was purified from 3.0 liters of infected cells.

MsTsf1 was purified from hemolymph following a procedure previously described (Brummett et al., 2017) with minor modifications. Briefly, 96 larvae were reared to day two of the fifth instar larval stage. From the larvae, 120 mL of hemolymph was collected at 4˚C into saturated ammonium sulfate and adjusted to a final saturation of 55%. The solution was stirred for 30 minutes to allow proteins to precipitate, followed by centrifugation at 12000 × g to remove precipitants. The remaining supernatant was dialyzed three times against 4 liters of 20 mM Tris, pH 8.3 (4˚C). The sample was loaded onto a DEAE Sephacel column (2.5 x 22 cm),

and proteins were eluted with a linear gradient of 0-120 mM NaCl in 20 mM Tris, pH 8.3 (4˚C). Fractions were analyzed by western blot, pooled and concentrated with Amicon Ultracel centrifugal filters with a 30 kDa molecular weight cut-off. The concentrated sample was divided into two parts (~ 4 mL each), and each was applied to a HiLoad 16/60 Superdex 200 column (GE Healthcare) equilibrated in 20 mM Tris, 150 mM NaCl, pH 7.4. Fractions containing transferrin were pooled and concentrated, and the buffer was adjusted to 0.5 M NaCl. The sample was applied to a series of two 1 mL HiTrap ConA 4B columns (GE Healthcare), and bound proteins were eluted with buffer containing 20 mM Tris, 0.5 M NaCl, 1 mM MnCl2, 1 mM CaCl2, 0.5 M methyl-α-D-mannopyranoside, pH 7.4. Fractions containing transferrin were pooled, concentrated and dialyzed against 20 mM Tris, 10 mM NaCl, pH 8.3. The sample was applied to an UnoQ column (Bio-Rad), and proteins were eluted using a linear gradient of 10-500 mM NaCl in 20 mM Tris, pH 8.3. Following this method, 9.2 mg of MsTsf1 was purified from 120 mL of hemolymph.

Production of the apo- and holo-forms of MsTsf1, DmTsf1 and DmTsf1$_N$

It was previously reported that after purification of MsTsf1 the protein was already iron saturated (Brummett et al., 2017). To ensure this was true of the purified Tsf1s used for this study, an absorbance spectrum (from 250-700 nm) of each Tsf1 at ~ 5 mg/mL in 10 mM HEPES, 20 mM sodium bicarbonate, pH 7.4, was measured, then 0.1 molar equivalent of ferric-nitrilotriacetic acid was added and allowed to equilibrate for 5-10 minutes, and finally a spectrum was collected. We concluded that each Tsf1 sample was saturated after purification because their absorbance spectra (specifically the LMCT peak) did not change (data not shown).

The apo-form of the purified Tsf1s was made as previously described (Brummett et al., 2017) by dialyzing purified protein samples against two exchanges of 1 liter of 0.1 M sodium acetate, 10 mM EDTA, pH 5, and then removing the EDTA by dialysis against two exchanges of 1 liter of 10 mM HEPES, pH 7.4. The Tsf1 samples changed from a yellowish-orange color in their holo-form to colorless in their apo-form.

Equilibrium dialysis

Experimental conditions were adapted from previous studies on transferrins using equilibrium dialysis to measure Fe^{3+} affinity (Aisen et al., 1978; Tinoco et al., 2008). Measurements were made using microdialyzers composed of two cells separated by a 5 kDa molecular weight cut-off membrane (Nest Group Company). Apo-Tsf1s produced as described in the previous section were used. Dialysis buffer was composed of 1.5 mM citrate, 0.1 M sodium nitrate, 10 mM HEPES and 20 mM sodium bicarbonate, pH 7.4. Citrate keeps the Fe^{3+} from precipitating and does not compete with carbonate anion at the binding site of the proteins (Aisen et al., 1978). Sodium nitrate was added to the dialysis buffer so that we could use previously calculated equilibrium constants for ferric-citrate complexes (Spiro et al., 1967; Warner and Weber, 1953). Known concentrations of either apo-DmTsf1 or apo-MsTsf1 in dialysis buffer were added to one cell of the dialyzer, while various concentrations of Fe^{3+}-citrate were added to both cells. Refer to supplementary Tables 2-4 and 2-5 for details on concentrations of apo-Tsf1 and Fe^{3+}-citrate used in each experiment and Figure 2-6 for a diagram of equilibrium dialysis experimental setup. Experiments were carried out at 25 ± 1˚C, with gentle agitation over 2 days. Knowing the amount of apo-Tsf1, citrate and Fe^{3+} added allowed for the measurement of non-transferrin bound iron after dialysis via the FerroZine assay (see the proceeding section) and

the determination of the concentration Tsf1 bound iron, specific binding factor (r) and affinity constants.

Ferrozine-based assay

In order to measure the amount of non-transferrin bound iron after equilibrium dialysis, we used a Ferrozine-based assay (Stookey, 1970.). Ferrozine was added to $FeCl_3$ standards and samples, and the solutions were acidified and incubated at 25 ± 1˚C with mild agitation for 18 hours to increase sensitivity (Jeitner, 2014). The amount of iron-Ferrozine complex was measured at 562 nm for each standard and sample. Standards were made in duplicates, and the resultant standard curve was used to determine the concentration of non-transferrin bound iron in solution from the equilibrium dialysis experiments.

Binding equations

Equations used for past studies of human transferrin's affinity for iron in a competitive environment with citrate (Aasa et al., 1963; Aisen et al., 1978) were modified to account for the single iron binding site of DmTsf1 and MsTsf1. Equation 1 (see below) is the overall reaction of free iron ($[Fe^{3+}]_{free}$), protein ([Tsf1]), the bicarbonate anion ($[HCO_3^-]$), their complex formation ($[Fe^{3+} \cdot Tsf1 \cdot CO_3^{2-}]$) along with the release of three protons at pH 7.4:

Equation 1) $$Fe^{3+} + Tsf1 + HCO_3^- \rightleftharpoons (Fe^{3+} \cdot Tsf1 \cdot CO_3^{2-}) + 3H^+$$

$$K = \frac{[Fe^{3+} \cdot Tsf1 \cdot CO_3^{2-}][H^+]^3}{[Fe^{3+}]_{free}\,[Tsf1][HCO_3^-]}$$

The complex $[Fe^{3+} \cdot Tsf1 \cdot CO_3^{2-}]$ in this situation is equal to the concentration of Tsf1 bound iron ($[Fe^{3+}]_{Tsf\ bound}$) calculated from an equilibrium dialysis experiment ($[Fe^{3+}]_{Tsf\ bound}$ values are found in supplementary Tables 2-4 and 2-5). Because Fe^{3+} in this situation is chelated by citrate,

the four known equilibrium equations for Fe^{3+}-citrate complexes were used to determine $[Fe^{3+}]_{free}$ (Spiro et al., 1967; Warner and Weber, 1953) and are as follows:

(Equation 2a) $HCit(OH)^{2-} + Fe^{3+} \rightleftharpoons FeCitO^{-} + 2H^{+}$

$$K_{c1} = \frac{[FeCitO^{-}][H^{+}]^2}{[Fe^{3+}]\,[HCit(OH)^{2-}]}$$

(Equation 2b) $Cit(OH)^{3-} + Fe^{3+} \rightleftharpoons FeCitO^{-} + H^{+}$

$$K_{c2} = \frac{[FeCitO^{-}][H^{+}]}{[Fe^{3+}]\,[Cit(OH)^{3-}]}$$

(Equation 2c) $HCit(OH)^{2-} \rightleftharpoons Cit(OH)^{3-} + H^{+}$

$$K_{c3} = \frac{[Cit(OH)^{3-}][H^{+}]}{[HCit(OH)^{2-}]}$$

(Equation 2d) $FeCitO^{-} + Cit(OH)^{3-} \rightleftharpoons Fe(CitO)_2^{5-} + H^{+}$

$$K_{c4} = \frac{[Fe(CitO)_2^{5-}][H^{+}]}{[FeCitO^{-}]\,[Cit(OH)^{3-}]}$$

Adhering to past procedures (Aisen et al., 1978), we used the following values for the Fe^{3+}-citrate equilibrium constants: log K_{c1} = 3.64; log K_{c2} = 9.46; log K_{c3} = -5.82; log K_{c4} = -6.17. Taken together with the known concentrations of citrate ($[Cit]_{add}$) and Fe^{3+} ($[Fe^{3+}]_{add}$) added to the equilibrium dialysis experiment, these equations provided us with enough information to determine citrate's effect on the concentration of $[Fe^{3+}]_{free}$ by Equation 3:

(Equation 3) $$[Fe^{3+}]_{free} = \frac{(C_{eq})\left(([H^{+}]^2)(K_{c2}) + ([H^{+}])(K_{c1}) + (C_{eq})(K_{c1})(K_{c4})\right)}{(K_{c1})(K_{c2})([Cit]_{add} - [Fe^{3+}]_{add})}$$

where $$C_{eq} = \frac{-y + (y^2 - 4xz)^{1/2}}{2x}$$

and $x = (K_{c3})(K_{c4})$

$$y = ([H^+])(K_{c3}) + [H^+]^2 + ([Cit]_{add})(K_{c3})(K_{c4}) - (2)([Fe^{3+}]_{add})(K_{c3})(K_{c4})$$

$$z = -(([Fe^{3+}]_{add})([H^+])(K_{c3}) + ([Fe^{3+}]_{add})([H^+]^2))$$

Because the reactions took place at a constant pH and [HCO_3^-], the overall affinity constant (*K*) can be corrected to give an effective affinity constant (*K'*) using Equation 4 (Aasa et al., 1963; Aisen et al., 1978):

(Equation 4) $$K' = (\frac{[HCO_3^-]}{[H^+]^3})(K)$$

Using these equations and the equilibrium dialysis results in supplementary Tables 2-4 and 2-5, the average *K*' (M^{-1}) was calculated and is reported as log *K*' for DmTsf1 and MsTsf1 in Table 2. An example calculation using these equations can be found in supplementary Table 2-6.

Ultraviolet-visible spectroscopy

To characterize and analyze the LMCT λ_{max} caused by iron binding to serum transferrin, MsTsf1, DmTsf1 and $DmTsf1_N$, we followed previous procedures for generating difference spectra for transferrins complexed with metals (Gasdaska et al., 1996; Harris and Pecoraro, 1983). Apo-Tsf1s were prepared as described above in buffer containing 100 mM HEPES and 15 mM sodium bicarbonate at pH 7.4. Human apo-serum transferrin was purchased from Sigma and prepared in the same buffer. Apo-transferrin solutions at ~4 mg/mL were added to both a sample and reference well. Sufficient ferric-nitrilotriacetate was added to the sample to saturate iron binding, and an equal volume of buffer was added to the reference well. Nitrilotriacetate is both an Fe^{3+} chelator and can act as the synergistic anion bound to transferrins (Aisen et al., 1978). When it is bound to transferrin at the anion binding site, it can cause shifts in the LMCT λ_{max} compared to the carbonate—which is the typical anion in physiological conditions (He et al., 2000b). To avoid this artifact and to get a true comparison of LMCT peaks, the sodium

bicarbonate concentration in the buffer was kept significantly higher than that of nitrilotriacetate. UV-Vis spectra from 280 to 900 nm were obtained, and saturation of the iron binding site was signified by no change in the LMCT λ_{max} for each transferrin. The difference spectrum for each transferrin was determined by subtracting the absorbance spectrum of the reference from the absorbance spectrum of the sample.

pH mediated iron release assay

Previous methods for iron release from transferrins as a function of pH were followed (Baker et al., 2003; Day et al., 1992; Nicholson et al., 1997). Human holo-lactoferrin was purchased from Sigma, and human holo-serum transferrin was made as previously described (see material and methods section: Production of the apo- and holo-forms of MsTsf1, DmTsf1 and DmTsf1$_N$). The iron-saturated transferrin samples (~ 5 mg/mL) were extensively dialyzed for 24 to 48 hours against various buffers over the pH range of 2.0 to 8.0. The buffers used were as follows: 50 mM HEPES, 50 mM MES, 50 mM sodium acetate and 100 mM glycine-HCl. The Tsf1s were not dialyzed below a pH of 4 because they precipitated at low pH. The ratio of the absorbance of the LMCT λ_{max} for each sample before and after dialysis gave the percent saturation at each pH unit. The data was plotted and fit with a sigmoidal dose response curve using GraphPad Prism Software.

Results

Conservation of iron binding residues in Tsf1s

Insect Tsf1s' iron binding residues have been previously predicted based on alignments with serum transferrins and lactoferrins (Baker, 1994; Geiser and Winzerling, 2012; Lambert et

al., 2005). To enable us to choose representative Tsf1s for our study, we wanted a more comprehensive list of the substitutions in Tsf1s from many different orders of insects. By using a sequence alignment of 98 insect Tsf1s, two lactoferrins, two serum transferrins and two ovotransferrins, we were able to gather a comprehensive collection of the predicted residues involved in iron binding (Table 2-1). (Note that the numbering of iron-coordinating residues in Table 2-1 and in the rest of this paper are based on the position in the human serum transferrin sequence.)

Table 2-1. Tsf1 residues predicted to be involved in iron and anion binding.

	Amino-lobe						**Carboxyl-lobe**					
	Iron				**Anion**		**Iron**				**Anion**	
	D[a]	Y	Y	H	T	R	D	Y	Y	H	T	R
	63[b]	95	188	249	120	124	392	426	517	585	452	456
Blattodea												
(5[c])	+[d]	+	+	Q	+	+	+	+	+	+	+	+
Coleoptera												
(3)	+	+	+	Q	+	+	+	+	+	+	+	+
(2)	+	+	+	Q	+	+						
Diptera												
(21)	+	+	+	Q	+	+						
(13)	E	+	+	S	+	+						
(12)	E	+	+	T	+	+						
(1)	+	+	+	P	+	+						
(1)	E	+	+	M	+	+						
Hemiptera												
(5)	+	+	+	Q	+	+						
(4)	E	+	+	P	+	+						
Hymenoptera												
(16)	+	+	+	Q	+	+						
(1)	+	+	+	Q	+	L						
Lepidoptera												
(13)	+	+	+	Q	+	+						
Orthoptera												
(1)	+	+	+	Q	+	+	+	+	+	+	+	+

[a]Consensus iron and anion binding residues of serum transferrin, lactoferrin and ovotransferrin sequences are shown.

[b]Position numbers are based on human serum transferrin.

[c]The number in parentheses is the number of species within an order to have the particular sequence shown. Species and accession numbers are listed in supplementary Table 2-3.

[d]Plus signs indicate conservation of consensus residues; empty spaces indicate a lack of conservation.

Several consistencies in the alignments are worth describing. First, in the amino-lobe of Tsf1s, the iron-coordinating tyrosines (Tyr-95 and Tyr-188) are conserved in all 98 insects. Site-directed mutagenesis studies of these tyrosines in lactoferrin have shown that each is vital to the stability of the binding site (Ward et al., 1996). Also, in the Tsf1 amino-lobes, 97 out of the 98 sequences show conservation of the anion coordinating residues, Thr-120 and Arg-124. The anion and the residues that coordinate it are crucial to iron binding (Zak et al., 2002). Conservation of the two tyrosines and the two anion residues suggest that Tsf1s bind iron in their amino-lobe. Another consistent result is that none of the 98 Tsf1 amino-lobe sequences have the His-249. There are five different residues that are present in this position: Gln (68), Ser (13), Thr (12), Pro (5) and Met (1). (The number in parenthesis indicates the number of times it was found.) Previous studies have probed the importance of the His-249 residue in serum transferrin's and lactoferrin's iron binding and release properties (Grady et al., 1995; He et al., 2000a; He et al., 2000b; MacGillivray et al., 2000; Mason and He, 2002; Nicholson et al., 1997). All of the His-249 mutants could bind iron, but most of them more readily released iron in response to a decrease in pH.

Less consistently seen in the alignments is the substitution of Asp-63 with glutamate, which occurs in 30 of the 98 Tsf1 sequences. The D63E change, which extends this iron coordinating sidechain by one methyl group, has been studied by site-directed mutagenesis in the human serum transferrin amino-lobe (Baker et al., 2003; He et al., 1997a; He et al., 1997c). The D63E mutant had similar iron coordinating characteristics as the wild type amino-lobe, but it more readily released its iron in the presence of a chelator, and it released iron at a higher pH.

Only nine Tsf1s show conservation of iron-binding residues in their carboxyl-lobe. One of these, BdTsf1, has been analyzed biochemically and was found to bind two equivalents of iron and to release iron in a similar pH-mediated manner as serum transferrin (Gasdaska et al., 1996).

From the data provided in Table 2-1, we decided to study the binding properties of MsTsf1, because it would give insight into the effect of the common H249Q substitution, and DmTsf1 because it would provide insight into the combined effect of D63E and H249S substitutions.

Production of MsTsf1, DmTsf1, and DmTsf1$_N$

In order to analyze the biochemical properties of MsTsf1, DmTsf1, and DmTsf1$_N$, we needed to obtain pure forms of each protein. MsTsf1was purified from *M. sexta* larval hemolymph as previously described (Brummett et al., 2017) through a number of steps: ammonium sulfate precipitation, anion exchange chromatography, gel filtration and high resolution ion exchange chromatography. From 96 larvae, 120 ml of hemolymph was collected, and 9.2 mg of MsTsf1 (~ 67 kDa) was purified (Figure 2-1 A). Recombinant full length DmTsf1 and DmTsf1$_N$ (residues 1-379) were expressed in an insect cell line using a baculovirus expression system. We used similar purification steps for these proteins: ammonium sulfate precipitation, anion exchange chromatography and gel filtration. DmTsf1$_N$ required an extra high resolution ion exchange chromatography step at the end of the process. From 3.2 liters of infected cells, 35.0 mg of DmTsf1 (~ 66 kDa) was purified, and from 3.0 liters of infected cells, 22.3 mg of DmTsf1$_N$ (~ 39.5 kDa) was purified (Figure 2-1 A).

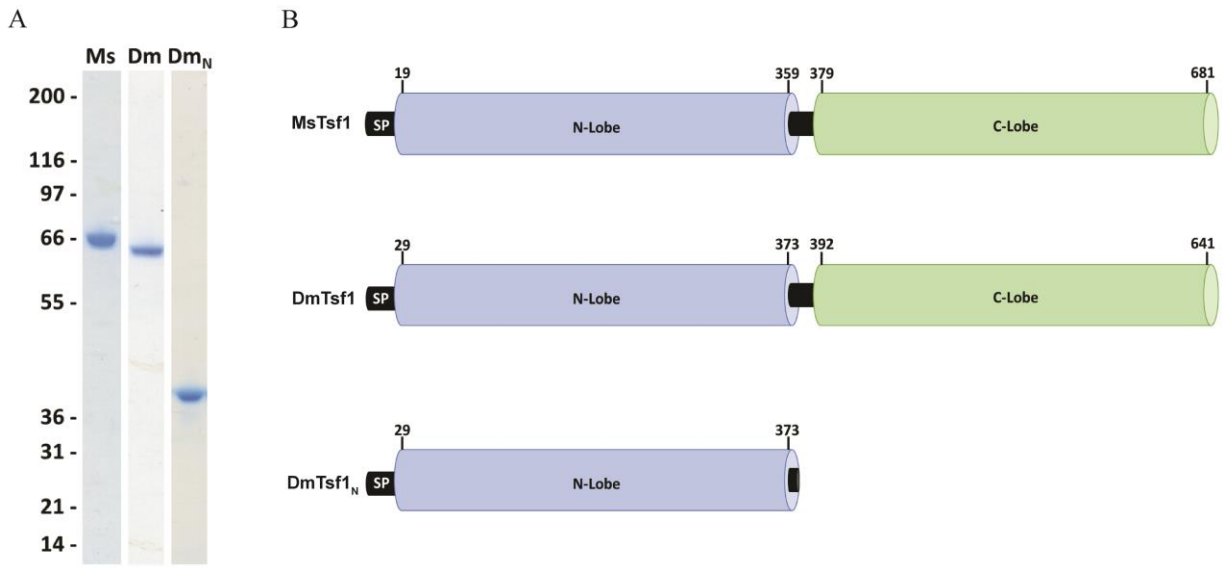

Figure 2-1. Analysis and domain architecture of purified Tsf1s.
(A) Tsf1 purified from the *M. sexta* larval hemolymph (Ms) and recombinantly expressed and purified *D. melanogaster* full-length (Dm) and amino-terminal lobe of Tsf1 (DmN) were analyzed by reducing SDS-PAGE followed by Coomassie staining. The positions of molecular mass standards are shown on the left and were used to estimate the size of the proteins. (B) The domain architecture of the purified Tsf1s based on alignment information. Represented here by their position in the amino acid sequence is the signal peptide (SP), the amino-lobe (N-lobe) colored in blue and carboxyl-lobe (C-lobe) in green.

DmTsf1 and MsTsf1 spectroscopic characterization for the binding of Fe^{3+}

Holo-serum transferrin and holo-lactoferrin have a red-orange color that results from a ligand-to-metal charge transfer (LMCT) band caused by the excitation of a pi orbital electron, believed to be from the phenol group of one tyrosine ligand, into a dpi* orbital of the iron (Baker, 1994; Patch and Carrano, 1981). It was evident after purification of DmTsf1 and MsTsf1 that they bind iron, because the concentrated protein solutions had a yellow-orange color. After removal of the iron by dialysis of the proteins in buffer at pH 5 in the presence of the iron

chelator EDTA, the color of the apo-protein solutions was clear. This visible characteristic of holo-Tsf1 is similar to that of holo-serum transferrin and holo-lactoferrin but less red.

In diferric serum transferrin and lactoferrin the LMCT band typically gives a pronounced λ_{max} of ~470 nm, but the peak can shift if the binding site is altered by substitution of the iron coordinating residues or a loss of one of the lobes (Day et al., 1992; He et al., 2000b; Nicholson et al., 1997; Peterson et al., 2000). The binding of metals at the site also perturbs pi-pi* transitions in the phenolic ring of the ligating tyrosines. This gives rise to characteristic absorption peaks in the UV region at ~295 and ~245 nm (Baker, 1994). The UV-Vis spectra for iron-bound DmTsf1 and MsTsf1 shows the characteristic absorption peaks in the UV region at ~ 295 nm (supplementary Figure 2-5). Thus, it is likely that the two iron coordinating tyrosine residues are conserved in the amino-lobe, as suggested by the alignment data in Table 2-1. However, the λ_{max} of the LMCT band in the visible region for both proteins is blue-shifted considerably from the 470 nm we observe for serum transferrin and lactoferrin (Figure 2-2). The λ_{max} is ~434 nm for DmTsf1 and ~420 nm for MsTsf1 (Table 2-2). We expected to see shifts in the LMCT bands because of the substitutions of D63E and H249S in DmTsf1 and H249Q in MsTsf1. These shifts of the LCMT band resemble those of His-249 and Asp-63 amino-lobe mutants of lactoferrin and serum transferrin, which exhibited blue-shifts in the range of 6 to 30 nm (He et al., 1997c; Nicholson et al., 1997). Like the alignment data, these results suggest that these Tsf1s coordinate iron binding differently than serum transferrin and lactoferrin.

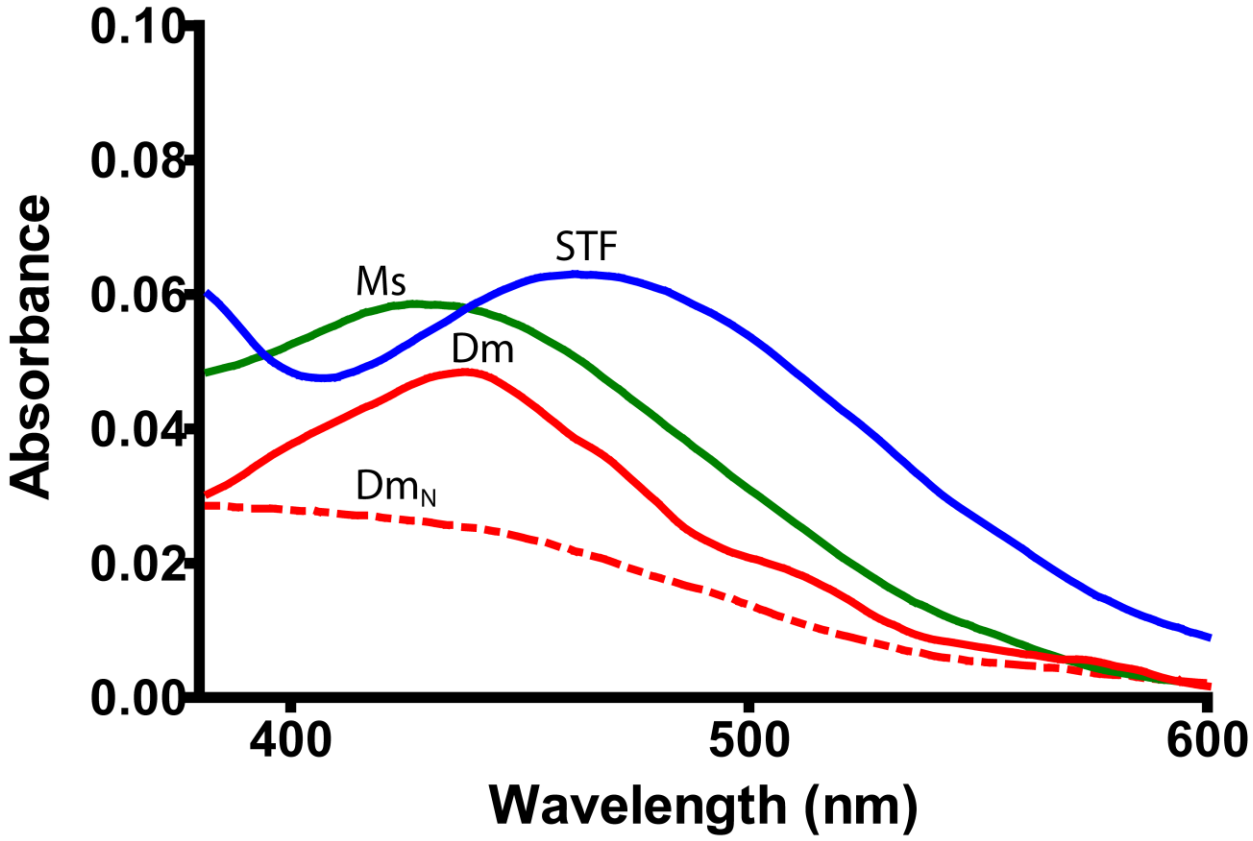

Figure 2-2. Visible difference spectra of the LMCT peak for the Fe^{3+}-transferrin complexes.

Serum transferrin (STF) is indicated by a blue line, MsTsf1 (Ms) by a green line, DmTsf1 (Dm) by a solid red line, and $DmTsf1_N$ (Dm_N) by a dashed red line. Proteins were at a concentration of approximately 4 mg/ml. The absorbance spectrum from the reference well containing the apo-protein was subtracted from the sample well containing fully iron-saturated holo-protein at the same concentration. A more complete spectrum showing the large 295 nm peak of each transferrin can be seen in supplementary Figure 2-5.

In the case of $DmTsf1_N$, the λ_{max} was shifted even further, to ~408 nm, and is more of a shoulder of the large 295 nm peak. This result demonstrates that the amino-lobe can bind iron without the presence of the carboxyl-lobe. However, binding in the amino-lobe is different from that of the full-length DmTsf1, suggesting altered iron coordination and the possibility of

decreased stability of iron binding—similar to other transferrin amino-lobe mutants (Day et al., 1992; Tinoco et al., 2008).

Fe^{3+} affinity of DmTsf1 and MsTsf1

With the putative substitutions at the iron binding site in both DmTsf1 and MsTsf1, we questioned if these proteins have a strong affinity for Fe^{3+}. We also wanted to quantitatively test whether they bind only one Fe^{3+} ion. We employed an equilibrium dialysis technique to measure the affinity of DmTsf1 and MsTsf1 for Fe^{3+} in the presence of citrate and HCO_3^- at 25±1˚C at pH 7.4. The specific binding (r) values derived from binding isotherms (Figure 2-3) show iron saturation of the Tsf1s occurring at an r_{max} of 1.11 for DmTsf1 and an r_{max} of 1.08 for MsTsf1 (Table 2-2). These results support the hypothesis, based on our alignment data, that many Tsf1s have only one Fe^{3+} binding site, and are consistent with the observation that iron makes up 0.05% of the weight of holo-MsTsf1 (Huebers, et al., 1988). These results, combined with the spectral evidence that $DmTsf1_N$ binds iron, demonstrate that binding occurs in the amino-lobe only. Moreover, these results quantitatively support our use of a single binding site model in determining affinity constants.

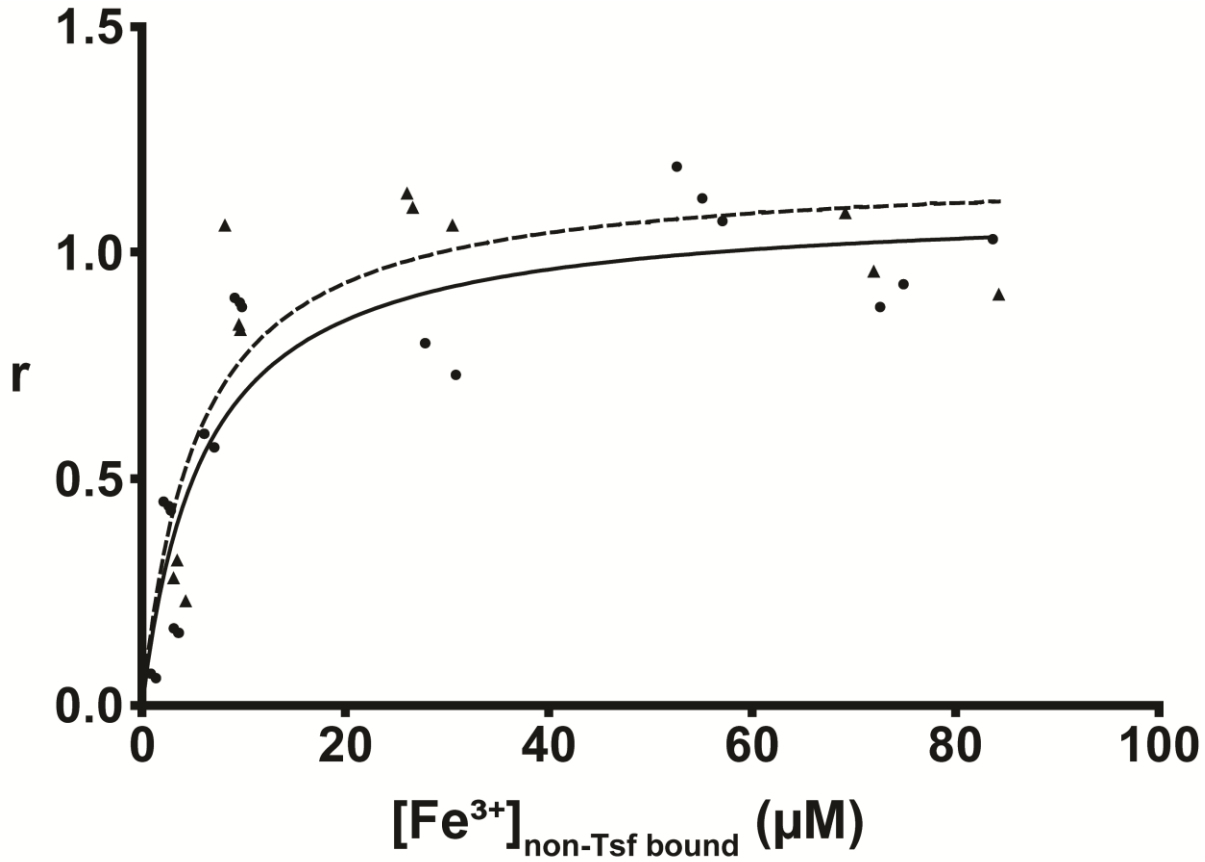

Figure 2-3. Binding isotherms of DmTsf1 and MsTsf1.

The DmTsf1 results are represented by dots and a solid line and MsTsf1 results by triangles and a dashed line. After equilibrium was reached in each experiment, the contents of the dialyzer were analyzed for the amount non-transferrin bound iron ($[Fe^{3+}]_{non\text{-}Tsf\ bound}$) using a ferrozine-based assay. From this assay the specific binding factor (r) for each experiment was determined by calculating the ratio of the concentration of transferrin bound iron ($[Fe^{3+}]_{Tsf\ bound}$) to the total Tsf1 concentration added [Tsf1] in the dialyzer. The r value at which saturation has occurred indicates the number of binding sites. Curve fitting and analysis of the r_{max} values (reported in Table 2-2) was performed using GraphPad Prism Software.

We used our equilibrium dialysis data (supplementary Tables 2-4 and 2-5) and binding equations (see Materials and Methods section) to calculate the Fe^{3+} affinity of DmTsf1 and MsTsf1. The known binding constants of Fe^{3+}-citrate complexes (Equation 2a-c) (Spiro et al.,

1967; Warner and Weber, 1953) were used to calculate the effective concentration of free Fe^{3+} in Equation 3. Under the assumption that three protons are being released from a single binding site upon binding of Fe^{3+} (Aisen et al., 1978; Tinoco et al., 2008), we calculated overall equilibrium constants (K) of the Fe^{3+}-Tsf1 complexes at pH 7.4 using Equation 1. Using Equation 4, the *K* values were then corrected for an environment with constant pH and HCO_3^- to get the effective dissociation constant (*K*') (an example calculation is provided in supplementary Table 2-6). The average log *K*' for DmTsf1 was 18.2, and the average log *K*' for MsTsf1 was 18.4. These values are less than those of human serum transferrin (amino-lobe log *K*' of 20.7 and carboxyl-lobe log *K*' of 19.4) under similar conditions (Aisen et al., 1978), although they indicate that both Tsf1s have a very high affinity for Fe^{3+} despite iron binding site substitutions.

pH-mediated iron release from DmTsf1, DmTsf1$_N$ and MsTsf1

Iron retention as a function of pH is a major difference between lactoferrin and serum transferrin, and this difference is important to their function in either immunity, in the case of lactoferrin, or iron transport, in the case of serum transferrin (Baker, 1994; Day et al., 1992). A previous study demonstrated that BdTsf1 releases iron in a manner similar to that of serum transferrin in response to lowered pH (Gasdaska et al., 1996). We decided to examine the iron release profiles of the more representative DmTsf1 and MsTsf1 to provide more information about possible mechanisms of Tsf1 function in immunity and iron transport. We also tested DmTsf1$_N$'s iron release properties, for insight into the possible role of the non-iron binding carboxyl-lobe in stabilizing iron coordination. Iron-saturated Tsf1 was dialyzed against buffers with a pH range of 2.0-8.0, and then percent iron-saturation was measured. Dialysis results indicate that both MsTsf1 and DmTsf1 behave similarly to serum transferrin, with an estimated

pH_{50} of 5.5 for both proteins (Figure 2-4, Table 2-2). Nearly identical to the pH release profile of serum transferrin (Day et al., 1992), DmTsf1 starts to release its iron at pH 6.25, while MsTsf1 does not start release until pH 5.75. Interestingly, neither Tsf1 is as stable as serum transferrin or lactoferrin at a pH of less than 4, which causes DmTsf1 and MsTsf1 to precipitate. In contrast to the full length Tsf1, $DmTsf1_N$ begins to release iron at ~pH 7 and has a pH_{50} of 6.0, indicating that iron release in the amino-lobe is affected by the presence of the carboxyl-lobe.

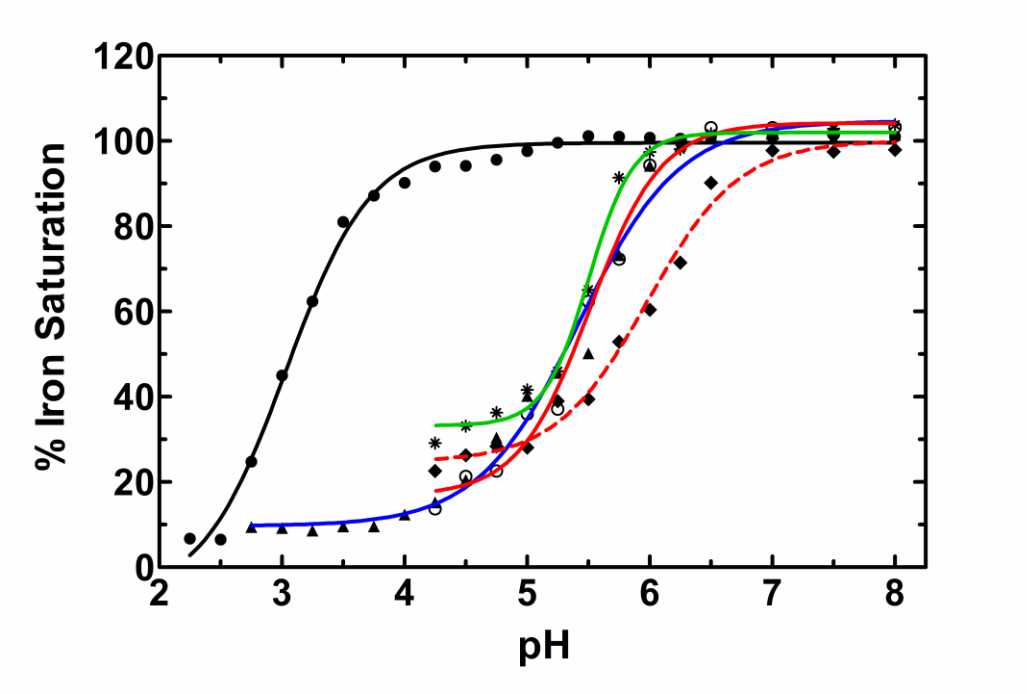

Figure 2-4. The pH-mediated release of iron from transferrins.
Serum transferrin is indicated by a blue line and triangles, lactoferrin by a black line and filled dots, MsTsf1 by a green line and asterisks, DmTsf1 by a solid red line and open dots, and $DmTsf1_N$ by a dashed red line and diamonds. Iron saturated protein samples, at ~5 mg/mL concentration, were dialyzed to equilibrium against various buffers at each indicated pH. The percent Fe^{3+}-saturation of the protein sample after dialysis was calculated by comparing the absorbance of the LMCT λ_{max} for each protein before and after dialysis. A sigmoidal dose response curve was used for curve fitting and analysis of the pH_{50} values (reported in Table 2-2).

Table 2-2. Summary of the iron binding and release properties of MsTsf1, DmTsf1, DmTsf1$_N$, serum transferrin and lactoferrin.

Protein	Fe^{3+} coordinating residues	LMCT λmax (nm)	Average Log *K*'	r_{max}	pH_{50}[c]
MsTsf1	D Y Y Q[a]	420	18.4	1.08	5.5
DmTsf1	E Y Y S[a]	434	18.2	1.11	5.5
DmTsf1$_N$	E Y Y S[a]	408	-	-	6.0
Serum transferrin amino-/carboxyl-lobe	D Y Y H	470	20.7 / 19.4[b]	-	5.4
Lactoferrin	D Y Y H	470	-	-	3.0

[a]Putative residues determined through sequence alignments.
[b]Calculated from values of *K*1' and *K*2' from Aisen et al. (1978) (Aisen et al., 1978).
[c]pH at 50% iron saturation.

Discussion

Comparison of Tsf1s to serum transferrin and lactoferrin

We found that the LMCT peak for DmTsf1 and MsTsf1 is blue-shifted relative to serum transferrin and lactoferrin. This is consistent with mutation studies of the amino-lobe of human serum transferrin, where a D63E mutation showed a LMCT λ_{max} shift from 472 nm to 450 nm (He et al., 1997c). To our knowledge there have been no studies of the effects of a H249S substitution; however, studies of mutants with substitutions of His-249 with other polar and uncharged resides in the amino-lobe of lactoferrin showed a LMCT λ_{max} shift from 450 nm to 428 nm for H249Q and 426 nm for H249T (Nicholson et al., 1997). The spectral characteristics of DmTsf1 and MsTsf1 support the alignment data in suggesting that these two Tsf1s differ in some residues that coordinate iron compared with serum transferrin and lactoferrin.

The effective binding affinity (expressed as log *K*') of DmTsf1 and MsTsf1 for Fe^{3+} is lower than that of serum transferrin under similar conditions. Lower affinity is likely due to the predicted differences in iron coordinating residues. Although the Tsf1s have lower Fe^{3+} affinity than serum transferrin and lactoferrin, their affinity (log *K*' of 17) is extremely high and functionally comparable to those of serum transferrin and lactoferrin. It is likely that DmTsf1

and MsTsf1 have an affinity for iron that is suitable for a physiological role in iron scavenging—a similar assumption made for other transferrins with lower affinity (Tinoco et al., 2008).

Like serum transferrin and lactoferrin, Tsf1s release iron at lowered pH. Both DmTsf1 and MsTsf1 have a pH_{50} of 5.5. This value is somewhat surprising given the His-249 substitution in both Tsf1s. A mutation of this histidine in the amino-lobe of lactoferrin has a dramatic effect on pH stability, such that H253Q/G/P mutants release all iron at pH 7.1 or higher (Nicholson et al., 1997). Despite changes in their iron coordination, Tsf1s had profiles of pH mediated iron release that are nearly identical to that of serum transferrin. The fact that serum transferrin has an amino-lobe with a pH_{50} of 5.7 and a carboxyl-lobe with a pH_{50} of 4.7, enables it to release iron in the acidifying environment of the endosome (a property necessary for its role in iron transport) (Baker, 1994; Peterson et al., 2000). Localization of Tsf1 within endosomes has not been demonstrated, and a Tsf1-receptor has not been identified in insects; however, the iron release properties of DmTsf1 and MsTsf1 support the possibility that Tsf1s could release iron in an endosomal environment.

Role of the DmTsf1 carboxyl-lobe

It appears that many Tsf1s have lost the ability to bind iron in their carboxyl-lobe. This conclusion is based on our finding that only nine out of 98 species have conserved iron-binding residues in their carboxyl-lobe, and also based on our demonstration that DmTsf1 and MsTsf1 have an r_{max} value of ~1, and, thus, must bind only one ferric ion. With these results in mind, we questioned the functional role of the carboxyl-lobe. One interesting hypothesis is that the carboxyl-lobe may act as a decoy for certain pathogens that have developed specific receptors to steal iron specifically from this lobe of transferrins (Yoshiga et al., 1997). Another possibility is

that the carboxyl-lobe is needed for receptor recognition. When holo-serum transferrin is recognized by the transferrin receptor, there is a large surface interaction between the C1 domain of the carboxyl-lobe and the transferrin receptor (Cheng et al., 2004).

While the above hypotheses have yet to be tested, our results indicate that the carboxyl-lobe stabilizes iron binding in the amino-lobe of DmTsf1. $DmTsf1_N$, which lacks the entire carboxyl-lobe, has spectral characteristics that clearly show it is capable of binding iron; however, there is a blue-shift of the LMCT peak relative to the full-length DmTsf1. In addition, $DmTsf1_N$ released iron at a higher pH than full-length DmTsf1. (It is important to note that attempts to perform Fe^{3+} affinity experiments with $DmTsf1_N$ in a competitive environment with citrate failed. This failure is probably due to an inability of $DmTsf1_N$ to compete effectively with citrate for Fe^{3+}.) $DmTsf1_N$ had properties similar to an amino-lobe mutant of lactoferrin (Lf_N) but not an amino-lobe mutant of serum transferrin (sTf_N) (Day et al., 1992; Peterson et al., 2000). Lf_N has a noticeable blue-shift of its LMCT peak from 465 nm to 454 nm and an increase in its pH_{50} compared with full-length lactoferrin, whereas the sTf_N counterpart has a red-shift and no change in pH_{50}. The difference between Lf_N and sTf_N pH stability has been explained in part by inter-lobe interactions that occur in lactoferrin but not in serum transferrin. Therefore, we suggest a similar hypothesis for Tsf1s: the carboxyl-lobe has a functional role in stabilizing iron coordination and in mediating proper release of iron as a function of pH.

Implications for insect immunity and iron homeostasis

Previous physiological studies have shown that Tsf1 functions in immunity, iron transport, and the prevention of oxidative stress; however, the biochemical mechanisms underlying these physiological roles are still poorly understood (Brummett et al., 2017; Geiser

and Winzerling, 2012; Huebers et al., 1988; Kim et al., 2008; Kurama et al., 1995; Lee et al., 2006; Xiao et al., 2019; Yoshiga et al., 1997). Our study provides important information for understanding these mechanisms.

Our results support the model that Tsf1 protects against infection by sequestering iron (Geiser and Winzerling, 2012; Brummett et al., 2017). We found that DmTsf1 and MsTsf1 bind iron with high affinity despite a difference in iron coordination properties compared with mammalian lactoferrin. In acidic conditions, the insect transferrins would not be as efficient at withholding iron as lactoferrin; however, the ability of lactoferrin to withhold iron at low pH may have evolved specifically for secretion into mammalian milk, which ends up in the acidic digestive tract of infants (Baker, 1994).

Though there is no known Tsf1 receptor in insects, iron from Tsf1 can be transported into cells (Huebers et al., 1988). This observation and the high concentration of Tsf1 in the hemolymph suggest that Tsf1 has a role in iron transport. Our results demonstrating that Tsf1 has a high affinity for iron and the ability to release iron over a physiologically relevant pH range are particularly interesting regarding its proposed role in iron transport (Huebers et al., 1988; Xiao et al., 2019). Two recent models of how Tsf1 may function in iron transport include the following scenarios for iron-binding: 1) Tsf1 binds iron in the secretory pathway of the midgut cells and is secreted into the hemolymph as holo-Tsf1, and 2) apo-Tsf1 in the hemolymph binds to iron that has been exported out of the midgut cells by an unknown mechanism (Xiao et al., 2019). Our results are compatible with both proposed pathways. Although there is mild acidification of some compartments of the secretory pathway, including the Golgi complex (Schapiro and Grinstein, 2000), release of iron from Tsf1 does not occur until the pH drops below 6; therefore, Tsf1 could potentially be loaded with iron in the secretory system of midgut cells as the first model

suggests. With high iron affinity of DmTsf1 and MsTsf1 at pH 7.4, apo-Tsf1 should bind iron in the hemolymph, as suggested by the second model. Future work is required to determine how holo-Tsf1 delivers iron into cells, but we have shown that Tsf1 would be capable of releasing iron in endosomes in a manner similar to that of serum transferrin.

Compared with the immune and iron transport functions of Tsf1, less is known about its ability to protect insects against oxidative stress. However, studies of two species of beetles have shown that Tsf1 is upregulated in response to various types of stress and that a lack of Tsf1 leads to increased oxidative stress (Kim et al., 2008; Lee et al., 2006). Our study supports the model that high concentrations of Tsf1 in hemolymph and other extracellular fluids would keep free iron levels exceedingly low and, thus, protect the insect from iron-induced oxidative stress.

Future Directions

The analysis of DmTsf1, DmTsf1$_N$, and MsTsf1's iron binding and release characteristics leads to three major topics for future work:

(1) Despite sequence analysis results, which indicated that a histidine is not conserved at the iron coordination site in DmTsf1 and MsTsf1, the iron binding and release characteristics are not vastly different from vertebrate transferrins. This contradiction led to the following question: is there an alternative method of iron coordination in Tsf1s, or possibly different structural folds of Tsf1s that bring an alternative histidine into the coordination sphere? Based on this question, future work (covered in Chapters 3 and 4) was aimed toward elucidating the structure and iron coordinating residues of a Tsf1 protein and probing the importance of certain residues to iron binding and release in Tsf1s.

(2) Tsf1's method of iron delivery into cells is unknown, but here we show the release of iron from DmTsf1 and MsTsf1 is at nearly the same pH as serum transferrin. This result suggests that Tsf1 could be delivering iron to cells via endocytosis, like serum transferrin. Future work presented in Chapter 5 was aimed toward testing this hypothesis.

(3) Though the carboxyl-lobe of DmTsf1 does not bind iron, it seems to aid in stabilizing iron binding and release in the amino-lobe. A future structure of Tsf1 could explain this stabilizing effect of the carboxyl-lobe. Also, to get a better sense of the functional importance of the carboxyl-lobe, a future study could be to compare the ability of $DmTsf_N$ and wild-type DmTsf1 to withhold iron from bacteria growing in culture media.

Acknowledgements

I would like to thank Dr. Maureen Gorman and Dr. Michael Kanost for their time providing writing and editing suggestions for the published manuscript based on this chapter. Dr. Gorman also provided a great amount of support and guidance during the purification and protein analysis. I also thank Dr. Michal Zolkiewski and Dr. Lawrence Davis for helpful suggestions regarding this work and Lisa Brummett for making the DmTsf1 recombinant baculovirus. This work was supported by National Science Foundation Grant 1656388 and National Institute of General Medical Sciences grant R37 GM041247. This is contribution 20-166-J from the Kansas Agricultural Experiment Station.

References

Aasa, R., Malmström, B.G., Saltman, P., Vänngård, T., 1963. The specific binding of iron(III) and copper(II) to transferrin and conalbumin. Biochim. Biophys. Acta 75, 203–222. https://doi.org/10.1016/0006-3002(63)90599-7

Aisen, P., Leibman, A., Zweier, J., 1978. Stoichiometric and site characteristics of the binding of iron to human transferrin. J. Biol. Chem. 253, 1930–1937.

Anderson, B.F., Baker, H.M., Dodson, E.J., Norris, G.E., Rumball, S.V., Waters, J.M., Baker, E.N., 1987. Structure of human lactoferrin at 3.2-A resolution. Proc. Natl. Acad. Sci. U.S.A. 84, 1769–1773. https://doi.org/10.1073/pnas.84.7.1769

Anderson, B.F., Baker, H.M., Norris, G.E., Rice, D.W., Baker, E.N., 1989. Structure of human lactoferrin: crystallographic structure analysis and refinement at 2.8 A resolution. J. Mol. Biol. 209, 711–734. https://doi.org/10.1016/0022-2836(89)90602-5

Bai, L., Qiao, M., Zheng, R., Deng, C., Mei, S., Chen, W., 2016. Phylogenomic analysis of transferrin family from animals and plants. Comp. Biochem. Physiol. D 17, 1–8. https://doi.org/10.1016/j.cbd.2015.11.002

Bailey, S., Evans, R.W., Garratt, R.C., Gorinsky, B., Hasnain, S., Horsburgh, C., Jhoti, H., Lindley, P.F., Mydin, A., Sarra, R., 1988. Molecular structure of serum transferrin at 3.3-A resolution. Biochemistry 27, 5804–5812. https://doi.org/10.1021/bi00415a061

Baker, E.N., 1994. Structure and reactivity of transferrins, in: Sykes, A.G. (Ed.), Advances in Inorganic Chemistry. Academic Press, pp. 389–463. https://doi.org/10.1016/S0898-8838(08)60176-2

Baker, E.N., Lindley, P.F., 1992. New perspectives on the structure and function of transferrins. J. Inorg. Biochem. 47, 147–160. https://doi.org/10.1016/0162-0134(92)84061-q

Baker, H.M., He, Q.-Y., Briggs, S.K., Mason, A.B., Baker, E.N., 2003. Structural and functional consequences of binding site mutations in transferrin: crystal structures of the Asp63Glu and Arg124Ala mutants of the N-lobe of human transferrin. Biochemistry 42, 7084–7089. https://doi.org/10.1021/bi020689f

Baldwin, D.A., Jenny, E.R., Aisen, P., 1984. The effect of human serum transferrin and milk lactoferrin on hydroxyl radical formation from superoxide and hydrogen peroxide. J. Biol. Chem. 259, 13391–13394.

Barber, M.F., Elde, N.C., 2015. Buried treasure: evolutionary perspectives on microbial iron piracy. Trends Genet. 31, 627–636. https://doi.org/10.1016/j.tig.2015.09.001

Bartfeld, N.S., Law, J.H., 1990. Isolation and molecular cloning of transferrin from the tobacco hornworm, Manduca sexta. Sequence similarity to the vertebrate transferrins. J. Biol. Chem. 265, 21684-21691.

Bonilla, M.L., Todd, C., Erlandson, M., Andres, J., 2015. Combining RNA-seq and proteomic profiling to identify seminal fluid proteins in the migratory grasshopper Melanoplus sanguinipes (F). BMC Genomics 16, 1096. https://doi.org/10.1186/s12864-015-2327-1

Brummett, L.M., Kanost, M.R., Gorman, M.J., 2017. The immune properties of Manduca sexta transferrin. Insect Biochem. Mol. Biol. 81, 1–9. https://doi.org/10.1016/j.ibmb.2016.12.006

Calap-Quintana, P., González-Fernández, J., Sebastiá-Ortega, N., Llorens, J.V., Moltó, M.D., 2017. Drosophila melanogaster models of metal-related human diseases and metal toxicity. Int. J. Mol. Sci. 18. https://doi.org/10.3390/ijms18071456

Cheng, Y., Zak, O., Aisen, P., Harrison, S.C., Walz, T., 2004. Structure of the human transferrin receptor-transferrin complex. Cell 116, 565–576. https://doi.org/10.1016/s0092-8674(04)00130-8

Day, C.L., Stowell, K.M., Baker, E.N., Tweedie, J.W., 1992. Studies of the N-terminal half of human lactoferrin produced from the cloned cDNA demonstrate that interlobe interactions modulate iron release. J. Biol. Chem. 267, 13857–13862.

Enns, C.A., Rutledge, E.A., Williams, A.M., 1996. The transferrin receptor, in: Lee, A.G. (Ed.), Biomembranes: A Multi-Volume Treatise, Endoctosis and Exocytosis. JAI, pp. 255–287. https://doi.org/10.1016/S1874-5342(96)80012-2

Farnaud, S., Evans, R.W., 2003. Lactoferrin - a multifunctional protein with antimicrobial properties. Mol. Immunol. 40, 395–405. https://doi.org/10.1016/s0161-5890(03)00152-4

Gasdaska, J.R., Law, J.H., Bender, C.J., Aisen, P., 1996. Cockroach transferrin closely resembles vertebrate transferrins in its metal ion-binding properties: a spectroscopic study. J. Inorg. Biochem. 64, 247–258. https://doi.org/10.1016/s0162-0134(96)00052-9

Geiser, D.L., Winzerling, J.J., 2012. Insect transferrins: multifunctional proteins. Biochim. Biophys. Acta 1820, 437–451. https://doi.org/10.1016/j.bbagen.2011.07.011

Giansanti, F., Leboffe, L., Pitari, G., Ippoliti, R., Antonini, G., 2012. Physiological roles of ovotransferrin. Biochim. Biophys. Acta 1820, 218–225. https://doi.org/10.1016/j.bbagen.2011.08.004

Grady, J.K., Mason, A.B., Woodworth, R.C., Chasteen, N.D., 1995. The effect of salt and site-directed mutations on the iron(III)-binding site of human serum transferrin as probed by EPR spectroscopy. Biochem. J. 309, 403–410. https://doi.org/10.1042/bj3090403

Harris, W.R., Pecoraro, V.L., 1983. Thermodynamic binding constants for gallium transferrin. Biochemistry 22, 292–299. https://doi.org/10.1021/bi00271a010

Hattori, M., Komatsu, S., Noda, H., Matsumoto, Y., 2015. Proteome analysis of watery saliva secreted by green rice leafhopper, Nephotettix cincticeps. PloS One 10, e0123671. https://doi.org/10.1371/journal.pone.0123671

He, Q.Y., Mason, A.B., Nguyen, V., MacGillivray, R.T., Woodworth, R.C., 2000a. The chloride effect is related to anion binding in determining the rate of iron release from the human transferrin N-lobe. Biochem. J. 350, 909–915.

He, Q.Y., Mason, A.B., Pakdaman, R., Chasteen, N.D., Dixon, B.K., Tam, B.M., Nguyen, V., MacGillivray, R.T., Woodworth, R.C., 2000b. Mutations at the histidine 249 ligand profoundly alter the spectral and iron-binding properties of human serum transferrin N-lobe. Biochemistry 39, 1205–1210. https://doi.org/10.1021/bi9915216

He, Q. Y., Mason, A.B., Woodworth, R.C., 1997a. Iron release from recombinant N-lobe and single point Asp63 mutants of human transferrin by EDTA. Biochem. J. 328, 439–445.

He, Q. Y., Mason, A.B., Woodworth, R.C., Tam, B.M., MacGillivray, R.T., Grady, J.K., Chasteen, N.D., 1997b. Inequivalence of the two tyrosine ligands in the N-lobe of human serum transferrin. Biochemistry 36, 14853–14860. https://doi.org/10.1021/bi9719556

He, Q. Y., Mason, A.B., Woodworth, R.C., Tam, B.M., Wadsworth, T., MacGillivray, R.T., 1997c. Effects of mutations of aspartic acid 63 on the metal-binding properties of the recombinant N-lobe of human serum transferrin. Biochemistry 36, 5522–5528. https://doi.org/10.1021/bi963028p

Huebers, H.A., Huebers, E., Finch, C.A., Webb, B.A., Truman, J.W., Riddiford, L.M., Martin, A.W., Massover, W.H., 1988. Iron binding proteins and their roles in the tobacco hornworm, Manduca sexta (L.). J. Comp. Physiol. B 158, 291–300. https://doi.org/10.1007/bf00695327

Jameson, G.B., Anderson, B.F., Norris, G.E., Thomas, D.H., Baker, E.N., 1998. Structure of human apolactoferrin at 2.0 Å resolution. Refinement and analysis of ligand-induced conformational change. Acta Crystallogr. D 54, 1319–1335. https://doi.org/10.1107/S0907444998004417

Jeitner, T.M., 2014. Optimized ferrozine-based assay for dissolved iron. Anal. Biochem. 454, 36–37. https://doi.org/10.1016/j.ab.2014.02.026

Jenssen, H., Hancock, R.E.W., 2009. Antimicrobial properties of lactoferrin. Biochimie 91, 19–29. https://doi.org/10.1016/j.biochi.2008.05.015

Kim, B.Y., Lee, K.S., Choo, Y.M., Kim, I., Je, Y.H., Woo, S.D., Lee, S.M., Park, H.C., Sohn, H.D., Jin, B.R., 2008. Insect transferrin functions as an antioxidant protein in a beetle larva. Comp. Biochem. Physiol. B 150, 161–169. https://doi.org/10.1016/j.cbpb.2008.02.009

Kosman, D.J., 2010. Redox cycling in iron uptake, efflux, and trafficking. J. Biol. Chem. 285, 26729–26735. https://doi.org/10.1074/jbc.R110.113217

Kurama, T., Kurata, S., Natori, S., 1995. Molecular characterization of an insect transferrin and its selective incorporation into eggs during oogenesis. Eur. J. Biochem. 228, 229–235. https://doi.org/10.1111/j.1432-1033.1995.0229n.x

Kurokawa, H., Mikami, B., Hirose, M., 1995. Crystal structure of diferric hen ovotransferrin at 2.4 A resolution. J. Mol. Biol. 254, 196–207. https://doi.org/10.1006/jmbi.1995.0611

Lambert, L.A., 2012. Molecular evolution of the transferrin family and associated receptors. Biochim. Biophys. Acta 1820, 244–255. https://doi.org/10.1016/j.bbagen.2011.06.002

Lambert, L.A., Perri, H., Halbrooks, P.J., Mason, A.B., 2005. Evolution of the transferrin family: conservation of residues associated with iron and anion binding. Comp. Biochem. Physiol. B 142, 129–141. https://doi.org/10.1016/j.cbpb.2005.07.007

Lee, K.S., Kim, B.Y., Kim, H.J., Seo, S.J., Yoon, H.J., Choi, Y.S., Kim, I., Han, Y.S., Je, Y.H., Lee, S.M., Kim, D.H., Sohn, H.D., Jin, B.R., 2006. Transferrin inhibits stress-induced apoptosis in a beetle. Free Radic. Biol. Med. 41, 1151–1161. https://doi.org/10.1016/j.freeradbiomed.2006.07.001

MacGillivray, R.T., Bewley, M.C., Smith, C.A., He, Q.Y., Mason, A.B., Woodworth, R.C., Baker, E.N., 2000. Mutation of the iron ligand His 249 to Glu in the N-lobe of human transferrin abolishes the dilysine "trigger" but does not significantly affect iron release. Biochemistry 39, 1211–1216. https://doi.org/10.1021/bi991522y

MacGillivray, R.T., Moore, S.A., Chen, J., Anderson, B.F., Baker, H., Luo, Y., Bewley, M., Smith, C.A., Murphy, M.E., Wang, Y., Mason, A.B., Woodworth, R.C., Brayer, G.D., Baker, E.N., 1998. Two high-resolution crystal structures of the recombinant N-lobe of human transferrin reveal a structural change implicated in iron release. Biochemistry 37, 7919–7928. https://doi.org/10.1021/bi980355j

Madeira, F., Park, Y.M., Lee, J., Buso, N., Gur, T., Madhusoodanan, N., Basutkar, P., Tivey, A.R.N., Potter, S.C., Finn, R.D., Lopez, R., 2019. The EMBL-EBI search and sequence analysis tools APIs in 2019. Nucleic Acids Res. 47, W636–W641. https://doi.org/10.1093/nar/gkz268

Mandilaras, K., Pathmanathan, T., Missirlis, F., 2013. Iron absorption in Drosophila melanogaster. Nutrients 5, 1622–1647. https://doi.org/10.3390/nu5051622

Mason, A., He, Q.-Y., 2002. Molecular aspects of release of iron from transferrin. https://doi.org/10.1201/9780824744175.ch4

Mason, A.B., Halbrooks, P.J., James, N.G., Connolly, S.A., Larouche, J.R., Smith, V.C., MacGillivray, R.T.A., Chasteen, N.D., 2005. Mutational analysis of C-lobe ligands of human serum transferrin: Insights into the mechanism of iron release. Biochemistry 44, 8013–8021. https://doi.org/10.1021/bi050015f

Nicholson, H., Anderson, B.F., Bland, T., Shewry, S.C., Tweedie, J.W., Baker, E.N., 1997. Mutagenesis of the histidine ligand in human lactoferrin: Iron binding properties and crystal structure of the histidine-253 → methionine mutant,. Biochemistry 36, 341–346. https://doi.org/10.1021/bi961908y

Octave, J.-N., Schneider, Y.-J., Trouet, A., Crichton, R.R., 1983. Iron uptake and utilization by mammalian cells. I: Cellular uptake of transferrin and iron. Trends Biochem. Sci. 8, 217–220. https://doi.org/10.1016/0968-0004(83)90217-7

Patch, M.G., Carrano, C.J., 1981. The origin of the visible absorption in metal transferrins. Inorg. Chim. Acta 56, L71–L73. https://doi.org/10.1016/S0020-1693(00)88536-9

Peterson, N.A., Anderson, B.F., Jameson, G.B., Tweedie, J.W., Baker, E.N., 2000. Crystal structure and iron-binding properties of the R210K mutant of the N-lobe of human lactoferrin: implications for iron release from transferrins. Biochemistry 39, 6625–6633. https://doi.org/10.1021/bi0001224

Qu, M., Ma, L., Chen, P., Yang, Q., 2014. Proteomic analysis of insect molting fluid with a focus on enzymes involved in chitin degradation. J. Proteome Res. 13, 2931–2940. https://doi.org/10.1021/pr5000957

Schapiro, F.B., Grinstein, S., 2000. Determinants of the pH of the Golgi complex. J. Biol. Chem. 275, 21025–21032. https://doi.org/10.1074/jbc.M002386200

Simmons, L.W., Tan, Y.-F., Millar, A.H., 2013. Sperm and seminal fluid proteomes of the field cricket Teleogryllus oceanicus: identification of novel proteins transferred to females at mating. Insect Mol. Biol. 22, 115–130. https://doi.org/10.1111/imb.12007

Spiro, T.G., Bates, George., Saltman, Paul., 1967. Hydrolytic polymerization of ferric citrate. II. Influence of excess citrate. J. Am. Chem. Soc. 89, 5559–5562. https://doi.org/10.1021/ja00998a009

Stookey, L.L., 1970. Ferrozine - a new spectrophotometric reagent for iron. Anal. Chem. 42, 779-781.

Tang, X., Zhou, B., 2013. Iron homeostasis in insects: Insights from Drosophila studies. IUBMB Life 65, 863–872. https://doi.org/10.1002/iub.1211

Tinoco, A.D., Peterson, C.W., Lucchese, B., Doyle, R.P., Valentine, A.M., 2008. On the evolutionary significance and metal-binding characteristics of a monolobal transferrin from Ciona intestinalis. Proc. Natl. Acad. Sci. U.S.A. 105, 3268–3273. https://doi.org/10.1073/pnas.0705037105

UniProt Consortium, 2019. UniProt: a worldwide hub of protein knowledge. Nucleic Acids Res. 47, D506–D515. https://doi.org/10.1093/nar/gky1049

Ward, P.P., Zhou, X., Conneely, O.M., 1996. Cooperative interactions between the amino- and carboxyl-terminal lobes contribute to the unique iron-binding stability of lactoferrin. J. Biol. Chem. 271, 12790–12794. https://doi.org/10.1074/jbc.271.22.12790

Warner, R.C., Weber, I., 1953. The cupric and ferric citrate complexes. J. Am. Chem. Soc. 75, 5086–5094. https://doi.org/10.1021/ja01116a055

Xiao, G., Liu, Z.-H., Zhao, M., Wang, H.-L., Zhou, B., 2019. Transferrin 1 functions in iron trafficking and genetically interacts with ferritin in Drosophila melanogaster. Cell Rep. 26, 748-758.e5. https://doi.org/10.1016/j.celrep.2018.12.053

Yoshiga, T., Hernandez, V.P., Fallon, A.M., Law, J.H., 1997. Mosquito transferrin, an acute-phase protein that is up-regulated upon infection. Proc. Natl. Acad. Sci. U.S.A. 94, 12337–12342. https://doi.org/10.1073/pnas.94.23.12337

Zak, O., Ikuta, K., Aisen, P., 2002. The synergistic anion-binding sites of human transferrin: chemical and physiological effects of site-directed mutagenesis. Biochemistry 41, 7416–7423. https://doi.org/10.1021/bi0160258

Zhang, J., Lu, A., Kong, L., Zhang, Q., Ling, E., 2014. Functional analysis of insect molting fluid proteins on the protection and regulation of ecdysis. J. Biol. Chem. 289, 35891–35906. https://doi.org/10.1074/jbc.M114.599597

Supplementary Material

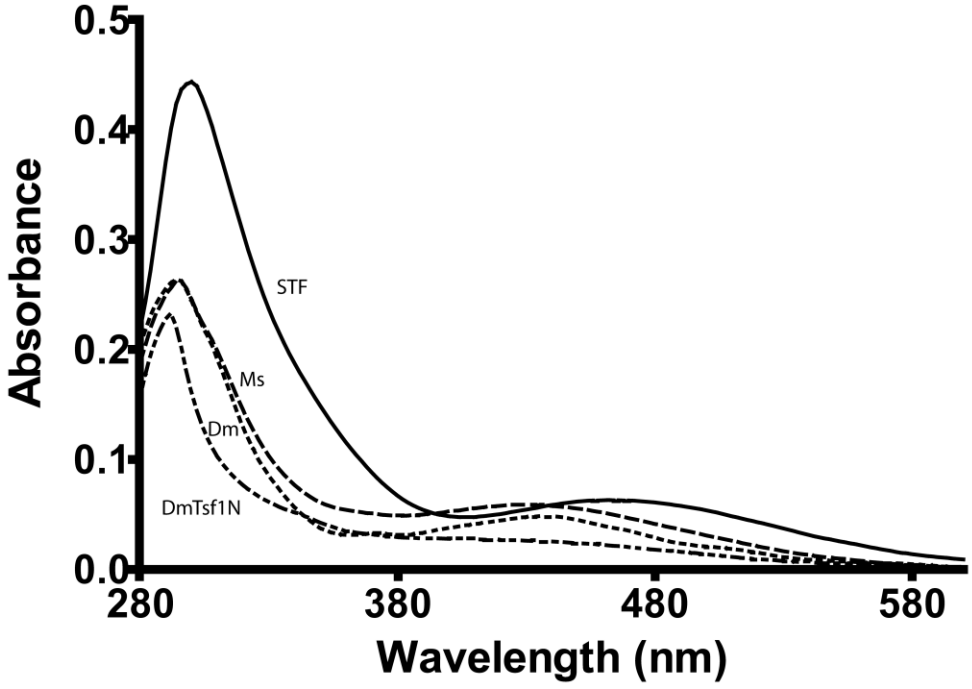

Figure 2-5. UV-Vis difference spectra of the LMCT peak for the Fe^{3+}-transferrin complexes.

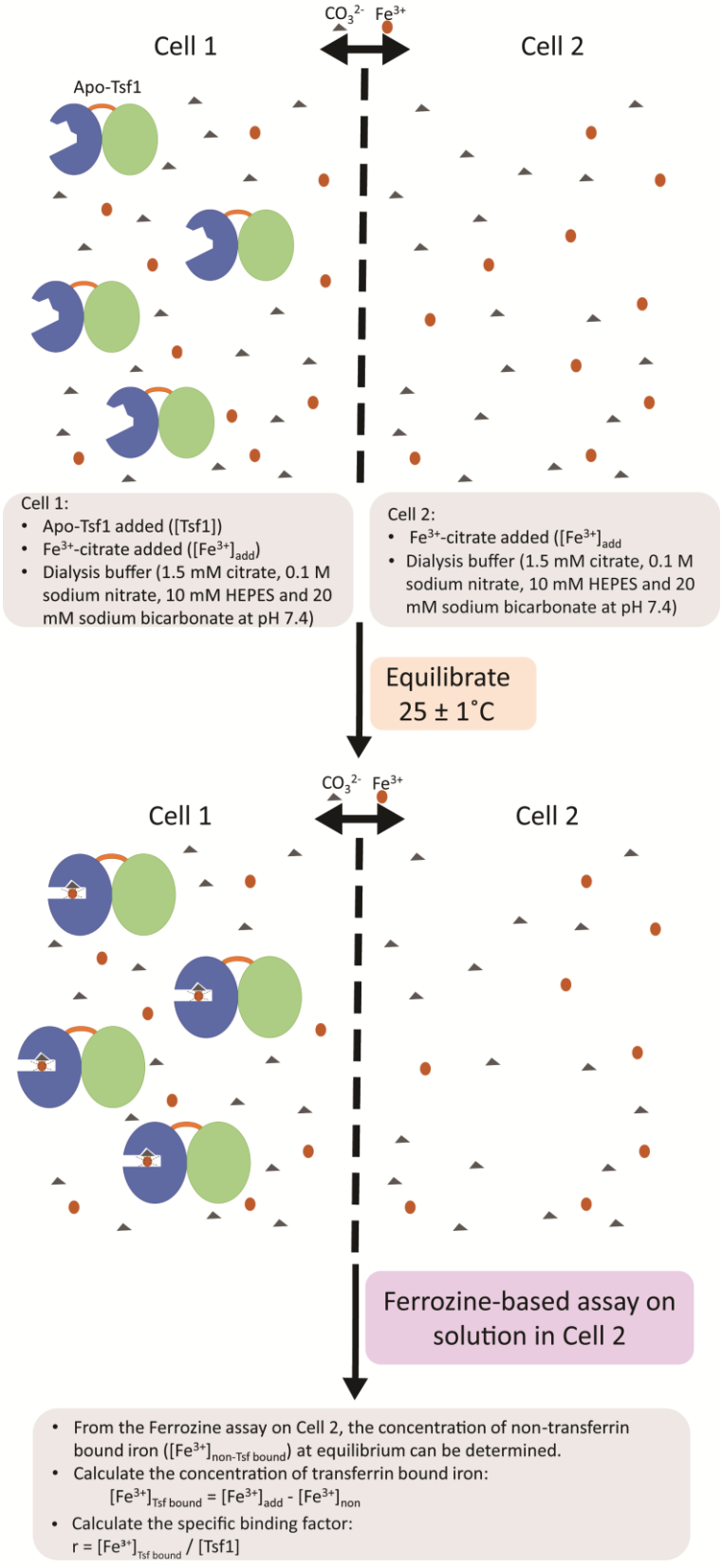

Figure 2-6. Diagram of equilibrium dialysis setup.

Table 2-3. Transferrin sequences used in alignment.

Order	Species	Accession #
Blattodea	*Blaberus discoidalis*	Q02942
Blattodea	*Cryptotermes secundus*	A0A2J7RCH3
Blattodea	*Mastotermes darwiniensis*	Q8MU80
Blattodea	*Periplaneta americana*	H2F490
Blattodea	*Zootermopsis nevadensis*	A0A067R8G2
Coleoptera	*Agrilus planipennis*	A0A1W4WDU6
Coleoptera	*Apriona germari*	Q5FX34
Coleoptera	*Monochamus alternatus*	A0A172WCD8
Coleoptera	*Protaetia brevitarsis*	Q0GB80
Coleoptera	*Tribolium castaneum*	A0A139WAX1
Diptera	*Aedes aegypti*	Q16894
Diptera	*Aedes albopictus*	A0A182HAB5
Diptera	*Anopheles dirus*	A0A182N8I6
Diptera	*Anopheles epiroticus*	A0A182PR24
Diptera	*Anopheles minimus*	A0A182W5Q6
Diptera	*Anopheles christyi*	A0A240PK04
Diptera	*Anopheles gambiae*	Q7QF98
Diptera	*Anopheles culicifacies*	A0A182MQL1
Diptera	*Anopheles arabiensis*	A0A182IAY0
Diptera	*Anopheles funestus*	A0A182RHN9
Diptera	*Anopheles farauti*	A0A182Q8L3
Diptera	*Anopheles merus*	A0A182UU15
Diptera	*Anopheles atroparvus*	A0A182IKA9
Diptera	*Anopheles stephensi*	A0A182YCV1
Diptera	*Anopheles melas*	A0A182TU06
Diptera	*Anopheles albimanus*	A0A182FAJ2
Diptera	*Anopheles quadriannulatus*	A0A182XK00
Diptera	*Anopheles maculatus*	A0A182TBM8
Diptera	*Bactrocera dorsalis*	A0A034VS68
Diptera	*Corethrella appendiculata*	U5EVY8
Diptera	*Culex tarsalis*	A0A1Q3FQK8
Diptera	*Culex quinquefasciatus*	B0X886
Diptera	*Drosophila persimilis*	B4H7J4
Diptera	*Drosophila virilis*	B4MD52
Diptera	*Drosophila grimshawi*	B4JJ24
Diptera	*Drosophila erecta*	B3NTD3
Diptera	*Drosophila ananassae*	B3MWK3
Diptera	*Drosophila mojavensis*	B4L3P8
Diptera	*Drosophila sechellia*	B4I6R8
Diptera	*Drosophila willistoni*	B4NEK7
Diptera	*Drosophila melanogaster*	Q9VWV6
Diptera	*Drosophila silvestris*	O97356
Diptera	*Drosophila pseudoobscura pseudoobscura*	B5DNN0
Diptera	*Drosophila ficusphila*	A0A1W4UDD6

Diptera	*Drosophila busckii*	A0A0M4EU20
Diptera	*Drosophila yakuba*	B4Q2X7
Diptera	*Glossina brevipalpis*	A0A1A9W323
Diptera	*Glossina pallidipes*	A0A1B0A3D5
Diptera	*Glossina fuscipes fuscipes*	A0A1A9YDI2
Diptera	*Glossina austeni*	A0A1A9VBV2
Diptera	*Glossina palpalis gambiensis*	A0A1B0BX64
Diptera	*Glossina morsitans morsitans*	Q8MX87
Diptera	*Lucilia cuprina*	A0A0L0C0K4
Diptera	*Lutzomyia longipalpis*	A0A1B0CHE7
Diptera	*Musca domestica*	A0A1I8M1D8
Diptera	*Sarcophaga peregrina*	Q26643
Diptera	*Stomoxys calcitrans*	A0A1I8PR12
Diptera	*Zeugodacus cucurbitae*	A0A0A1X109
Hemiptera	*Diaphorina citri*	A0A1S3CYM8
Hemiptera	*Lygus hesperus*	A0A146LNB5
Hemiptera	*Nephotettix cincticeps*	A0A0E4AVN5
Hemiptera	*Panstrongylus lignarius*	A0A224XL75
Hemiptera	*Pristhesancus plagipennis*	A0A1Q1NPJ1
Hemiptera	*Pyrrhocoris apterus*	M4WMH6
Hemiptera	*Rhodnius prolixus*	B8LJ43
Hemiptera	*Riptortus clavatus*	O96418
Hemiptera	*Riptortus pedestris*	R4WJB4
Hymenoptera	*Acromyrmex echinatior*	F4W957
Hymenoptera	*Apis cerana cerana*	J7F1T1
Hymenoptera	*Apis mellifera*	A0A088AFH7
Hymenoptera	*Atta cephalotes*	A0A158P0A5
Hymenoptera	*Atta colombica*	A0A195B5L1
Hymenoptera	*Bombus ignitus*	A8D919
Hymenoptera	*Cyphomyrmex costatus*	A0A151ID51
Hymenoptera	*Fopius arisanus*	A0A0C9RQZ4
Hymenoptera	*Habropoda laboriosa*	A0A0L7QKR3
Hymenoptera	*Harpegnathos saltator*	E2B326
Hymenoptera	*Melipona quadrifasciata*	A0A0M9A935
Hymenoptera	*Nasonia vitripennis*	K7J4P3
Hymenoptera	*Ooceraea biroi*	A0A026WB04
Hymenoptera	*Solenopsis invicta*	Q3MJL5
Hymenoptera	*Trachymyrmex cornetzi*	A0A195EDU2
Hymenoptera	*Trachymyrmex septentrionalis*	A0A195F369
Hymenoptera	*Trachymyrmex zeteki*	A0A151WU63
Lepidoptera	*Bombyx mori*	O97158
Lepidoptera	*Asiatic rice borer moth*	Q6F4J2
Lepidoptera	*Choristoneura fumiferana*	Q6Q2Z2
Lepidoptera	*Danaus plexippus plexippus*	A0A212FLE3
Lepidoptera	*Ephestia kuehniella*	D5M9Y5
Lepidoptera	*Galleria mellonella*	Q6UQ29

Lepidoptera	*Helicoverpa armigera*	A0A0B5H6A8
Lepidoptera	*Manduca sexta*	P22297
Lepidoptera	*Papilio machaon*	A0A194RH67
Lepidoptera	*Papilio xuthus*	A0A194PSJ1
Lepidoptera	*Pararge aegeria*	S4NYG0
Lepidoptera	*Plutella xylostella*	A0JCK0
Lepidoptera	*Spodoptera litura*	A7IT76
Orthoptera	*Romalea microptera*	Q6USR2
Artiodactyla	*Bos Taurus (bovine)*	P24627
Artiodactyla	*Bos Taurus (bovine)*	Q29443
Primates	*Homo sapien (human)*	P02787
Primates	*Homo sapien (human)*	P02788
Anseriformes	*Anas platyrhynchos (mallard)*	P56410
Galliformes	*Gallus gallus (chicken)*	P02789

Table 2-4. Equilibrium dialysis results for DmTsf1.

Pre-dialysis			Post-Dialysis		r^e	Log *K*'
[DmTsf1][a]	$[Fe^{3+}]_{add}$[b]		$[Fe^{3+}]_{Tsf\ bound}$[c]	$[Fe^{3+}]_{non\text{-}Tsf\ bound}$[d]		
µM	µM	trial	µM			
		1	2.3	1.4	0.1	18.2
40	3.6	2	2.8	0.9	0.1	18.3
		3	2.8	0.9	0.1	18.3
		1	6.5	3.5	0.2	18.2
40	10	2	6.9	3.1	0.2	18.3
		3	6.4	3.6	0.2	18.2
		1	17.2	2.8	0.4	18.4
40	20	2	17.9	2.1	0.4	18.4
		3	17.4	2.6	0.4	18.4
		1	23.9	6.1	0.6	18.3
40	30	2	23.9	6.1	0.6	18.3
		3	22.9	7.1	0.6	18.3
		1	35.2	9.8	0.9	18.3
40	45	2	35.4	9.6	0.9	18.3
		3	35.9	9.1	0.9	18.3
		1	29.2	30.9	0.7	18.1
40	60	2	32.2	27.8	0.8	18.1
		3	32.2	27.9	0.8	18.1
		1	42.9	57.1	1.1	18.0
40	100	2	44.9	55.1	1.1	18.1
		3	47.4	52.6	1.2	18.1
		1	41.3	83.7	1.0	18.0
40	115	2	35.0	72.6	0.9	17.9
		3	37.1	74.9	0.9	17.9
						18.2 ± 0.2[f]

[a]Total concentration of DmTsf1 after addition to dialyzer; used in Equation 1 as [Tsf1].
[b]Total concentration of Fe^{3+} in solution after addition to dialyzer (added in the form of Fe^{3+}-citrate).
[c]Transferrin bound iron; $[Fe^{3+}]_{Tsf\ bound} = [Fe^{3+}]_{add} - [Fe^{3+}]_{non\text{-}Tsf\ bound}$; used in Equation 1 as $[Fe^{3+} \cdot Tsf1 \cdot CO_3^{2-}]$.
[d]Concentration of non-transferrin bound iron measure by the Ferrozine assay (see in material and methods section)
[e]Specific binding factor of DmTsf1; $r = [Fe^{3+}]_{Tsf\ bound} / [DmTsf1]$.
[f]Log *K*' average ± standard deviation.

Table 2-5. Equilibrium dialysis results for MsTsf1.

Pre-dialysis			Post-Dialysis		r^e	Log *K*'
$[MsTsf1]^a$	$[Fe^{3+}]_{add}{}^b$		$[Fe^{3+}]_{Tsf\ bound}{}^c$	$[Fe^{3+}]_{non\text{-}Tsf\ bound}{}^d$		
µM	µM	trial	µM			
		1	7.0	3.4	0.3	18.6
21.9	9.7	2	5.0	4.3	0.2	18.4
		3	6.2	3.1	0.3	18.5
		1	23.1	8.1	1.1	18.6
21.9	29.0	2	18.4	9.5	0.8	18.5
		3	18.2	9.7	0.8	18.5
18.0		1	20.5	26.1	1.1	18.4
18.0	46.5	2	19.9	26.6	1.1	18.4
15.0		3	16.0	30.5	1.1	18.4
		1	19.9	84.3	0.9	18.0
21.9	96.7	2	23.8	69.2	1.1	18.1
		3	21.0	72.0	1.0	18.0
						18.4 ± 0.2^f

[a]Total concentration of MsTsf1 after addition to dialyzer; used in Equation 1 as [Tsf1].
[b]Total concentration of Fe^{3+} in solution after addition to dialyzer (added in the form of Fe^{3+}-citrate).
[c]Transferrin bound iron; $[Fe^{3+}]_{Tsf\ bound} = [Fe^{3+}]_{add} - [Fe^{3+}]_{non\text{-}Tsf\ bound}$; used in Equation 1 as $[Fe^{3+} \cdot Tsf1 \cdot CO_3^{2-}]$.
[d]Concentration of non-transferrin bound iron measure by the Ferrozine assay (see in material and methods section).
[e]Specific binding factor of MsTsf1; $r = [Fe^{3+}]_{Tsf\ bound} / [MsTsf1]$.
[f]Log *K*' average ± standard deviation.

Table 2-6. Example calculation of equilibrium dialysis results from 40 µM [DmTsf1] incubated with 100 µM $[Fe^{3+}]_{add}$ (trial 1) applied to binding equations.

Constants:	**Value**	**Derivation**
[Tsf1]	4.0×10^{-5} M	experimentally added (see $[DmTsf1]_{add}$ in Table S2)
[H+]	$10^{-7.4}$ M	experimentally added (see material and methods)
$[Cit]_{add}$	1.5×10^{-3} M	experimentally added (see material and methods)
$[HCO_3^-]$	2.0×10^{-2} M	experimentally added (see material and methods)
K_{c1}	$10^{3.64}$	Equation 2a (Warner and Weber, 1953)
K_{c2}	$10^{9.46}$	Equation 2b (Warner and Weber, 1953)
K_{c3}	$10^{-5.82}$	Equation 2c (Warner and Weber, 1953)
K_{c4}	$10^{-6.17}$	Equation 2d (Spiro et al., 1967)
Variables:		
$[Fe^{3+}]_{add}$	1.0×10^{-4} M	experimentally added (see Table S2)
$[Fe^{3+} \cdot Tsf1 \cdot CO_3^{2-}]$	4.3×10^{-5} M	experimentally determined; equal to [Fe3+]Tsf bound in Table S2
Calculations:		
x	1.0×10^{-12}	Eq. 3: $(K_{c3})(K_{c4})$
y	6.3×10^{-14}	Eq. 3: $([H^+])(K_{c3}) + [H^+]^2 + ([Cit]_{add})(K_{c3})(K_{c4}) - (2)([Fe^{3+}]_{add})(K_{c3})(K_{c4})$
z	-6.2×10^{-18}	Eq. 3: $-(([Fe^{3+}]_{add})([H^+])(K_{c3}) + ([Fe^{3+}]_{add})([H^+]^2))$
C_{eq}	9.8×10^{-5}	Eq. 3: $\frac{-y+(y^2-4xz)^{1/2}}{2x}$
$[Fe^{3+}]_{free}$	9.9×10^{-19}	Eq. 3: $\frac{(C_{eq})\left(([H^+]^2)(K_{c2})+([H^+]\right)(K_{c1})+(C_{eq})(K_{c1})(K_{c4}))}{(K_{c1})(K_{c2})([Cit]_{add}-[Fe^{3+}]_{add})}$
K	3.4×10^{-3} M	Eq. 1: $\frac{[Fe^{3+} \cdot Tsf1 \cdot CO_3^{2-}][H^+]^3}{[Fe^{3+}]_{free}\,[Tsf1][HCO_3^-]}$
K'	1.1×10^{18} M^{-1}	Eq. 4: $(\frac{[HCO_3^-]}{[H^+]^3})(K)$

Chapter 3 - Structural insight into the novel iron-coordination and domain interactions of transferrin-1 from a model insect, *Manduca sexta*[1]

Abstract

Transferrins function in iron sequestration and iron transport by binding iron tightly and reversibly. Vertebrate transferrins coordinate iron through interactions with two tyrosines, an aspartate, a histidine, and a carbonate anion (CO_3^{2-}), and conformational changes that occur upon iron binding and release have been described. Much less is known about the structure and functions of insect transferrin-1 (Tsf1), which is present in hemolymph and influences iron homeostasis mostly by unknown mechanisms. Amino acid sequence and biochemical analyses have suggested that iron coordination by Tsf1 differs from that of the vertebrate transferrins. Here we report the first crystal structure (2.05 Å resolution) of an insect transferrin. *Manduca sexta* (MsTsf1) in the holo form exhibits a bilobal fold similar to that of vertebrate transferrins, but its carboxyl-lobe adopts a novel orientation and contacts with the amino-lobe. The structure revealed coordination of a single Fe^{3+} ion in the amino-lobe through Tyr90, Tyr204, and two CO_3^{2-} anions. One CO_3^{2-} is buried near the ferric ion and is coordinated by four residues, whereas the other CO_3^{2-} is solvent exposed and coordinated by Asn121. Notably, these residues are highly conserved in Tsf1 orthologs. Docking analysis suggested that the solvent exposed CO_3^{2-} position is capable of binding alternative anions. These findings provide a structural basis for understanding Tsf1 function in iron sequestration and transport in insects as well as insight regarding the similarities and differences in iron homeostasis between insects and humans.

[1]This chapter was published as follows: Weber, J.J., Kashipathy, M.M., Battaile, K.P., Go, E., Desaire, H., Kanost, M.R., Lovell, S., Gorman, M.J., 2021. Structural insight into the novel iron-coordination and domain interactions of transferrin-1 from a model insect, *Manduca sexta*. *Protein Science* 30(2), 408 – 422.

Key words: transferrin, insect, iron homeostasis, metal binding, protein structure, hemolymph, iron coordination

Significance: This first structural analysis of an insect transferrin demonstrates that insect and human transferrins have important differences in iron coordination and other structural features, including domain interactions. These dissimilarities likely reflect mechanistic differences in biochemical function; therefore, model insect studies of iron-related diseases should be interpreted within this new framework. The novel aspects of the structure of MsTsf1 provides a basis for deeper understanding of iron homeostasis in insects, the largest class of animals.

Introduction

Members of the transferrin protein superfamily are known for their roles in the iron homeostasis of animals (Baker, 1994). Their functions are mediated by the ability to bind iron tightly and, in some cases, reversibly (Baker, 1994; Mizutani et al., 2012; Sun et al., 1999). The well-understood transferrins are those found in vertebrates and include mammalian serum transferrin, which sequesters iron in the blood and delivers it into cells via receptor mediated endocytosis (Octave et al., 1983); mammalian lactoferrin, which sequesters iron in secreted fluids as an iron withholding mechanism of innate immunity (Farnaud and Evans, 2003; Jenssen and Hancock, 2009); and avian ovotransferrin that has both an iron transport and immune

function (Giansanti et al., 2012). These proteins are typically 70-80 kDa monomeric glycoproteins that form two distinct lobes, an amino-lobe and carboxyl-lobe (N-lobe and C-lobe, respectively) (Baker, 1994; Mizutani et al., 2012; Sun et al., 1999). Each lobe has the ability to bind a ferric (Fe^{3+}) ion with high affinity at neutral pH (Aisen et al., 1978; Brandts and Lin, 1990; Pakdaman et al., 1998), and to release the Fe^{3+} ion as a function of pH decrease (Day et al., 1992).

High resolution crystal structures of lactoferrin (Anderson et al., 1987) and serum transferrin (Bailey et al., 1988) have demonstrated that these mammalian transferrins have remarkably similar iron binding sites and several common structural features that facilitate iron binding. The iron binding site in each of the N- and C- lobes is in a deep cleft that separates each lobe into two domains: the N1 and N2 domains of the N-lobe and the C1 and C2 domains of the C-lobe (Harris, 2012). Each iron binding site contains an aspartate, a histidine and two tyrosines, which, along with an anion, typically carbonate (CO_3^{2-}), coordinate a ferric ion (Baker, 1994; Harris, 2012; Mizutani et al., 2012; Sun et al., 1999). Coordination of the CO_3^{2-} occurs through the side chains of a threonine and an arginine, and the amide groups of two N-terminal helix residues (Harris, 2012). The binding of CO_3^{2-} at the site is considered synergistic because it is crucial for the formation of a stable Fe^{3+}- CO_3^{2-}-transferrin complex (Harris, 2012; Schlabach and Bates, 1975). Domain 1 (N1 or C1) contains the ligating aspartate, domain 2 (N2 or C2) contains one of the tyrosines, and a hinge region between domains 1 and 2 contains the histidine and second tyrosine (Mizutani et al., 2001). With the four ligating side chains from the protein and two from the synergistic anion, the site has a distorted octahedral coordination sphere. The iron release characteristic of vertebrate serum transferrins arises from conformational changes that occur during binding of transferrin to its receptor and protonation of residues in the intralobe

binding cleft (Eckenroth et al., 2011; Mizutani et al., 2012). As domains 1 and 2 begin to separate and as the coordination of iron at the binding site is abolished, the tertiary structure of the protein changes from a “closed” conformation in the holo-form to an “open” conformation in the apo-form (Yang et al., 2012) (supplementary Figure 3-8).

The roles of insect transferrin-1 (Tsf1) in iron homeostasis are functionally similar to those of lactoferrin and serum transferrin (Brummett et al., 2017; Geiser and Winzerling, 2012; Huebers et al., 1988; Iatsenko et al., 2020; Kim et al., 2008; Kurama et al., 1995; Lee et al., 2006; Xiao et al., 2019; Yoshiga et al., 1997). Recent in vivo studies in Drosophila melanogaster have provided strong evidence for the function of Tsf1 in iron transport and immunity (Iatsenko et al., 2020; Xiao et al., 2019). Xiao et al. (Xiao et al., 2019) showed that Tsf1 functions in the transportation of iron from the gut to the fat body (insect liver and adipose equivalent). Iatsenko et al. (Iatsenko et al., 2020) demonstrated that after infection, Tsf1 functions in relocating iron from the hemolymph to the fat body. However, unlike vertebrates, insects have no known Tsf1 receptor, and the mechanism by which iron bound to Tsf1 enters the cell remains elusive. In addition, Tsf1’s iron binding and release mechanisms appear to differ from the well-studied vertebrate transferrins (Weber et al., 2020). Bioinformatic studies have suggested that most Tsf1s have only a single iron binding site, in their N-lobe, and that this site lacks an iron coordinating histidine (Geiser and Winzerling, 2012; Lambert et al., 2005; Najera et al., 2021; Weber et al., 2020). Spectroscopic analysis of the ligand-to-metal charge transfer (LMCT) peak, which occurs when transferrins bind iron (Sun et al., 1999), was done for Tsf1s from Manduca sexta (MsTsf1) and D. melanogaster (DmTsf1). Both iron saturated MsTsf1 and DmTsf1 showed large LMCT peak shifts compared to the 470 nm peak for serum transferrin and lactoferrin, with MsTsf1 having a peak at 420 nm and DmTsf1 at 434 nm. These results indicate that Tsf1s coordinate

iron differently than the two mammalian transferrins (Weber et al., 2020). Despite their spectroscopic differences, biochemical analysis of MsTsf1 and DmTsf1 showed that both bind a single Fe^{3+} with high affinity (log K' = 18 at pH 7.4), and release Fe^{3+} under moderately acidic conditions, similar to iron release by serum transferrin.

The goal of this study was to further our understanding of iron coordination in Tsf1s through structural analysis. To this end, the first crystal structure of a Tsf1 (MsTsf1) was obtained using protein purified from M. sexta larval hemolymph in an iron bound and glycosylated form. The structure of MsTsf1 revealed a single Fe^{3+} binding site in the N-lobe that surprisingly is coordinated by two tyrosine ligands, Tyr90 and Tyr204, and two CO_3^{2-} anions. Moreover, the positioning of the C-lobe suggests that it acts as wedge between the N1 and N2 domains leaving the iron bound N-lobe in a relatively open conformation. These novel findings provide a structural explanation for the differences in the biochemical properties of Tsf1s compared to vertebrate transferrins.

Materials and Methods

Crystallization and data collection (performed in collaboration with Scott Lovell and Maithri Kashipathy)

MsTsf1 was purified from larval hemolymph following a procedure previously described (Weber et al., 2020). Purified MsTsf1 was extensively dialyzed in 50 mM NaCl, 20 mM Tris pH 7.4, 5 mM sodium bicarbonate and concentrated to 9.2 mg/mL for crystallization screening. All crystallization experiments were setup using an NT8 drop setting robot (Formulatrix Inc.) and UVXPO MRC (Molecular Dimensions) sitting drop vapor diffusion plates at 18 ˚C. 100 nL of protein and 100 nL crystallization solution were dispensed and equilibrated against 50 uL of the

latter. Initial crystals that formed needle clusters were obtained from the Index HT screen (Hampton Research) condition D10 (20% (w/v) PEG 5,000 MME, 100 mM Bis-Tris pH 6.5). These crystals were reproduced in a new crystallization plate in order to generate a crystal seed stock and 20 nL of seeds were added to each drop of new crystallization experiments dispensed with the NT8 robot as described above. Crystals that displayed a needle morphology were obtained in 2 weeks from the Proplex HT screen (Molecular Dimensions) condition F6 (15% (w/v) PEG 20,000, 100 mM Hepes pH 7.5). These crystals could be reproducibly obtained overnight by streak seeding new crystallization drops in a sitting drop plate. Heavy atom derivatized crystals were obtained by transferring native crystals to a solution containing crystallant supplemented with 10 mM K2PtCl4 and incubating for 18 hours. Crystals were transferred to a cryoprotectant solution composed of 80% crystallization solution and 20% PEG 200 before storing in liquid nitrogen. X-ray diffraction data were collected at the Advanced Photon Source beamline 17-ID using a Dectris Pilatus 6M pixel array detector.

Structure solution and refinement (performed by Scott Lovell and Maithri Kashipathy)

Intensities were integrated using XDS (Kabsch, 2010, 1988) via Autoproc (Vonrhein et al., 2011) and the Laue class analysis and data scaling were performed with Aimless (Evans, 2011). Structure solution, using two data sets that were scaled together from Pt-derivatized crystals, was conducted by SAD phasing with Crank2 (Skubák and Pannu, 2013) using the Shelx (Sheldrick, 2010), Refmac (Murshudov et al., 1997), Solomon (Abrahams and Leslie, 1996), Parrot (Zhang et al., 1997) and Buccaneer (Cowtan, 2006) pipeline via the CCP4 (Winn et al., 2011) interface. Eleven Pt sites were located with occupancies greater than 0.25 and

phasing/density modification resulted in a mean figure of merit of 0.44 in the space group $P2_12_12_1$. Subsequent model building utilizing density modification and phased refinement yielded R/R_{free} = 0.352/0.425 for the initial model. This model was used for molecular replacement with Phaser (McCoy et al., 2007) against the higher resolution native data set and the top solution was obtained for two molecules of MsTsf1 in the asymmetric unit in the space group *P*212121 (TFZ=51.5, LLG=2,945). The model was further improved by automated model building with Phenix and additional refinement and manual model building were conducted with Phenix and Coot (Emsley et al., 2010) respectively. Disordered side chains were truncated to the point for which electron density could be observed. Structure validation was conducted with Molprobity (Chen et al., 2010) and figures were prepared using the CCP4MG package (Potterton et al., 2004) and Pymol (The PyMOL Molecular Graphics System, Version 2.3.2 Schrödinger, LLC). Surface electrostatics were determined using APBS (Jurrus et al., 2018). Crystallographic data are provided in Table 3-1. The coordinates and structure factors were deposited in the Protein Data Bank with the code 6WB6.

Table 3-1. Crystallographic data for MsTsf1.

	MsTsf1 (K_2PtCl_4)	**MsTsf1 (Native)**
Data Collection		
Unit-cell parameters (Å, °)	*a*=65.61, *b*=141.42, *c*=150.40	*a*=64.49, *b*=139.06, *c*=146.70
Space group	$P2_12_12_1$	$P2_12_12_1$
Resolution (Å)[1]	49.44-2.85 (2.99-2.85)	47.28-2.05 (2.09-2.05)
Wavelength (Å)	1.0000	1.0000
Temperature (K)	100	100
Observed reflections	545,842	544,369
Unique reflections	33,530	83,612
$\langle I/\sigma(I)\rangle$[1]	10.8 (2.1)	7.6 (2.2)
Completeness (%)[1]	99.9 (99.6)	100 (100)
Multiplicity[1]	16.3 (17.1)	6.5 (6.6)
R_{merge} (%)[1, 2]	24.1 (187.2)	16.2 (82.7)
R_{meas} (%)[1, 4]	24.9 (193.0)	17.6 (89.8)
R_{pim} (%)[1, 4]	6.2 (46.6)	6.9 (34.8)
$CC_{1/2}$ [1, 5]	0.997 (0.777)	0.991 (0.697)
DelAnom CC[6]	0.481 (0.039)	-

Refinement		
Resolution (Å)[1]		40.00-2.05
Reflections (working/test)[1]		79,455/4,065
R_{factor} / R_{free} (%)[1,3]		20.9/27.2
No. of atoms (Protein/Fe^{3+}/CO_3/water)		9,925/2/16/422
Model Quality		
R.m.s deviations		
Bond lengths (Å)		0.008
Bond angles (°)		0.964
Average *B*-factor (Å^2)		
All Atoms		33.4
Protein		33.5
Fe^{3+}	18.7	
CO_3	22.6	
Water	49.3	
Coordinate error (maximum likelihood) (Å)	0.30	
Ramachandran Plot		
Most favored (%)	94.8	
Additionally allowed (%)	4.6	

[1]Values in parenthesis are for the highest resolution shell.
[2]$R_{merge} = \Sigma_{hkl}\Sigma_i |I_i(hkl) - \langle I(hkl)\rangle| / \Sigma_{hkl}\Sigma_i I_i(hkl)$, where $I_i(hkl)$ is the intensity measured for the *i*th reflection and $\langle I(hkl)\rangle$ is the average intensity of all reflections with indices hkl.
[3]$R_{factor} = \Sigma_{hkl} ||F_{obs}(hkl)| - |F_{calc}(hkl)|| / \Sigma_{hkl} |F_{obs}(hkl)|$; R_{free} is calculated in an identical manner using 5% of randomly selected reflections that were not included in the refinement.
[4]R_{meas} = redundancy-independent (multiplicity-weighted) R_{merge} (Evans, 2006, 2011). R_{pim} = precision-indicating (multiplicity-weighted) R_{merge} (Diederichs and Karplus, 1997; Weiss, 2001).
[5]$CC_{1/2}$ is the correlation coefficient of the mean intensities between two random half-sets of data (Evans, 2012; Karplus and Diederichs, 2012).
[6]DelAnom CC is the correlation coefficient between the Bijvoet differences ($I_{(hkl)} - I_{(-h-k-l)}$) from two random half-sets of data (Evans, 2011) and is used to estimate the anomalous signal strength.

Mass spectrometry and chromatography (performed by Eden Go and Heather Desaire)

A 25 µg aliquot of MsTsf1 sample at a concentration of 9.25 mg/mL was denatured with 7 M urea in 100 mM Tris buffer (pH 8.5), then reduced with 5 mM TCEP at room temperature for one hour, followed by alkylation with 20 mM iodoacetamide for an additional hour in the dark. The reduced and alkylated sample was buffer exchanged with 50 mM ammonium

bicarbonate (pH 8) using a 30-kDa MWCO filter (Millipore) prior to trypsin digestion. The sample was digested with trypsin at a 30:1 protein:enzyme ratio and was incubated overnight at 37°C for 18 hours.

High-resolution LC/MS experiment was performed using an Orbitrap Fusion Lumos Tribrid (Thermo Scientific) mass spectrometer equipped with ETD that is coupled to an Acquity UPLC M-Class system (Waters). Mobile phases consisted of solvent A: 99.9% deionized H2O + 0.1% formic acid and solvent B: 99.9 % CH3CN + 0.1% formic acid. Three microliters of the sample were injected onto C18 PepMap™ 300 column (300 µm i.d. x 15 cm, 300 Å, Thermo Fisher Scientific) at a flow rate of 3 µL/min. The CH3CN/H2O gradient ramping from 3% to 40% B in 45 min was used to separate the MsTsfl digest. All mass spectrometric analysis was performed in the positive ion mode using data-dependent acquisition with the instrument set to run in 3-sec cycles for the survey and two consecutive MS/MS scans with CID and ETD. Mass spectrometry data acquisition parameters include: a survey scan in the mass range, 350-1800 *m/z* at a resolution of 60000 at *m/z* 200 with an AGC target of 4 $x10^5$ and a maximum injection time of 50 ms, CID collision energy of 30%, and ETD was performed using the calibrated charge dependent reaction time. Data dependent acquisition was carried out by dynamic selection of ions with intensity greater than 5000. Resulting fragments were detected using rapid scan rate in the ion trap. Glycopeptide compositions were manually identified in the LC/MS data file and were confirmed by a combination of high-resolution MS data, CID, and ETD data.

Structure preparation and molecular docking

Water molecules and ligands were removed from the MsTsf1 PDB file and the structure was subjected to the fpocket online server (Le Guilloux et al., 2009). Pockets located in the N-

lobe cleft were identified and grouped as one pocket. The size (x = 15.0 Å, y = 28.5 Å, and z = 15.0 Å) and center (x = -16.2 Å, y = -7.4 Å and z = 4.2 Å) coordinates of this grouped pocket were determined. The structures of the candidate anions were drawn using MolView (molview.org) and converted to MOL2 files using the program OpenBabel (O'Boyle et al., 2011). The anions and MsTsf1 structures were prepared for docking in AutoDockTools version 1.5.6 (Sanner, 1999) and structural files in PDBQT format were generated for use in AutoDock Vina (Trott and Olson, 2010).

AutoDock Vina 1.1.2 was used to carry out the docking simulations of the organic anions in the identified pocket of MsTsf1. The parameters of experiments were carried out under default conditions except that the searchable area was set to the size and center of the pocket in the N-lobe cleft and the exhaustiveness was set to 100. Four independent trials were conducted. This program predicted the global minimum binding energy (kcal/mol) of the anions in the given pocket dimensions and reported the top nine poses for each trial. The poses that had an RMSD of 4 Å or less from CO_3^{2-}-1 were further analyzed to determine if they would sterically clash with the Fe^{3+} in the original structure. The average RMSD from CO_3^{2-}-1 and the average binding energy of these sterically acceptable poses were then calculated. A carbonate anion structure was generated and used as positive control for the study. It had poses at both the CO_3^{2-}-1 and CO_3^{2-}-2 positions; therefore, the average energy and average RMSD from each position was analyzed and reported. A phosphonium cation was generated as a negative control and we analyzed its predicted binding poses. Pockets, coordinates, and poses were analyzed using Pymol (The PyMOL Molecular Graphics System, Version 2.3.2 Schrödinger, LLC).

Alignment analysis

To identify possible anion-binding residues in transferrin sequences, we analyzed sequence alignments of 107 Tsf1 and Tsf1-like sequences and 14 non-insect hexapod transferrin sequences (Najera et al., 2021; Weber et al., 2020). We evaluated whether these sequences had the five anion-binding residues identified in the MsTsf1 crystal structure. To identify transferrins from other types of animals that may also have these anion-binding residues, we used BLASTP at NCBI to search non-redundant protein databases for Crustacea, Arachnida, Myriapoda, Xiphosura, Mollusca, Annelida, Nematoda and Deuterostomia.

The sequence alignment of MsTsf1, human lactoferrin and human serum transferrin was created by collecting sequences through the UniProt data base ("UniProt," 2019). The signal peptide sequences were removed. A sequence alignment was generated with Clustal Omega using the EMBL-EBI server (Madeira et al., 2019). The accession numbers used in the alignment are as follows: P22297 for MsTsf1, P02788 for human lactoferrin and P02787 for human serum transferrin.

Results

Overall structure of MsTsf1

The final MsTsf1 model contained two molecules in the asymmetric unit and included residues spanning Ser3-Leu662 (subunit A) and Tyr5-Gly661 (subunit B). Residues Ala1-Lys2, Pro508-Pro514 and Ala663 in subunit A as well as Ala1-Ser4, Gly445, Asn511-Ser513 and Leu662-Ala663 in subunit B could not be modeled due to disorder. Crystallographic data are provided in Table 3-1 (see in Material and Methods sections). The overall structure of MsTsf1 subunit A along with the non-crystallographic dimer is shown in Figure 3-1 A and B

respectively. Each subunit contains an Fe^{3+} ion and a single N-glycosylation site, and MsTsf1 adopts an overall bilobal fold. The amino- and carboxyl-lobes are labeled N-lobe (Ser3-Glu343) and C- lobe (Val352-Leu662), respectively, and are covalently connected by a short linker peptide (Arg344-Leu351). Furthermore, each lobe contains two domains delineated by residues

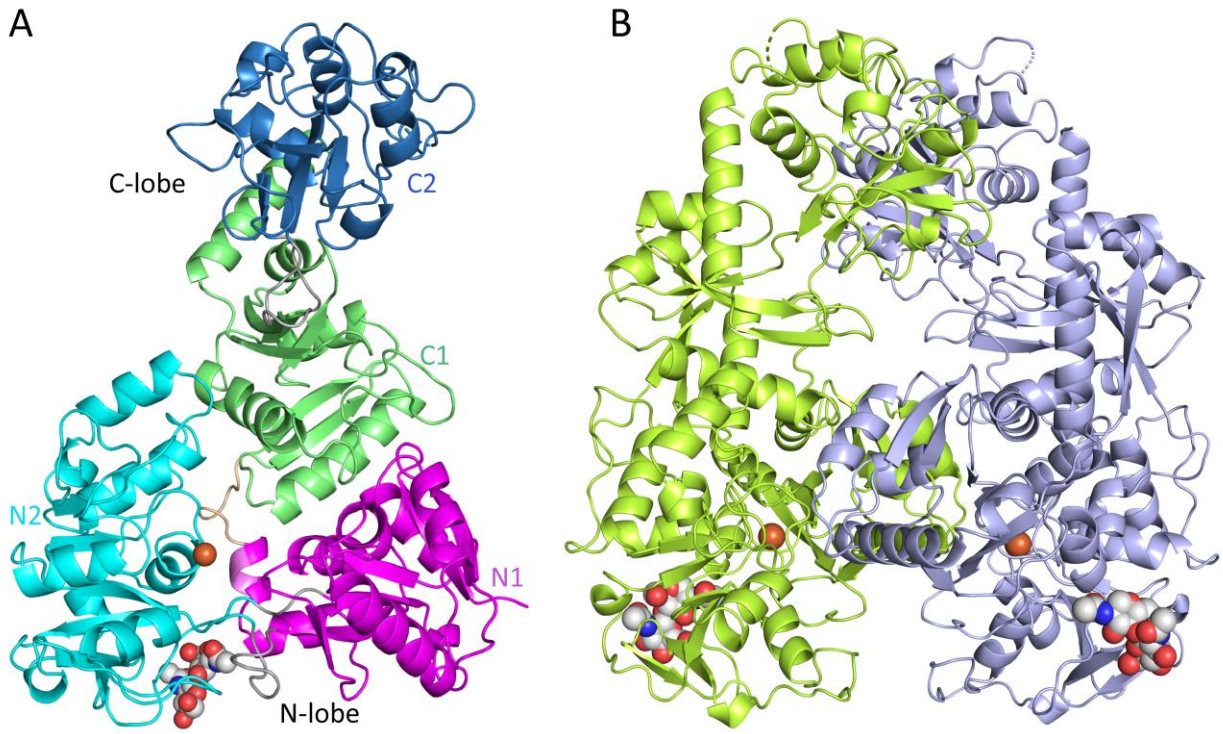

Figure 3-1. Structure of MsTsf1.

A) Individual domains of subunit A with N1 in magenta, N2 in cyan, C1 in green and C2 in blue. Also shown are the interlobe linker peptide in wheat and the intralobe "hinge" segments in grey. B) Non-crystallographic dimer showing subunit A (yellow-green) and B (light blue). The Fe^{3+} ions (brown) and NAG molecules are modeled as spheres.

Ser3-Arg79 and Gly275-Glu343 (domain N1), Arg89-Arg271 (domain N2), Val352-Tyr429 and Thr587-Leu662 (domain C1) and Tyr437-Met582 (domain C2). The topology of the secondary structure elements for each domain is depicted in supplementary Figure 3-9. The MsTsf1 structure is composed of 20 α-helices, 26 β-strands and twelve disulfide bonds (Figure 3-2). The

structure of MsTsf1 was subjected to a DALI (Holm and Laakso, 2016; Holm and Rosenström, 2010) search in an effort to identify structures that display a similar fold, and the top 100 hits are listed in supplementary Table 3-4. Not surprisingly, the top hits consisted of various transferrin type proteins. However, one interesting observation was that only a small number of residues were aligned (lali). The average number of aligned residues was 269 amongst the top 100 hits even though the MsTsf1 protein contains 663 amino acids and most transferrin proteins are of similar length, which is evident in supplementary Table 3-4 (nres). It should be noted that the hits in supplementary Table 3-4 that contain "nres" in the 300 amino acid range are structures of individual N- or C-lobes of transferrins. To compare MsTsf1 further with other transferrin proteins, superposition of apo-human serum transferrin in the glycosylated form (PDB 2HAV) was conducted, which yielded an RMSD deviation of 2.46 Å between Cα atoms (282 residues aligned). The N-lobe domains had the highest sequence similarity and comparatively displayed a similar spatial arrangement of the secondary structure elements (Figure 3-3A). However, the C-lobe domains were in completely different orientations relative to the N-lobe core and would need to rotate approximately 180˚ about the linker peptide that connects the N1 and C1 domains in order to superimpose (Figure 3-3B). Superposition of the individual C-lobe domains of 2HAV and MsTsf1 yielded an RMSD deviation of 3.38 Å between Cα atoms (258 residues aligned, supplementary Figure 3-10A). Although the secondary structure elements in the C-terminus were similar, their overall spatial arrangements differ, which accounts for the high RMSD deviation.

The N- and C-lobes of transferrins are believed to have arisen from a gene duplication event from a single lobed ancestral gene (Lambert, 2012). The N1 and C1 domains and the N2 and C2 domains of MsTsf1 were subjected to a pairwise structure comparison using the DALI server (Holm, 2020) to assess their sequence and structure similarity. Superposition of the N1

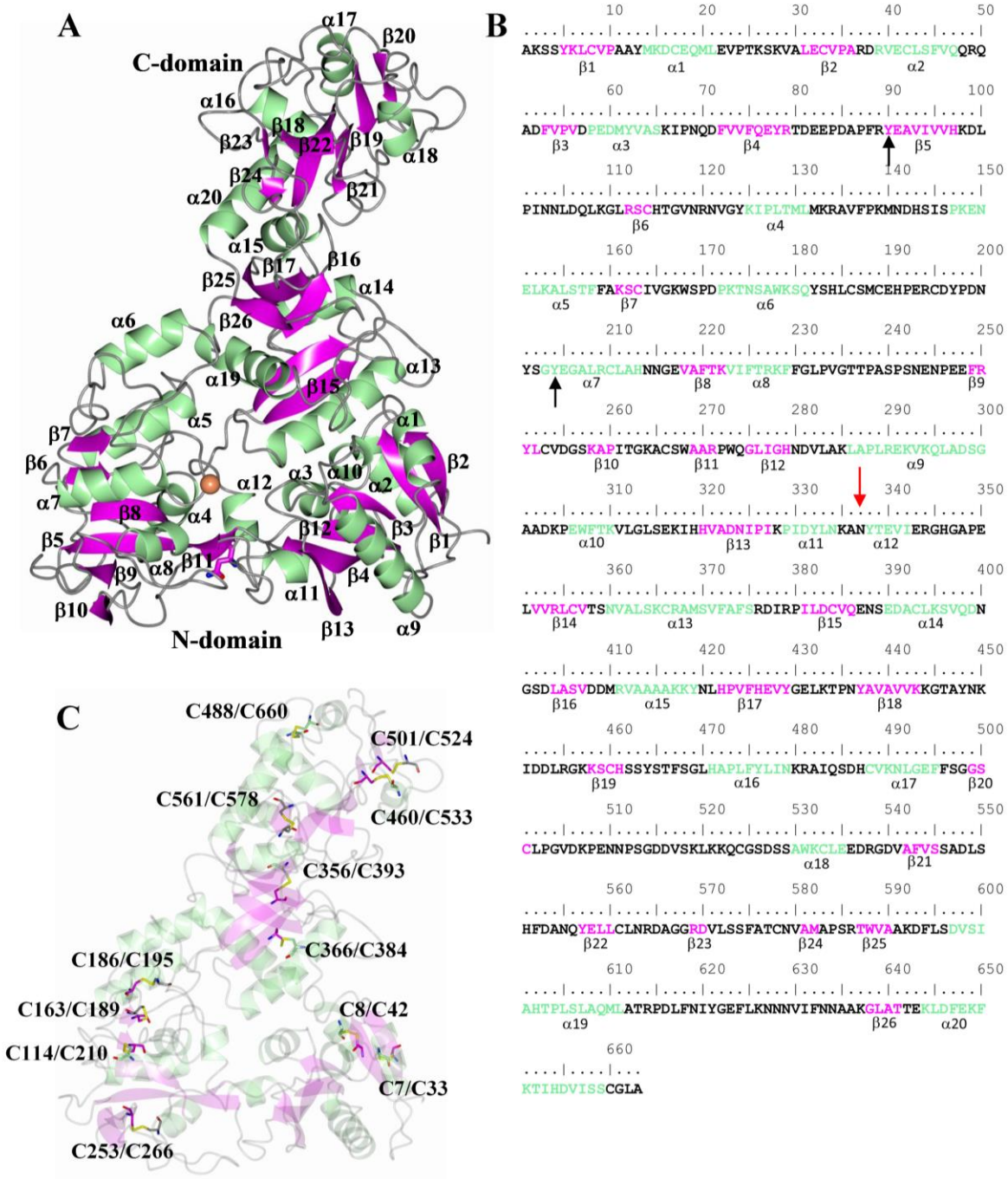

Figure 3-2. Secondary structure elements relative to the MsTsf1 sequence.

A) MsTsf1 structure showing the secondary structure elements and B) secondary structure annotation relative to the amino acid sequence. The red arrow and black arrows indicate the glycosylation site and residues that coordinate the Fe^{3+} ion, respectively. C) Locations of the disulfide bonds.

and C1 domains yielded an RMSD deviation of 2.8 Å between Cα atoms (135 out of 154 residues aligned). Superposition of the N2 and C2 domains yielded an RMSD deviation of 2.3 Å between Cα atoms (134 out of 139 residues aligned). The structural alignments show that despite having low amino acid sequence identity (24%) and no metal binding ability by the C-lobe, the lobes do have homologous folding patterns (supplementary Figure 3-10B).

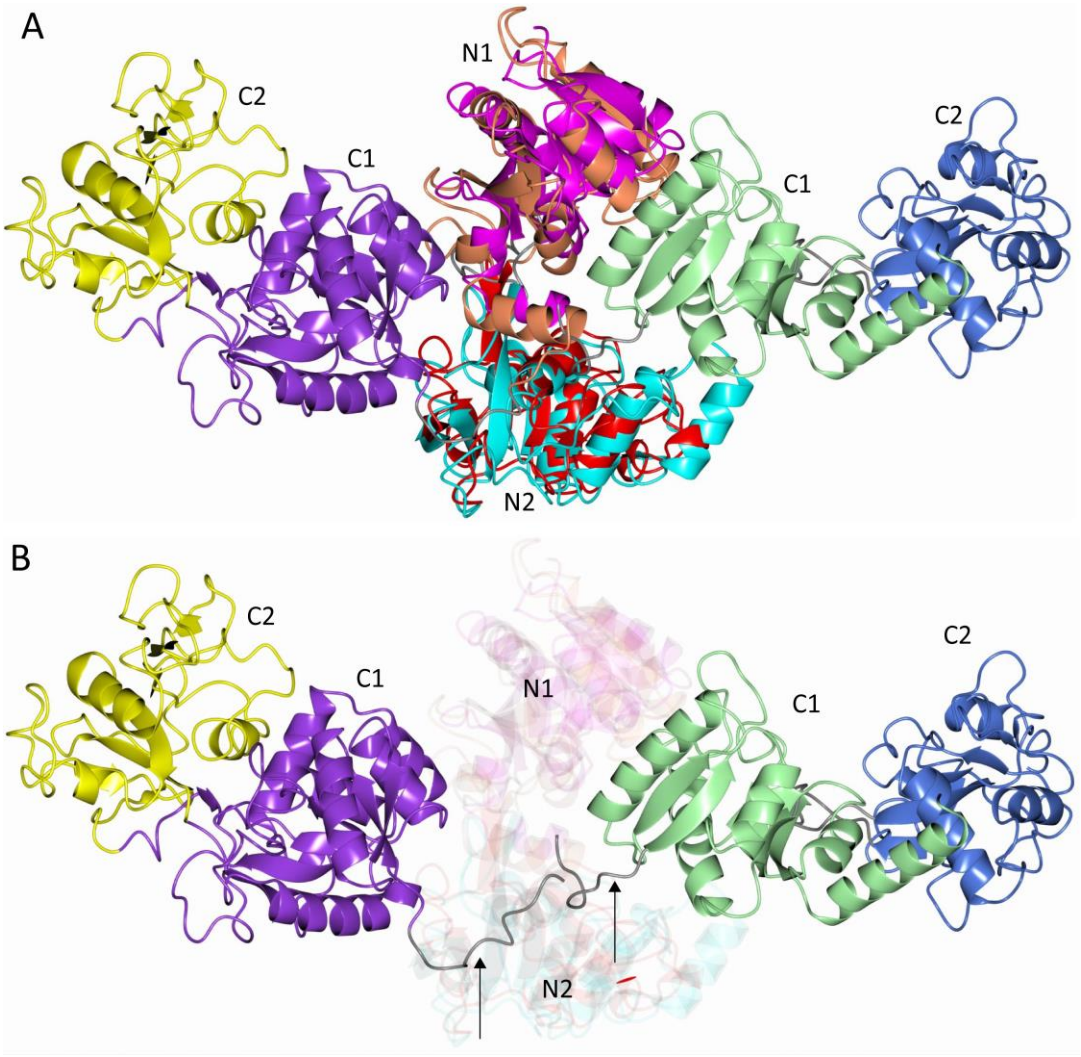

Figure 3-3. Comparison of MsTsf1 with human serum transferrin 2HAV.
A) The domains are colored as follows. MsTsf1: magenta (N1), cyan (N2), green (C1) and blue (C2); 2HAV: orange (N1), red (N2), purple (C1) and yellow (C2) B) Same as panel A highlighting the differences in the orientation of the C1 and C2 domains. The linker peptides that connect the N1 and C1 domains are indicated by the arrows and colored as grey.

The solvent exposed surface of MsTsf1 does not contain patches of positive charge on the surface as was observed for lactoferrin (Baker and Baker, 2012). However, one notable area in the intralobe cleft of the N-lobe contains a large mass of positive charge. This positive patch surrounds the Fe^{3+} binding site (supplementary Figure 3-11) and is formed by residues Arg89, Arg120, Lys125, Lys222, and Arg271.

Structure of the Fe^{3+} and CO_3^{2-} binding sites

The MsTsf1 structure showed difference electron density consistent with the Fe^{3+} in each subunit and displayed appreciable peak heights (8.6 and 7.4 σ) in the phased anomalous difference maps using diffraction data collected at a wavelength of 1.0000 Å. Additionally, electron density for two CO_3^{2-} anions was observed at each Fe^{3+} ion site. It should be noted that at this resolution it is not clear whether these resonance stabilized anions are carbonate or bicarbonate; however, for simplicity and to adhere to past nomenclature in transferrin research, we have used the term carbonate (CO_3^{2-}) for both anions. The Fe^{3+} ion is positioned in the N2 domain and adopts an octahedral coordination from six coordinating oxygens: two phenolic oxygens of residues Tyr90 and Tyr204, which are located in strand β5 and helix α7 respectively, and two oxygen atoms from each of the carbonate ions (CO_3^{2-}-1 and CO_3^{2-}-2) (Figure 3-4A). Tyr90 and Tyr204 are highly conserved in all iron binding transferrins, including human serum transferrin and lactoferrin (supplementary Figure 3-12), and have been predicted to be involved in iron coordination in Tsf1s (Geiser and Winzerling, 2012; Lambert et al., 2005; Najera et al., 2021; Weber et al., 2020). However, the presence of two CO_3^{2-} ions in the coordination of iron is a novel observation amongst all transferrin structures. The bond lengths of the six coordinating ligands to the Fe^{3+} are within the range of 1.9-2.3 Å, and the bond angles of the octahedral

coordination are distorted from their ideal geometry (supplementary Figure 3-13A and Table 3-2).

The carbonate ions are coordinated by residues Thr116, Arg120, Asn121, Val122 and Gly123, which are located in the loop connecting strand β6 and helix α4 in the N2 domain. CO_3^{2-}-2 forms hydrogen bonds with the $O_{\gamma 1}$ atom of Thr116, the N_{ε} atom of Arg120 and the backbone nitrogen group of Val122 and Gly123. CO_3^{2-}-1 forms hydrogen bonds with the backbone nitrogen group and the $N_{\Delta 2}$ atom of Asn121 (Figure 3-4B and Table 3-2). A surface representation of the iron binding site shows that one carbonate ion (CO_3^{2-}-2) is deeply buried at the site, while the other carbonate ion (CO_3^{2-}-1) is solvent exposed (supplementary Figure 3-13B). Superposition of the MsTsf1 and human serum transferrin (PDB 1D3K) iron binding site shows that the position of CO_3^{2-}-1 around the Fe^{3+} in MsTsf1 is similar to the position of the iron-coordinating histidine and aspartate in human serum transferrin (supplementary Figure 3-13C). Moreover, CO_3^{2-}-2 is very similar in its position and hydrogen bonding network to the carbonate anion bound to serum transferrin (supplementary Figure 3-13D).

By performing an analysis of amino acid sequence alignments of Tsf1 sequences (Najera et al., 2021; Weber et al., 2020), we found that all five carbonate binding residues are highly conserved (supplementary Table 3-5); therefore, anion coordination appears to be conserved in Tsf1 orthologs. To predict whether any non-insect transferrins have an N-lobe that binds two anions, we analyzed transferrin sequences from non-insect species. We identified sequences that have the conserved carbonate-binding residues in four non-insect arthropod species (supplementary Table 3-5), but we did not find this consensus in other types of animals, including molluscs, annelids, nematodes, and deuterostomes; therefore, the binding of a solvent exposed anion by Asn121 is likely to be specific to arthropods.

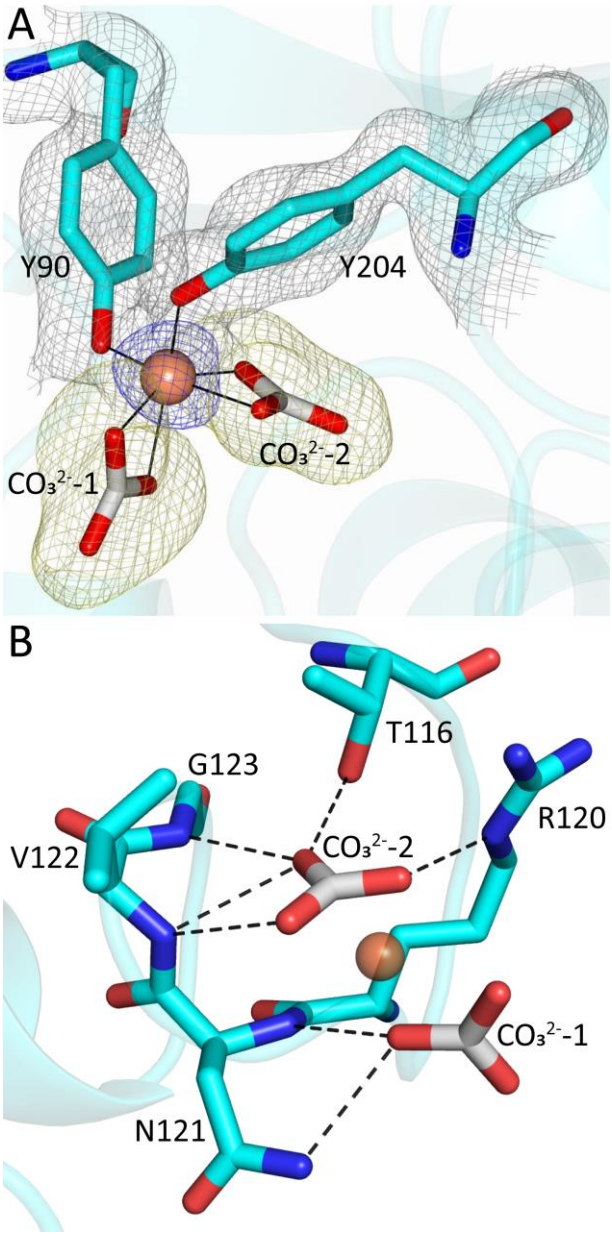

Figure 3-4. The coordination of Fe^{3+} and two CO_3^{2-} ions in MsTsf1.

A) The site of Fe^{3+} coordination. The ligating tyrosines, Tyr90 and Tyr204, and two CO_3^{2-} ions are in cyan, and the Fe^{3+} is shown as a brown sphere. The blue anomalous difference map and yellow Fo-Fc are contoured at 3.0 σ and the grey 2Fo-Fc map is contoured at 1.0 σ. B) Hydrogen bond interactions (dashed lines) between MsTsf1 residues (cyan) and the CO_3^{2-} ions (grey).

Table 3-2. Bonds lengths (Å) of Fe^{3+}, CO_3^{2-}-1, and CO_3^{2-}-2 to coordinating residues and bond angles (°) of Fe^{3+} to coordinating residues.

bond	length	bonds	angle
Fe—O_η (Y90)	2.1	O_η (Y90)---Fe---O_η (Y204)	101.9
Fe—O_η (Y204)	1.9	O_η (Y90)---Fe---O_3 (CO_3^{2-}-2)	89.9
Fe—O_3 (CO_3^{2-}-2)	2.0	O_η (Y90)---Fe---O_1 (CO_3^{2-}-2)	157.6
Fe—O_1 (CO_3^{2-}-2)	2.1	O_η (Y90)---Fe---O_3 (CO_3^{2-}-1)	92.6
Fe—O_3 (CO_3^{2-}-1)	2.2	O_η (Y90)---Fe---O_1 (CO_3^{2-}-1)	111.6
Fe—O_1 (CO_3^{2-}-1)	2.3	O_η (Y204)---Fe---O_3 (CO_3^{2-}-2)	102.2
$O_{\gamma1}$ (T116)---O_2 (CO_3^{2-}-2)	2.8	O_η (Y204)---Fe---O_1 (CO_3^{2-}-2)	85.9
N_ε (R120)---O_1 (CO_3^{2-}-2)	2.7	O_η (Y204)---Fe---O_3 (CO_3^{2-}-1)	157.9
N (G123)---O_2 (CO_3^{2-}-2)	3.1	O_η (Y204)---Fe---O_1 (CO_3^{2-}-1))	95.9
N (V122)---O_2 (CO_3^{2-}-2)	3.1	O_3 (CO_3^{2-}-2)---Fe---O_1 (CO_3^{2-}-2)	67.8
N (V122)---O_3 (CO_3^{2-}-2)	3.0	O_3 (CO_3^{2-}-2)---Fe---O_3 (CO_3^{2-}-1)	94.3
$N_{\Delta2}$ (N121)---O_3 (CO_3^{2-}-1)	3.0	O_3 (CO_3^{2-}-2)---Fe---O_1 (CO_3^{2-}-1)	148.4
		O_1 (CO_3^{2-}-2)---Fe---O_3 (CO_3^{2-}-1)	86.9
		O_1 (CO_3^{2-}-2)---Fe---O_1 (CO_3^{2-}-1)	88.1
		O_3 (CO_3^{2-}-1)---Fe---O_1 (CO_3^{2-}-1)	63.0

Domain interactions

The N- and C-lobe of the MsTsf1 structure are connected by a linker peptide (Arg344-Leu351) between the N1 and C1 domains (Figure 3-1). The MsTsf1 linker peptide adopts a loop conformation, similar to the linker peptides in serum transferrin (Yang et al., 2012), which is different from lactoferrin linker peptides, that form an α-helical structure (Wally and Buchanan, 2007). The linker peptide further connects the two lobes through several of its residues forming bonds with the N1, N2 and C1 domains (supplementary Figure 3-14). One residue of the linker peptide, Arg344, interacts with all three domains. The $N_{\eta1}$ and $N_{\eta2}$ atoms of Arg344 form a salt bridge with the $O_{\varepsilon2}$ atom of Glu151 as well as the $O_{\delta2}$ atom of Asp377. The backbone nitrogen of Arg344 forms hydrogen bonds with the backbone oxygen of Val341 and Glu340 while the backbone oxygen of Arg344 forms hydrogen bonds with the N_ε and $N_{\eta2}$ atoms of Arg379 (Figure 3-5A).

Non-covalent interlobe contact in the form of direct hydrogen bonds and salt bridges comes solely from the N1 and C1 domains. The $N_{\eta 1}$ and $N_{\eta 2}$ atoms of Arg376 form a salt bridge with $O_{\delta 2}$ of Asp57. The $N_{\eta 2}$ atom of Arg376 also engages in hydrogen bonds with the $O_{\delta 1}$ and $O_{\delta 2}$ atoms of Asp60. Atom $N_{\eta 2}$ of Arg379 forms a hydrogen bond with the backbone oxygen of Ile342. The N-terminal end of helix α2 in the N1 domain, three hydrogen bonds are formed with a disordered region of the C1-domain. The $O_{\delta 2}$ atom of Asp38 bonds with the backbone nitrogen of Asn619, the backbone nitrogen of Arg39 with the backbone oxygen of Asp616 and the backbone nitrogen of Val40 with the backbone oxygen of Leu617 (Figure 3-5B). While there is no direct interaction of the C-lobe with the N2-domain, there is a notable hydrogen bond network mediated by several water molecules located in the space between the N2 and C1 domain. This network is composed of side chain and backbone groups of residues from the C1 domain (Asp377, Arg379, Gln609 and Thr641) and the N2 domain (Asn119, Lys148, Lys167, Pro170 and Asp171) (supplementary Figure 3-15).

Despite the N1 domain having no direct interaction with the bound Fe^{3+} or anions, it does make several intralobe contacts with the N2 domain. Two peptide segments covalently connect the two lobes (Thr80-Phe88 and Pro272-Gln274). These two segments help to form the back of the cleft between the two lobes (Figures 3-1A and 3-2A), similar in position to the hinge regions in the N- and C-lobes of serum transferrin and lactoferrin (Mizutani et al., 2012, 2001; Sun et al., 1999). Because these two covalent segments adopt loop structures, they may provide flexibility to the two domains to facilitate any conformational changes. There are also several non-covalent contacts that occur between the N1 and N2 domain. A salt bridge is formed between the N_{ζ} atom of Lys133 and the $O_{\varepsilon 1}$ atom of Glu340. Two residues, Ala336 and Asn337 (Asn337 is also the site of glycosylation), between helix α11 and α12 form hydrogen bonds with

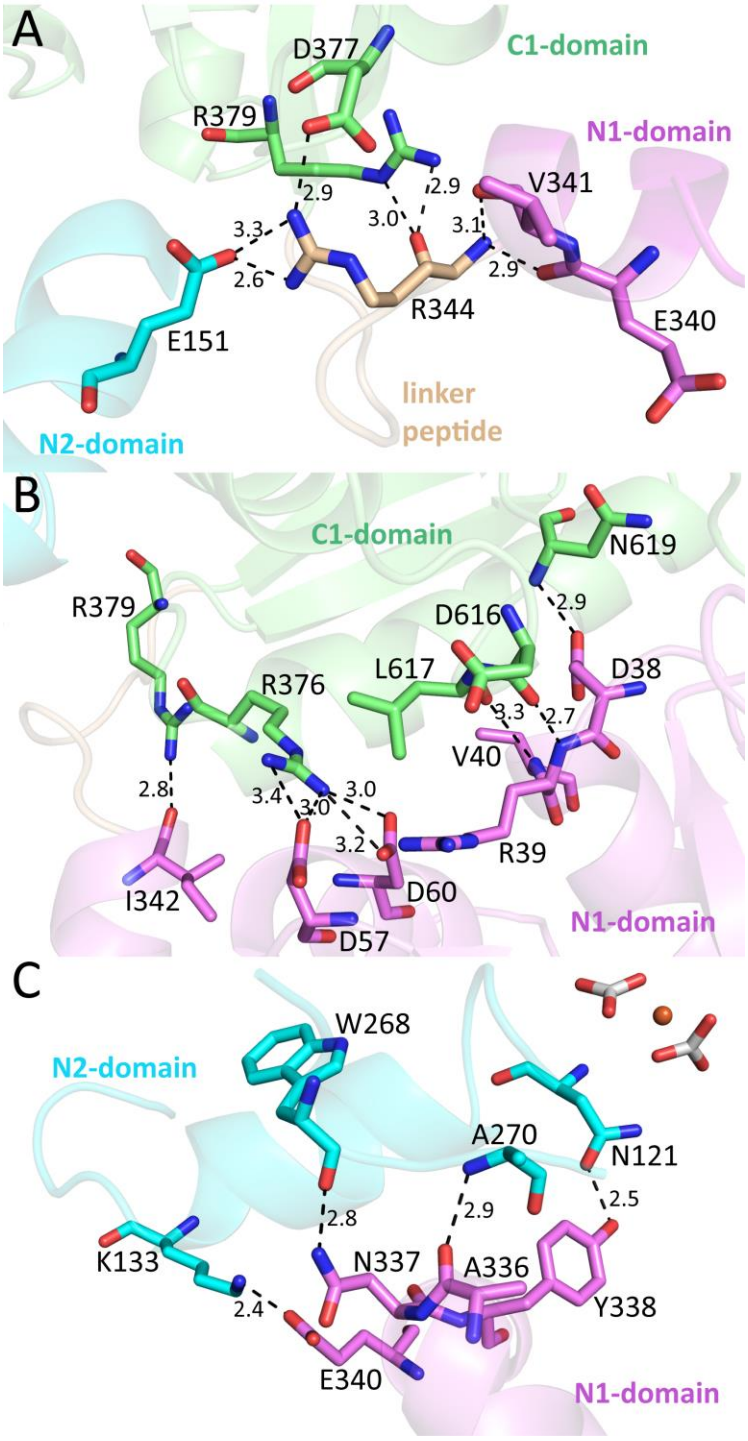

Figure 3-5. Interactions between the domains of MsTsf1.

A) The interaction of the linker peptide residue, Arg344, with residues of the N1, N2 and C1 domains. B) The non-covalent interlobe contacts between the N1 and C1 domains. C) The non-covalent intralobe contacts in the N-lobe. For clarity, the NAGs were removed from Asn337. All residues and domains are colored according to Figure 3-1A.

the N2 domain residues Trp268 and Ala270. The most interesting contact comes from a hydrogen bond formed between the O_{η} atom of Tyr338 and the $O_{\delta 1}$ atom of the CO_3^{2-}-1 coordinating Asn121 (Figure 3-5C). This 2.5 Å interaction between Tyr338 and Asn121 is not only an intralobe contact connecting the N1 domain to the N2 domain, but also closely links the N1 domain to anion coordination and likely also to iron binding.

The C2 domain of MsTsf1 makes no contact with the N-lobe. Besides the two covalent peptide linkages made with the C1 domain (Gly430-Asn436 and Ala583-Arg586), the C2 domain's only other direct contact comes through a disulfide linkage between its Cys488 and the Cys660 very near to the C-terminal end in the C1 domain.

Glycosylation site

Characteristic of the transferrin family, MsTsf1 is glycosylated. MsTsf1 has three potential glycosylation sites at Asn200, Asn337 and Asn400, as predicted from the N-GlyDE server (Pitti et al., 2019). However, electron density consistent with glycosylation was only observed at Asn337 in each subunit (Figure 3-6 A-B), which is located in the N1 domain within the loop connecting α11 and α12. Two N-Acetylglucosamine (NAG) glycans could be modeled at each Asn337 residue, although there was weaker electron density present that suggested that more extensive glycan branching was present. Therefore, the glycosylated MsTsf1 was analyzed by mass spectrometry, using a site-specific glycosylation analysis, in an effort to identify the glycans on each potential N-glycosylation site. The mass spectrometry results (Figure 3-6C) confirmed the observations from the crystal structure that glycosylation was only present at Asn337. Additionally, heterogeneous glycosylation of high mannose variants was observed at Asn337 which explains why only the NAG-NAG glycans could only be modeled to the electron

density, as the mannose occupancies presumably varied and/or were disordered. This level of glycosylation of MsTsf1 is consistent with previous reports of mannose and NAG being at a 5:1 ratio in MsTsf1 (Bartfeld and Law, 1990).

Studies of vertebrate transferrins have revealed highly variable sites of N-glycosylation; however, these post-translational modifications have mostly been found on the protein surface and are not believed to alter iron binding and release (Baker, 1994; Baker and Baker, 2009). The glycosylation of Asn337 in the N-lobe of MsTsf1 is unique because of its location at the intralobe contact points (Figure 3-5C) and near the hinge-like region. In vertebrate transferrins, this region would normally be buried in the interlobe interface, but it is exposed due to the difference in the orientation of the MsTsf1 C-lobe. The positioning of glycosylation at the hinge-like region of MsTsf1's N-lobe could influence the flexibility of the domains to form open or closed conformations.

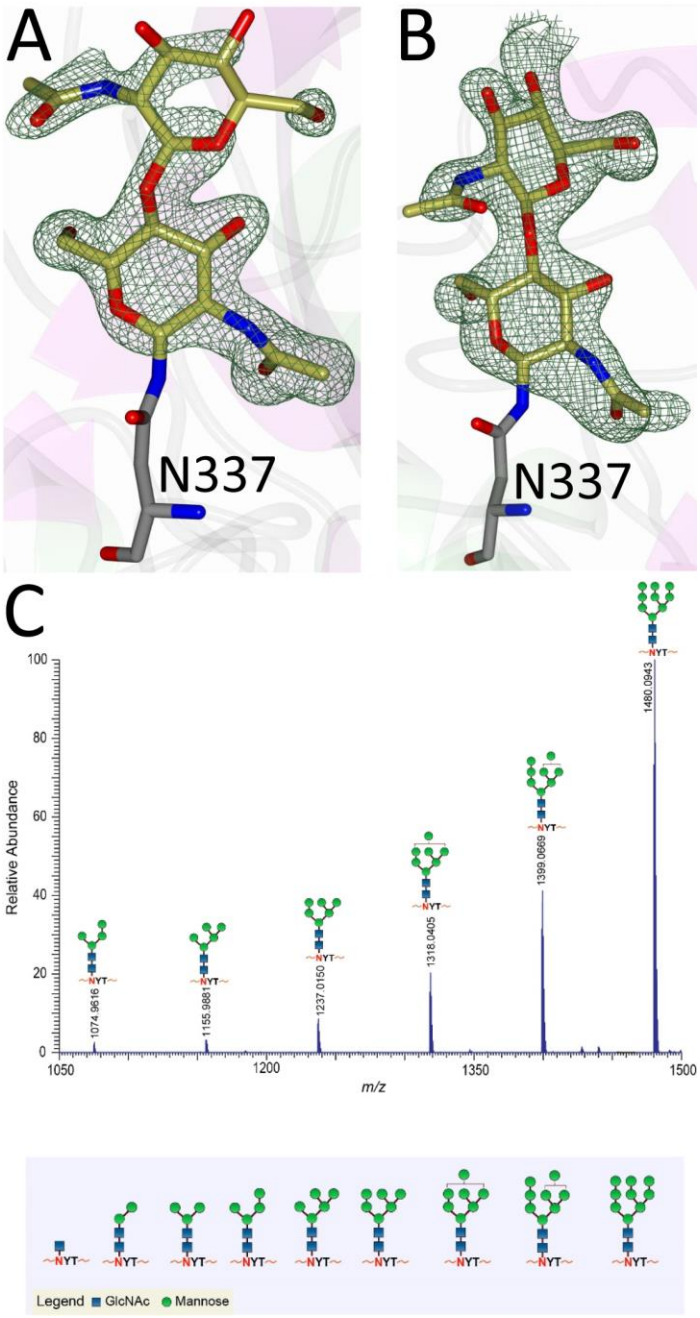

Figure 3-6. Glycosylation in MsTsf1.

Fo-Fc Polder omit electron density map (green mesh) contoured at 3σ showing the modeled glycans in A) subunit A and B) subunit B. C) Mass spectrometry results showing the most abundant glycoforms present at residue Asn337.

Molecular docking of organic anions

Substitutes for carbonate as the synergistic anion bound to vertebrate transferrins have been previously studied (Dubach et al., 1991; Harris, 2012; Schlabach and Bates, 1975). While many organic anions can form weak Fe^{3+}-anion-transferrin complexes, oxalate is the only substitute that forms a relatively similar stable complex to that of carbonate (Halbrooks et al., 2004; Schlabach and Bates, 1975). In the case of MsTsf1, CO_3^{2-}-2 has a similar coordination as the carbonate in vertebrate transferrins, but CO_3^{2-}-1 is solvent exposed and has less steric restrictions. The concentration of carbonate in insect hemolymph (Jungreis, 1978) is similar to many other organic acids (Wyatt, 1961). Thus, our hypothesis is that the CO_3^{2-}-1 binding site is susceptible to the binding of alternative anions that could form a stable Fe^{3+}-anion-MsTsf1 complex. As an initial probe of this hypothesis, we performed a molecular docking study. Candidate anions were selected from reported organic anions and acids found in insect hemolymph (Phalaraksh et al., 2008; Wyatt, 1961): acetoacetate, α-ketoglutarate, ascorbate, fumarate, glycine, glyoxylate, lactate, malate, oxaloacetate, pyruvate and succinate. Searchable pockets in the cleft between the N1 and N2 domains were identified (Figure 3-16A) and docking experiments were performed using AutoDock Vina (Trott and Olson, 2010). Nearly all of the candidate anions had poses within an RMSD of 4 Å of CO_3^{2-}-1; however, not all positions were sterically possible with respect to where the iron is located in the pocket. Analysis of the sterically acceptable docking poses at the iron binding site are found in Table 3-3. Figure 3-16 B-L shows the sterically acceptable poses for each anion with the Fe^{3+} ion and CO_3^{2-}-2 replaced in the MsTsf1 structure. Citrate was the exception, as no poses were found near the site, which explains its high average RMSD from the CO_3^{2-}-1 position, >11 Å. The binding of the dicarboxylic acid candidates, α-ketoglutarate, fumarate, malate, oxaloacetate and succinate, were

consistently more energetically favorable because one carboxyl group becomes the oxygen ligands for the iron and the other carboxyl group can interact with nearby positively charged residues Lys125 and Arg271 that protrude into the cleft. Figure 3-7 shows an example of α-ketoglutarate's predicted interactions at the iron binding site.

Table 3-3. Analysis of sterically acceptable organic anions docked at the iron binding site of MsTsf1.

Anion	Structure	Average RMSD deviation from carbonate (Å)	Average energy (kcal/mol)
acetoacetate	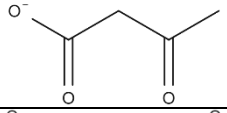	1.52	-4.0
α-ketoglutarate	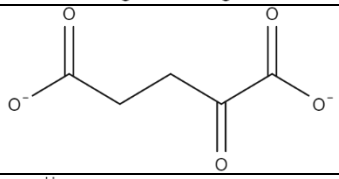	1.40	-4.8
ascorbate	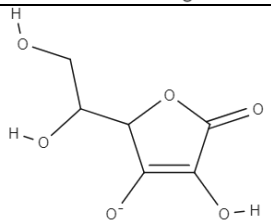	2.86	-5.3
carbonate[1]	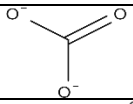	1.16 / 0.27	-3.2 / -3.5
fumarate	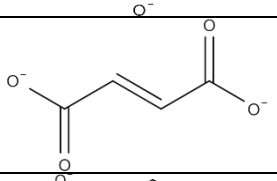	2.21	-4.0
glycine	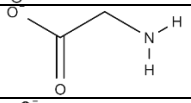	0.84	-3.1
glyoxylate	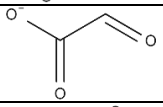	1.68	-3.6
lactate	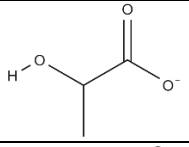	1.24	-3.6
malate	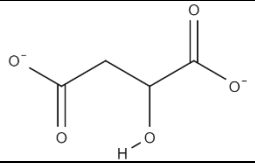	3.42	-4.4

oxaloacetate	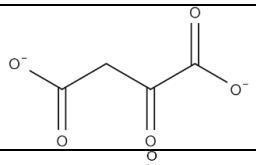	1.21	-4.6
pyruvate	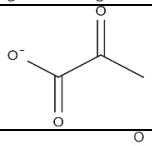	1.74	-3.8
succinate	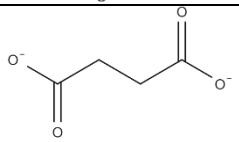	2.30	-4.3

[1]The docked carbonate results have two values, the first being the measurements of the docking result at the CO_3^{2-}-1 position (solvent exposed carbonate) and the second being the CO_3^{2-}-2 position (buried carbonate).

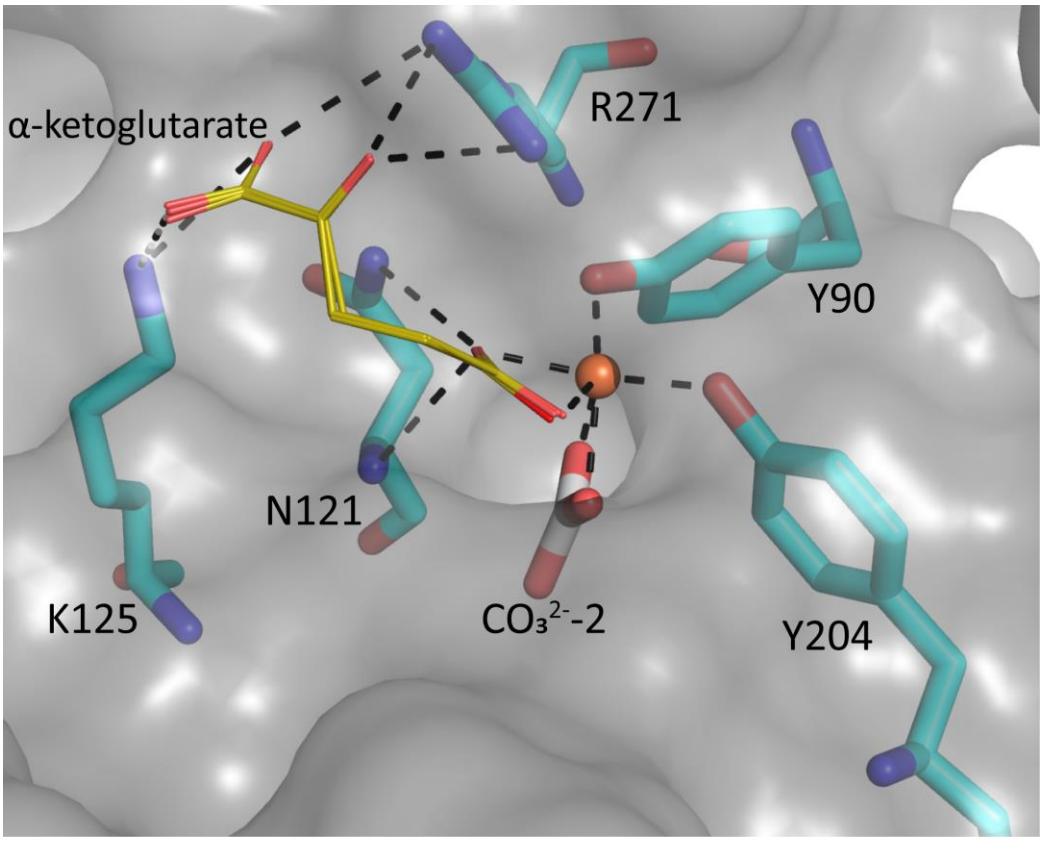

Figure 3-7. Docking poses of α-ketoglutarate and the possible interaction in MsTsf1 N-lobe. A surface representation of the predicted interactions of α-ketoglutarate (gold stick) with iron and residues Asn121, Lys125, and Arg271 (cyan). Predicted bonds are shown as dashed lines and are within 3.5 Å. The Fe^{3+} ion (brown sphere) and known coordinating ligands, Tyr90 and Tyr204, and CO_3^{2-}-2 are also shown.

To assess the robustness of the search area and docking parameters, two controls were applied to the study. As a positive control, carbonate was redocked in the structure. This proved to be a good control, as it was the only anion that had poses at the CO_3^{2-}-1 and CO_3^{2-}-2 positions (Figure 3-16M); moreover, carbonate had low RMSD values for both positions (CO_3^{2-}-1 = 1.16 Å and CO_3^{2-}-2 = 0.27 Å). The cation phosphonium was used as a negative control because of its positive charge. The average energy of the phosphonium binding poses was considerably higher (-0.5 kcal/mol) than all the anions and had no poses near the iron binding site.

Discussion

Previous studies have provided bioinformatic and biochemical evidence that that Tsf1s have different iron binding properties than the well-characterized vertebrate transferrins (Geiser and Winzerling, 2012; Lambert et al., 2005; Najera et al., 2021; Weber et al., 2020). Most Tsf1s have only one iron-binding site, and it is found in the N-lobe (Geiser and Winzerling, 2012; Lambert et al., 2005; Najera et al., 2021; Weber et al., 2020). Moreover, while Tsf1s are predicted to have two tyrosines at the iron binding site, the histidine and, in many species, the aspartate are substituted with other amino acid residues. In addition, Tsf1 and vertebrate transferrins differ in their spectroscopic properties (Weber et al., 2020). Despite these differences between Tsf1s and vertebrate transferrins, DmTsf1 and MsTsf1 bind iron tightly and reversibly (Weber et al., 2020).

This structural analysis of MsTsf1 verifies that one iron binding site is present in the N-lobe but not the C-lobe. It also demonstrates that the iron binding site differs from other transferrin structures. The distorted octahedral coordination of the Fe^{3+} is mediated by two N2 domain residues, Tyr90 and Tyr204, and two carbonate anions. These two tyrosine ligands and

the residues that hydrogen bond with the two carbonates, Thr116, Arg120, Asn121, Val122 and Gly123, are highly conserved in all available Tsf1 sequences, leading us to believe that similar coordination is likely to occur in other species of insects. The use of a second carbonate instead of histidine and aspartate in iron coordination explains the differences in the spectroscopic characteristics of Tsf1s compared to serum transferrin and lactoferrin (Weber et al., 2020). One of the carbonate anions, CO_3^{2-}-2, is buried behind the Fe^{3+} in a pocket within the N1 domain and adopts a similar position observed for the structures of other transferrins (Anderson et al., 1989, 1987; Bailey et al., 1988; Kurokawa et al., 1995). The other carbonate, CO_3^{2-}-1, is more solvent exposed and held in place through hydrogen bounds with Asn121 which is also involved in intralobe contacts within the N-lobe. The intralobe contacts suggest that Asn121 influences the integrity of the iron binding site during expected conformational changes.

The overall structure of MsTsf1 is bilobal, with each lobe separated into two domains, forming folds similar to those of vertebrate transferrin structures (Anderson et al., 1989, 1987; Bailey et al., 1988; Kurokawa et al., 1995). However, the orientation of the MsTsf1 C-lobe differs from other transferrin structures in that it is rotated approximately 180˚ from the core of the N-lobe. Thus, the interaction of the C1 domain with the N1 and N2 domains is at the opening of the N-lobe cleft. The C1 domain appears to act as a wedge between the N1 and N2 domains, hindering further closing of the N-lobe around the iron binding site. This most likely explains why the first several hits of the DALI search were vertebrate transferrin structures in the open conformation. The glycosylation site of MsTsf1 at Asn337 makes it unlikely that the C-lobe orientation is induced by crystal contacts, because the glycosylation at Asn337 is positioned on the backside of the N-lobe cleft, near the hinge-like region, thereby sterically inhibiting the C-lobe from the positioning itself like the vertebrate transferrin structures.

The finding of iron-bound MsTsf1 in an open conformation was surprising. However, our docking study provides evidence that this conformation results in a solvent exposed anion binding site that is accessible to several different organic anions found in insect hemolymph. The concentration of carbonate (10 mM) in Manduca sexta hemolymph (Jungreis, 1978) is similar to other organic anions, many of which fall within the 3-7 mM range in similar lepidopteran insects (Wyatt, 1961). With the numerous organic anions found in insect hemolymph and their fluctuating concentrations during development (Jungreis, 1978; Phalaraksh et al., 2008; Wyatt, 1961), this flexibility to bind alternative anions could be functionally significant.

The functional role of the C-lobe in Tsf1s is still unknown. In the MsTsf1 structure, the C-lobe is in a novel orientation that makes contacts with the N-lobe domains and likely stabilizes the tertiary structure. However, why the C-lobe adopts a secondary structure similar to vertebrate transferrins but does not bind iron, remains unknown. One hypothesis is that the C-lobe could act as a decoy for receptors of iron scavenging pathogens (Noinaj et al., 2012; Yoshiga et al., 1997). Future work is needed to elucidate the conformational changes and interplay between domains that takes place in MsTsf1.

In summary, this paper describes the first structure of an insect transferrin and details several novel structural features, including iron coordination, domain interactions, C-lobe orientation, and glycosylation position. Two tyrosines from the N2 domain and two carbonate anions coordinate iron binding. The C1 domain is wedged at the cleft opening between the N1 and N2 domains. The unique properties of this transferrin structure illustrate the important fact that insect and vertebrate transferrins have evolved different structural features, and suggest that Tsf1s have different mechanisms for carrying out their proposed roles in iron homeostasis. It will

be important to consider these differences when evaluating model insect studies of iron homeostasis and iron-related diseases of humans.

Future Directions

The investigation of the first Tsf1 structure was exciting and provided several explanations to previous questions about iron coordination in Tsf1s, but the findings in this chapter also brought about a series of new questions for future studies:

(1) In the vertebrate transferrin structures, there are large tertiary movements of the domains when the proteins change conformations from their apo- to holo-form. So, what does the apo-structure of MsTsf1 look like? Towards answering this question, we have sent apo-MsTsf1 to our collaborators to see if we can obtain its crystal structure. Also, following this study, a qualitative study of apo-MsTsf1 secondary structure was performed utilizing circular dichroism and compared to holo-MsTsf1 (discussed in Chapter 4).

(2) This study showed that the solvent exposed carbonate is hydrogen bonded with Asn121, and that this Asn121 is conserved in most Tsf1 sequences. Based on these findings, future work focused on determining the importance of Asn121 in anion binding and iron coordination (discussed in Chapter 4).

(3) The docking analysis of various other anions found in insect hemolymph showed that they could potentially bind at the solvent-exposed anion position. Future work could focus on *in vitro* experiments to test this hypothesis. The difficulty in these experiments would be to make carbonate free-conditions in which the binding of anion could be read by UV-Vis spectroscopy, but this can be done following previous methods used for studies of vertebrate transferrins (Schlabach and Bates, 1975; Dubach et al., 1991).

Acknowledgements

I would like to thank our collaborator Dr. Scott Lovell at the University of Kansas for his major contribution to this study, including obtaining this structure, his thorough report on his team's findings, and his helpful comments and edits that went into the publishing the manuscript this chapter is based on. I would also like to thank Dr. Brian Geisbrecht for helpful suggestions regarding the crystallization and protein preparation, and Dr. Gorman and Dr. Kanost for their suggestions and aid in writing the manuscript. This work was supported by National Science Foundation Grant 1656388, National Institute of General Medical Sciences grant R37 GM041247 and grant R35 GM130354 and the Johnson Cancer Research Center. This is contribution 21-023-J from the Kansas Agricultural Experiment Station. Use of the IMCA-CAT beamline 17-ID at the Advanced Photon Source was supported by the companies of the Industrial Macromolecular Crystallography Association through a contract with Hauptman-Woodward Medical Research Institute. Use of the Advanced Photon Source was supported by the U.S. Department of Energy, Office of Science, Office of Basic Energy Sciences, under Contract No. DE-AC02-06CH11357.

References

Abrahams, J.P., Leslie, A.G., 1996. Methods used in the structure determination of bovine mitochondrial F1 ATPase. Acta Crystallogr. D Biol. Crystallogr. 52, 30–42. https://doi.org/10.1107/S0907444995008754

Aisen, P., Leibman, A., Zweier, J., 1978. Stoichiometric and site characteristics of the binding of iron to human transferrin. J. Biol. Chem. 253, 1930–1937.

Anderson, B.F., Baker, H.M., Dodson, E.J., Norris, G.E., Rumball, S.V., Waters, J.M., Baker, E.N., 1987. Structure of human lactoferrin at 3.2-A resolution. Proc. Natl. Acad. Sci. U.S.A. 84, 1769–1773. https://doi.org/10.1073/pnas.84.7.1769

Anderson, B.F., Baker, H.M., Norris, G.E., Rice, D.W., Baker, E.N., 1989. Structure of human lactoferrin: crystallographic structure analysis and refinement at 2.8 A resolution. J. Mol. Biol. 209, 711–734. https://doi.org/10.1016/0022-2836(89)90602-5

Bailey, S., Evans, R.W., Garratt, R.C., Gorinsky, B., Hasnain, S., Horsburgh, C., Jhoti, H., Lindley, P.F., Mydin, A., Sarra, R., 1988. Molecular structure of serum transferrin at 3.3-A resolution. Biochemistry 27, 5804–5812. https://doi.org/10.1021/bi00415a061

Baker, E.N., 1994. Structure and Reactivity of Transferrins, in: Sykes, A.G. (Ed.), Advances in Inorganic Chemistry. Academic Press, pp. 389–463. https://doi.org/10.1016/S0898-8838(08)60176-2

Baker, E.N., Baker, H.M., 2009. A structural framework for understanding the multifunctional character of lactoferrin. Biochimie, Advances in Lactoferrin Research 91, 3–10. https://doi.org/10.1016/j.biochi.2008.05.006

Baker, H.M., Baker, E.N., 2012. A structural perspective on lactoferrin function. Biochemistry and Cell Biology 90, 320–328.

Bartfeld, N.S., Law, J.H., 1990. Isolation and molecular cloning of transferrin from the tobacco hornworm, Manduca sexta. Sequence similarity to the vertebrate transferrins. Journal of Biological Chemistry 265, 21684–21691. https://doi.org/10.1016/S0021-9258(18)45794-8

Brandts, J.F., Lin, L.N., 1990. Study of strong to ultratight protein interactions using differential scanning calorimetry. Biochemistry 29, 6927–6940. https://doi.org/10.1021/bi00481a024

Brummett, L.M., Kanost, M.R., Gorman, M.J., 2017. The immune properties of Manduca sexta transferrin. Insect Biochem. Mol. Biol. 81, 1–9. https://doi.org/10.1016/j.ibmb.2016.12.006

Chen, V.B., Arendall, W.B., Headd, J.J., Keedy, D.A., Immormino, R.M., Kapral, G.J., Murray, L.W., Richardson, J.S., Richardson, D.C., 2010. MolProbity: all-atom structure validation for macromolecular crystallography. Acta Crystallogr. D Biol. Crystallogr. 66, 12–21. https://doi.org/10.1107/S0907444909042073

Cowtan, K., 2006. The Buccaneer software for automated model building. 1. Tracing protein chains. Acta Crystallogr. D Biol. Crystallogr. 62, 1002–1011. https://doi.org/10.1107/S0907444906022116

Day, C.L., Stowell, K.M., Baker, E.N., Tweedie, J.W., 1992. Studies of the N-terminal half of human lactoferrin produced from the cloned cDNA demonstrate that interlobe interactions modulate iron release. J. Biol. Chem. 267, 13857–13862.

Diederichs, K., Karplus, P.A., 1997. Improved R -factors for diffraction data analysis in macromolecular crystallography. Nature Structural Biology 4, 269–275. https://doi.org/10.1038/nsb0497-269

Dubach, J., Gaffney, B.J., More, K., Eaton, G.R., Eaton, S.S., 1991. Effect of the synergistic anion on electron paramagnetic resonance spectra of iron-transferrin anion complexes is consistent with bidentate binding of the anion. Biophysical Journal 59, 1091–1100. https://doi.org/10.1016/S0006-3495(91)82324-4

Eckenroth, B.E., Steere, A.N., Chasteen, N.D., Everse, S.J., Mason, A.B., 2011. How the binding of human transferrin primes the transferrin receptor potentiating iron release at endosomal pH. Proc Natl Acad Sci USA 108, 13089–13094. https://doi.org/10.1073/pnas.1105786108

Emsley, P., Lohkamp, B., Scott, W.G., Cowtan, K., 2010. Features and development of Coot. Acta Crystallogr. D Biol. Crystallogr. 66, 486–501. https://doi.org/10.1107/S0907444910007493

Evans, P., 2012. Resolving Some Old Problems in Protein Crystallography. Science 336, 986–987. https://doi.org/10.1126/science.1222162

Evans, P., 2006. Scaling and assessment of data quality. Acta Crystallogr. D Biol. Crystallogr. 62, 72–82. https://doi.org/10.1107/S0907444905036693

Evans, P.R., 2011. An introduction to data reduction: space-group determination, scaling and intensity statistics. Acta Crystallogr. D Biol. Crystallogr. 67, 282–292. https://doi.org/10.1107/S090744491003982X

Farnaud, S., Evans, R.W., 2003. Lactoferrin--a multifunctional protein with antimicrobial properties. Mol. Immunol. 40, 395–405. https://doi.org/10.1016/s0161-5890(03)00152-4

Geiser, D.L., Winzerling, J.J., 2012. Insect transferrins: multifunctional proteins. Biochim. Biophys. Acta 1820, 437–451. https://doi.org/10.1016/j.bbagen.2011.07.011

Giansanti, F., Leboffe, L., Pitari, G., Ippoliti, R., Antonini, G., 2012. Physiological roles of ovotransferrin. Biochim. Biophys. Acta 1820, 218–225. https://doi.org/10.1016/j.bbagen.2011.08.004

Halbrooks, P.J., Mason, A.B., Adams, T.E., Briggs, S.K., Everse, S.J., 2004. The Oxalate Effect on Release of Iron from Human Serum Transferrin Explained. Journal of Molecular Biology 339, 217–226. https://doi.org/10.1016/j.jmb.2004.03.049

Harris, W.R., 2012. Anion binding properties of the transferrins. Implications for function. Biochimica et Biophysica Acta (BBA) - General Subjects 1820, 348–361. https://doi.org/10.1016/j.bbagen.2011.07.017

Holm, L., 2020. DALI and the persistence of protein shape. Protein Science 29, 128–140. https://doi.org/10.1002/pro.3749

Holm, L., Laakso, L.M., 2016. Dali server update. Nucleic Acids Res 44, W351–W355. https://doi.org/10.1093/nar/gkw357

Holm, L., Rosenström, P., 2010. Dali server: conservation mapping in 3D. Nucleic Acids Res 38, W545–W549. https://doi.org/10.1093/nar/gkq366

Huebers, H.A., Huebers, E., Finch, C.A., Webb, B.A., Truman, J.W., Riddiford, L.M., Martin, A.W., Massover, W.H., 1988. Iron binding proteins and their roles in the tobacco hornworm, Manduca sexta (L.). J. Comp. Physiol. B, Biochem. Syst. Environ. Physiol. 158, 291–300. https://doi.org/10.1007/bf00695327

Iatsenko, I., Marra, A., Boquete, J.-P., Peña, J., Lemaitre, B., 2020. Iron sequestration by transferrin 1 mediates nutritional immunity in Drosophila melanogaster. PNAS 117, 7317–7325. https://doi.org/10.1073/pnas.1914830117

Jenssen, H., Hancock, R.E.W., 2009. Antimicrobial properties of lactoferrin. Biochimie 91, 19–29. https://doi.org/10.1016/j.biochi.2008.05.015

Jungreis, A.M., 1978. The composition of larval-pupal moulting fluid in the tobacco hornworm, Manduca sexta. Journal of Insect Physiology 24, 65–73. https://doi.org/10.1016/0022-1910(78)90013-6

Jurrus, E., Engel, D., Star, K., Monson, K., Brandi, J., Felberg, L.E., Brookes, D.H., Wilson, L., Chen, J., Liles, K., Chun, M., Li, P., Gohara, D.W., Dolinsky, T., Konecny, R., Koes, D.R., Nielsen, J.E., Head-Gordon, T., Geng, W., Krasny, R., Wei, G.-W., Holst, M.J., McCammon, J.A., Baker, N.A., 2018. Improvements to the APBS biomolecular solvation software suite. Protein Sci. 27, 112–128. https://doi.org/10.1002/pro.3280

Kabsch, W., 2010. XDS. Acta Cryst D 66, 125–132. https://doi.org/10.1107/S0907444909047337

Kabsch, W., 1988. Automatic indexing of rotation diffraction patterns. J Appl Cryst 21, 67–72. https://doi.org/10.1107/S0021889887009737

Karplus, P.A., Diederichs, K., 2012. Linking Crystallographic Model and Data Quality. Science 336, 1030–1033. https://doi.org/10.1126/science.1218231

Kim, B.Y., Lee, K.S., Choo, Y.M., Kim, I., Je, Y.H., Woo, S.D., Lee, S.M., Park, H.C., Sohn, H.D., Jin, B.R., 2008. Insect transferrin functions as an antioxidant protein in a beetle larva. Comp. Biochem. Physiol. B, Biochem. Mol. Biol. 150, 161–169. https://doi.org/10.1016/j.cbpb.2008.02.009

Kurama, T., Kurata, S., Natori, S., 1995. Molecular Characterization of an Insect Transferrin and its Selective Incorporation into Eggs During Oogenesis. European Journal of Biochemistry 228, 229–235. https://doi.org/10.1111/j.1432-1033.1995.0229n.x

Kurokawa, H., Mikami, B., Hirose, M., 1995. Crystal structure of diferric hen ovotransferrin at 2.4 A resolution. J. Mol. Biol. 254, 196–207. https://doi.org/10.1006/jmbi.1995.0611

Lambert, L.A., 2012. Molecular evolution of the transferrin family and associated receptors. Biochim. Biophys. Acta 1820, 244–255. https://doi.org/10.1016/j.bbagen.2011.06.002

Lambert, L.A., Perri, H., Halbrooks, P.J., Mason, A.B., 2005. Evolution of the transferrin family: conservation of residues associated with iron and anion binding. Comp. Biochem. Physiol. B, Biochem. Mol. Biol. 142, 129–141. https://doi.org/10.1016/j.cbpb.2005.07.007

Le Guilloux, V., Schmidtke, P., Tuffery, P., 2009. Fpocket: An open source platform for ligand pocket detection. BMC Bioinformatics 10, 168. https://doi.org/10.1186/1471-2105-10-168

Lee, K.S., Kim, B.Y., Kim, H.J., Seo, S.J., Yoon, H.J., Choi, Y.S., Kim, I., Han, Y.S., Je, Y.H., Lee, S.M., Kim, D.H., Sohn, H.D., Jin, B.R., 2006. Transferrin inhibits stress-induced apoptosis in a beetle. Free Radical Biology and Medicine 41, 1151–1161. https://doi.org/10.1016/j.freeradbiomed.2006.07.001

Madeira, F., Park, Y.M., Lee, J., Buso, N., Gur, T., Madhusoodanan, N., Basutkar, P., Tivey, A.R.N., Potter, S.C., Finn, R.D., Lopez, R., 2019. The EMBL-EBI search and sequence analysis tools APIs in 2019. Nucleic Acids Res. 47, W636–W641. https://doi.org/10.1093/nar/gkz268

McCoy, A.J., Grosse-Kunstleve, R.W., Adams, P.D., Winn, M.D., Storoni, L.C., Read, R.J., 2007. Phaser crystallographic software. J Appl Cryst 40, 658–674. https://doi.org/10.1107/S0021889807021206

Mizutani, K., Mikami, B., Hirose, M., 2001. Domain closure mechanism in transferrins: new viewpoints about the hinge structure and motion as deduced from high resolution crystal structures of ovotransferrin N-lobe. Journal of Molecular Biology 309, 937–947. https://doi.org/10.1006/jmbi.2001.4719

Mizutani, K., Toyoda, M., Mikami, B., 2012. X-ray structures of transferrins and related proteins. Biochimica et Biophysica Acta (BBA) - General Subjects, Transferrins: Molecular mechanisms of iron transport and disorders 1820, 203–211. https://doi.org/10.1016/j.bbagen.2011.08.003

Murshudov, G.N., Vagin, A.A., Dodson, E.J., 1997. Refinement of Macromolecular Structures by the Maximum-Likelihood Method. Acta Cryst D 53, 240–255. https://doi.org/10.1107/S0907444996012255

Najera, D.G., Dittmer, N.T., Weber, J.J., Kanost, M.R., Gorman, M.J., 2021. Phylogenetic and sequence analyses of insect transferrins suggest that only transferrin 1 has a role in iron homeostasis. Insect Science 28, 495–508. https://doi.org/10.1111/1744-7917.12783

Noinaj, N., Easley, N.C., Oke, M., Mizuno, N., Gumbart, J., Boura, E., Steere, A.N., Zak, O., Aisen, P., Tajkhorshid, E., Evans, R.W., Gorringe, A.R., Mason, A.B., Steven, A.C., Buchanan, S.K., 2012. Structural basis for iron piracy by pathogenic Neisseria. Nature 483, 53–58. https://doi.org/10.1038/nature10823

O'Boyle, N.M., Banck, M., James, C.A., Morley, C., Vandermeersch, T., Hutchison, G.R., 2011. Open Babel: An open chemical toolbox. Journal of Cheminformatics 3, 33. https://doi.org/10.1186/1758-2946-3-33

Octave, J.-N., Schneider, Y.-J., Trouet, A., Crichton, R.R., 1983. Iron uptake and utilization by mammalian cells. I: Cellular uptake of transferrin and iron. Trends in Biochemical Sciences 8, 217–220. https://doi.org/10.1016/0968-0004(83)90217-7

Pakdaman, R., Petitjean, M., Chahine, J.-M.E.H., 1998. Transferrins. European Journal of Biochemistry 254, 144–153. https://doi.org/10.1046/j.1432-1327.1998.2540144.x

Phalaraksh, C., E. Reynolds, S., D. Wilson, I., M. Lenz, E., K. Nicholson, J., C. Lindon, J., 2008. A metabonomic analysis of insect development: 1H-NMR spectroscopic characterization of changes in the composition of the haemolymph of larvae and pupae of the tobacco hornworm, Manduca sexta. ScienceAsia 34, 279. https://doi.org/10.2306/scienceasia1513-1874.2008.34.279

Pitti, T., Chen, C.-T., Lin, H.-N., Choong, W.-K., Hsu, W.-L., Sung, T.-Y., 2019. N-GlyDE: a two-stage N-linked glycosylation site prediction incorporating gapped dipeptides and pattern-based encoding. Scientific Reports 9, 15975. https://doi.org/10.1038/s41598-019-52341-z

Potterton, L., McNicholas, S., Krissinel, E., Gruber, J., Cowtan, K., Emsley, P., Murshudov, G.N., Cohen, S., Perrakis, A., Noble, M., 2004. Developments in the CCP4 molecular-graphics project. Acta Crystallogr. D Biol. Crystallogr. 60, 2288–2294. https://doi.org/10.1107/S0907444904023716

Sanner, M.F., 1999. Python: a programming language for software integration and development. J. Mol. Graph. Model. 17, 57–61.

Schlabach, M.R., Bates, G.W., 1975. The synergistic binding of anions and Fe3+ by transferrin. Implications for the interlocking sites hypothesis. J. Biol. Chem. 250, 2182–2188.

Sheldrick, G.M., 2010. Experimental phasing with SHELXC/D/E: combining chain tracing with density modification. Acta Crystallogr. D Biol. Crystallogr. 66, 479–485. https://doi.org/10.1107/S0907444909038360

Skubák, P., Pannu, N.S., 2013. Automatic protein structure solution from weak X-ray data. Nat Commun 4, 2777. https://doi.org/10.1038/ncomms3777

Sun, H., Li, H., Sadler, P.J., 1999. Transferrin as a Metal Ion Mediator. Chem. Rev. 99, 2817–2842. https://doi.org/10.1021/cr980430w

Trott, O., Olson, A.J., 2010. AutoDock Vina: improving the speed and accuracy of docking with a new scoring function, efficient optimization and multithreading. J Comput Chem 31, 455–461. https://doi.org/10.1002/jcc.21334

UniProt: a worldwide hub of protein knowledge, 2019. . Nucleic Acids Res 47, D506–D515. https://doi.org/10.1093/nar/gky1049

Vonrhein, C., Flensburg, C., Keller, P., Sharff, A., Smart, O., Paciorek, W., Womack, T., Bricogne, G., 2011. Data processing and analysis with the autoPROC toolbox. Acta Cryst D 67, 293–302. https://doi.org/10.1107/S0907444911007773

Wally, J., Buchanan, S.K., 2007. A structural comparison of human serum transferrin and human lactoferrin. Biometals 20, 249–262. https://doi.org/10.1007/s10534-006-9062-7

Weber, J.J., Kanost, M.R., Gorman, M.J., 2020. Iron binding and release properties of transferrin-1 from Drosophila melanogaster and Manduca sexta: Implications for insect iron homeostasis. Insect Biochemistry and Molecular Biology 125, 103438. https://doi.org/10.1016/j.ibmb.2020.103438

Weiss, M.S., 2001. Global indicators of X-ray data quality. J Appl Cryst 34, 130–135. https://doi.org/10.1107/S0021889800018227

Winn, M.D., Ballard, C.C., Cowtan, K.D., Dodson, E.J., Emsley, P., Evans, P.R., Keegan, R.M., Krissinel, E.B., Leslie, A.G.W., McCoy, A., McNicholas, S.J., Murshudov, G.N., Pannu, N.S., Potterton, E.A., Powell, H.R., Read, R.J., Vagin, A., Wilson, K.S., 2011. Overview of the CCP4 suite and current developments. Acta Crystallogr. D Biol. Crystallogr. 67, 235–242. https://doi.org/10.1107/S0907444910045749

Wyatt, G.R., 1961. The Biochemistry of Insect Hemolymph. Annual Review of Entomology 6, 75–102. https://doi.org/10.1146/annurev.en.06.010161.000451

Xiao, G., Liu, Z.-H., Zhao, M., Wang, H.-L., Zhou, B., 2019. Transferrin 1 Functions in Iron Trafficking and Genetically Interacts with Ferritin in Drosophila melanogaster. Cell Rep 26, 748-758.e5. https://doi.org/10.1016/j.celrep.2018.12.053

Yang, N., Zhang, H., Wang, M., Hao, Q., Sun, H., 2012. Iron and bismuth bound human serum transferrin reveals a partially-opened conformation in the N-lobe. Sci Rep 2, 999. https://doi.org/10.1038/srep00999

Yoshiga, T., Hernandez, V.P., Fallon, A.M., Law, J.H., 1997. Mosquito transferrin, an acute-phase protein that is up-regulated upon infection. Proc. Natl. Acad. Sci. U.S.A. 94, 12337–12342. https://doi.org/10.1073/pnas.94.23.12337

Zhang, K.Y.J., Cowtan, K., Main, P., 1997. [4] Combining constraints for electron-density modification, in: Methods in Enzymology, Macromolecular Crystallography Part B. Academic Press, pp. 53–64. https://doi.org/10.1016/S0076-6879(97)77006-X

Supplementary Material

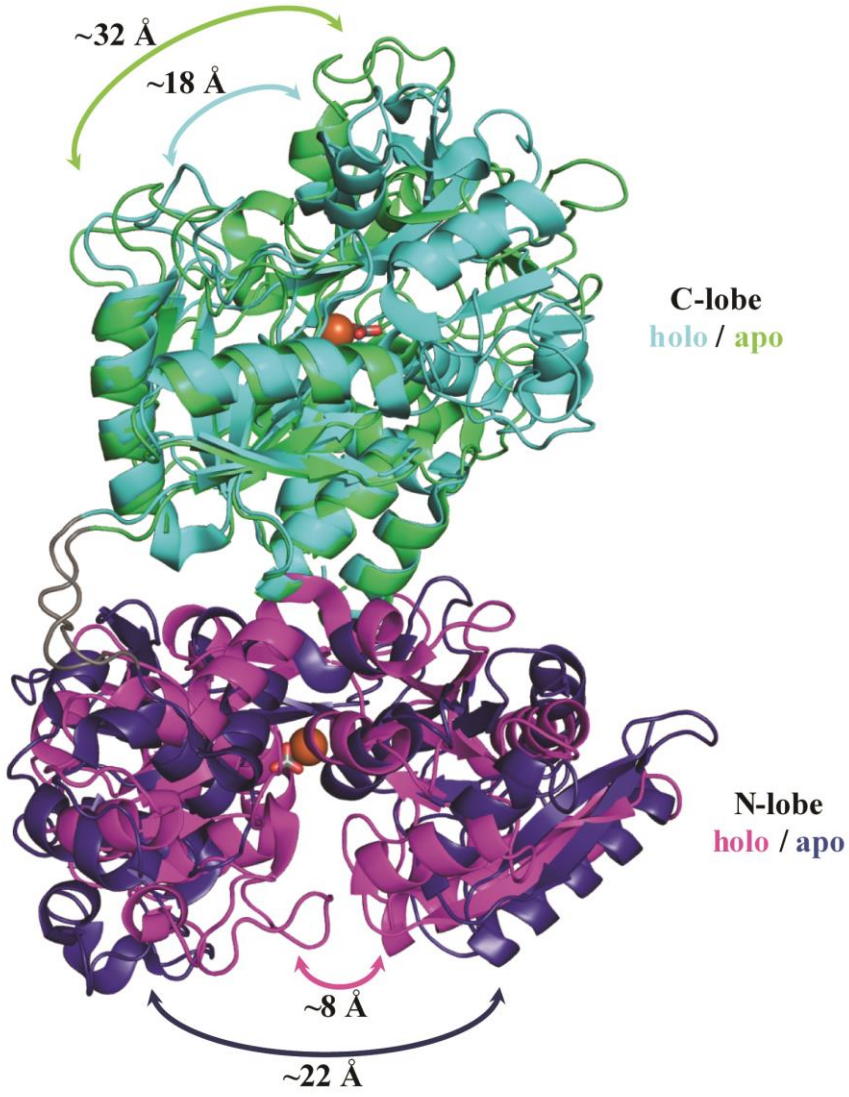

Figure 3-8. Comparison of human serum transferrin (hSTF) in the holo- and apo-form. Proteins used in alignment are as follows: apo form is PDB 2HAU; holo N-lobe, PDB 1D3K; holo C-lobe, PDB 3QYT. The domains are colored as follows. Holo-hSTF: magenta (N-lobe) and cyan (C-lobe); apo-hSTF: blue (N-lobe) and green (C-lobe).

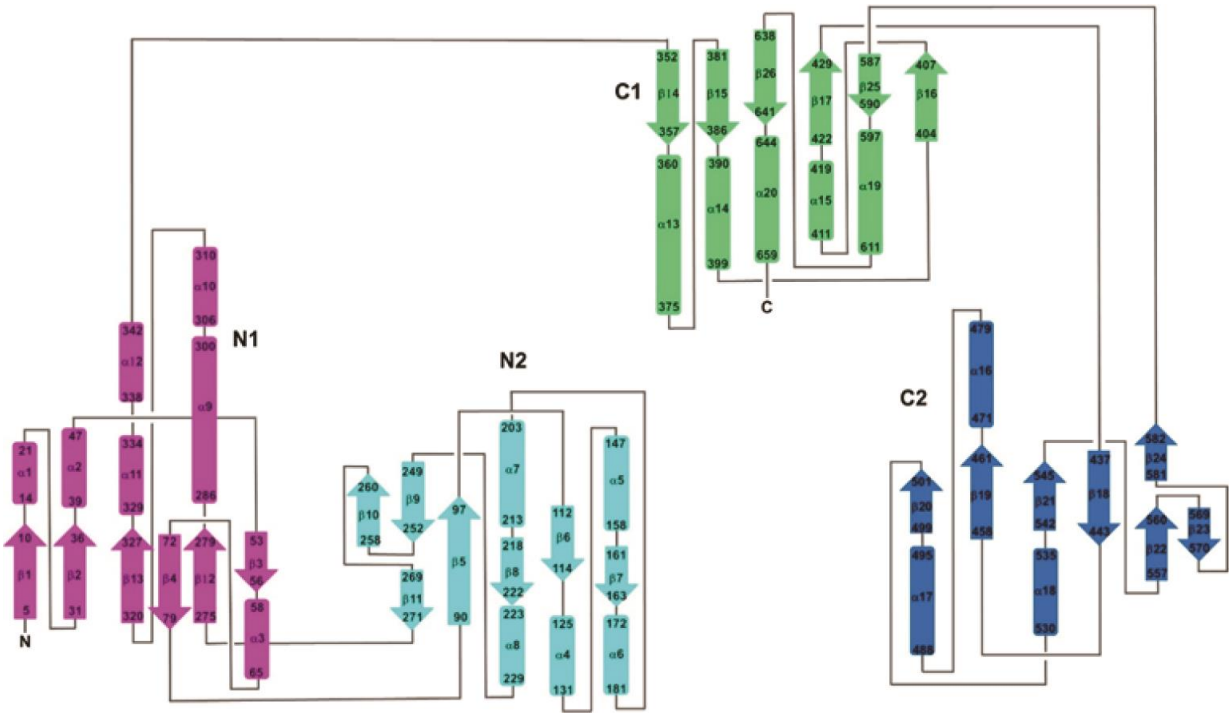

Figure 3-9. Topology diagram of MsTsf1 showing the helices (tubes) and strands (arrows) for each of the domains.

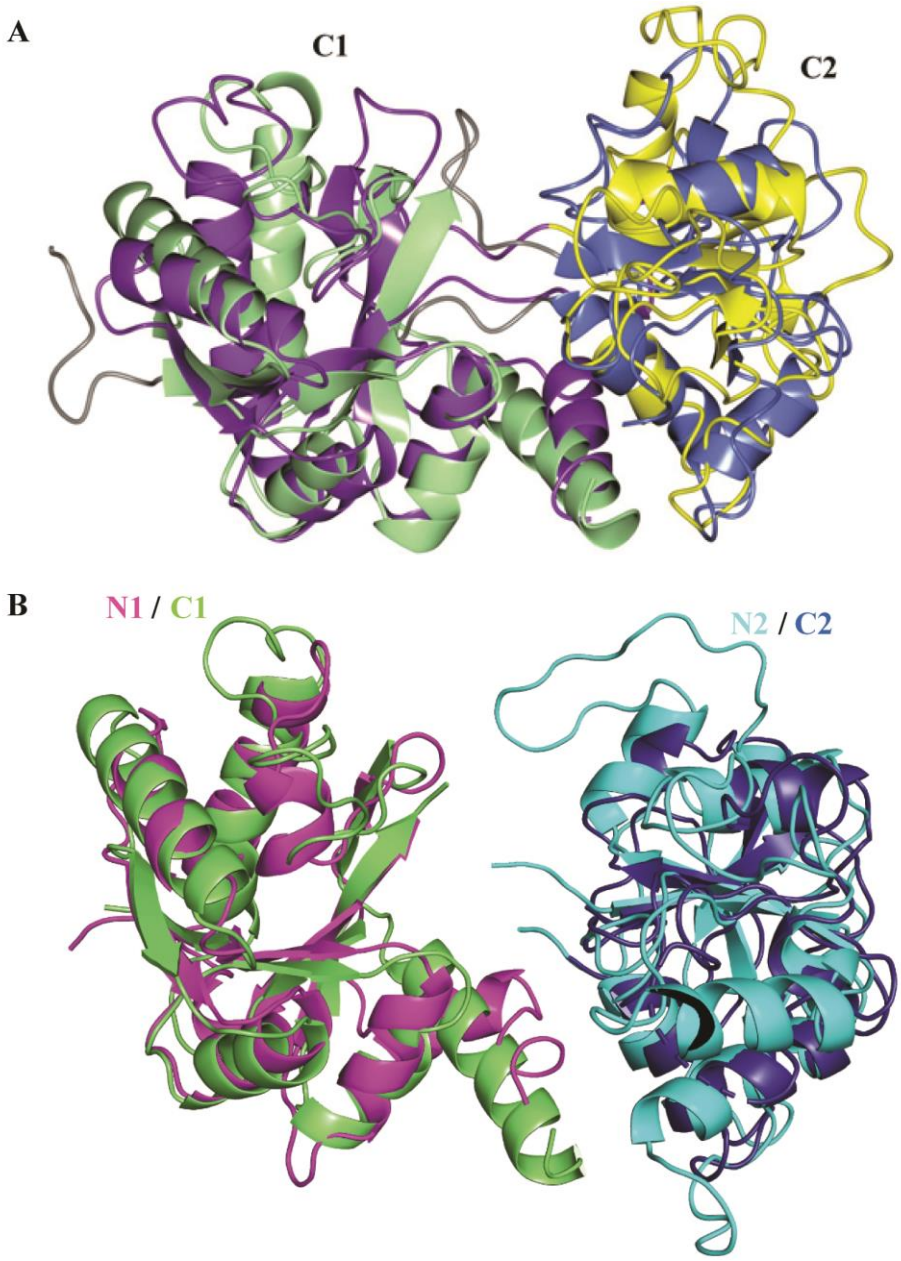

Figure 3-10. Structural alignments of transferrin lobes.

A) Comparison of the C-lobe of MsTsf1 with human serum transferrin (apo, PDB 2HAV). The domains are colored as follows. MsTsf1: green (C1) and blue (C2); 2HAV: purple (C1) and yellow (C2). B) Comparison of the N1- and C1 domains and the N2 and C2 domains of MsTsf1. The domains are colored as follows: magenta (N1), cyan (N2), green (C1) and blue (C2).

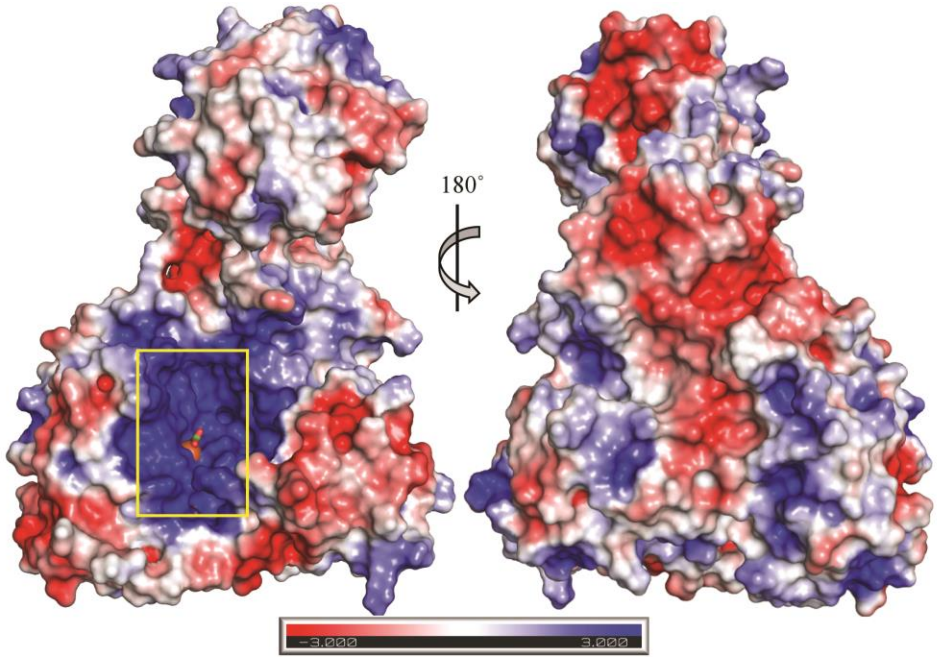

Figure 3-11. Electrostatic surface charge of MsTsf1.

A yellow box highlights the positive patch surrounding the Fe^{3+} binding site in the N-lobe. At the center of the yellow box is the bound Fe^{3+} (modeled as a tan sphere) and the solvent exposed CO_3^{2-} (shown in licorice). Electrostatic surface coloring ranges from -3 K_bT/e_c to +3 K_bT/e_c.

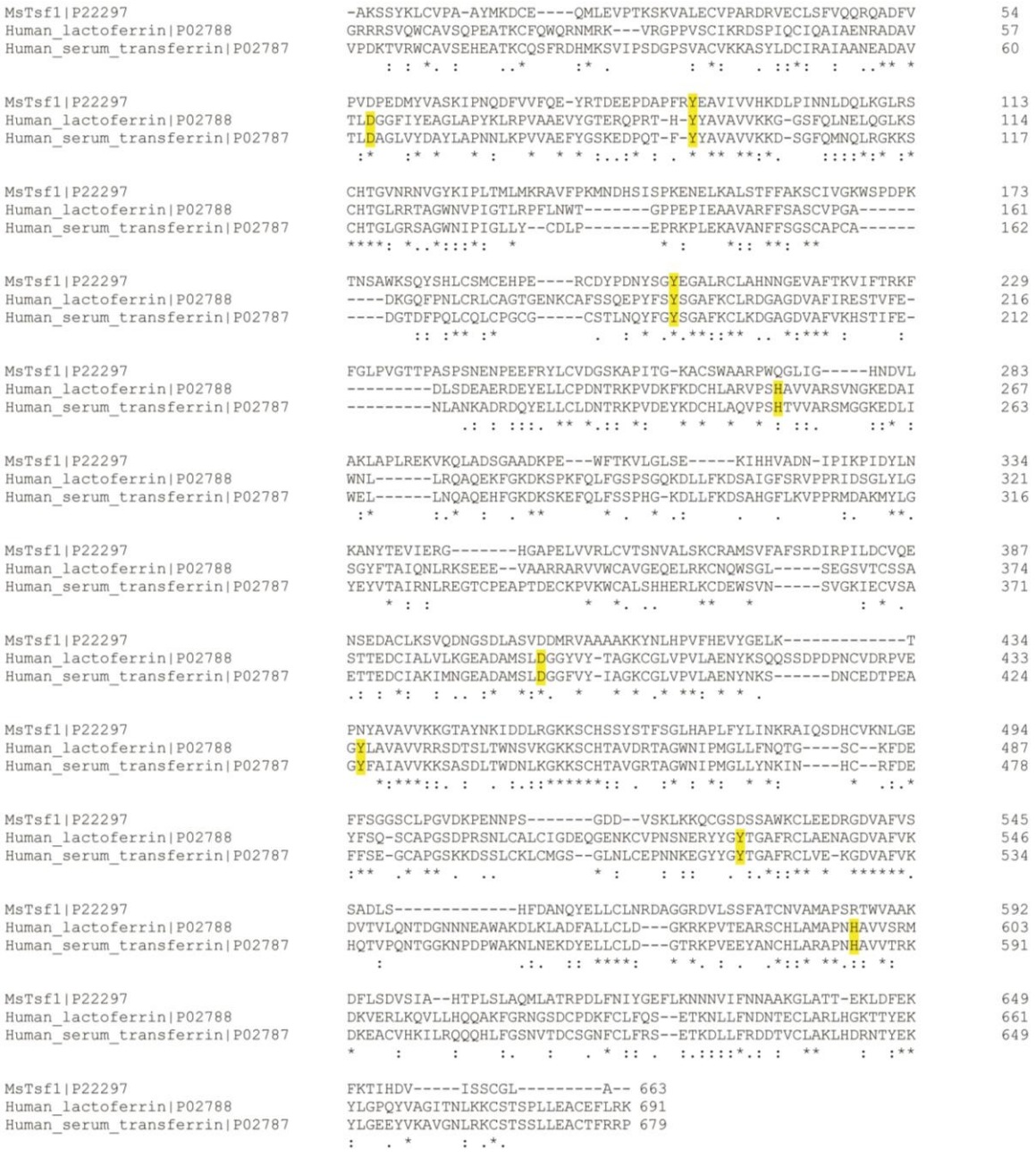

Figure 3-12. Sequence alignment of MsTsf1, human lactoferrin and human serum transferrin.

The iron binding residues are highlighted in yellow.

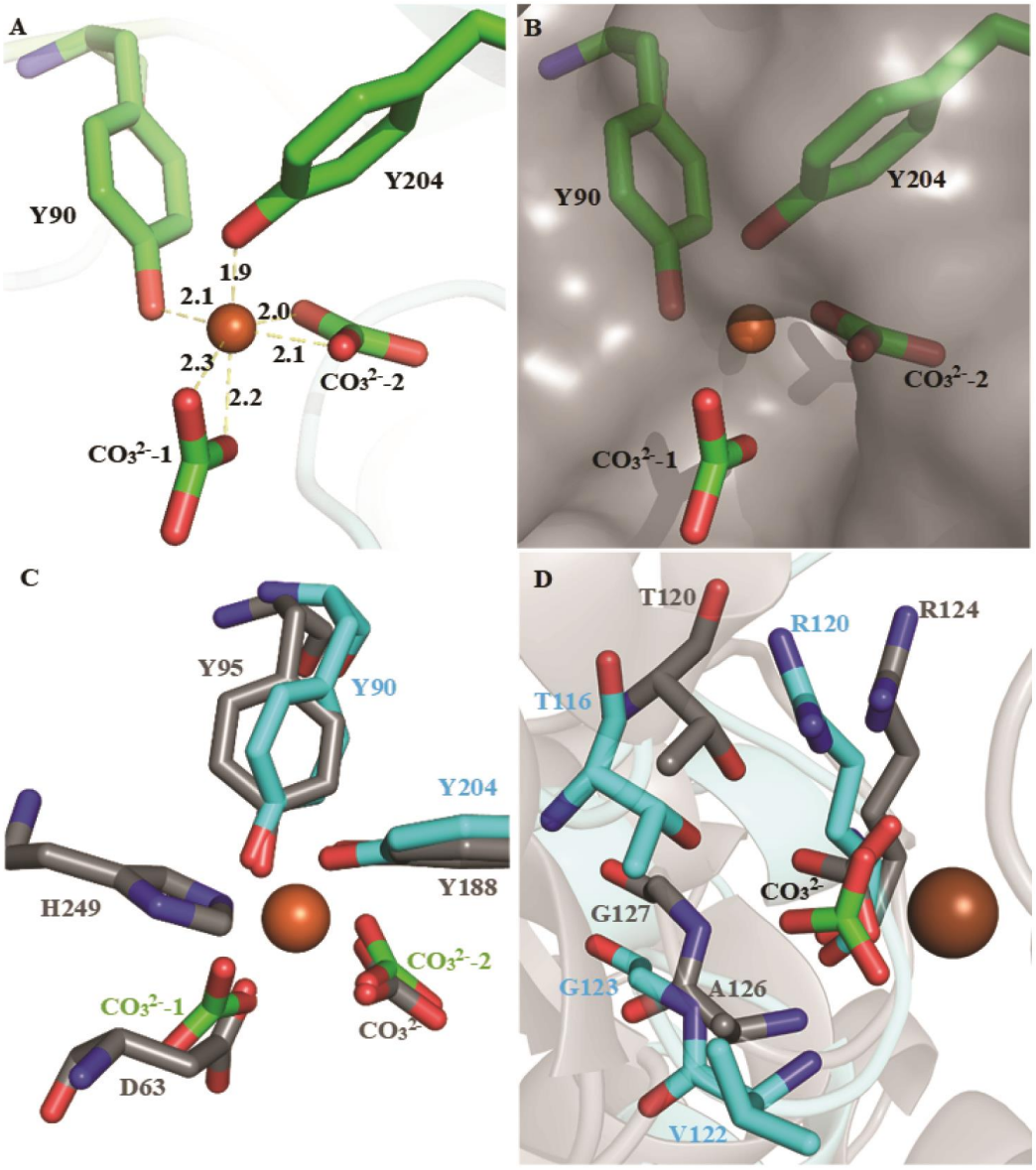

Figure 3-13. Characteristics of Fe^{3+} and carbonate coordination in MsTsf1.

A) Bond lengths (Å) of ligating residues and carbonates (green) to Fe^{3+} (tan sphere) showing the distorted octahedral coordination of Fe^{3+}. B) A surface representation of the Fe^{3+} site highlighting the difference in solvent exposure of the two ligating carbonate anions, CO_3^{2-}-1 and CO_3^{2-}-2. C) Superposition relative to the position of the Fe^{3+} in the binding site of MsTsf1 and in the N-lobe of human serum transferrin (PDB 1D3K). The Fe^{3+} coordinating residues of MsTsf1 are represented in cyan (licorice) and carbonates in green, while those of 1D3K are in grey (licorice). D) Superposition relative to the position of Fe^{3+} of the buried carbonate (CO_3^{2-}-2) (green) of MsTsf1 and the iron coordinating CO_3^{2-} (grey) of 1D3K. The CO_3^{2-} coordinating residues of MsTsf1 are represented in cyan (licorice) and those of 1D3K in grey (licorice).

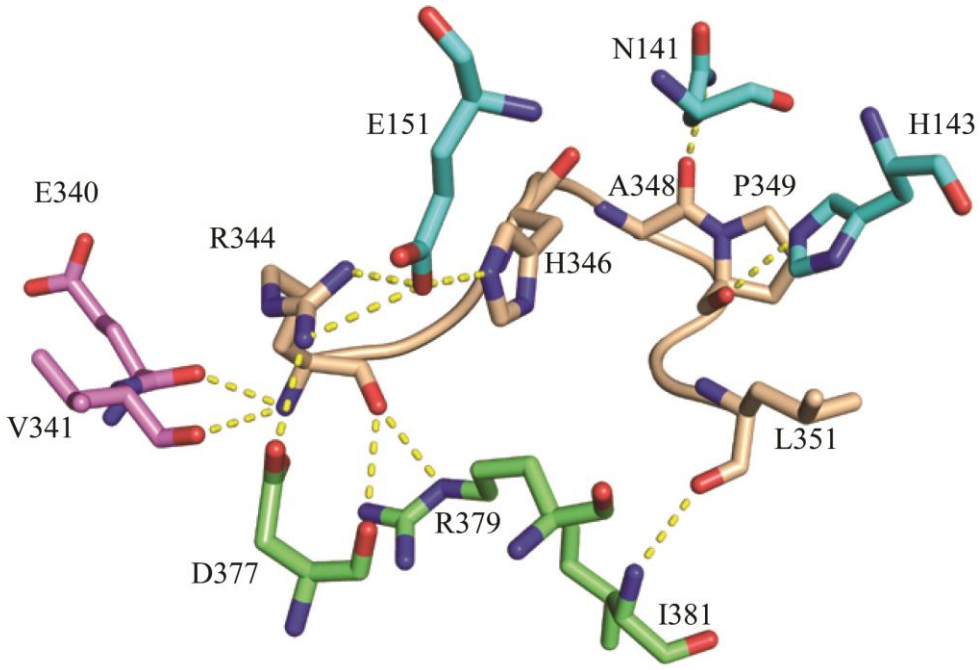

Figure 3-14. Non-covalent interactions between the linker peptide (wheat) and the N1 (magenta), N2 (cyan) and C1 (green) domains.

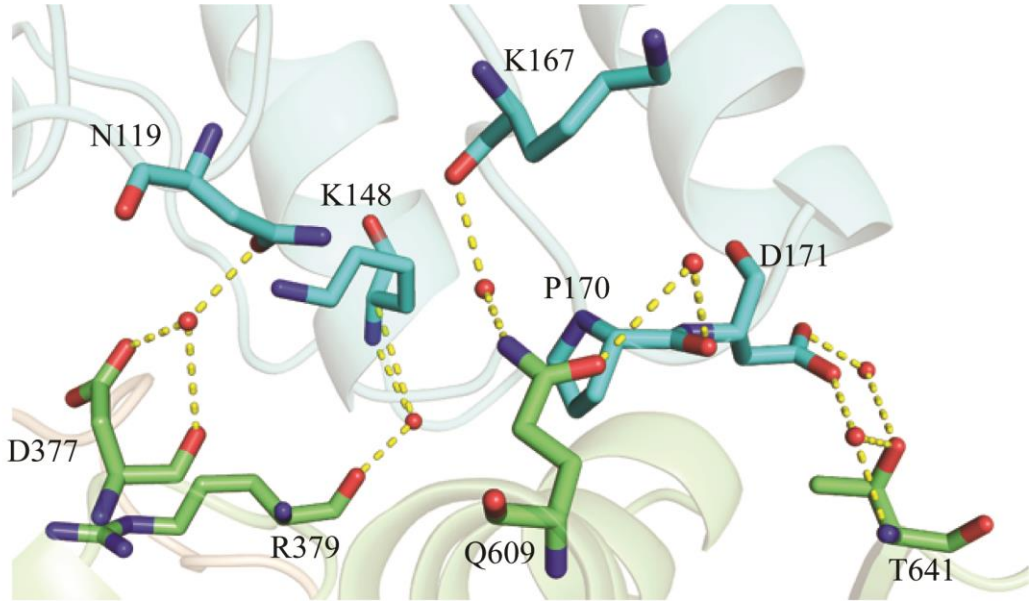

Figure 3-15. The mediated contacts between the C1 and N2 domains.

In the space between the two domains, side chain and backbone groups of residues from the C1-domain (Asp377, Arg379, Gln609 and Thr641) and the N2-domain (Asn119, Lys148, Lys167, Pro170 and Asp171) engage in hydrogen bonds with water molecules. Water molecules are rendered as red spheres and residues as licorice colored according to their domain.

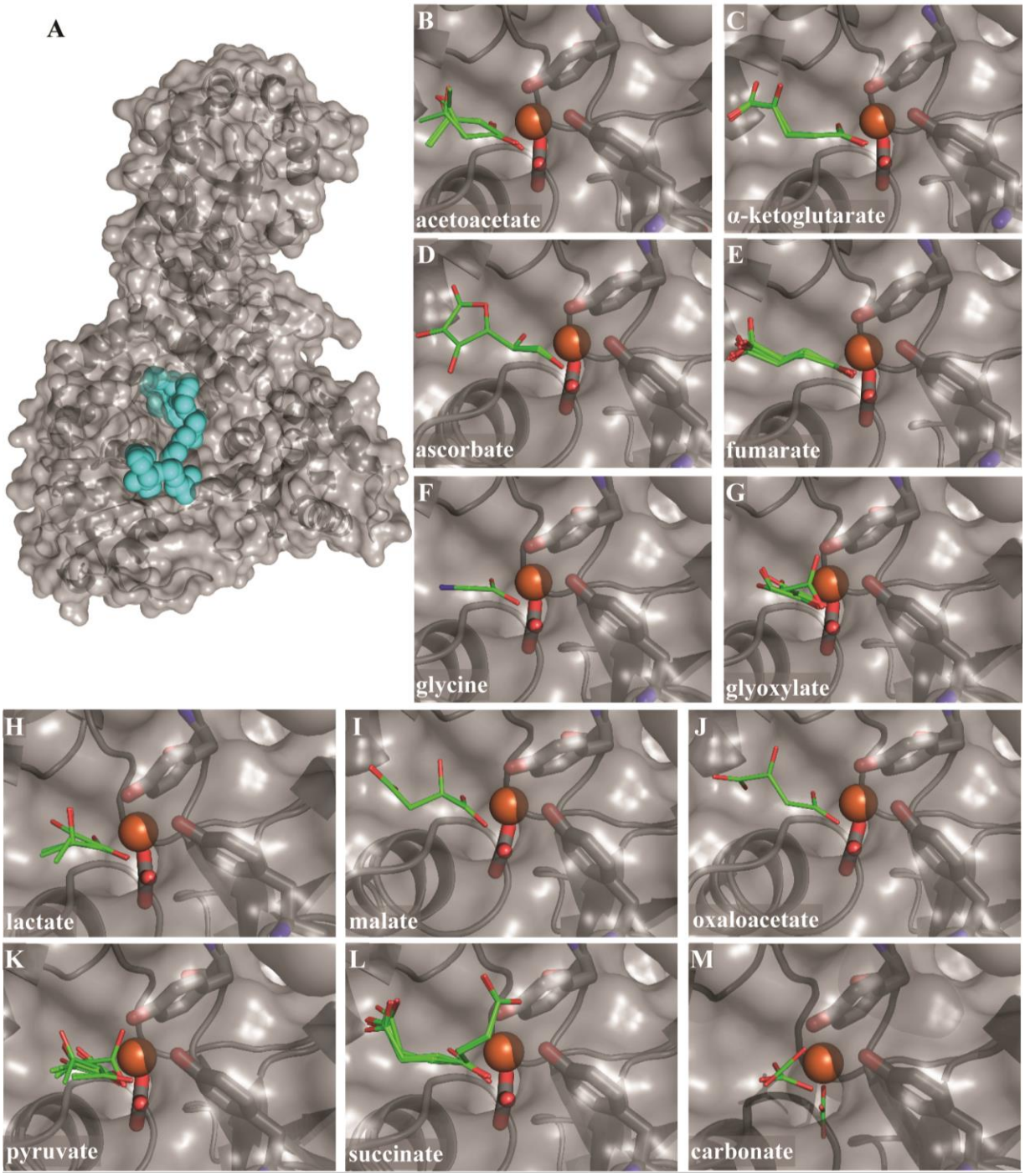

Figure 3-16. Results from docking study of organic anions in the N-lobe cleft of MsTsf1. A) Structure of MsTsf1 (grey cartoon and surface) and the identified searchable pockets in the cleft (cyan spheres). B-L) Poses of organic anions docked at the iron binding site of MsTsf1. Docked anions are modeled as green sticks, the ligating molecules, Tyr 90, Tyr204 and CO_3^{2-}-2, are modeled as grey licorice and the iron as a tan sphere. M) Poses of carbonate (green sticks) docked at both the solvent exposed (CO_3^{2-}-1) and buried position (CO_3^{2-}-2).

Table 3-4. Top 100 hits from the DALI search.

No:	Chain[a]	Z[b]	rmsd	lali[c]	nres[d]	%id[e]	Description
1:	1bp5-A	29.8	3.5	294	328	29	PROTEIN (SERUM TRANSFERRIN);
2:	6ctc-A	29.7	3.8	296	673	29	SEROTRANSFERRIN;
3:	5dyh-B	29.7	3.2	293	677	29	SEROTRANSFERRIN;
4:	1bp5-B	29.7	3.6	294	328	29	PROTEIN (SERUM TRANSFERRIN);
5:	5x5p-A	29.6	3.6	295	649	29	SEROTRANSFERRIN;
6:	6jas-A	29.5	3.6	295	656	29	SEROTRANSFERRIN;
7:	2hav-B	29.4	3.2	292	676	30	SEROTRANSFERRIN;
8:	2hau-B	29.4	3.3	292	676	29	SEROTRANSFERRIN;
9:	5h52-A	29.4	3.6	295	650	29	SEROTRANSFERRIN;
10:	1btj-B	29.3	3.6	294	333	29	PROTEIN (SERUM TRANSFERRIN);
11:	1bp5-C	29.3	3.5	294	334	30	PROTEIN (SERUM TRANSFERRIN);
12:	2hav-A	29.3	3.3	292	676	29	SEROTRANSFERRIN;
13:	1dtz-A	29.3	24.1	366	689	22	APO LACTOFERRIN;
14:	5dyh-A	29.2	3.4	293	677	29	SEROTRANSFERRIN;
15:	1btj-A	29.2	3.6	293	333	29	PROTEIN (SERUM TRANSFERRIN);
16:	4x1b-A	29.2	3.6	293	650	29	SEROTRANSFERRIN;
17:	1bp5-D	29.2	3.6	294	334	30	PROTEIN (SERUM TRANSFERRIN);
18:	1l5t-A	29.1	3.1	305	329	24	LACTOFERRIN;
19:	1cb6-A	29.1	23.4	365	691	22	LACTOTRANSFERRIN;
20:	1l5t-B	29.1	3.1	306	329	24	LACTOFERRIN;
21:	1nft-A	29.0	4.0	305	329	24	PROTEIN (OVOTRANSFERRIN);
22:	1tfa-A	28.9	3.9	303	329	24	PROTEIN (OVOTRANSFERRIN);
23:	6soy-C	28.7	3.4	295	652	29	ESAG6, SUBUNIT OF HETERODIMERIC TRANSFERRIN RECEP
24:	3v8x-B	28.4	3.6	292	676	29	TRANSFERRIN-BINDING PROTEIN 1;
25:	4h0w-A	28.2	22.7	348	679	22	SEROTRANSFERRIN;
26:	2hau-A	27.5	3.5	294	676	30	SEROTRANSFERRIN;
27:	2d3i-A	26.7	6.2	284	670	32	OVOTRANSFERRIN;
28:	1hse-A	26.2	5.8	279	317	28	LACTOFERRIN;
29:	3skp-A	26.2	3.8	299	338	26	SEROTRANSFERRIN;
30:	1biy-A	26.1	6.2	288	689	28	LACTOFERRIN;
31:	1aov-A	26.0	3.5	296	686	33	APO-OVOTRANSFERRIN;
32:	1n04-A	26.0	6.2	285	683	31	SERUM TRANSFERRIN;
33:	4oqo-A	26.0	4.0	278	348	28	LACTOTRANSFERRIN;
34:	2o7u-I	25.9	6.4	286	329	30	SEROTRANSFERRIN;
35:	2o7u-E	25.8	6.4	286	329	30	SEROTRANSFERRIN;
36:	4oqo-B	25.7	3.9	279	348	28	LACTOTRANSFERRIN;
37:	6o0e-B	25.3	19.5	317	815	24	SAXIPHILIN;
38:	6o0d-B	25.2	13.7	301	817	24	SAXIPHILIN;
39:	1i6q-A	25.1	3.2	296	689	24	LACTOFERRIN;
40:	1iq7-A	25.0	5.0	294	341	25	OVOTRANSFERRIN;
41:	2pms-B	24.8	6.9	303	331	24	LACTOTRANSFERRIN;
42:	1bka-A	24.1	20.7	344	688	22	LACTOFERRIN;
43:	1lfi-A	24.0	19.4	343	691	22	LACTOFERRIN;
44:	1lfg-A	23.9	13.5	335	691	22	LACTOFERRIN;
45:	1lcf-A	23.9	20.0	337	691	22	LACTOFERRIN;
46:	6o0f-B	23.9	19.0	310	816	25	SAXIPHILIN;
47:	3v89-B	23.7	5.9	294	339	26	TRANSFERRIN-BINDING PROTEIN A;
48:	1iej-A	23.5	7.3	291	329	25	OVOTRANSFERRIN;
49:	1ovt-A	23.5	17.4	338	682	22	OVOTRANSFERRIN;
50:	1ryx-A	23.2	4.8	290	686	25	OVOTRANSFERRIN;
51:	1vfd-A	23.2	7.0	291	321	23	LACTOFERRIN;
52:	1vfe-A	22.9	6.9	284	321	23	HUMAN LACTOFERRIN;
53:	1h43-A	22.7	5.4	188	309	24	LACTOFERRIN;
54:	1n84-A	22.5	7.3	280	329	24	SEROTRANSFERRIN;
55:	1h76-A	22.5	5.4	209	677	22	SEROTRANSFERRIN;
56:	1oqg-A	22.5	7.3	283	329	25	SEROTRANSFERRIN;
57:	5wtd-A	22.5	3.6	295	649	29	SEROTRANSFERRIN;
58:	1ryo-A	22.4	7.2	279	324	25	SEROTRANSFERRIN;
59:	1n7w-A	22.4	5.3	209	329	22	SEROTRANSFERRIN;
60:	4x1d-B	22.3	3.6	295	658	29	SEROTRANSFERRIN;
61:	3ve1-B	22.3	3.5	295	675	29	TRANSFERRIN-BINDING PROTEIN 2;
62:	3ve1-D	22.3	3.5	295	677	29	TRANSFERRIN-BINDING PROTEIN 2;
63:	5y6k-A	22.3	3.6	295	649	29	SEROTRANSFERRIN;
64:	3cr9-A	22.2	5.1	211	689	20	LACTOTRANSFERRIN;
65:	1dsn-A	22.2	5.4	196	315	20	LACTOFERRIN;
66:	3v83-E	22.2	5.5	211	674	20	SEROTRANSFERRIN;
67:	3v83-A	22.1	5.9	211	674	25	SEROTRANSFERRIN;
68:	6soz-C	22.1	3.4	294	651	29	ESAG6, SUBUNIT OF HETERODIMERIC FERRIN RECEP
69:	1sqy-A	22.0	4.7	207	691	23	LACTOFERRIN;
70:	3v83-F	22.0	5.4	210	676	22	SEROTRANSFERRIN;

```
 71:  1b1x-A 22.0  5.1  211   689   20    LACTOFERRIN;
 72:  2pms-A 22.0  4.7  210   331   22    LACTOTRANSFERRIN;
 73:  4x1d-A 22.0  3.6  295   658   29    SEROTRANSFERRIN;
 74:  1b7z-A 21.9  5.7  212   689   24    PROTEIN (LACTOFERRIN);
 75:  2o7u-G 21.9  5.6  210   329   26    SEROTRANSFERRIN;
 76:  1b0l-A 21.9 17.8  317   691   22    PROTEIN (LACTOFERRIN);
 77:  1f9b-A 21.8  5.5  206   689   24    LACTOTRANSFERRIN;
 78:  1blf-A 21.8  5.8  214   685   23    LACTOFERRIN;
 79:  1fqe-A 21.8  5.4  206   329   21    SEROTRANSFERRIN;
 80:  1d4n-A 21.8  5.4  211   329   22    TRANSFERRIN;
 81:  1fck-A 21.7  4.7  208   691   22    LACTOFERRIN;
 82:  3fgs-A 21.7  5.5  208   329   23    SEROTRANSFERRIN;
 83:  1h45-A 21.7  5.0  200   321   21    LACTOFERRIN;
 84:  1h44-A 21.7  5.0  197   322   21    LACTOFERRIN;
 85:  1b3e-A 21.7  6.2  210   330   25    PROTEIN (SERUM TRANSFERRIN);
 86:  2bjj-X 21.6  4.9  212   692   20    LACTOTRANSFERRIN;
 87:  2o7u-F 21.6  5.5  207   329   26    SEROTRANSFERRIN;
 88:  3v83-C 21.6  5.4  210   674   22    SEROTRANSFERRIN;
 89:  1lfh-A 21.5 24.9  373   691   24    LACTOFERRIN;
 90:  2o84-X 21.5  5.4  210   329   21    SEROTRANSFERRIN;
 91:  1oqh-A 21.4  5.3  206   329   21    SEROTRANSFERRIN;
 92:  1dtg-A 21.4  5.7  210   331   22    TRANSFERRIN;
 93:  1jqf-A 21.4  5.3  206   329   21    TRANSFERRIN;
 94:  3s9l-C 21.4  6.0  217   515   24    TRANSFERRIN RECEPTOR PROTEIN 1;
 95:  1suv-D 21.4  5.4  211   329   22    TRANSFERRIN RECEPTOR PROTEIN 1;
 96:  1d3k-A 21.4  5.3  209   329   22    SERUM TRANSFERRIN;
 97:  3qyt-A 21.4  4.1  298   679   29    SEROTRANSFERRIN;
 98:  1a8e-A 21.3  5.5  211   329   20    SERUM TRANSFERRIN;
 99:  2o7u-C 21.3  5.3  215   329   22    SEROTRANSFERRIN;
100:  1suv-C 21.3  5.6  213   329   21    TRANSFERRIN RECEPTOR PROTEIN 1;
```

[a]PDB structural code
[b]DALI Z-score to assess structural similarity
[c]Number structurally aligned residues
[d]Number of residues in the matched PDB structure
[c]Percent of amino acid sequence identity

Table 3-5. Predicted carbonate binding residues of the N-lobe of insect Tsf1 orthologs and other arthropod transferrins.

Descrip-tion[a]	Order	Species	Accession #[b]	Thr 116[c]	Arg 120	Asn 121	Val 122	Gly 123
Insect Tsf1	Blattodea	*Blaberus discoidalis*	Q02942	Thr	Arg	Asn	Val	Gly
Insect Tsf1	Blattodea	*Cryptotermes secundus*	A0A2J7RCH3	Thr	Arg	Asn	Val	Gly
Insect Tsf1	Blattodea	*Mastotermes darwiniensis*	Q8MU80	Thr	Arg	Asn	Val	Gly
Insect Tsf1	Blattodea	*Periplaneta americana*	H2F490	Thr	Arg	Asn	Val	Gly
Insect Tsf1	Blattodea	*Zootermopsis nevadensis*	A0A067R8G2	Thr	Arg	Asn	Val	Gly
Insect Tsf1	Coleoptera	*Agrilus planipennis*	A0A1W4WDU6	Thr	Arg	Asn	Val	Gly
Insect Tsf1	Coleoptera	*Apriona germari*	Q5FX34	Thr	Arg	Asn	Val	Gly

Insect Tsf1	Coleoptera	*Monochamus alternatus*	A0A172WCD8	Thr	Arg	Asn	Val	Gly
Insect Tsf1	Coleoptera	*Protaetia brevitarsis*	Q0GB80	Thr	Arg	Asn	Val	Gly
Insect Tsf1	Coleoptera	*Tribolium castaneum*	A0A139WAX1	Thr	Arg	Asn	Val	Gly
Insect Tsf1	Diptera	*Aedes aegypti*	Q16894	Thr	Arg	Asn	Val	Gly
Insect Tsf1	Diptera	*Aedes albopictus*	A0A182HAB5	Thr	Arg	Asn	Val	Gly
Insect Tsf1	Diptera	*Anopheles dirus*	A0A182N8I6	Thr	Arg	Asn	Val	Gly
Insect Tsf1	Diptera	*Anopheles epiroticus*	A0A182PR24	Thr	Arg	Asn	Val	Gly
Insect Tsf1	Diptera	*Anopheles minimus*	A0A182W5Q6	Thr	Arg	Asn	Val	Gly
Insect Tsf1	Diptera	*Anopheles christyi*	A0A240PK04	Thr	Arg	Asn	Val	Gly
Insect Tsf1	Diptera	*Anopheles gambiae*	Q7QF98	Thr	Arg	Asn	Val	Gly
Insect Tsf1	Diptera	*Anopheles culicifacies*	A0A182MQL1	Thr	Arg	Asn	Val	Gly
Insect Tsf1	Diptera	*Anopheles arabiensis*	A0A182IAY0	Thr	Arg	Asn	Val	Gly
Insect Tsf1	Diptera	*Anopheles funestus*	A0A182RHN9	Thr	Arg	Asn	Val	Gly
Insect Tsf1	Diptera	*Anopheles farauti*	A0A182Q8L3	Thr	Arg	Asn	Val	Gly
Insect Tsf1	Diptera	*Anopheles merus*	A0A182UU15	Thr	Arg	Asn	Val	Gly
Insect Tsf1	Diptera	*Anopheles atroparvus*	A0A182IKA9	Thr	Arg	Asn	Val	Gly
Insect Tsf1	Diptera	*Anopheles stephensi*	A0A182YCV1	Thr	Arg	Asn	Val	Gly
Insect Tsf1	Diptera	*Anopheles melas*	A0A182TU06	Thr	Arg	Asn	Val	Gly
Insect Tsf1	Diptera	*Anopheles albimanus*	A0A182FAJ2	Thr	Arg	Asn	Val	Gly
Insect Tsf1	Diptera	*Anopheles quadriannulatus*	A0A182XK00	Thr	Arg	Asn	Val	Gly
Insect Tsf1	Diptera	*Anopheles maculatus*	A0A182TBM8	Thr	Arg	Asn	Val	Gly
Insect Tsf1	Diptera	*Bactrocera dorsalis*	A0A034VS68	Thr	Arg	Asn	Val	Gly
Insect Tsf1	Diptera	*Corethrella appendiculata*	U5EVY8	Thr	Arg	Asn	Val	Gly

Insect Tsf1	Diptera	*Culex tarsalis*	A0A1Q3FQK8	Thr	Arg	Asn	Val	Gly
Insect Tsf1	Diptera	*Culex quinquefasciatus*	B0X886	Thr	Arg	Asn	Val	Gly
Insect Tsf1	Diptera	*Drosophila persimilis*	B4H7J4	Thr	Arg	Asn	Val	Gly
Insect Tsf1	Diptera	*Drosophila virilis*	B4MD52	Thr	Arg	Asn	Val	Gly
Insect Tsf1	Diptera	*Drosophila grimshawi*	B4JJ24	Thr	Arg	Asn	Val	Gly
Insect Tsf1	Diptera	*Drosophila erecta*	B3NTD3	Thr	Arg	Asn	Val	Gly
Insect Tsf1	Diptera	*Drosophila ananassae*	B3MWK3	Thr	Arg	Asn	Val	Gly
Insect Tsf1	Diptera	*Drosophila mojavensis*	B4L3P8	Thr	Arg	Asn	Val	Gly
Insect Tsf1	Diptera	*Drosophila sechellia*	B4I6R8	Thr	Arg	Asn	Val	Gly
Insect Tsf1	Diptera	*Drosophila willistoni*	B4NEK7	Thr	Arg	Asn	Val	Gly
Insect Tsf1	Diptera	*Drosophila melanogaster*	Q9VWV6	Thr	Arg	Asn	Val	Gly
Insect Tsf1	Diptera	*Drosophila silvestris*	O97356	Thr	Arg	Asn	Val	Gly
Insect Tsf1	Diptera	*Drosophila pseudoobscura pseudoobscura*	B5DNN0	Thr	Arg	Asn	Val	Gly
Insect Tsf1	Diptera	*Drosophila ficusphila*	A0A1W4UDD6	Thr	Arg	Asn	Val	Gly
Insect Tsf1	Diptera	*Drosophila busckii*	A0A0M4EU20	Thr	Arg	Asn	Val	Gly
Insect Tsf1	Diptera	*Drosophila yakuba*	B4Q2X7	Thr	Arg	Asn	Val	Gly
Insect Tsf1	Diptera	*Glossina brevipalpis*	A0A1A9W323	Thr	Arg	Asn	Val	Gly
Insect Tsf1	Diptera	*Glossina pallidipes*	A0A1B0A3D5	Thr	Arg	Asn	Val	Gly
Insect Tsf1	Diptera	*Glossina fuscipes fuscipes*	A0A1A9YDI2	Thr	Arg	Asn	Val	Gly
Insect Tsf1	Diptera	*Glossina austeni*	A0A1A9VBV2	Thr	Arg	Asn	Val	Gly
Insect Tsf1	Diptera	*Glossina palpalis gambiensis*	A0A1B0BX64	Thr	Arg	Asn	Val	Gly
Insect Tsf1	Diptera	*Glossina morsitans morsitans*	Q8MX87	Thr	Arg	Asn	Val	Gly
Insect Tsf1	Diptera	*Lucilia cuprina*	A0A0L0C0K4	Thr	Arg	Asn	Val	Gly

Insect Tsf1	Diptera	*Lutzomyia longipalpis*	A0A1B0CHE7	Thr	Arg	Thr[d]	Val	Gly
Insect Tsf1	Diptera	*Musca domestica*	A0A1I8M1D8	Thr	Arg	Asn	Val	Gly
Insect Tsf1	Diptera	*Sarcophaga peregrina*	Q26643	Thr	Arg	Asn	Val	Gly
Insect Tsf1	Diptera	*Stomoxys calcitrans*	A0A1I8PR12	Thr	Arg	Asn	Val	Gly
Insect Tsf1	Diptera	*Zeugodacus cucurbitae*	A0A0A1X109	Thr	Arg	Asn	Val	Gly
Insect Tsf1	Hemiptera	*Diaphorina citri*	A0A1S3CYM8	Thr	Arg	Asn	Val	Gly
Insect Tsf1	Hemiptera	*Lygus hesperus*	A0A146LNB5	Thr	Arg	Asn	Val	Gly
Insect Tsf1	Hemiptera	*Nephotettix cincticeps*	A0A0E4AVN5	Thr	Arg	Asn	Val	Gly
Insect Tsf1	Hemiptera	*Panstrongylus lignarius*	A0A224XL75	Thr	Arg	Asn	Val	Gly
Insect Tsf1	Hemiptera	*Pristhesancus plagipennis*	A0A1Q1NPJ1	Thr	Arg	Asn	Val	Gly
Insect Tsf1	Hemiptera	*Pyrrhocoris apterus*	M4WMH6	Thr	Arg	Asn	Val	Gly
Insect Tsf1	Hemiptera	*Rhodnius prolixus*	B8LJ43	Thr	Arg	Asn	Val	Gly
Insect Tsf1	Hemiptera	*Riptortus clavatus*	O96418	Thr	Arg	Asn	Val	Gly
Insect Tsf1	Hemiptera	*Riptortus pedestris*	R4WJB4	Thr	Arg	Asn	Val	Gly
Insect Tsf1	Hymenoptera	*Acromyrmex echinatior*	F4W957	Thr	Arg	Asn	Val	Gly
Insect Tsf1	Hymenoptera	*Apis cerana cerana*	J7F1T1	Thr	Arg	Asn	Val	Gly
Insect Tsf1	Hymenoptera	*Apis mellifera*	A0A088AFH7	Thr	Arg	Asn	Val	Gly
Insect Tsf1	Hymenoptera	*Atta cephalotes*	A0A158P0A5	Thr	Arg	Asn	Val	Gly
Insect Tsf1	Hymenoptera	*Atta colombica*	A0A195B5L1	Thr	Arg	Asn	Val	Gly
Insect Tsf1	Hymenoptera	*Bombus ignitus*	A8D919	Thr	Arg	Asn	Val	Gly
Insect Tsf1	Hymenoptera	*Cyphomyrmex costatus*	A0A151ID51	Thr	Arg	Asn	Val	Gly
Insect Tsf1	Hymenoptera	*Fopius arisanus*	A0A0C9RQZ4	Thr	Arg	Asn	Val	Gly
Insect Tsf1	Hymenoptera	*Habropoda laboriosa*	A0A0L7QKR3	Thr	Arg	Asn	Val	Gly

Insect Tsf1	Hymenoptera	*Harpegnathos saltator*	E2B326 edited	Thr	Arg	Asn	Val	Gly
Insect Tsf1	Hymenoptera	*Melipona quadrifasciata*	A0A0M9A935	Thr	Arg	Asn	Val	Gly
Insect Tsf1	Hymenoptera	*Nasonia vitripennis*	K7J4P3	Thr	Arg	Asn	Ala	Gly
Insect Tsf1	Hymenoptera	*Ooceraea biroi*	A0A026WB04	Thr	Arg	Asn	Val	Gly
Insect Tsf1	Hymenoptera	*Solenopsis invicta*	Q3MJL5	Thr	Arg	Asn	Val	Gly
Insect Tsf1	Hymenoptera	*Trachymyrmex cornetzi*	A0A195EDU2	Thr	Arg	Asn	Val	Gly
Insect Tsf1	Hymenoptera	*Trachymyrmex septentrionalis*	A0A195F369	Thr	Arg	Asn	Val	Gly
Insect Tsf1	Hymenoptera	*Trachymyrmex zeteki*	A0A151WU63	Thr	Arg	Asn	Val	Gly
Insect Tsf1	Lepidoptera	*Bombyx mori*	O97158	Thr	Arg	Asn	Val	Gly
Insect Tsf1	Lepidoptera	*Asiatic rice borer moth*	Q6F4J2	Thr	Arg	Asn	Val	Gly
Insect Tsf1	Lepidoptera	*Choristoneura fumiferana*	Q6Q2Z2	Thr	Arg	Asn	Val	Gly
Insect Tsf1	Lepidoptera	*Danaus plexippus plexippus*	A0A212FLE3	Thr	Arg	Asn	Val	Gly
Insect Tsf1	Lepidoptera	*Ephestia kuehniella*	D5M9Y5	Thr	Arg	Asn	Val	Gly
Insect Tsf1	Lepidoptera	*Galleria mellonella*	Q6UQ29	Thr	Arg	Asn	Val	Gly
Insect Tsf1	Lepidoptera	*Helicoverpa armigera*	A0A0B5H6A8	Thr	Arg	Asn	Val	Gly
Insect Tsf1	Lepidoptera	*Manduca sexta*	P22297	Thr	Arg	Asn	Val	Gly
Insect Tsf1	Lepidoptera	*Papilio machaon*	A0A194RH67	Thr	Arg	Asn	Val	Gly
Insect Tsf1	Lepidoptera	*Papilio xuthus*	A0A194PSJ1	Thr	Arg	Asn	Val	Gly
Insect Tsf1	Lepidoptera	*Pararge aegeria*	S4NYG0	Thr	Arg	Asn	Val	Gly
Insect Tsf1	Lepidoptera	*Plutella xylostella*	A0JCK0	Thr	Arg	Asn	Val	Gly
Insect Tsf1	Lepidoptera	*Spodoptera litura*	A7IT76	Thr	Arg	Asn	Val	Gly
Insect Tsf1	Odonata	*Ladona fulva*	LFUL008155_PA	Thr	Arg	Thr	Val	Gly
Insect Tsf1	Orthoptera	*Romalea microptera*	Q6USR2	Thr	Arg	Asn	Val	Gly

Insect Tsf1	Orthoptera	*Locusta migratoria*	BBE27867	Thr	Arg	Asn	Val	Gly
Insect Tsf1	Phasmatodea	*Medauroidea extradentata*	GAWD01077063	Thr	Arg	Asn	Val	Gly
Insect Tsf1	Siphonoptera	*Ctenocephalides felis*	XP_026466165	Thr	Arg	Asn	Val	Gly
Insect Tsf1	Trichoptera	*Annulipalpia* species	GATX01086443	Thr	Arg	Asn	Val	Gly
Insect Tsf1	Zygentoma	*Atelura formicaria*	GAYJ02040055	Thr	Arg	Asn	Ala	Gly
Insect Tsf1	Zygentoma	*Thermobia domestica*	GASN02065056	Thr	Arg	Thr	Ala	Gly
Insect Tsf1-like	Archaeognatha	*Meinertellua cundinamarcensis*	GAUG02039070	Thr	Arg	Asn	Ala	Gly
Insect Tsf1-like	Archaeognatha	*Meinertellua cundinamarcensis*	GAUG02047150	Thr	Arg	Asn	Ala	Gly
Non-insect hexa-pod Tsf	Collembola	*Folsomia candida*	XP_021946057	Thr	Arg	Asn	Ala	Gly
Non-insect Hexa-pod Tsf	Collembola	*Orchesella cincta*	ODM93913	Thr	Arg	Asn	Ala	Gly
Crusta-cean Tsf	Decapoda	*Portunus trituberculatus*	MPC36721	Thr	Arg	Asn	Ala	Gly
Arach-nid Tsf	Thrombid-iformes	*Tetranychus urticae*	XP_015790183.1	Thr	Arg	Asn	Ala	Gly
Bovine LF	Artiodactyla	*Bos taurus*	P24627	Thr	Arg	Ser	Ala	Gly
Bovine STF	Artiodactyla	*Bos taurus*	Q29443	Thr	Arg	Ser	Ala	Gly

[a]Tsf = transferrin, Lf = lactoferrin, STF = serum transferrin.
[b]Data sets of insect and non-insect hexapod sequences were described previously (Najera et al., 2020; Weber et al., 2020).
[c]Amino acid residue numbers correspond to the MsTsf1 sequence.
[d]Red text indicates non-conserved amino acid residues.

Chapter 4 - Mutational analysis of iron-coordinating and anion-binding ligands of transferrin-1 from *Manduca sexta*

Abstract

Transferrin 1 (Tsf1) is an insect-specific, multifunctional iron-binding protein. Its high affinity for iron at neutral pH and release of iron under slightly acidic conditions are comparable to the iron binding and release properties of mammalian serum transferrin; however, iron coordination by Tsf1 differs from that of serum transferrin and other well-characterized transferrins. The iron-binding ligands in *Manduca sexta* Tsf1 are Tyr90, Tyr204, a buried carbonate anion, and a novel solvent-exposed carbonate anion. The solvent-exposed carbonate anion is bound by a single, conserved amino acid residue, Asn121. The goal of this study was to determine how Tyr90, Tyr204, and Asn121 contribute to iron binding and pH-mediated iron release. We analyzed five forms of Tsf1: wild-type, a double tyrosine mutant (Y90F/Y204F), and three Asn121 mutants (N121A, N121S and N121D). As expected, the Y90F/Y204F mutant did not bind iron. The Asn121 mutants exhibited altered spectral characteristics, indicating changes in iron coordination; in addition, the N121S and N121D mutations decreased iron binding at pH 7.4, and caused iron release at pH $\leq$ 7.0. These results confirm that Asn121 contributes to iron coordination. Surprisingly, the N121A mutation did not affect affinity for iron or pH-mediated iron release. Given the high conservation of Asn121 in Tsf1 orthologs, this finding suggests a difference in in vivo and in vitro mechanisms of iron coordination, with the possibility that iron coordination in vivo involves organic anions other than carbonate in the novel solvent-exposed position. Ultimately, these findings will help to explain the mechanisms of Tsf1 function in insects.

Introduction

Animals maintain iron homeostasis and limit iron-induced toxicity through mechanisms of iron sequestration, absorption, transport, and storage (Crichton et al., 2002; Han, 2011; Kosman, 2010). Some mechanisms of iron sequestration and transport involve the transferrin family of extracellular iron-binding proteins (Baker and Baker, 2009; Gkouvatsos et al., 2012). One well-studied transferrin is mammalian lactoferrin, which sequesters iron in bodily fluids to protect against iron-scavenging pathogens (Farnaud and Evans, 2003; Jenssen and Hancock, 2009). Another is mammalian serum transferrin, which transports iron in the blood and delivers it to cells in a regulated manner (Gkouvatsos et al., 2012; Kosman, 2010). Both mammalian transferrins keep free iron levels extremely low in extracellular fluids, which protects against iron-induced oxidative stress.

The structures of vertebrate transferrins, including lactoferrin, serum transferrin, ovotransferrin, and melanotransferrin, are similar (Anderson et al., 1987; Bailey et al., 1988; Hayashi et al., 2021; Kurokawa et al., 1995). They comprise two homologous lobes, termed the amino- and carboxyl-lobe (N- and C-lobe, respectively) (Mizutani et al., 2012). The first three proteins have a single ferric ion-binding site in each lobe, whereas melanotransferrin has a ferric ion-binding site only in the N-lobe (Anderson et al., 1987; Bailey et al., 1988; Hayashi et al., 2021; Kurokawa et al., 1995). The iron-binding sites have identical ligands for iron coordination: two tyrosines, an aspartate, a histidine, and a single bound carbonate anion (Anderson et al., 1987; Bailey et al., 1988; Hayashi et al., 2021; Kurokawa et al., 1995; Mizutani et al., 2012).

Lactoferrin and serum transferrin are known to bind iron with high affinity ($\log K > 20$ for each binding site) (Aisen et al., 1978; Aisen and Leibman, 1972); and they release iron in a pH-dependent manner that corresponds to their physiological functions (Day et al., 1992).

Lactoferrin releases iron over the pH range of 4.0 to 2.5, which provides it with iron-withholding properties in a variety of environments, while serum transferrin releases iron in the pH range of 6.0 to 4.0, which facilitates the release of iron in the mildly acidic endosome (Day et al., 1992). Iron will not bind to these transferrins without a carbonate anion being present at the iron-binding site; moreover, conformational shifts at the anion binding site are part of the initiation process for iron release (Adams et al., 2003; Harris, 2012).

Insect transferrin-1 (Tsf1) is one of four transferrin family members found in insects (Bai et al., 2016; Najera et al., n.d.). Of the four, Tsf1 is the only one that is both secreted into hemolymph (blood) and other extracellular fluids (Bonilla et al., 2015; Brummett et al., 2017; Geiser and Winzerling, 2012; Hattori et al., 2015; Qu et al., 2014; Simmons et al., 2013; Zhang et al., 2014), and known to reversibly bind iron (Bartfeld and Law, 1990; Brummett et al., 2017; Gasdaska et al., 1996; Huebers et al., 1988; Weber et al., 2020). Tsf1s from *Drosophila melanogaster* (DmTsf1), *Manduca sexta* (MsTsf1), and *Blaberus discoidalis* (BdTsf1) have biochemical characteristics compatible with iron sequestration and iron transport (Gasdaska et al., 1996; Weber et al., 2020). MsTsf1 and DmTsf1 have high affinity for iron at neutral pH (log K ~18) (Weber et al., 2020), and all three Tsf1s are known to release iron under moderately acidic conditions (Gasdaska et al., 1996; Weber et al., 2020), similar to serum transferrin (Day et al., 1992). Several studies of various insects have shown that Tsf1 plays a role in immunity, protection against iron-induced oxidative stress, and iron transport (Brummett et al., 2017; Huebers et al., 1988; Iatsenko et al., 2020; Kim et al., 2008; Kurama et al., 1995; Lee et al., 2006; Xiao et al., 2019; Xue et al., 2020; Zhang et al., 2018); however, it is not yet clear how Tsf1 is involved in iron transport, because, unlike serum transferrin, Tsf1 has no identified

receptor (Geiser and Winzerling, 2012; Lambert, 2012), and the mechanism by which Tsf1 releases iron for delivery to the cell is unknown (Xiao et al., 2019).

A recent report on the first crystal structure of a Tsf1 ortholog, isolated from *M. sexta* hemolymph, described its overall structure and the coordination of iron at the iron-binding site (Weber et al., 2021). The iron-bound (holo) MsTsf1 has an overall fold that includes an N-lobe and a C-lobe, and each lobe is divided into two domains, N1/N2 in the N-lobe and C1/C2 in the C-lobe (Figure 4-1A). The location of the single ferric ion-binding site is found in the cleft between the N1 and N2 domains (Figure 4-1A). Similar to vertebrate transferrins, MsTsf1 binds iron in the cleft of the N-lobe through an octahedral coordination of six ligands (Anderson et al., 1987; Bailey et al., 1988; Kurokawa et al., 1995; Weber et al., 2021); however, a novel feature of MsTsf1 is that it uses two tyrosine residues in the N2 domain (Tyr90 and Tyr204) and two bound bidenate carbonate anions as ligands to bind iron (Figure 4-1B). One of the carbonate anions in MsTsf1 is buried near the iron-coordination site, and it forms hydrogen bonds with the side chains of Thr116 and Arg120 and the backbone amide groups of Val122 and Gly123 (Figure 4-1C). This buried carbonate anion is bound in nearly identical fashion to the single carbonate anion in serum transferrin and lactoferrin (Weber et al., 2021). The other carbonate anion in MsTsf1 is located on the opposite side of the iron-binding site from the buried carbonate and is in a solvent-exposed position. This solvent-exposed carbonate is held in place by a single amino acid residue, Asn121 (Figure 4-1C). The importance of the solvent-exposed carbonate and Asn121 to the iron-binding and release mechanisms of MsTsf1 is unknown.

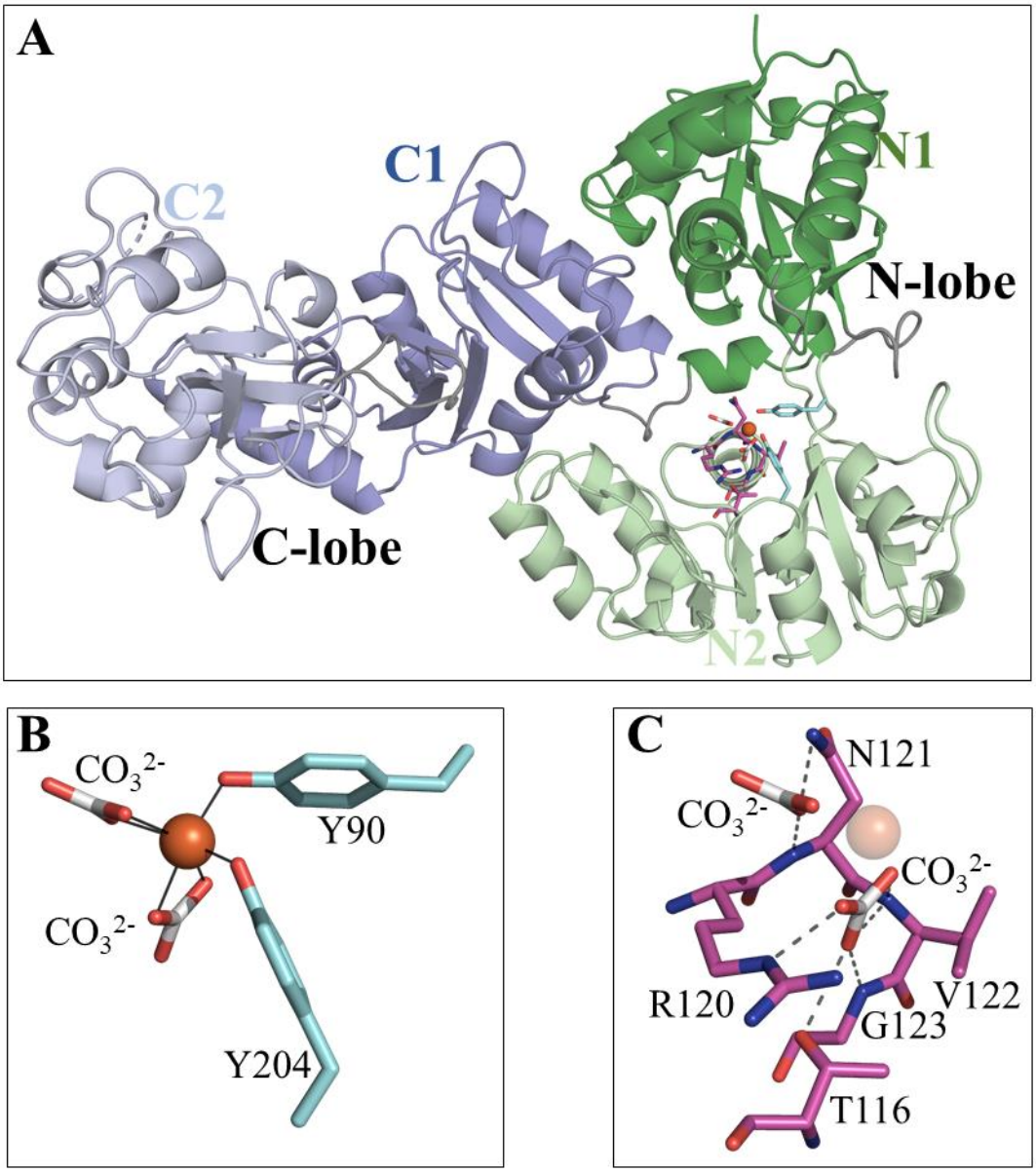

Figure 4-1. Overall structure and iron coordination and anion binding in MsTsf1.
A) A cartoon representation of the overall structure of MsTsf1 (PDB code 6WB6) showing the location of the Fe^{3+} and CO_3^{2-} anion ligating residues (in licorice). The C-lobe is shown in blue, with the C1 domain in dark blue and the C2 domain in light blue. The N-lobe is shown in green, with the N1 in dark green and the N2 in light green. B) A close-up view of the N-lobe showing coordination of Fe^{3+} (orange sphere), with the ligating residues Tyr90 and Tyr204 in cyan and the two bound CO_3^{2-} anions in grey. The solid lines depict the coordinating bonds formed with the Fe^{3+}. C) A close-up view of the anion-binding residues (magenta). The hydrogen bonds formed between the amino acid residues and the CO_3^{2-} anions are shown as dashed lines.

Amino acid sequence analyses of Tsf1s and non-insect transferrins have shown that the iron-coordinating residues Tyr90 and Tyr204 and the residues whose side chains are ligands for the buried carbonate anion, Thr116 and Arg120, are highly conserved among all iron-binding transferrin sequences (Lambert et al., 2005; Najera et al., n.d.; Weber et al., 2021, 2020). However, an analysis of the Asn121 residue, which binds the solvent-exposed carbonate, showed that conservation of this residue occurs only in arthropods and is highly conserved in insects (Weber et al., 2021). Therefore, the binding of the solvent-exposed carbonate and its involvement in iron coordination are likely to be specific to insects.

One goal of this study was to probe the importance of Asn121 in the stability of iron coordination in MsTsf1 through site-directed mutagenesis and biochemical analysis. We made three substitutions at position 121 to test its involvement in iron binding and release. A second goal was to determine if the iron-ligating tyrosines are essential to iron binding by creating and analyzing a Tyr90/Tyr204 double mutant. We expressed and purified recombinant MsTsf1 in the following forms: wild-type (WT), Asn121 to alanine mutant (N121A), Asn121 to serine mutant (N121S), Asn121 to aspartate mutant (N121D), and a double Tyr-90/Tyr-204 to phenylalanines mutant (Y90F/Y204F). The purified recombinant proteins were characterized by three types of experiments: 1) UV-visible spectroscopy to examine if the mutations affect iron coordination, 2) equilibrium dialysis to assess each mutation's effect on affinity for iron and pH-mediated iron release, and 3) far-UV circular dichroism (CD) to determine if the mutations or iron binding cause any secondary structural changes to the proteins. We found that Asn121 contributes in a nonessential way to iron coordination, and we found that Y90 and/or Y204 are essential to iron binding in MsTsf1. We also found that iron binding is not likely to cause major changes to the secondary structure of MsTsf1.

Materials and Methods

Isolation of MsTsf1 cDNA

A cDNA that encodes the entire MsTsf1 protein was amplified by PCR with the use of a *M. sexta* fat body cDNA pool as the template and the following primers: 5' GAC CAT GGC TTT GAA AC 3' and 5' TTA GGC GAG ACC ACA TG 3'. The predicted amino acid sequence encoded by the MsTsf1 cDNA is reported in Figure 4-9 and is 99.7% identical to the reported sequence in UniProtKB (entry P22297). The MsTsf1 cDNA was cloned into the pCR4-TOPO vector (Invitrogen) by TA cloning.

Plasmid preparation and site-directed mutagenesis

The MsTsf1+pCR4-TOPO recombinant plasmid was used as a template to amplify the full coding region of MsTsf1 (PCR primers are listed in supplementary Table 4-2). The PCR product was digested with *Apa*I and *Not*I and inserted into the pOET3 baculovirus transfer plasmid (Oxford Expression Technologies) for use in recombinant wild-type MsTsf1 production and as a template for mutagenesis. The QuickChange Multi Site-Directed Mutagenesis Kit (Agilent) was used to mutagenize the MsTsf1+pOET3 plasmid using mutagenic primers for N121, Y90 and Y204 (supplementary Table 4-2). DNA sequencing verified the correct sequences of the mutant plasmids. The flashBAC Gold system (Oxford Expression Technologies) was used to generate a recombinant baculovirus stock for WT and mutant forms of MsTsf1.

Protein expression and purification

The same expression and purification procedures were used for the production of WT and mutant forms of MsTsf1 (culture volumes are listed in supplementary Table 4-2). Recombinant baculovirus was used to infect Sf9 cells at 2 x 10^6 cells/ml in Sf900III serum free medium, using a multiplicity of infection of 1 pfu/cell. After two days, the culture was centrifuged at 500 × *g*, and the cell pellet was discarded. While stirring, ammonium sulfate was slowly added to the supernatant to obtain 100% saturation, and protein precipitation occurred over a two-day period at 4°C. Floating brown precipitate was collected with a pipet and dialyzed three times against 20 mM Tris, pH 8.3 (4°C). The dialyzed sample was collected, centrifuged at 10,000 × *g*, and applied to a Q-Sepharose Fast Flow column (1.5 x 10 cm). Proteins were eluted from the column with a linear gradient of 0-1 M NaCl in 20 mM Tris, pH 8.3 (4°C). Following SDS-PAGE analysis, fractions containing transferrin were pooled and concentrated with 30 kDa molecular weight cut-off Amicon Ultracel centrifugal filters. The samples were then applied to a HiLoad 16/60 Superdex 200 column (GE Healthcare) equilibrated in 20 mM Tris, 150 mM NaCl, pH 7.4. Fractions were analyzed by SDS-PAGE and pooled. Protein yield was determined using the Pierce Coomassie Plus (Bradford) Assay Reagent (Thermo Scientific) (supplementary Table 4-2).

Apo- and holo-MsTsf1 preparation and spectral analysis

Apo- and holo-forms of the proteins were produced following a previously described protocol (Brummett et al., 2017; Weber et al., 2020). At ~10 mg/ml, the holo-WT and N121 mutants had a distinct orange color, while at ~20 mg/ml the Y90F/Y204F mutant had a slight yellow color. In their apo-forms, all the protein solutions were clear in color.

UV-visible difference spectra were generated for each protein as previously described (Weber et al., 2020) with minor changes. Briefly, the absorbance of proteins in their apo- and holo-forms (~ 2 mg/ml) were measured from 280 to 600 nm, and the apo-protein spectra was subtracted from the holo-protein spectra.

Far-UV CD analysis

Circular dichroism (CD) measurements were carried out using a J815 JASCO spectropolarimeter and a 1.0 mm cell on WT and mutant forms of MsTsf1 in their apo- and holo-forms. All proteins were at concentrations from 1-2 mg/ml and in 10 mM HEPES, 20 mM sodium bicarbonate, pH 7.4. An average of five spectral readings for each sample was used for analysis, and a buffer blank was subtracted from each protein spectra. The CD spectra were converted from millidegrees to molar ellipticity (Θ) to normalize the readings based on protein concentration. Difference CD spectra were generated by subtracting the apo-protein spectra from the holo-protein spectra.

Iron affinity measurements

Competition assays to measure the affinity for iron of the various forms of MsTsf1 were performed using equilibrium dialysis as described previously (Weber et al., 2020) with minor modifications. Apo-MsTsf1 proteins at 20 µM in dialysis buffer, 1.5 mM citrate, 0.1 M sodium nitrate, 10 mM HEPES and 20 mM sodium bicarbonate, pH 7.4, were added to one cell of a micro-dialyzer (Nest Group Company), and to the second cell was added dialysis buffer prepared with known Fe^{3+} concentrations. Each cell had a total volume of 50 µL. The cells were separated by a 10 kDa membrane so that the protein could not pass through to the second cell.

Simultaneous experiments with buffer containing 7.2, 18, or 45 µM of total Fe^{3+} were performed with gentle agitation at 25 ± 1˚C to equilibrium (24 hours minimum incubation time). Each experimental variation of the three iron concentrations was performed in duplicate. Following equilibration, the amount of non-Tsf1-bound iron in the cell containing no protein was measured using a Ferrozine-based assay (Jeitner, 2014). The amount of Tsf1-bound iron was calculated using the known concentration of added protein and the measured amount of non-Tsf1-bound iron (equations in supplementary Table 4-3). The iron affinity constants for each protein were calculated (supplementary Table 4-3) using previously described equations (Aasa et al., 1963; Aisen et al., 1978; Weber et al., 2020). It should be noted that that the equations used for calculating the MsTsf1 iron affinity constant (Weber et al., 2020) do not reflect the recent finding that MsTsf1 binds two carbonate anions (Weber et al., 2021); however, since the carbonate concentration is held constant in the closed environment of the dialysis chamber, this new information does not change the outcome of the protein's measured affinity for iron. To assess the significance of the difference in affinity, a statistical unpaired *t* test to compare the log *K* of the WT Tsf1 and each mutant was performed using GraphPad Prism software.

Iron release measurements

An assay for measuring pH-mediated iron release from transferrins has been previously described (Day et al., 1992; Nicholson et al., 1997; Weber et al., 2020). Only minor modifications to the assay were made for this study. Briefly, iron-saturated proteins (5 mg/ml) were extensively dialyzed against buffers over the range of 4.0 to 8.0 for a two-day period. The percent iron saturation was calculated by measuring the change of each protein's specific LCMT λ_{max} in the visible spectrum. A sigmoidal dose response curve was fitted to the data using

GraphPad Prism software, and the resultant curve was used to determine the pH range of iron release and pH_{50}.

Results

Asn121 mutant modeling

The Asn121 side chain forms a hydrogen bond with the solvent-exposed carbonate anion and another hydrogen bond with Tyr338 to create an intralobal interaction (Figure 4-2A); therefore, we predicted that Asn121 would have a critical role in iron coordination and possibly intralobal stability. To test this hypothesis, we made three Asn121 mutants, each with different predicted side chain interactions: N121S was hypothesized to disrupt the intralobal contact, N121D was hypothesized to repel the solvent-exposed carbonate, and N121A was hypothesized to disrupt both the intralobal interaction and the hydrogen bond with the solvent-exposed carbonate anion. To illustrate what effect the mutations may have on the iron-binding site and the surrounding protein environment, we used the mutagenesis function in PyMOL (The PyMOL Molecular Graphics System, Version 2.3.2 Schrödinger, LLC) to make alterations of the MsTsf1 structure (PDB code 6WB6) and model the mutant residues at amino acid residue position 121 (Figure 4-2).

The serine mutation had two modeled positions, termed S-p1 and S-p2 (Figure 4-2B). In the S-p1 position, the hydroxyl group on the side chain is positioned between the oxygen group on Tyr338 (3.7 Å) and an oxygen group of the carbonate (3.5 Å). In the S-p1 position, we predicted the hydroxyl group would likely interact with closer oxygen group of the carbonate and, thus, would disrupt the intralobal contact. In the S-p2 position, the serine's hydroxyl group is > 4.4 Å away from both the Tyr338 and the carbonate, and, at this distance, it is unlikely the

serine would make either bond and, thus, would disrupt iron binding and the intralobal interaction.

Modeling of the aspartate rendered several positions, and two of these positions, D-p1 and D-p2, showed the aspartate side chain interacting with its surroundings, (Figure 4-2C). In the D-p1 position, the carboxyl group of the aspartate's side chain could interact with the ferric ion. ($O_{\delta 1}$ is 3.3 Å from the iron ion and $O_{\delta 2}$ is 3.3 Å.) In the D-p1 position, we predicted that the aspartate side chain would replace the carbonate anion and coordinate the iron, which could lead to destabilization of the iron binding site. The D-p2 position shows a possible positioning of the carboxyl group that would allow it to form a hydrogen bond with Tyr338, but would also bring the negatively charged side chain near the carbonate anion, which could cause the repulsion of the anion and disrupt iron binding.

The modeling of the alanine mutant rendered a single position (Figure 4-2D). The shorter alanine side chain should be sterically acceptable at this position because the closest atom to the hydrophobic methyl group of the side chain is an oxygen group of the solvent-exposed carbonate 3.7 Å away. The alanine mutation should disrupt the hydrogen bonds made by the Asn121 side chain in the WT protein. Since the shorter side chain of the alanine mutant would create fewer steric restrictions for surrounding residues, we looked to see what other residues in proximity to the solvent-exposed carbonate and the Tyr338 could potentially reorient to fill the space. The best candidate is Arg271 (Figure 4-2D), which, in the WT MsTsf1 structure, has an Nη1 group that is 3.6 Å from an oxygen of the solvent-exposed carbonate. Moreover, Arg271 is positioned in the solvent-exposed cleft of the N-lobe and has limited steric restrictions, giving its side chain the flexibility needed to orient closer to the carbonate anion and hydroxyl group of Tyr338 in the N121A mutant.

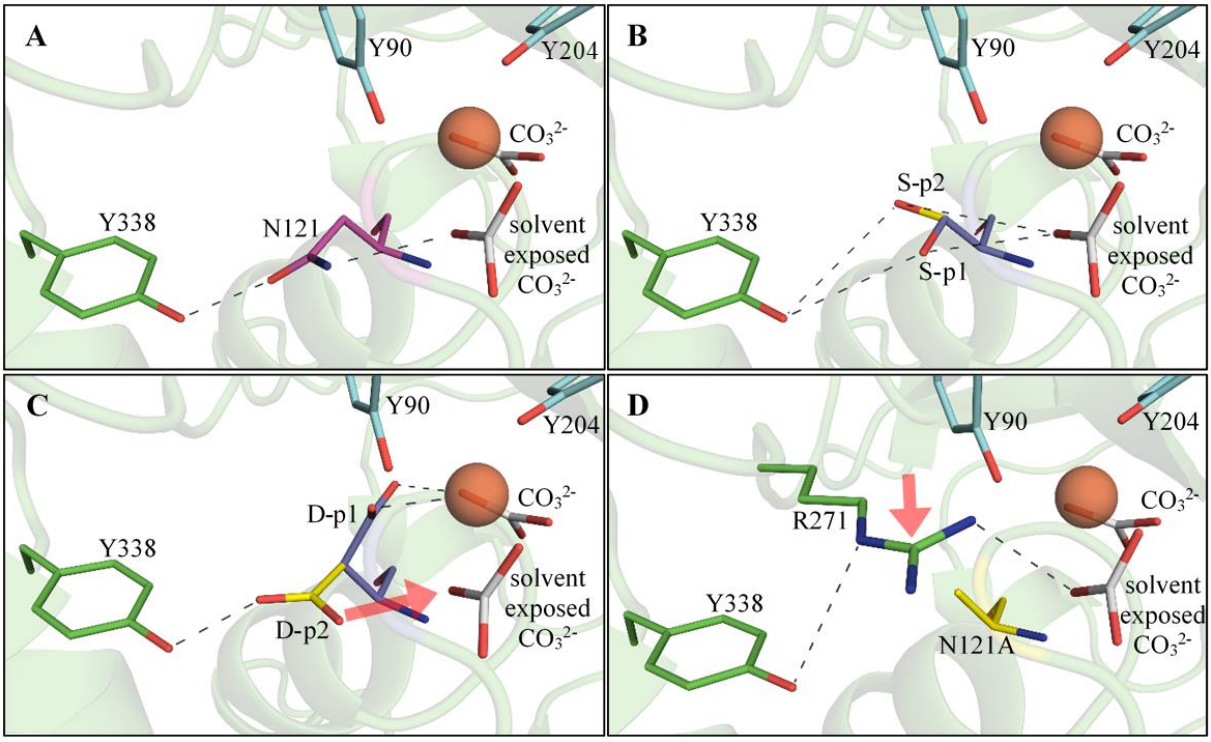

Figure 4-2. Modeling of the Asn121 position in the WT protein and N121 mutants.
A-D) The iron ligating tyrosines are represented as cyan sticks and the two CO_3^{2-} as grey sticks. Iron is shown as an orange sphere, and bonds are depicted as dashed lines. A) The anion and intralobal hydrogen bond interactions made by the side chain of Asn121 (magenta sticks) with the solvent-exposed anion and Tyr338 (green sticks). B) The modeled positions of the N121S mutant. Position 1 is labeled S-p1 (blue sticks) and position 2 is labeled S-p2 (yellow sticks). C) Two modeled positions of the N121D mutant. Position 1 is labeled D-p1 (blue sticks) and position 2 is labeled D-p2 (yellow sticks). The red arrow indicates the possible charge repulsion of the solvent exposed CO_3^{2-} by the aspartate side chain. D) The modeled N121A mutant (yellow sticks) and the position of Arg271. The red arrow indicates the possible movement of Arg271 towards the solvent-exposed CO_3^{2-} and Tyr338. Modeling of the Asn121 mutants was done using the MsTsf1 structure (PDB code 6WB6) as a template, and residues were altered using the PyMOL mutagenesis wizard (The PyMOL Molecular Graphics System, Version 2.3.2 Schrödinger, LLC).

Production of recombinant forms of MsTsf1

MsTsf1 was previously purified in its native form from the hemolymph of M. sexta larvae (Brummett et al., 2017; Weber et al., 2020) prior to characterization. For this study, we expressed and purified recombinant forms of MsTsf1, including WT, N121A, N121D, N121S and Y90F/Y204F. The recombinant proteins were expressed in the Sf9 insect cell line using a baculovirus expression system. The WT and mutant proteins were purified with the same procedure: ammonium sulfate precipitation followed by anion exchange and size exclusion chromatography. The proteins were determined to be very pure (Figure 4-3). The protein yield from each expression was in the range of 11 to 25 mg/liter (supplementary Table 4-2).

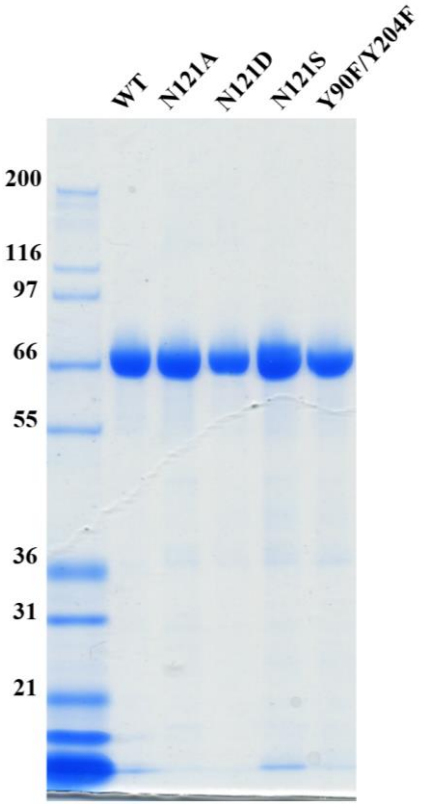

Figure 4-3. SDS-PAGE analysis of the purified forms of MsTsf1.
Purified WT, N121A, N121D, N121S and Y90F/Y204F forms of MsTsf1 were analyzed by reducing SDS-PAGE followed by Coomassie staining. The molecular mass standards (in kDa) are shown to the left. The expected mass of MsTsf1 was 73 kDa.

Spectroscopic characterization of the transferrin-Fe^{3+} complex

Iron-binding transferrins have spectral characteristics in the ultraviolet and visible spectrum due to the interaction of electrons from the bound Fe^{3+} and ligating tyrosines (Baker, 1994; Patch and Carrano, 1981). This interaction, termed a ligand-to-metal-charge transfer (LMCT) transition, results in a visible absorbance maximum (λ_{max}) in the 400 to 470 nm range, depending on the transferrin, and provides a noticeable yellowish-orange or sometimes pinkish-salmon color in concentrated transferrin samples (Baker, 1994). Previous studies of the residues involved in iron coordination and anion binding in vertebrate transferrins have demonstrated shifts in the λ_{max} that have been attributed to changes in the ligand coordination geometry of the Fe^{3+} ion (Day et al., 1992; Halbrooks et al., 2004; Nicholson et al., 1997).

Following purification, WT MsTsf1 and the N121 mutants all had a similar orange color, but the Y90F/Y204F mutant was nearly clear with a slight hint of yellow. The λ_{max} of the WT at 420 nm is identical to the reported λ_{max} of native MsTsf1 (Weber et al., 2020) (Figure 4-4, Table 4-1). As indicated by their visible color and their difference spectra, the N121 mutants all bind iron, but their λ_{max}'s are shifted from 420 nm, indicating differences in iron coordination (Figure 4-4, Table 4-1). Despite the slight yellowish color, the difference spectrum of the Y90F/Y204F mutant did not show convincing evidence of bound iron. Even after several additions of 0.1 M equivalent ferric-NTA to the solution containing Y90F/Y204F, no pronounced LMCT λ_{max} was observed nor did the color change. However, the full UV-visible spectrum of Y90F/Y204F has a small peak in the UV spectral region at ~290 nm (Figure 4-10). A λ_{max} in the UV spectrum of vertebrate holo-transferrins is attributed to disturbances of the pi-pi* transitions that occur in the phenolic ring of the ligating tyrosines (Baker, 1994), but a peak at ~290 nm can also be the result of anion binding (Harris, 2012). In the case of Y90F/Y204F, the small λ_{max} at ~290 nm could be

caused by non-specific or low affinity interactions with iron at the site leading to a disturbance of aromatic pi electrons of the mutant phenylalanine residues, or it could be due to the binding of the carbonate anion(s).

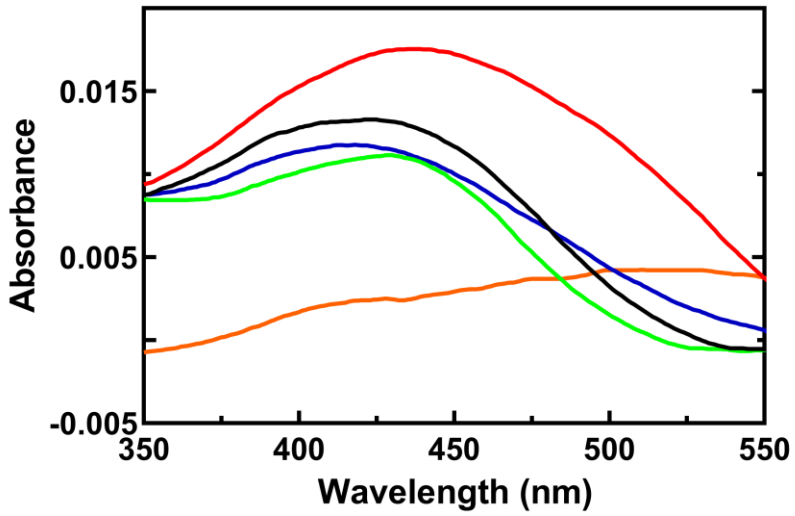

Figure 4-4. Difference spectra of the LMCT peak for WT and mutant forms of MsTsf1. WT MsTsf1 is indicated by a black line, N121A by a red line, N121D by a blue line, N121S by green line and Y90F/Y204F by an orange line. Proteins were at approximately 2 mg/mL in 10 mM HEPES, 20 mM sodium bicarbonate, pH 7.4. To obtain the difference spectra, the apo-protein spectra was subtracted from the holo-protein spectra. The full UV-visible spectra are presented in supplementary Figure 4-10.

Iron affinity and release measurements

To determine the effect of each mutation on iron binding and pH-mediated iron release, we compared the log *K'* and pH_{50} of each mutant to those of the recombinant WT and the previously reported native WT MsTsf1 (Weber et al., 2020).

We used equilibrium dialysis to measure the affinity for iron of recombinant WT MsTsf1 and the N121A, N121S, N121D and Y90F/Y204F mutants. The experiments were set up as an

iron competition assay (Aisen et al., 1978; Tinoco et al., 2008; Weber et al., 2020) between MsTsf1 and citrate, which has a high affinity for iron, with log *K* values as high as 9.5 (Warner and Weber, 1953). Thus, any measurable affinity of MsTsf1 for iron should be due to its ability to out-compete citrate. Recombinant WT MsTsf1 had a high affinity for iron, with log *K'* = 18.3. This result is essentially the same as that reported for native MsTsf1, with log *K'* = 18.4 (Weber et al., 2020) (Table 4-1). There was no difference in log *K'* between the N121A mutant and WT MsTsf1. The N121S and N121D mutants had slightly lower affinities, with average log *K'* = 18.1 (P = 0.037) and 17.9 (P = 0.0009), respectively (Table 4-1). There was no measurable binding of iron by the Y90F/Y204F mutant, which is consistent with the results of the spectroscopic characterization of the Y90F/Y204Y mutant (described above).

The release of iron as a function of pH from WT Tsf1 and the N121 mutants was measured by dialyzing the iron-saturated forms of the proteins against buffers in the pH range of 8 to 4, and calculating the percent iron saturation from the change in the LMCT λ_{max}. Recombinant WT MsTsf1 behaved identically to native MsTsf1, with a pH_{50} of 5.5, and iron release in the pH range of 6.2 to 5.0 (Figure 4.5, Table 4-1). The N121S and N121D mutants released iron at a much higher pH, near pH 7, while the N121A mutant released iron similarly to WT MsTsf1 (Figure 4.5). The N12S mutant had a pH_{50} of 6.0, which is markedly higher than the pH_{50} of WT MsTsf1 (Table 4-1), and the overall release profile was almost linear rather than sigmoidal like that of the other proteins (Figure 4.5). Iron release by WT MsTsf1 and the N121A mutant could not be measured at pH 4 because these proteins precipitated at this pH.

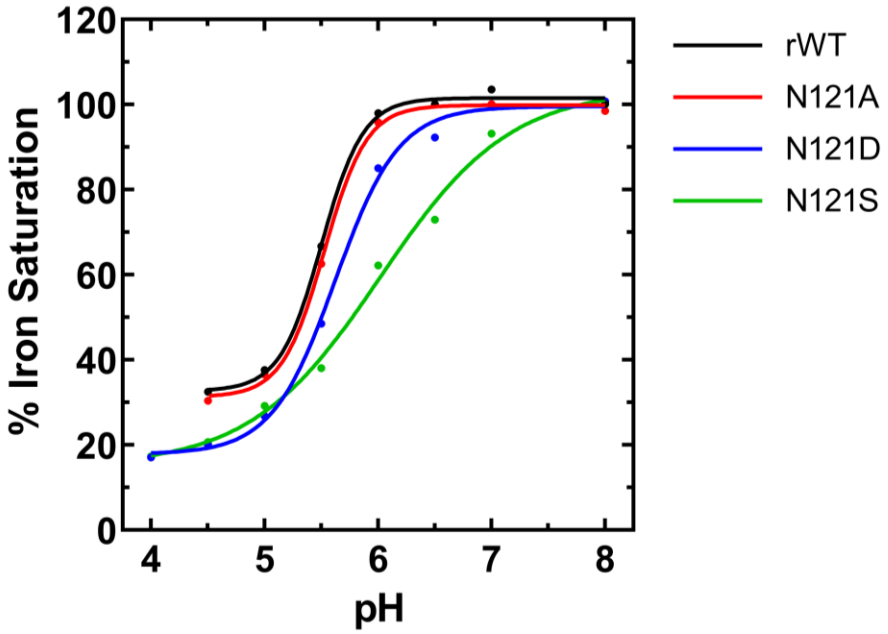

Figure 4-5. The pH-mediated release of iron from WT MsTsf1 and N121 mutants. Data for WT MsTsf1 is colored in black, N121A in red, N121D in blue, and N121S in green. Holo-proteins at 5 mg/mL were dialyzed against various buffers with a pH range of 8 to 4. The percent iron saturation was calculated by measuring the absorbance change in the LMCT λ_{max} before and after dialysis. The pH range of iron release and the point at which the proteins are half saturated with iron (pH_{50}) are reported in Table 4-1.

Secondary structure analysis using far-UV circular dichroism

Far-UV CD spectral analysis is often used to assess secondary structural changes that may occur in proteins under different conditions (Berova et al., 2000). We used far-UV CD to qualitatively assess any obvious changes to the secondary structure of WT and mutant forms of holo- and apo-MsTsf1. We had two main goals when conducting these experiments: 1) to determine if the mutations caused any secondary structural changes to MsTsf1, and 2) to determine if the binding of iron by the WT protein causes structural changes or perturbations.

The CD spectra profile of the apo-proteins were almost identical (Figure 4-6A). The holo-forms of WT MsTsf1 and the N121A, N121D, and Y90F/Y204F mutants have similar spectra, but the spectrum of the holo-N121S mutant is considerably different from those of WT MsTsf1 and the other mutants (Figure 4-6B).

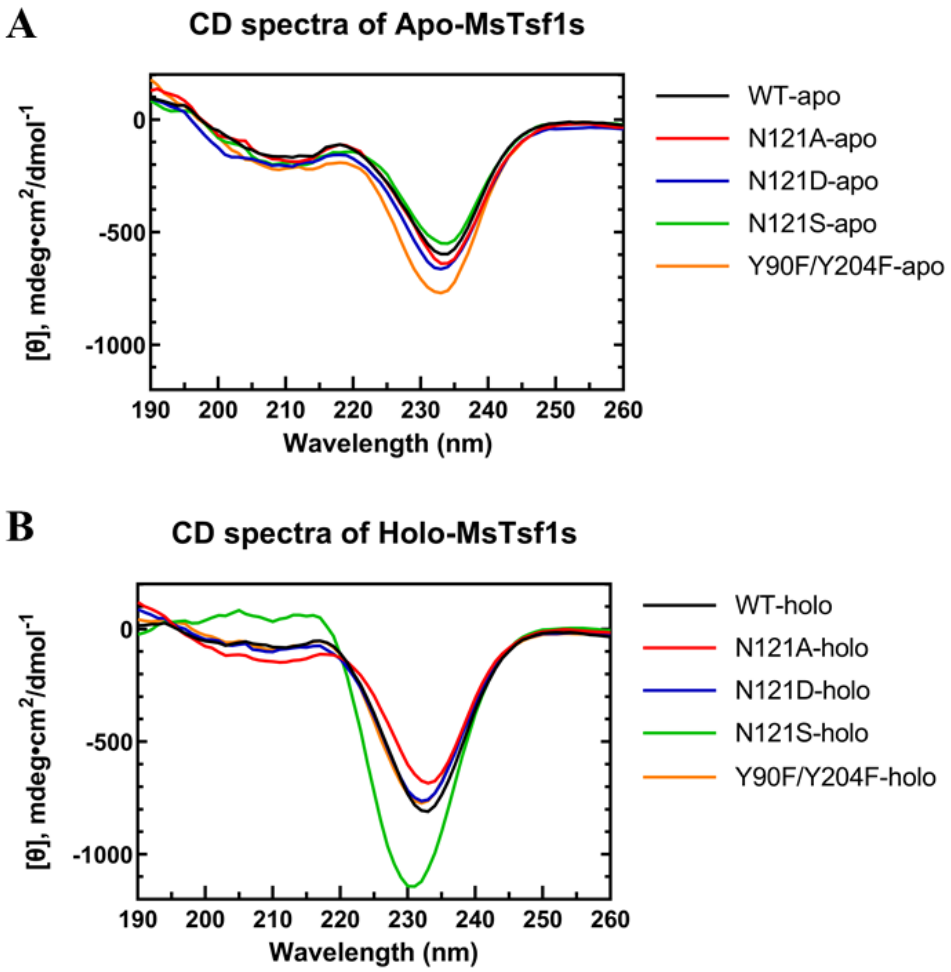

Figure 4-6. Far-UV CD spectra of the apo- and holo-forms of WT and mutant forms of MsTsf1.

A) The CD spectra of the apo-proteins. B) The CD spectra of the holo-proteins. The spectra of the various forms of the proteins are colored the same in each in graph and are as follows: WT in black, N121A in red, N121D in blue, N121S in green, and Y90F/Y204F in orange. Proteins were in a buffer containing 10 mM HEPES, 20 mM sodium bicarbonate, pH 7.4, and a buffer blank was subtracted from each protein spectrum. All spectra were normalized to the protein concentration by converting the units to molar ellipticity (mdeg•cm^2/$dmol^{-1}$).

To determine if iron binding causes secondary structural changes, we compared the difference spectra of WT MsTsf1 and the iron-binding defective mutant, Y90F/Y204F (Figure 4-7). Because Y90F/Y204F does not bind iron in a specific manner, any spectral differences in the apo- and holo-forms of the Y90F/Y204F mutant can be attributed to noise or possibly slight differences in the samples due to apo- and holo- protein sample preparation (e.g. the apo-proteins underwent an extensive dialysis step to remove the bound iron, while the holo-proteins did not). A comparison of the difference spectra demonstrates that the 233 nm peak changes upon iron binding in the WT, but a similar change does not occur in this region for the Y90F/Y204F mutant.

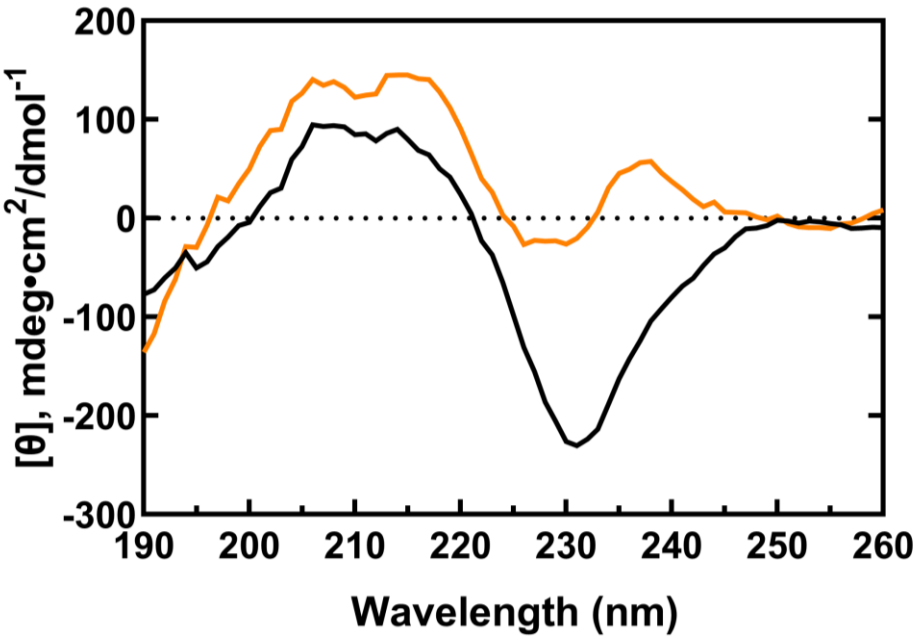

Figure 4-7. Difference CD spectra of WT MsTsf1 and the Y90F/Y204F mutant.
The difference spectra were produced by subtracting the apo-protein spectra from the holo-protein spectra. The difference spectrum of WT MsTsf1 is in black and the difference spectrum of the Y90F/Y204F mutant is in orange. The Y90F/Y204F mutant lacks the 233 nm peak.

Table 4-1. Iron binding and release characteristics of MsTsf WT and mutants

protein	λ_{max} (nm)	average log K' ± S.E.	iron release[a]	pH_{50}[b]
WT	420	18.3 ± 0.06 n=6	6.2—5.0	5.5
N121A	438	18.3 ± 0.07 n=6	6.2—5.0	5.5
N121S	428	18.1 ± 0.08 n=6	>7.1	6.0
N121D	414	17.9 ± 0.05 n=6	7.0—4.5	5.6
Y90F/Y204F	no peak	no measurable affinity	n.a.	n.a.
native-MsTsf1[c]	420	18.4 ± 0.06 n=12	6.2—5.0	5.5

[a]pH range of iron release
[b]pH at 50% iron saturation
[c]Results of native MsTsf1 (Weber et al., 2020)

Discussion

Asn121 contributes to iron coordination in MsTsf1

Asn121 is highly conserved in Tsf1 orthologs from diverse insect species (Weber et al., 2021). The backbone nitrogen group and the side chain $N_{\Delta 2}$ atom of Asn121 form hydrogen bonds with the novel solvent-exposed carbonate anion that functions as an iron ligand. The side chain oxygen of Asn121 forms a hydrogen bond with Tyr338 in the N1 domain, thus creating an N1-N2 intralobal interaction that is closely associated with the iron-binding site (Weber et al., 2021). In vertebrate transferrins, conformational changes occur in the N1 and N2 domains as iron is bound and released (Andersen et al., 1990; Mizutani et al., 2012; Thakurta et al., 2004). If similar conformational changes occur in MsTsf1, the intralobal contact between Asn121 and Tyr338 could influence iron binding and release. Taken together, these findings suggested to us that Asn121 is essential to the function of MsTsf1.

When Asn121 was replaced with serine, aspartate, or alanine, the protein exhibited a shift in its LMCT λ_{max} from 420 nm, which indicates a change in the iron coordination geometry. This result establishes that Asn121 contributes to iron coordination in MsTsf1. Therefore, it was

surprising to find that the Asn121 mutants and WT Tsf1 have similar iron-binding affinities and that the N121A mutant releases iron under the same mildly acidic conditions as WT MsTsf1.

We hypothesized that the N121S mutation would disrupt the N1-N2 intralobal contact but still bind the solvent-exposed carbonate. The serine side chain is one carbon shorter and lacks the carboxamide functional group of asparagine, but it does have a polar hydroxyl group, which modelling suggests is likely to hydrogen bond with the carbonate. The N121S mutant in its holo-form showed a significant difference in the far-UV CD spectral profile. In addition, the N121S mutant had a slightly lower affinity for iron, and it released iron at a much higher pH. Taken together, these results indicate secondary structural perturbations caused by iron binding, and a destabilization of the iron binding and release mechanisms. It is not clear, however, whether a disrupted intralobal contact, altered anion binding, or an unknown interaction of the serine led to these results. Future work is required to determine whether the intralobal contact between Asn121 (N2 domain) and Tyr338 (N1 domain) affects iron binding and release.

The side chain of the aspartate residue in the N121D mutant has a similar length to the side chain of asparagine, but it has a negative charge due to the carboxyl functional group. We had two hypotheses about this negatively charged side chain: 1) the negative charge could repel the negatively charged carbonate anion at the solvent-exposed position, or 2) the aspartate could act as an iron ligand, similar to the iron-ligating aspartate present in vertebrate transferrins (Anderson et al., 1987; Bailey et al., 1988; Kurokawa et al., 1995). Either position of the aspartate would likely lead to a shift of the iron ion and the ligating anions and amino acid residues, leading to destabilization at the iron binding site. The N121D mutant did show a measurable decrease in its affinity for iron, and it released iron at a higher pH. These results

confirm that a negatively charged residue at this position, regardless of the mechanism, is detrimental to the biochemical function of MsTsf1.

Asn121 is not essential to iron binding or release in MsTsf1

The N121A mutant showed no major differences from the WT MsTsf1 in its affinity for iron or pH-mediated iron release. This result was surprising, given that we hypothesized that the shorter, hydrophobic side chain would disrupt both carbonate binding and the Asn121-Tyr388 intralobal contact. How could this mutant disrupt these two bonds without affecting log *K'* or pH_{50}? One possibility is that the hydrogen bonds made by the Asn121 side chain are not important in keeping the carbonate anion bound or in forming the intralobal contact with Tyr33; however, this would contradict the N121D and N121S mutant results, which showed measurable changes in log *K'* and pH_{50}. Moreover, N121A had the largest shift in LMCT λ_{max}, from 420 to 438 nm, suggesting major changes in iron coordination geometry. Another possibility is that in N121A, carbonate binding and the intralobal contact with Tyr338 is replaced by a different residue that can fill the vacant space created by alanine's shorter side chain. The space may be filled by Arg271 because it is relatively close to the anion, it is solvent-exposed with very little steric inhibition of its side chain, and its guanidinium side chain can provide multiple hydrogen bond donor interactions. Modelling showed that it is sterically possible for Arg271 to create hydrogen bonds with the solvent-exposed carbonate and/or the Tyr338. While unexpected, the N121A mutant results are important because they show that an asparagine residue at position 121 does influence iron coordination but that it is not essential for iron binding and release of MsTsf1 *in vitro*.

Asn121 as just one ligand within an anion-binding site

Studies of serum transferrin have probed the protein's ability to substitute carbonate with alternative anions (Dubach et al., 1991; Halbrooks et al., 2004; Harris, 2012; Schlabach and Bates, 1975). Due to steric restrictions, oxalate has proven to be the only organic anion that results in a highly stable iron-anion-transferrin complex (Halbrooks et al., 2004). We have a similar interest in MsTsf1. A computational docking analysis suggested that the buried anion-binding site in MsTsf1 is likely to be specific for a carbonate anion, but that the solvent-exposed position is compatible with other anions (Weber et al., 2021).

Carbonate is present in *M. sexta* hemolymph at 10 mM (Jungreis, 1978). Other organic anions in the hemolymph of *M. sexta* and related insect species are present at similar concentrations (Jungreis, 1978; Phalaraksh et al., 2008; Wyatt, 1961). Several of the reported anions are larger organic acids with various functional groups, for example, the dicarboxylic acids succinate, fumarate, α-ketoglutarate, malate, and oxaloacetate. A computational docking study of these hemolymph anions at the solvent-exposed anion position predicted that the larger anions could bind at this position, and that Asn121, Arg271, and Lys125 would be the ligands (Weber et al., 2021). Despite the different functional groups of the organic anions that were analyzed, Asn121 was predicted to form a hydrogen bond with each of them (Weber et al., 2021). Both of the positively charged residues, Arg271 and Lys125, were predicted to electrostatically interact with one negatively charged end of the dicarboxylic acid anion, while the other negative end of the anion was predicted to coordinate iron.

We hypothesize that Asn121 may be an important part of a larger scheme of anion coordination, which allows insects to utilize the numerous organic anions in their hemolymph at the solvent-exposed anion position (Figure 4.8). This hypothesis is supported by our finding that

the side chain of the amino acid residue at position 121 influences iron coordination, affinity for iron, and iron release. The importance of an asparagine at position 121 may be that it accommodates alternative anions because its carboxamide side chain has the ability to be a hydrogen bond donor and acceptor. This hypothesis is supported by the presence of a threonine residue at position 121 in Tsf1 orthologs from a sandfly, dragonfly, and firebrat (Weber et al., 2021), given that the threonine side chain can also act as a hydrogen bond donor and acceptor. Thus, Asn121's versatility in hydrogen bond formation could facilitate the binding of anions with a variety of functional groups (Figure 4.8). In the case of organic anions with smaller functional groups, like carbonate, the side chain of Asn121 may aid in its coordination but not be essential to the formation of a bond between the anion and iron. Future work is required to determine if other anions can bind at the solvent-exposed position and if the Arg271 and Lys125 residues are involved in their coordination.

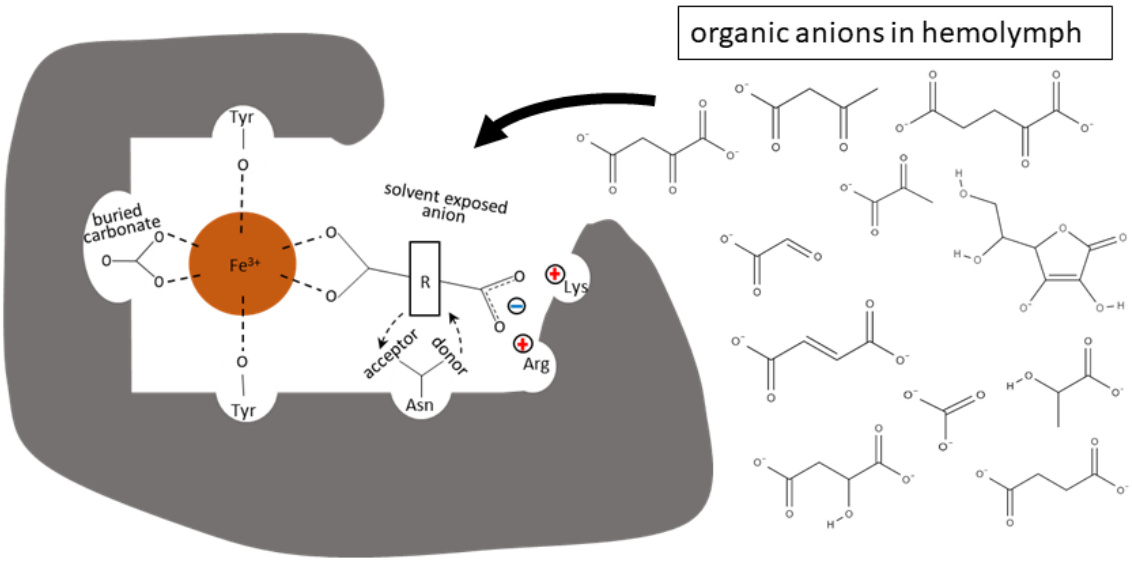

Figure 4-8. Schematic of the solvent-exposed anion position.
Binding of organic acids found in the hemolymph of insects may occur with Asn121, Arg271 and Lys125 as ligands. The coordination of the Fe^{3+} ion through bonds (dashed lines) with the solvent-exposed anion, buried carbonate, and two tyrosines (Tyr90 and Tyr204) are also shown.

Tyr90 and/or Tyr204 are essential to the high-affinity iron binding function of MsTsf1

A previous study of the vertebrate transferrin, lactoferrin, demonstrated that mutating the two iron-ligating tyrosines resulted in the loss of iron binding (Ward et al., 1996). Analyses of amino-acid sequence alignments have suggested that these tyrosine residues are critical for iron binding by *D. melanogaster* Tsf1 (Iatsenko et al., 2020; Weber et al., 2020); moreover, structural analysis of MsTsf1 showed that the two iron-ligating tyrosines are the only amino acid residues that directly coordinate the iron ion (Weber et al., 2021). Our Y90F/Y204F mutant did not have a measurable LMCT λ_{max} in the visible spectrum, and it was unable to out-compete citrate in the equilibrium dialysis assay. This iron-binding defective mutant proved to be a useful control in the affinity and CD analyses, and it showed that these tyrosines in MsTsf1 are essential to its function of binding iron. This mutant validates the use of the Tyr90/Tyr204 mutant as an iron-binding defective mutant for *in vivo* functional studies.

Iron binding does not cause major changes to the secondary structure of MsTsf1

It is known from structural and UV CD studies of vertebrate transferrins that iron binding causes major changes in tertiary but not secondary structure (Andersen et al., 1990; Kurokawa et al., 1995; Messori et al., 1997; Mizutani et al., 2012; Thakurta et al., 2004). The structure of Tsf1 in its apo-form is unknown, but, based on the novel iron binding site and significant interaction of the C-lobe with the N-lobe, we hypothesized that iron binding may induce secondary structural changes in MsTsf1. Far-UV CD analysis of the apo- and holo-forms of WT MsTsf1 and the Y90F/Y204F mutant allowed us to assess any major secondary structural changes associated with iron binding. The far CD spectra of apo- and holo-WT MsTsf1 were nearly

identical in the 190 to 220 nm range, indicating no major changes in the secondary structure upon iron binding; however, the 233 nm negative peak is larger for holo-WT MsTsf1 than apo-WT MsTsf1. The difference spectrum of the Y90F/Y204F mutant, which does not bind iron, lacks a significant negative peak at 233 nm. Previous studies of non-insect holo- and apo-transferrins have shown a similar peak in the CD spectra and attributed it to aromatic side chains, not the secondary structure of the protein polypeptide backbone (Tang et al., 1995; Tinoco et al., 2008). Near-UV CD is often the technique used to measure interactions of aromatic residues; however, far-UV CD can also detect aromatic interactions, with bands typically in the 225-235 nm region (Berova et al., 2000). Disulfide bonds can also contribute to the far-UV CD spectrum, with band intensity and wavelength depending on the number and bond angle of the disulfide bonds (Kelly and Price, 2000). In addition to the iron ligands Tyr90 and Tyr204, MsTsf1 has other aromatic residues, including tryptophan residues that are near the iron-binding site; moreover, MsTsf1 contains twelve disulfide bonds (Weber et al., 2021). Any of these amino acid residues could contribute to the change in the 233 nm peak when MsTsf1 binds to iron. The conformational changes that occur when iron is bound by vertebrate transferrins cause flexing and stress on the secondary structure of N-lobe, which changes disulfide bond angles; however, these changes do not alter the secondary structure content (Andersen et al., 1990; Kurokawa et al., 1995). Future work is needed to determine if the difference we see in the far-UV CD spectra of the apo- and holo-forms of MsTsf1 is due to a direct interaction of the iron with its coordinating ligands, or to perturbations caused by changes in the tertiary structure.

Conclusions

From our mutant analysis of MsTsf1, we conclude that binding of the solvent-exposed carbonate anion by Asn121 contributes to iron coordination, but that Asn121 is not essential for iron binding and release *in vitro*. These results suggest a hypothesis that the importance of Asn121 in Tsf1 comes from its side chain's versatility as a hydrogen bond donor and acceptor, giving it the ability to coordinate numerous organic anions in insect hemolymph. This work also demonstrated that one or both of the two iron-ligating residues of MsTsf1, Tyr90 and Tyr204, are essential to iron binding. Finally, our study indicates that major secondary structural changes do not occur when iron binds to MsTsf1, but, instead, it is likely that there are perturbations of specific aromatic residues or shifts of disulfide bond angles. Our study of iron coordination and anion binding in MsTsf1 resulted in some unexpected findings that will contribute to a mechanistic understanding of how Tsf1 functions in insect iron homeostasis.

Future Directions

The investigation of the iron-coordinating and solvent-exposed anion binding ligands of MsTsf1 answered some questions about the iron-binding and release mechanism of Tsf1, but it also opened the door to further areas of exploration:

(1) The intralobal interaction between Tyr338 and Asn121 closely associates the N1 domain with the iron-binding site in the N2 domain. The importance of this intralobal contact was not directly addressed in the study because it was not clear to what extent the Asn121 mutations disrupted this interaction or anion binding. A future study could further investigate the intralobal contact by mutating the Tyr338 and analyzing its iron binding and iron release characteristics.

(2) The mutational analysis of Asn121 provided more evidence toward the hypothesis that alternative anions may bind at the solvent-exposed anion position. To further verify this hypothesis, future work could attempt to form a stable iron-anion-transferrin complex with these alternative anions (described in detail in the "Future Directions" section of Chapter 3). We are also interested in obtaining a crystal structure of MsTsf1 in complex with one of these alternative anions. Experiments by our collaborators have attempted to soak MsTsf1 crystals with buffer containing these anions, but no promising results have been shown yet. If this hypothesis is verified, a mutational analysis of Arg271 and Lys125 could test whether these amino acid residues are also involved in binding the solvent-exposed anion.

(3) The Y90F/Y204F mutant showed the importance of these two residues in iron coordination, but it did not distinguish if one tyrosine is more important than the other. He et al., (1997) showed that the second tyrosine in the N-lobe of human serum transferrin (equivalent to Tyr204 in Tsf1) is essential to the iron binding function of the protein, but the first tyrosine (Tyr90 in Tsf1) is not (He et al., 1997). To better understand the iron coordinating mechanism of Tsf1, a future study could involve the individual mutation of these tyrosine residues followed by an assessment of their iron binding properties.

Acknowledgements

We thank Neal Dittmer and Kristin Michel for helpful suggestions regarding this work, Lisa Brummett for isolating the MsTsf1 cDNA, and Susan Whitaker at the Kansas State University Biotechnology Core Facility for instrument training and guidance on using circular dichroism. This work was supported by National Science Foundation Grant 1656388. In addition, research reported in this publication was supported by the National Institute of General

Medical Sciences of the National Institutes of Health (NIH) under Award Numbers R37GM041247 and R35GM141859, and by the United States Department of Agriculture National Institute of Food and Agriculture, Hatch Project No. 1013197. The content is solely the responsibility of the authors and does not necessarily represent the official views of the NIH.

References

Aasa, R., Malmström, B.G., Saltman, P., Vänngård, T., 1963. The specific binding of iron(III) and copper(II) to transferrin and conalbumin. Biochimica et Biophysica Acta 75, 203–222. https://doi.org/10.1016/0006-3002(63)90599-7

Adams, T.E., Mason, A.B., He, Q.-Y., Halbrooks, P.J., Briggs, S.K., Smith, V.C., MacGillivray, R.T.A., Everse, S.J., 2003. The Position of Arginine 124 Controls the Rate of Iron Release from the N-lobe of Human Serum Transferrin: A STRUCTURAL STUDY *. Journal of Biological Chemistry 278, 6027–6033. https://doi.org/10.1074/jbc.M210349200

Aisen, P., Leibman, A., 1972. Lactoferrin and transferrin: A comparative study. Biochimica et Biophysica Acta (BBA) - Protein Structure 257, 314–323. https://doi.org/10.1016/0005-2795(72)90283-8

Aisen, P., Leibman, A., Zweier, J., 1978. Stoichiometric and site characteristics of the binding of iron to human transferrin. J. Biol. Chem. 253, 1930–1937.

Andersen, B.F., Baker, H.M., Morris, G.E., Rumball, S.V., Baker, E.N., 1990. Apolactoferrin structure demonstrates ligand-induced conformational change in transferrins. Nature 344, 784–787. https://doi.org/10.1038/344784a0

Anderson, B.F., Baker, H.M., Dodson, E.J., Norris, G.E., Rumball, S.V., Waters, J.M., Baker, E.N., 1987. Structure of human lactoferrin at 3.2-A resolution. Proc. Natl. Acad. Sci. U.S.A. 84, 1769–1773. https://doi.org/10.1073/pnas.84.7.1769

Bai, L., Qiao, M., Zheng, R., Deng, C., Mei, S., Chen, W., 2016. Phylogenomic analysis of transferrin family from animals and plants. Comp. Biochem. Physiol. Part D Genomics Proteomics 17, 1–8. https://doi.org/10.1016/j.cbd.2015.11.002

Bailey, S., Evans, R.W., Garratt, R.C., Gorinsky, B., Hasnain, S., Horsburgh, C., Jhoti, H., Lindley, P.F., Mydin, A., Sarra, R., 1988. Molecular structure of serum transferrin at 3.3-A resolution. Biochemistry 27, 5804–5812. https://doi.org/10.1021/bi00415a061

Baker, E.N., 1994. Structure and Reactivity of Transferrins, in: Sykes, A.G. (Ed.), Advances in Inorganic Chemistry. Academic Press, pp. 389–463. https://doi.org/10.1016/S0898-8838(08)60176-2

Baker, E.N., Baker, H.M., 2009. A structural framework for understanding the multifunctional character of lactoferrin. Biochimie, Advances in Lactoferrin Research 91, 3–10. https://doi.org/10.1016/j.biochi.2008.05.006

Bartfeld, N.S., Law, John H., 1990. Biochemical and Molecular Characterization of Transferrin from Manduca sexta, in: Hagedorn, H.H., Hildebrand, J.G., Kidwell, M.G., Law, J. H. (Eds.), Molecular Insect Science. Springer US, Boston, MA, pp. 125–130. https://doi.org/10.1007/978-1-4899-3668-4_15

Berova, N., Nakanishi, K., Woody, R.W., 2000. Circular Dichroism: Principles and Applications. John Wiley & Sons.

Bonilla, M.L., Todd, C., Erlandson, M., Andres, J., 2015. Combining RNA-seq and proteomic profiling to identify seminal fluid proteins in the migratory grasshopper Melanoplus sanguinipes (F). BMC Genomics 16, 1096. https://doi.org/10.1186/s12864-015-2327-1

Brummett, L.M., Kanost, M.R., Gorman, M.J., 2017. The immune properties of Manduca sexta transferrin. Insect Biochem. Mol. Biol. 81, 1–9. https://doi.org/10.1016/j.ibmb.2016.12.006

Crichton, R.R., Wilmet, S., Legssyer, R., Ward, R.J., 2002. Molecular and cellular mechanisms of iron homeostasis and toxicity in mammalian cells. Journal of Inorganic Biochemistry 91, 9–18. https://doi.org/10.1016/S0162-0134(02)00461-0

Day, C.L., Stowell, K.M., Baker, E.N., Tweedie, J.W., 1992. Studies of the N-terminal half of human lactoferrin produced from the cloned cDNA demonstrate that interlobe interactions modulate iron release. J. Biol. Chem. 267, 13857–13862.

Dubach, J., Gaffney, B.J., More, K., Eaton, G.R., Eaton, S.S., 1991. Effect of the synergistic anion on electron paramagnetic resonance spectra of iron-transferrin anion complexes is consistent with bidentate binding of the anion. Biophysical Journal 59, 1091–1100. https://doi.org/10.1016/S0006-3495(91)82324-4

Farnaud, S., Evans, R.W., 2003. Lactoferrin--a multifunctional protein with antimicrobial properties. Mol. Immunol. 40, 395–405. https://doi.org/10.1016/s0161-5890(03)00152-4

Gasdaska, J.R., Law, J.H., Bender, C.J., Aisen, P., 1996. Cockroach transferrin closely resembles vertebrate transferrins in its metal ion-binding properties: a spectroscopic study. J. Inorg. Biochem. 64, 247–258. https://doi.org/10.1016/s0162-0134(96)00052-9

Geiser, D.L., Winzerling, J.J., 2012. Insect transferrins: multifunctional proteins. Biochim. Biophys. Acta 1820, 437–451. https://doi.org/10.1016/j.bbagen.2011.07.011

Gkouvatsos, K., Papanikolaou, G., Pantopoulos, K., 2012. Regulation of iron transport and the role of transferrin. Biochimica et Biophysica Acta (BBA) - General Subjects 1820, 188–202. https://doi.org/10.1016/j.bbagen.2011.10.013

Halbrooks, P.J., Mason, A.B., Adams, T.E., Briggs, S.K., Everse, S.J., 2004. The Oxalate Effect on Release of Iron from Human Serum Transferrin Explained. Journal of Molecular Biology 339, 217–226. https://doi.org/10.1016/j.jmb.2004.03.049

Han, O., 2011. Molecular mechanism of intestinal iron absorption. Metallomics 3, 103. https://doi.org/10.1039/c0mt00043d

Harris, W.R., 2012. Anion binding properties of the transferrins. Implications for function. Biochimica et Biophysica Acta (BBA) - General Subjects 1820, 348–361. https://doi.org/10.1016/j.bbagen.2011.07.017

Hattori, M., Komatsu, S., Noda, H., Matsumoto, Y., 2015. Proteome Analysis of Watery Saliva Secreted by Green Rice Leafhopper, Nephotettix cincticeps. PLOS ONE 10, e0123671. https://doi.org/10.1371/journal.pone.0123671

Hayashi, K., Longenecker, K.L., Liu, Y.-L., Faust, B., Prashar, A., Hampl, J., Stoll, V., Vivona, S., 2021. Complex of human Melanotransferrin and SC57.32 Fab fragment reveals novel interdomain arrangement with ferric N-lobe and open C-lobe. Sci Rep 11, 566. https://doi.org/10.1038/s41598-020-79090-8

He, Q. Y., Mason, A.B., Woodworth, R.C., Tam, B.M., MacGillivray, R.T., Grady, J.K., Chasteen, N.D., 1997. Inequivalence of the two tyrosine ligands in the N-lobe of human serum transferrin. Biochemistry 36, 14853–14860. https://doi.org/10.1021/bi9719556

Huebers, H.A., Huebers, E., Finch, C.A., Webb, B.A., Truman, J.W., Riddiford, L.M., Martin, A.W., Massover, W.H., 1988. Iron binding proteins and their roles in the tobacco hornworm, Manduca sexta (L.). J. Comp. Physiol. B, Biochem. Syst. Environ. Physiol. 158, 291–300. https://doi.org/10.1007/bf00695327

Iatsenko, I., Marra, A., Boquete, J.-P., Peña, J., Lemaitre, B., 2020. Iron sequestration by transferrin 1 mediates nutritional immunity in Drosophila melanogaster. PNAS 117, 7317–7325. https://doi.org/10.1073/pnas.1914830117

Jeitner, T.M., 2014. Optimized ferrozine-based assay for dissolved iron. Anal. Biochem. 454, 36–37. https://doi.org/10.1016/j.ab.2014.02.026

Jenssen, H., Hancock, R.E.W., 2009. Antimicrobial properties of lactoferrin. Biochimie 91, 19–29. https://doi.org/10.1016/j.biochi.2008.05.015

Jungreis, A.M., 1978. The composition of larval-pupal moulting fluid in the tobacco hornworm, Manduca sexta. Journal of Insect Physiology 24, 65–73. https://doi.org/10.1016/0022-1910(78)90013-6

Kelly, S., Price, N., 2000. The Use of Circular Dichroism in the Investigation of Protein Structure and Function. CPPS 1, 349–384. https://doi.org/10.2174/1389203003381315

Kim, B.Y., Lee, K.S., Choo, Y.M., Kim, I., Je, Y.H., Woo, S.D., Lee, S.M., Park, H.C., Sohn, H.D., Jin, B.R., 2008. Insect transferrin functions as an antioxidant protein in a beetle larva. Comp. Biochem. Physiol. B, Biochem. Mol. Biol. 150, 161–169. https://doi.org/10.1016/j.cbpb.2008.02.009

Kosman, D.J., 2010. Redox cycling in iron uptake, efflux, and trafficking. J. Biol. Chem. 285, 26729–26735. https://doi.org/10.1074/jbc.R110.113217

Kurama, T., Kurata, S., Natori, S., 1995. Molecular Characterization of an Insect Transferrin and its Selective Incorporation into Eggs During Oogenesis. European Journal of Biochemistry 228, 229–235. https://doi.org/10.1111/j.1432-1033.1995.0229n.x

Kurokawa, H., Mikami, B., Hirose, M., 1995. Crystal structure of diferric hen ovotransferrin at 2.4 A resolution. J. Mol. Biol. 254, 196–207. https://doi.org/10.1006/jmbi.1995.0611

Lambert, L.A., 2012. Molecular evolution of the transferrin family and associated receptors. Biochim. Biophys. Acta 1820, 244–255. https://doi.org/10.1016/j.bbagen.2011.06.002

Lambert, L.A., Perri, H., Halbrooks, P.J., Mason, A.B., 2005. Evolution of the transferrin family: conservation of residues associated with iron and anion binding. Comp. Biochem. Physiol. B, Biochem. Mol. Biol. 142, 129–141. https://doi.org/10.1016/j.cbpb.2005.07.007

Lee, K.S., Kim, B.Y., Kim, H.J., Seo, S.J., Yoon, H.J., Choi, Y.S., Kim, I., Han, Y.S., Je, Y.H., Lee, S.M., Kim, D.H., Sohn, H.D., Jin, B.R., 2006. Transferrin inhibits stress-induced apoptosis in a beetle. Free Radic. Biol. Med. 41, 1151–1161. https://doi.org/10.1016/j.freeradbiomed.2006.07.001

Messori, L., Dal Poggetto, G., Monnanni, R., Hirose, J., 1997. [No title found]. Biometals 10, 303–313. https://doi.org/10.1023/A:1018328517603

Mizutani, K., Toyoda, M., Mikami, B., 2012. X-ray structures of transferrins and related proteins. Biochimica et Biophysica Acta (BBA) - General Subjects, Transferrins: Molecular mechanisms of iron transport and disorders 1820, 203–211. https://doi.org/10.1016/j.bbagen.2011.08.003

Najera, D.G., Dittmer, N.T., Weber, J.J., Kanost, M.R., Gorman, M.J., n.d. Phylogenetic and sequence analyses of insect transferrins suggest that only transferrin 1 has a role in iron homeostasis. Insect Science n/a. https://doi.org/10.1111/1744-7917.12783

Nicholson, H., Anderson, B.F., Bland, T., Shewry, S.C., Tweedie, J.W., Baker, E.N., 1997. Mutagenesis of the Histidine Ligand in Human Lactoferrin: Iron Binding Properties and Crystal Structure of the Histidine-253 → Methionine Mutant,. Biochemistry 36, 341–346. https://doi.org/10.1021/bi961908y

Patch, M.G., Carrano, C.J., 1981. The origin of the visible absorption in metal transferrins. Inorganica Chimica Acta 56, L71–L73. https://doi.org/10.1016/S0020-1693(00)88536-9

Phalaraksh, C., E. Reynolds, S., D. Wilson, I., M. Lenz, E., K. Nicholson, J., C. Lindon, J., 2008. A metabonomic analysis of insect development: 1H-NMR spectroscopic characterization of changes in the composition of the haemolymph of larvae and pupae of the tobacco hornworm, Manduca sexta. ScienceAsia 34, 279. https://doi.org/10.2306/scienceasia1513-1874.2008.34.279

Qu, M., Ma, L., Chen, P., Yang, Q., 2014. Proteomic analysis of insect molting fluid with a focus on enzymes involved in chitin degradation. J. Proteome Res. 13, 2931–2940. https://doi.org/10.1021/pr5000957

Schlabach, M.R., Bates, G.W., 1975. The synergistic binding of anions and Fe3+ by transferrin. Implications for the interlocking sites hypothesis. J. Biol. Chem. 250, 2182–2188.

Simmons, L.W., Tan, Y.-F., Millar, A.H., 2013. Sperm and seminal fluid proteomes of the field cricket Teleogryllus oceanicus: identification of novel proteins transferred to females at mating. Insect Mol. Biol. 22, 115–130. https://doi.org/10.1111/imb.12007

Tang, S., MacColl, R., Parsons, P.J., 1995. Spectroscopic study of the interaction of aluminum ions with human transferrin. Journal of Inorganic Biochemistry 60, 175–185. https://doi.org/10.1016/0162-0134(95)00018-J

Thakurta, P.G., Choudhury, D., Dasgupta, R., Dattagupta, J.K., 2004. Tertiary structural changes associated with iron binding and release in hen serum transferrin: a crystallographic and spectroscopic study. Biochemical and Biophysical Research Communications 316, 1124–1131. https://doi.org/10.1016/j.bbrc.2004.02.165

Tinoco, A.D., Peterson, C.W., Lucchese, B., Doyle, R.P., Valentine, A.M., 2008. On the evolutionary significance and metal-binding characteristics of a monolobal transferrin from Ciona intestinalis. PNAS 105, 3268–3273. https://doi.org/10.1073/pnas.0705037105

Ward, P.P., Zhou, X., Conneely, O.M., 1996. Cooperative interactions between the amino- and carboxyl-terminal lobes contribute to the unique iron-binding stability of lactoferrin. J. Biol. Chem. 271, 12790–12794. https://doi.org/10.1074/jbc.271.22.12790

Warner, R.C., Weber, I., 1953. The Cupric and Ferric Citrate Complexes1. J. Am. Chem. Soc. 75, 5086–5094. https://doi.org/10.1021/ja01116a055

Weber, J.J., Kanost, M.R., Gorman, M.J., 2020. Iron binding and release properties of transferrin-1 from Drosophila melanogaster and Manduca sexta: Implications for insect iron homeostasis. Insect Biochemistry and Molecular Biology 125, 103438. https://doi.org/10.1016/j.ibmb.2020.103438

Weber, J.J., Kashipathy, M.M., Battaile, K.P., Go, E., Desaire, H., Kanost, M.R., Lovell, S., Gorman, M.J., 2021. Structural insight into the novel iron-coordination and domain

interactions of transferrin-1 from a model insect, Manduca sexta. Protein Science 30, 408–422. https://doi.org/10.1002/pro.3999

Wyatt, G.R., 1961. The Biochemistry of Insect Hemolymph. Annual Review of Entomology 6, 75–102. https://doi.org/10.1146/annurev.en.06.010161.000451

Xiao, G., Liu, Z.-H., Zhao, M., Wang, H.-L., Zhou, B., 2019. Transferrin 1 Functions in Iron Trafficking and Genetically Interacts with Ferritin in Drosophila melanogaster. Cell Rep 26, 748-758.e5. https://doi.org/10.1016/j.celrep.2018.12.053

Xue, J., Wang, H.-L., Xiao, G., 2020. Transferrin1 modulates rotenone-induced Parkinson's disease through affecting iron homeostasis in Drosophila melanogaster. Biochem Biophys Res Commun 531, 305–311. https://doi.org/10.1016/j.bbrc.2020.07.025

Zhang, J., Lu, A., Kong, L., Zhang, Q., Ling, E., 2014. Functional analysis of insect molting fluid proteins on the protection and regulation of ecdysis. J. Biol. Chem. 289, 35891–35906. https://doi.org/10.1074/jbc.M114.599597

Zhang, L., Gao, J., Gao, X., 2018. Role for Transferrin in Triggering Apoptosis in Helicoverpa armigera Cells Treated with 2-Tridecanone. J. Agric. Food Chem. 66, 11426–11431. https://doi.org/10.1021/acs.jafc.8b02505

Supplementary Materials

MALKLLTLIALTCVAANAAKSSYKLCVPAAYMKDCEQMLEVPTKSKVALECVPARDRVEC
LSFVQQRQADFVPVDPEDMYVASKIPNQDFVVFQEYRTDEEPDAPFRYEAVIVVHKDLPI
NNLDQLKGLRSCHTGVNRNVGYKIPLTMLMKRAVFPKMNDHSISPKENELKALSTFFAKS
CIVGKWSPDPKTNSAWKSQYSHLCSMCEHPERCDYPDNYSGYEGALRCLAHNNGEVAFTK
VIFTRKFFGLPVGTTPASPSNENPEEFRYLCVDGSKAPITGKACSWAARPWQGLIGHNDV
LAKLAPLREKVKQLADSGAADKPEWFTKVLGLSEKIHHVADNIPIKPIDYLNKANYTEVI
ERGHGAPELVVRLCVTSNVALSKCRSMSVFAFSRDIRPILDCVQENSEDACLKSVQDNGS
DLASVDDMRVAAAAKKYNLHPVFHEVYGELKTPNYAVAVVKKGTAYNKIDDLRGKKSCHS
SYSTFSGLHAPLFYLINKRAIQSDHCVKNLGEFFSGGSCLPGVDKPENNPSGDDVSKLKK
QCGSDSSAWKCLEEDRGDVAFVSSADLSHFDANQYELLCLNRDAGGRDVLSSFATCNVAM
APSRTWVAAKDFLSDVSIAHTPLSLAQMLATRPDLFNIYGEFLKNNNVIFNNAAKGLATT
EKLDFEKFKTIHDVISSCGLA

Figure 4-9. Predicted amino acid sequence encoded by the isolated MsTsf1 cDNA.

Tyr90, Tyr204, and Asn121 are highlighted in yellow.

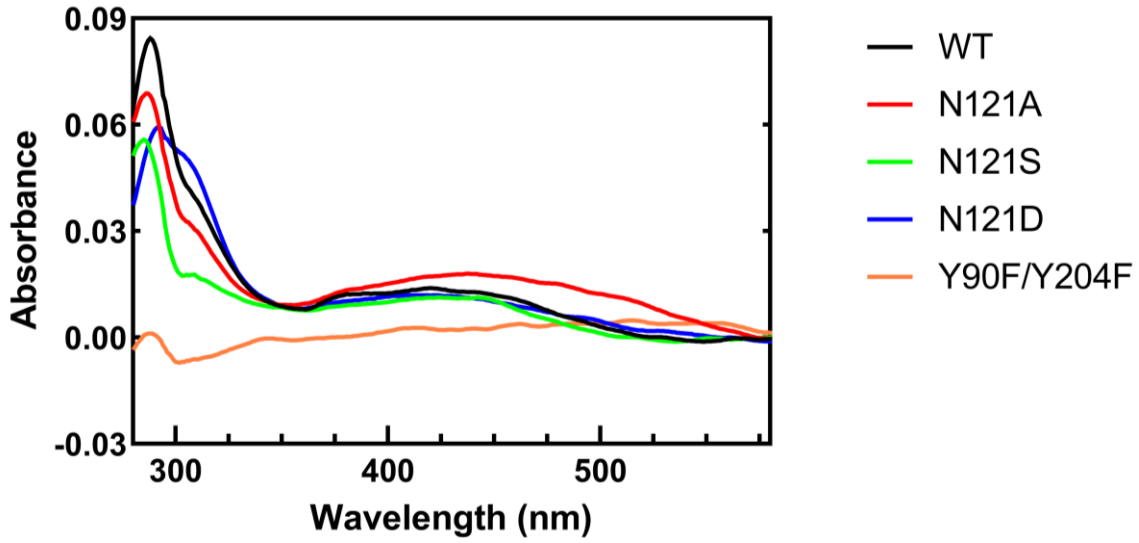

Figure 4-10. Full difference spectra showing the UV and visible LMCT peaks for MsTsf1 WT and mutants.

WT MsTsf1 is indicated by a black line, N121A by a red line, N121D by a blue line, N121S by green line and Y90F/Y204F by an orange line. Proteins were at approximately 2 mg/mL in 10 mM HEPES, 20 mM sodium bicarbonate, pH 7.4. To obtain the difference spectra, the apo-protein spectra was subtracted from the holo-protein spectra.

Table 4-2. Primers, culture volumes and yields for making, expressing, and purifying recombinant proteins

Protein	Primer	Sequence (5'— 3')	Expression volume (liters)	Yield (mg)
WT	cloning forward	GTTGTTGGGCCCATGGCTTTGAAACTTCTA	3.0	34.5
	cloning reverse	TGTGGTCTCGCCTAAGCGGCCGCGTTGTT		
N121A	mutagenic	GGAGTCAATCGTGCCGTCGGGTACAAGATC	1.0	13.5
N121D	mutagenic	GGAGTCAATCGTTCCGTCGGGTACAAGATCC	1.0	20.3
N121S	mutagenic	GGAGTCAATCGTGAC GTCGGGTACAAGATC	1.0	24.9
Y90F/Y204F	Y90F mutagenic	ACGCGCCATTCCGCTTCGAAGCCGTTATCGTGGTT	1.2	19.1
	Y204 mutagenic	GACAATTACAGCGGGTTCGAGGGCGCGTTGAGATG		

*Mutated nucleotides in the mutagenic primers are underlined

Table 4-3. Equilibrium dialysis results for MsTsf1 WT and mutant forms.

Protein	Pre-dialysis			Post-dialysis		Log K'[e]
	[protein][a]	$[Fe^{3+}]_{add}$[b]		$[Fe^{3+}]_{TB}$[c]	$[Fe^{3+}]_{NTB}$[d]	
	µM	µM	trial	µM	µM	
WT	20	7.2	1	4.3	3.0	18.5
			2	3.8	3.4	18.5
		18	1	9.1	8.9	18.4
			2	7.8	10.2	18.4
		45	1	12.1	33.0	18.2
			2	12.1	33.0	18.2
N121A	20	7.2	1	3.8	3.4	18.5
			2	4.2	3.0	18.5
		18	1	7.3	10.7	18.3
			2	7.3	10.7	18.3
		45	1	11.1	33.9	18.1
			2	11.1	33.9	18.1
N121D	20	7.2	1	1.1	6.1	17.9
			2	1.5	5.7	18.1
		18	1	3.2	14.8	18.0
			2	2.8	15.2	17.9
		45	1	5.2	39.8	17.8
			2	4.3	40.7	17.7
N121S	20	7.2	1	2.9	4.3	18.3
			2	2.4	4.8	18.3
		18	1	5.0	13.0	18.2
			2	4.6	13.4	18.1
		45	1	7.0	38.0	17.9
			2	6.1	38.9	17.9
Y90F/Y204F	20	7.2	1	-0.3	7.5	
			2	-0.8	8.0	
		18	1	-0.4	18.4	could not be calculated
			2	-0.9	18.9	
		45	1	0.2	44.8	
			2	-2.0	47.0	

[a]Final concentration of protein after addition to the microdialyzer.
[b]Final concentration of Fe^{3+} after addition to dialyzer (added in the form of Fe^{3+}-citrate).
[c]Tsf1 bound (TB) iron; $[Fe^{3+}]_{TB} = [Fe^{3+}]_{add} - [Fe^{3+}]_{NTB}$.
[d]Concentration of non-Tsf1 bound (NTB) iron measured by the Ferrozine assay.
[e]Calculated using equations described in Weber et al., 2020.

Chapter 5 - Immunohistochemistry and confocal imaging of transferrin-1 uptake in tissues from *Drosophila melanogaster*[1]

[1]Parts of this chapter are included in a manuscript that was submitted to *Insect Biochemistry and Molecular Biology* in June (2021) and is under review.

Introduction

Iron is an essential micronutrient, but it can initiate harmful chemical reactions in cells (Kosman, 2010). Unsurprisingly, animal lineages have evolved homeostatic processes, including iron transport mechanisms, that supply an adequate amount of iron to cells while limiting iron toxicity (Anderson and Leibold, 2014; Galay et al., 2015; Lambert, 2012; Tang and Zhou, 2013a).

In mammals, a key player in iron transport is serum transferrin, an extracellular protein composed of two homologous lobes, each with a high affinity iron-binding site (Gkouvatsos et al., 2012; Mizutani et al., 2012). In mammals, iron is transported out of cells as ferrous ions (Fe^{2+}), oxidized to ferric ions (Fe^{3+}), and loaded onto serum transferrin (De Domenico et al., 2007; Han, 2011). Iron uptake can occur via two pathways that involve transferrin and its receptor. The most widely known mechanism is receptor-mediated endocytic uptake of the Fe^{3+}-transferrin-receptor complex (Frazer and Anderson, 2014). A less recognized mechanism involves extracellular ferric reduction of iron bound to the transferrin-receptor complex followed by ferrous ion uptake (Kosman, 2020). Animals with a severe deficiency of serum transferrin die shortly after birth with symptoms of anemia and iron overload of various tissues; therefore, it appears that the main function of serum transferrin is to provide iron to cells in a regulated manner (Anderson and Vulpe, 2009; Bernstein, 1987; Hamill et al., 1991).

Information about iron transport in insects is surprisingly limited. Transferrin 1 (Tsf1), an insect-specific homolog of mammalian serum transferrin, appears to play a role, although the mechanisms involved have not been solved (Iatsenko et al., 2020a; Najera et al., 2020; Tang and Zhou, 2013b; Xiao et al., 2019). Tsf1 is thought to participate in iron transport because 1) Tsf1-bound iron can be taken up by insect cells, 2) Tsf1 is transported into oocytes, 3) knockdown of Tsf1 results in changes in iron distribution in the insect body, and 4) a lack of Tsf1 interferes with immune-induced transfer of iron from hemolymph to fat body (Huebers et al., 1988; Iatsenko et al., 2020a; Kurama et al., 1995; Xiao et al., 2019). Like serum transferrin, Tsf1 is an extracellular, bilobal protein with high affinity for iron at neutral pH and low affinity at acidic pH; however, many Tsf1 orthologs have only one iron-binding site, and iron coordination by Tsf1 differs from that of serum transferrin (Weber et al., 2020b, 2020a). Because the known aspects of iron transport in insects are quite different from those of the major iron transport pathways in mammals, it is not obvious how Tsf1 may function in iron transport. Whereas iron is transported out of mammalian cells as ferrous ions, iron is transported out of insect cells by the secretion of iron-loaded ferritin; therefore, the source of iron bound to Tsf1 in hemolymph is unknown (Nichol and Locke, 1990; Pham and Winzerling, 2010; Tang and Zhou, 2013b; Whiten et al., 2018; Xiao et al., 2014). In addition, insects lack a mammalian transferrin receptor homolog, and no Tsf1 receptor has been identified (Geiser and Winzerling, 2012; Lambert, 2012).

The goal of this study was to determine whether Tsf1 delivers iron into cells via endocytosis. To answer this question, we used *Drosophila melanogaster* as a model insect system, and used immunohistochemistry to evaluate in which tissue Tsf1 is located and whether

cells take up Tsf1 via endocytosis. Our results indicate that Tsf1 is endocytosed by nephrocytes and oocytes but not by other tissues.

Materials and Methods

Drosophila melanogaster stocks

Insects were cultured at 25.5 °C on K12 High Efficiency diet (United States Biological). The w^{1118} stock (#3605) was obtained from the Bloomington Drosophila Stock Center and was used as the control genotype.

$Tsf1^{m10m1}$, which has a deletion of the entire Tsf1 coding region, was made via CRISPR-Cas9 technology by GenetiVision Corporation. Briefly, guide RNAs (aaccggttgagtcaccacggtgg and gagtggtgtgaaaagccaattgg) and a donor construct containing 3xP3-GFP as a selectable marker were co-injected into *y w; nos-Cas9 (y+)/CyO* eggs, F1 progeny were screened for GFP-expressing individuals, and three independent stocks were established. PCR using genomic DNA as the template was performed by GenetiVision to confirm that the GFP cassette was inserted at the expected location.

Antisera and purification of Tsf1

Recombinant Tsf1 was expressed using a baculovirus expression system and purified as described previously (Weber et al., 2020a). Briefly, Sf9 cells were infected with a recombinant baculovirus made with a full-length Tsf1 cDNA (LP08340, from the Drosophila Genomics Resource Center), and secreted Tsf1 was purified from the medium with the use of ammonium sulfate precipitation, and anion exchange and size exclusion chromatography. Purified Tsf1 (0.3 mg) was sent to Cocalico Biologicals for the production of polyclonal antiserum in a guinea pig.

We used commercially available rabbit antiserum against *D. melanogaster* Rab5 (Abcam). This antiserum has been used by others to identify endosomes in neural tissue, wing discs, eye discs, and other tissues (Fan et al., 2013; Yuva-Aydemir et al., 2011; Zschätzsch et al., 2014).

Tissue preparation and immunohistochemistry

To detect endocytic uptake of Tsf1 in w^{1118} third instar larvae and adult females, we performed immunostaining of Tsf1 and an early endosome marker, Rab5, in whole mounted tissues. A *y w* $Tsf1^{m10m1}$ line was used as a negative control. Insects were dissected in phosphate buffered saline (PB), and samples were briefly rinsed in fresh PBS before processing. Larval tissues were prepared by snipping the anterior end and inverting the carcass by pushing in on the posterior end. Ovaries were dissected from adult females by making an incision in the cuticle on the ventral side of the abdomen and removing the ovaries. Pericardial cells were prepared in adult flies by pinning the down the thorax, making transverse incisions at the anterior and posterior ends of the ventral abdominal cuticle, followed by a longitudinal incision from anterior to posterior ends of the ventral abdominal cuticle, and then pinning down each side of the opening to reveal the abdominal contents. Some fat body and gut tissue was removed to better expose the dorsal vessel and pericardial cells. To analyze adult midguts, Malpighian tubules, and neural tissues, abdomens were prepared similarly to those used for analyzing pericardial cells, without the removal of these tissues.

The antisera used for immunohistochemistry are described in the previous section (Antisera and purification of Tsf1). Dissected samples were fixed in 4% (w/v) paraformaldehyde in PBS solution for 2 hours at 4 ˚C. The samples were washed five times with PBS plus 0.5%

(v/v) Triton X-100 (PBST), with a final incubation in PBST for 5 minutes with agitation at 25 ˚C to permeabilize tissues. Samples were then blocked for 1 hour in PBST and 10% (v/v) goat serum with agitation at 25 ˚C, washed five times with PBST, and incubated with Tsf1 antiserum (1:20,000) for 24 to 48 hours with agitation at 25 ˚C. Five brief washes with PBST were followed by an 8-hour wash with agitation at 25 ˚C. The samples were then incubated with Alexa Flour 568-conjugated goat anti-guinea pig secondary antibody (1:1,000; Invitrogen) with agitation overnight at 4 ˚C or 5 hours at 25 ˚C. Samples were then washed five times with PBST followed by a 4-hour wash with agitation at 25 ˚C. The procedure was repeated for Rab5 endosomal marker staining using Rab5 antiserum (1:1,000; Abcam) and Alexa Flour 488-conjugated goat anti-rabbit secondary antibody (1:1,000; Invitrogen). Samples were transferred to glass slides and mounted in Prolong Gold Antifade mountant (Invitrogen).

Imaging was performed using a Zeiss LSM 700 AxioObserver confocal microscope with Plan-Neofluar 20x/0.50 M27 and 40x/1.30 Oil M27 objectives. Alexa Flour 568 excitation was at 555 nm and emission was at 573 nm. Alexa Flour 488 excitation was at 488 nm and emission was at 518 nm. w^{1118} and $y\ w\ Tsf1^{m10m1}$ samples were imaged with identical settings. Zen 3.1 lite software was used for imaging and processing.

Results

Mammalian serum transferrin, which is transported into cells via receptor-mediated endocytosis, is detectable in endosomes by immunohistochemistry (Mayle et al., 2012); in contrast, endocytic uptake of Tsf1 has not been reported. We used immunohistochemistry to analyze dissected tissues for evidence of intracellular Tsf1 and for colocalization of Tsf1 with the endosome marker Rab5 (Zeigerer et al., 2012).

Tsf1 detection and uptake in oocytes and nephrocytes

We observed intracellular Tsf1 staining in developing oocytes. Co-staining of Tsf1 and Rab5 showed colocalization of the two proteins, which occurred primarily at the posterior apex of the oocyte (Figure 5-1). The Tsf1 staining further into in the cytoplasm was not colocalized with Rab5, and was in a spherical pattern. Endocytosed yolk proteins are often stored in yolk granules for later use during embryogenesis (Schonbaum et al., 2000); moreover, staining of yolk granules often show the same spherical pattern shown in our Tsf1 staining (Liu et al., 2015).

We also observed Tsf1 staining in two types of nephrocyte cells: pericardial cells (Figure 5-2) and garland cells (Figure 5-3). The pericardial cells are large uninucleate cells that flank the heart tube in pairs. The garland cells, also called wreath cells, are binucleate cells that form in a ring around the esophagus (Weavers et al., 2009). The major function of these cells is to filter circulating hemolymph through endocytic uptake, and they are equivalent to the function of kidney glomerular podocytes in humans (Weavers et al., 2009). Co-staining of Tsf1 and Rab5 showed colocalization of the two proteins in both the garland cells and pericardial cells (Figures 5-2 and 5-3).

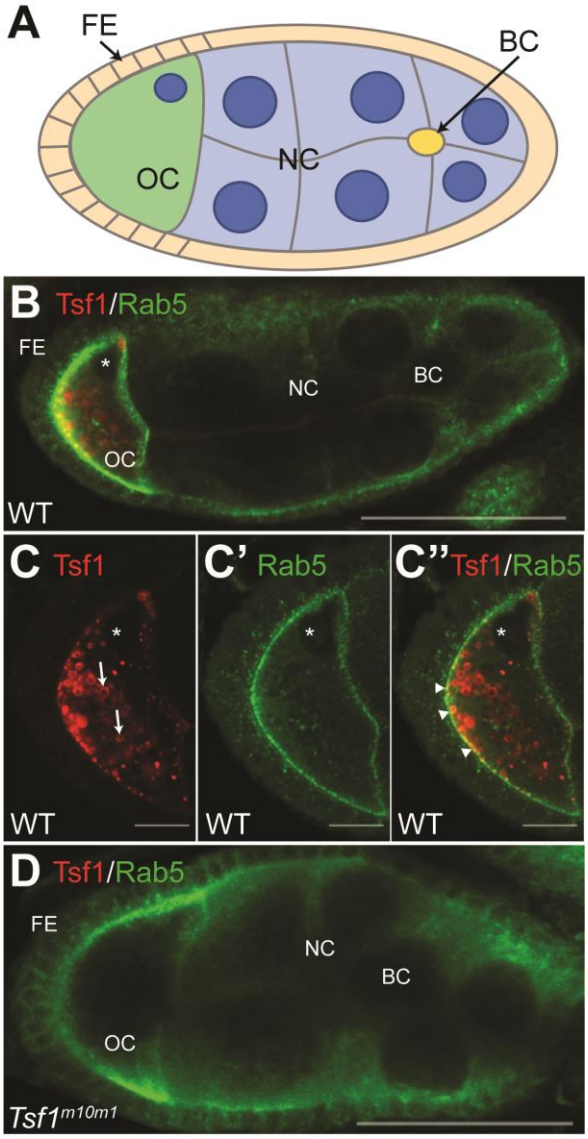

Figure 5-1. Tsf1 colocalized with Rab5 in oocytes.

(A) A schematic diagram of a developing egg chamber. The surrounding layer of follicle epithelium cells (FE) is shown in tan, the border cell (BC) in yellow, the nurse cells (NC) in light blue, and the oocyte (OC) in green, with nuclei in dark blue. (B and D) Egg chambers from wild-type (WT) and *Tsf1*^{m10ml} flies were fixed and processed for immunofluorescence using antibodies against Tsf1 (red) and Rab5 (green). (C - C") A magnified view of a single 0.48 µm slice taken from a Z-stack acquisition of the wild-type oocyte. The arrows in the first panel indicate Tsf1 accumulation in the yolk granules. Colocalization of Tsf1 and Rab5 occurs at the posterior apex of the oocyte, indicated by arrowheads in the third panel. An asterisk indicates the oocyte nucleus. Scale bars are 50 µm for panels B and D and 10 µm for panels C - C''.

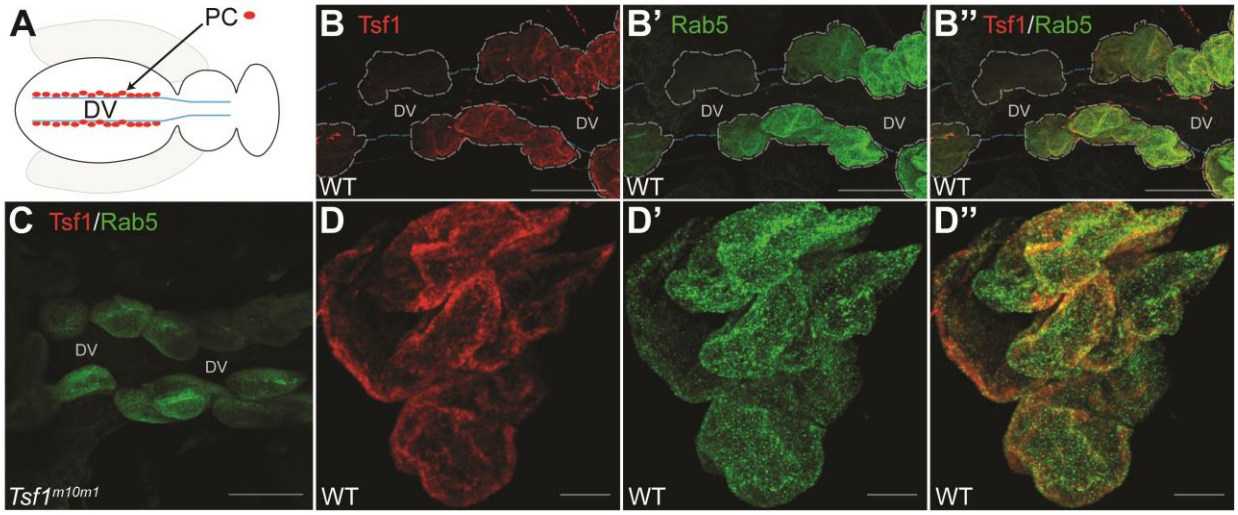

Figure 5-2. Tsf1 colocalized with Rab5 in pericardial cells.

(A) A schematic diagram of the location of pericardial cells (PC) surrounding the dorsal vessel (DV) in the abdomen of adult flies. Pericardial cells from wild-type (WT) and *Tsf1*^{m10ml} (C) flies were fixed and processed for immunofluorescence using antibodies against Tsf1 (red) and Rab5 (green). (B - B" and C) Images are a rendering of 20-30 optical slices from a confocal stack. "DV" indicates the dorsal vessel with its boundary outlined with dashes, while "PC" indicates pericardial cells with their boundaries outlined with dashes. (D - D") Magnified views of a 2 µm slice from the center of a wild-type pericardial cell. Scale bars are 50 µm for panels B - B" and C, and 10 µm for panels D - D".

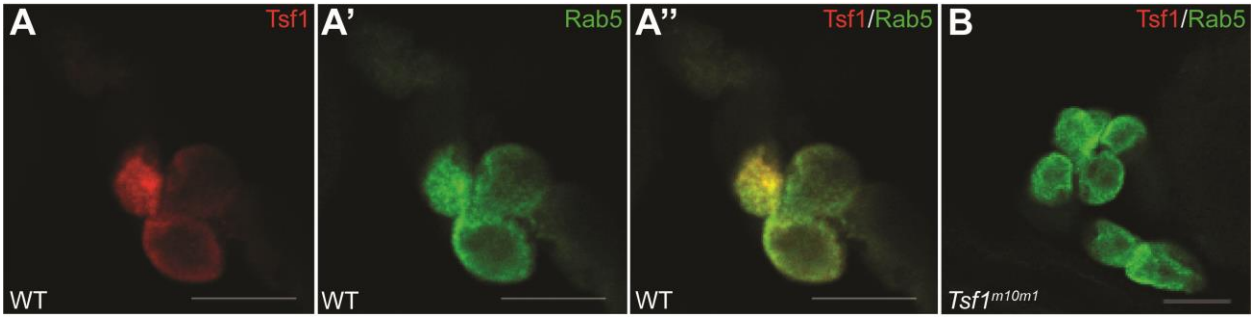

Figure 5-3. Tsf1 colocalized with Rab5 in garland cells.

Garland cells from wild-type (WT) and *Tsf1*^{m10ml} larvae were fixed and processed for immunofluorescence using antibodies against Tsf1 (red) and Rab5 (green). Scale bars are 20 µm.

Tsf1 detection in trachea

The delivery of oxygen to insect tissues occurs through their extensive network of trachea. The architecture of the trachea is comprised of a cuticle layer which is exposed to the lumen, an epithelial layer which surrounds the cuticle, and the basal lamina layer which is exposed to hemolymph or cellular tissue (Snelling et al., 2011). Tsf1 is highly expressed in the epithelial layer of the trachea, where it has been hypothesized to act as a bacteriostatic agent (Wagner et al., 2008a). We observed Tsf1 staining in the trachea (Figure 5-4); however, its localization with respect to Rab5 and the tracheal lumen was not clear.

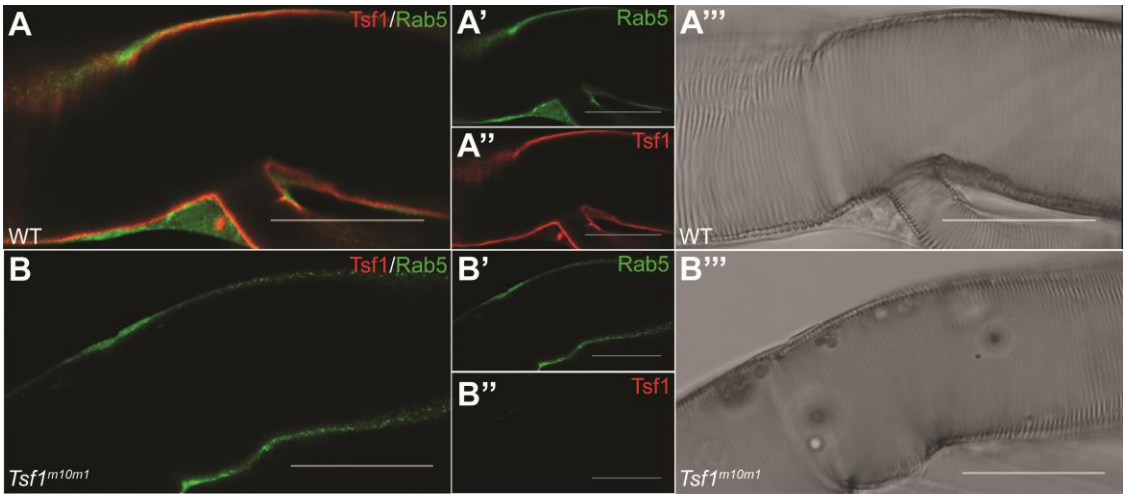

Figure 5-4. Tsf1 is present in tracheae.
Tracheae from wild-type (WT) and *Tsf1*^{m10ml} larvae were fixed and processed for immunofluorescence using antibodies against Tsf1 (red) and Rab5 (green). Images are of a single optical slice from the longitudinal center of the tracheal lumen. No Tsf1 immunoreactivity was observed in tracheae from *Tsf1*^{m10ml} larvae. It is unclear whether Tsf1 staining in wild-type tracheae is lumenal or intracellular. Scale bars are 50 µm.

Lack of Tsf1 detection in fat body and other tissues

We were particularly interested in whether Tsf1 is endocytosed by fat body cells because previous studies demonstrated that, under some circumstances, Tsf1 is involved in the transfer of

iron into the fat body (Iatsenko et al., 2020a; Xiao et al., 2019); however, we failed to detect intracellular Tsf1 in larval or adult fat body (Figures 5-5 and 5-6). In addition, we did not observe consistent or convincing Tsf1 staining within larval or adult Malpighian tubules, neural tissues, or midguts (data not shown).

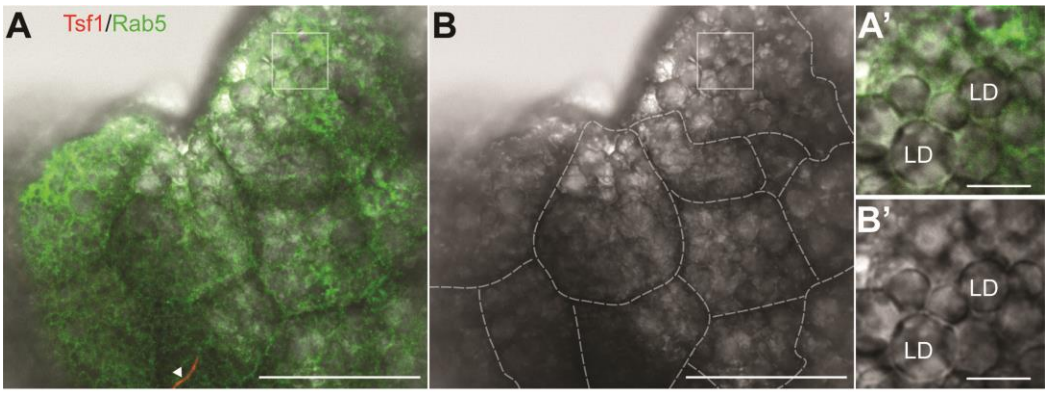

Figure 5-5. Tsf1 was not detected in larval fat body.
(A) Larval fat body was fixed and processed for immunofluorescence using antisera against Tsf1 (red) and Rab5 (green). (B) A brightfield image with the individual fat body cell boundaries outlined with grey dashes is shown. A' and B' are a magnified view of the area bounded by a box in A and B. Lipid droplets (LD) are visible. Note that except for a likely bit of the tracheal system (arrow head), no Tsf1 immunoreactivity was observed. Scale bars are 50 µm for panels A and B and 10 µm for panels A' and B'.

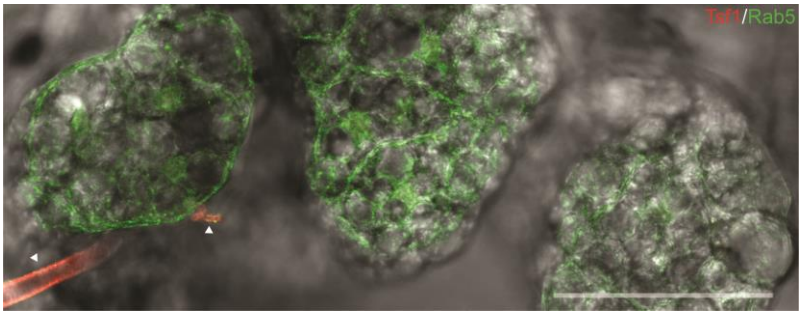

Figure 5-6. Tsf1 was not detected in adult fat body.
Adult fat body was fixed and processed for immunofluorescence using antisera against Tsf1 (red) and Rab5 (green). The brightfield channel is also shown. Note that except for the tracheal system (arrow heads), no Tsf1 immunoreactivity was observed. Scale bar is 50 µm.

Discussion

How iron is transported from one cell to another in insects is still not understood (Calap-Quintana et al., 2017; Mandilaras et al., 2013; Tang and Zhou, 2013b; Whiten et al., 2018). Because the main mechanisms of iron transport in mammals involve serum transferrin (Frazer and Anderson, 2014; Kosman, 2020), one reasonable hypothesis is that Tsf1 plays a similar role in insects. Both Tsf1 and serum transferrin release iron under moderately acidic conditions, suggesting that Tsf1 could release iron in acidified endosomes, as does serum transferrin (Baker et al., 2002; Weber et al., 2020a). Serum transferrin is detectable in endosomes by immunohistochemistry and is even sometimes used as an endosome marker (Mayle et al., 2012). However, we did not find evidence of endocytic uptake of Tsf1 by fat body, Malpighian tubules, neural tissues, or midguts, although our methods may not have been sensitive enough to detect Tsf1 in these tissues. The lack of an identifiable Tsf1 receptor indicates that, if endocytic uptake of Tsf1 does occur in these tissues, the uptake mechanism must have evolved separately from those of mammals.

Whereas most of the tissues analyzed lacked evidence of Tsf1 uptake, we did detect Tsf1 uptake in oocytes. At the start of egg development, the egg chambers of *D. melanogaster* contain 16 germline cells and are surrounded by a single layer of follicle cells. As the chamber develops, one of the 16 germline cells differentiates and becomes the oocyte, while the other 15 cells become nurse cells. As the oocyte develops, it eventually reaches a point of increased endocytic uptake of hemolymph proteins, called vitellogenesis, which usually occurs in stages 8 to 10 (Liu et al., 2015). During vitellogenesis, Rab5 is essential to proper uptake of yolk proteins via clathrin-mediated endocytosis, as well as the maturation of the endosome into yolk granules (Compagnon et al., 2009). We observed endocytic uptake of Tsf1 and colocalization with Rab5

in oocytes; moreover, we found that Tsf1 remained in the oocytes and appeared to be stored in yolk granules. This uptake seemed to occur only at stage 8-10 of their development. This result is consistent with previous studies demonstrating that Tsf1 is abundant in *D. melanogaster* eggs, but that Tsf1 is not expressed in *D. melanogaster* eggs or ovaries (Brown et al., 2014; Casas-Vila et al., 2017; Graveley et al., 2011; Harizanova et al., 2004). Similar results were observed for *Riptortus clavatus* (bean bug) and *Sarcophaga peregrina* (flesh fly) (Hirai et al., 2000; Kurama et al., 1995). Whether apo-Tsf1 is taken up by insect oocytes is not known, but iron-bound Tsf1 was shown to be transported into *S. pergrina* oocytes (Kurama et al., 1995). Interestingly, in separate experiments performed by Maureen Gorman, it was shown that eggs from w^{1118} $Tsf1^{m10ml}$ mothers are not iron deficient, the eggs have a wild-type hatch rate, and the offspring are viable (Gorman, personal communication). Taken together, these results indicate that Tsf1 is not essential for the uptake of iron by oocytes. Instead, the main function of Tsf1 in oocytes and eggs may be that it is stored in yolk granules for later use in immune-related iron sequestration (similar to the role of mammalian lactoferrin or avian ovotransferrin) or protection from iron-induced oxidative stress (Farnaud and Evans, 2003; Giansanti et al., 2012).

We also observed evidence of endocytic uptake of Tsf1 by two types of nephrocytes: pericardial cells and garland cells. Nephrocytes form extensive narrow channels through folding-in of their plasma membrane, and the entire cell is further enclosed in a basement membrane. The nephrocyte's channels and basement membrane allow for size and charge selectivity of particles (Weavers et al., 2009; Zhang et al., 2013). Nephrocytes endocytose these selected particles from hemolymph thereby regulating hemolymph composition (Denholm and Skaer, 2009; Helmstädter et al., 2017). The endocytic contents is either degraded in the lysosome, recycled back to the hemolymph, or stored within the nephrocyte (Helmstädter et al., 2017). *D.*

melanogaster nephrocytes have been implicated in iron homeostasis. Mehta et al. (Mehta et al., 2009) found that under high dietary intake of iron, ferritin was found to accumulate in both the garland and pericardial cells. It was not determined whether the ferritin in the cells was taken up from the hemolymph or if it was expressed endogenously (Mehta et al., 2009); however, with the size selectivity of nephrocytes (Zhang et al., 2013) and the large size of insect ferritin (400 – 600 kDa), it seems more likely that the ferritin is expressed endogenously as a result of high levels of iron in the diet.

But the question remains: if Tsf1 is not taken up into fat body, then how does Tsf1 influence iron transport to this tissue? One possibility is that Tsf1 delivers iron through interactions at plasma membrane and not the through endocytic uptake. Another possibility is that Tsf1 does not directly deliver iron to most tissues, but instead transfers the iron to ferritin. We propose that Tsf1 uptake by nephrocytes could provide a mechanism for Tsf1-bound iron to be released and transferred to ferritin (Figure 5-7). Our hypothesis is that Tsf1 is endocytosed by the nephrocytes, and, within the endosome, iron is released from Tsf1 and then transported into the secretory pathway, where the iron is bound by ferritin. In this way, Tsf1 would be relocating iron from the hemolymph into nephrocytes for redistribution to other tissues or storage via ferritin. This model would explain studies showing Tsf1's function in keeping the level of free iron low in the hemolymph (Huebers et al., 1988) and its influence on relocating and trafficking iron during infection or iron overload (Bartfeld and Law, 1990; Iatsenko et al., 2020b; Xiao et al., 2019), and it would explain ferritin's role in long-term storage of iron in nephrocytes when systemic iron levels are high (Mehta et al., 2009).

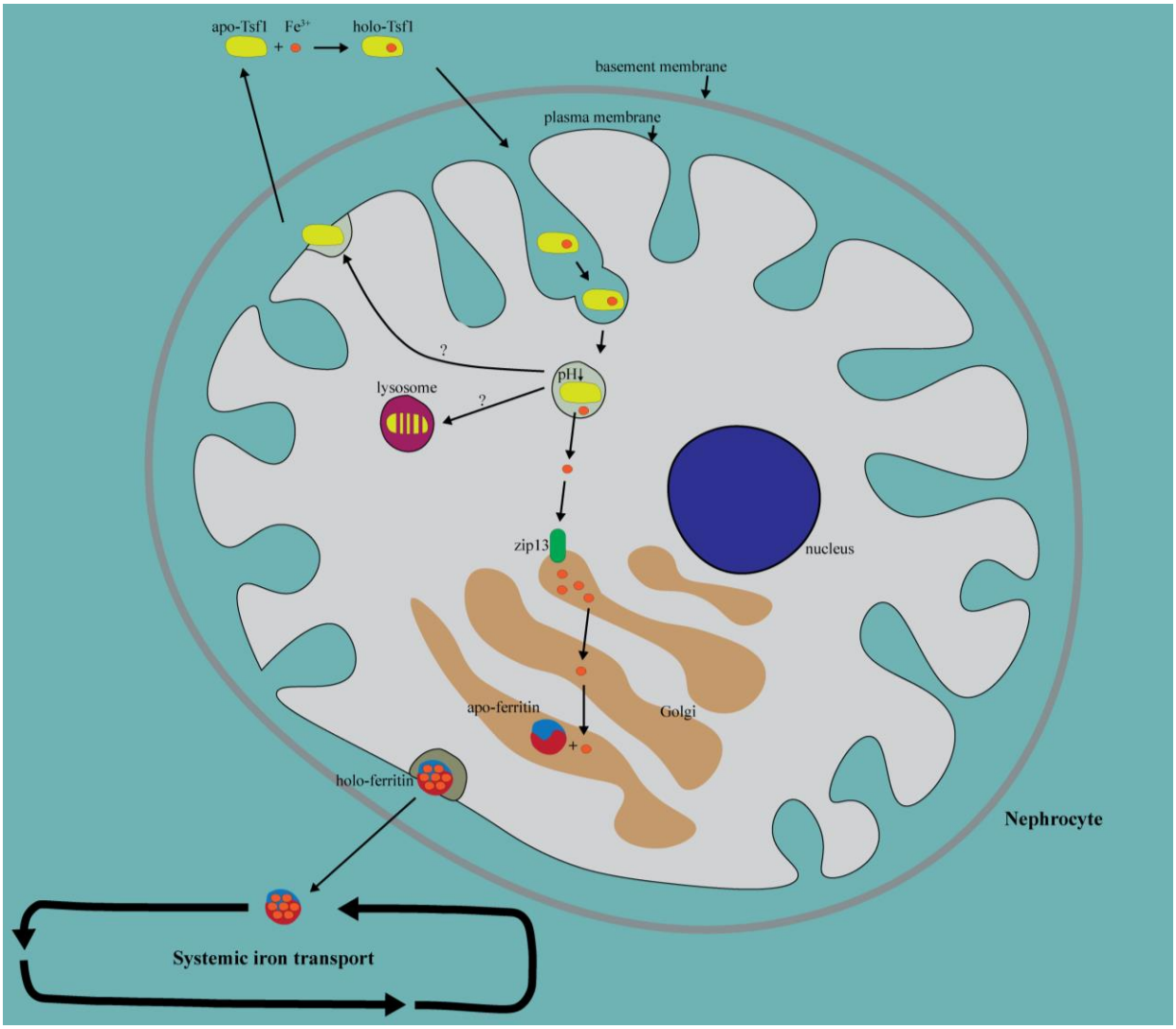

Figure 5-7. Model to explain the function of Tsf1 uptake in nephrocytes.
Iron-saturated Tsf1 in the hemolymph is endocytosed into the nephrocyte where the iron is released, transported into the Golgi and loaded into ferritin for storage or secretion.

Tsf1 orthologs from various insect species have antimicrobial activity, and the bacteriostatic activity of Tsf1 from *M. sexta* is dependent on its ability to sequester iron (Brummett et al., 2017; Ciencialová et al., 2008; Yun et al., 2009). This bacteriostatic activity is likely why Tsf1 is present in extracellular fluids such as molting fluid, saliva, and seminal fluid (Bonilla et al., 2015; Brummett et al., 2017; Geiser and Winzerling, 2012; Hattori et al., 2015;

Qu et al., 2014; Simmons et al., 2013; Zhang et al., 2014). We found that Tsf1 is also present in the tracheal system, where *Tsf1* is highly expressed (Chintapalli et al., 2007; Wagner et al., 2008b). Tsf1 may be secreted into the tracheal lumen or the space between the epithelial cells and cuticle where it could suppress microbial growth.

If the main function of Tsf1 under normal conditions is not to transport iron, then what are its primary functions? Tsf1 appears to protect insects from oxidative stress (Geiser and Winzerling, 2012; Kim et al., 2008; Lee et al., 2006; Xue et al., 2020; Zhang et al., 2018). Although we did not observe a large decrease in the longevity of w^{1118} $Tsf1^{m10ml}$ flies living in standard laboratory conditions (Gorman, personal communication), the presence of Tsf1 may protect against oxidative stress in flies that are exposed to oxidative-stress-inducing conditions (Xue et al., 2020). The bacteriostatic activity of Tsf1 and its presence in extracellular fluids are characteristics similar to those of mammalian lactoferrin (Farnaud and Evans, 2003). Like flies lacking Tsf1, mice lacking lactoferrin are viable and fertile and have apparently normal iron homeostasis (Ward et al., 2003). We suggest that the main functions of Tsf1 may be in protection against iron-induced oxidative stress and immune-related iron sequestration.

Future Directions

Analyzing the uptake of Tsf1 in tissues from *D. melanogaster* has led to several topics for future studies:

(1) Endocytic uptake of hemolymph proteins in nephrocytes and oocytes involves specific receptors. In *D. melanogaster* nephrocytes there are two receptors, Cubilin and Amnionless, which function as co-receptors for hemolymph protein uptake. During vitellogenesis in *D. melanogaster* oocytes, the receptor Yolkless mediates endocytosis of

hemolymph proteins. Future work could focus on the possible interaction of Tsf1 with these receptors and determining what domains of Tsf1 or the receptors are necessary for endocytic uptake into these specific tissues. Moreover, if there is an interaction, it could be determined whether apo- and holo-Tsf1 have different affinity for these receptors.

(2) It has been shown that Tsf1 is involved in the hypoferremic response by relocating iron from the hemolymph into the fat body during an immune challenge (Iatsenko et al., 2020a); however, under normal lab conditions, we did not see Tsf1 uptake in fat body. A future study could look at staining of Tsf1 in the fat body during an immune challenge.

My model of Tsf1 recycling iron in the nephrocytes could also explain this iron relocation function of Tsf1; therefore, it would also be interesting to look and see if there is increased iron content and/or Tsf1 uptake in the nephrocytes during an immune challenge.

(3) The fate Tsf1 in the nephrocytes was not clear from the immunostaining in this study. A future study could focus on whether Tsf1 is recycled back to the hemolymph, like the recycling of serum transferrin in mammals, or if it is degraded in the lysosome.

(4) The model of iron recycling in nephrocytes is reliant somewhat on ferritin being expressed in the nephrocytes (so that it can bind iron from endocytosed Tsf1 in the Golgi); however, the subcellular location and the level of expression of ferritin found in nephrocytes is not clear. Future work could focus on staining ferritin in nephrocytes to determine its subcellular location.

(5) Whether Tsf1 staining in the trachea occurred in the lumen was not clear. Future work could implement staining of chitin or other components of the tracheal system to get a better idea of the location of the Tsf1.

(6) It is not clear what the role of Tsf1 uptake into eggs is, but Maureen Gorman's experiments on survival and iron content of *Tsf1*^{m10ml} eggs show that Tsf1 is not necessary for delivering iron to this tissue. One hypothesis is that the Tsf1 is taken up and stored in yolk granules for later use as a bacteriostatic agent or sequestering free iron to reduce oxidative stress. In order to perform these functions, Tsf1 would need to be in its apo-form and would need to be eventually be free of the yolk granule. During vitellogenesis the yolk granules are equivalent to dormant lysosomes, but eventually during embryogenesis the granules turn acidic and become lysosomes, which could degrade the stored Tsf1. Future work on Tsf1 function in oocytes could focus on two questions: do oocytes specifically take up apo-Tsf1, and what is the fate of Tsf1 after it is stored in yolk granules?

Acknowledgements

I would like to thank Dr. Maureen Gorman and Dr. Yoonseong Park for their helpful suggestions in planning experiments and their time spent training me in dissection, staining, and imaging techniques. Dr. Gorman also had a role in writing some parts of this chapter, which was combined with additional work and submitted as a manuscript in June (2021). I would also like to thank Joel Sanneman for confocal microscopy training at the Kansas State University College of Veterinary Medicine Confocal Core Facility. This work was supported by National Science Foundation Grant 1656388. In addition, research reported in this chapter was supported by the National Institute of General Medical Sciences of the National Institutes of Health (NIH) under Award Numbers R37GM041247 and R35GM141859, and by the United States Department of Agriculture National Institute of Food and Agriculture, Hatch Project No. 1013197. This is contribution 21-324-J from the Kansas Agricultural Experiment Station. Stocks obtained from

the Bloomington Drosophila Stock Center (NIH P40OD018537) were used in this study. A cDNA clone was obtained from the Drosophila Genomics Resource Center, supported by NIH grant 2P40OD010949.

References

Anderson, C.P., Leibold, E.A., 2014. Mechanisms of iron metabolism in Caenorhabditis elegans. Front Pharmacol 5, 113. https://doi.org/10.3389/fphar.2014.00113

Anderson, G.J., Vulpe, C.D., 2009. Mammalian iron transport. Cell. Mol. Life Sci. 66, 3241. https://doi.org/10.1007/s00018-009-0051-1

Bartfeld, N.S., Law, John H., 1990. Biochemical and Molecular Characterization of Transferrin from Manduca sexta, in: Hagedorn, H.H., Hildebrand, J.G., Kidwell, M.G., Law, J. H. (Eds.), Molecular Insect Science. Springer US, Boston, MA, pp. 125–130. https://doi.org/10.1007/978-1-4899-3668-4_15

Bernstein, S.E., 1987. Hereditary hypotransferrinemia with hemosiderosis, a murine disorder resembling human atransferrinemia. J Lab Clin Med 110, 690–705.

Bonilla, M.L., Todd, C., Erlandson, M., Andres, J., 2015. Combining RNA-seq and proteomic profiling to identify seminal fluid proteins in the migratory grasshopper Melanoplus sanguinipes (F). BMC Genomics 16, 1096. https://doi.org/10.1186/s12864-015-2327-1

Brown, J.B., Boley, N., Eisman, R., May, G.E., Stoiber, M.H., Duff, M.O., Booth, B.W., Wen, J., Park, S., Suzuki, A.M., Wan, K.H., Yu, C., Zhang, D., Carlson, J.W., Cherbas, L., Eads, B.D., Miller, D., Mockaitis, K., Roberts, J., Davis, C.A., Frise, E., Hammonds, A.S., Olson, S., Shenker, S., Sturgill, D., Samsonova, A.A., Weiszmann, R., Robinson, G., Hernandez, J., Andrews, J., Bickel, P.J., Carninci, P., Cherbas, P., Gingeras, T.R., Hoskins, R.A., Kaufman, T.C., Lai, E.C., Oliver, B., Perrimon, N., Graveley, B.R., Celniker, S.E., 2014. Diversity and dynamics of the Drosophila transcriptome. Nature 512, 393–399. https://doi.org/10.1038/nature12962

Brummett, L.M., Kanost, M.R., Gorman, M.J., 2017. The immune properties of Manduca sexta transferrin. Insect Biochem. Mol. Biol. 81, 1–9. https://doi.org/10.1016/j.ibmb.2016.12.006

Casas-Vila, N., Bluhm, A., Sayols, S., Dinges, N., Dejung, M., Altenhein, T., Kappei, D., Altenhein, B., Roignant, J.-Y., Butter, F., 2017. The developmental proteome of Drosophila melanogaster. Genome Res. 27, 1273–1285. https://doi.org/10.1101/gr.213694.116

Chintapalli, V.R., Wang, J., Dow, J.A.T., 2007. Using FlyAtlas to identify better Drosophila melanogaster models of human disease. Nature Genetics 39, 715–720. https://doi.org/10.1038/ng2049

Ciencialová, A., Neubauerová, T., Šanda, M., Šindelka, R., Cvačka, J., Voburka, Z., Buděšínský, M., Kašička, V., Sázelová, P., Šolínová, V., Macková, M., Koutek, B., Jiráček, J., 2008. Mapping the peptide and protein immune response in the larvae of the fleshfly Sarcophaga bullata. J. Peptide Sci. 14, 670–682. https://doi.org/10.1002/psc.967

Compagnon, J., Gervais, L., Roman, M.S., Chamot-Bœuf, S., Guichet, A., 2009. Interplay between Rab5 and PtdIns(4,5) P 2 controls early endocytosis in the Drosophila germline. Journal of Cell Science 122, 25–35. https://doi.org/10.1242/jcs.033027

De Domenico, I., Ward, D.M., di Patti, M.C.B., Jeong, S.Y., David, S., Musci, G., Kaplan, J., 2007. Ferroxidase activity is required for the stability of cell surface ferroportin in cells expressing GPI-ceruloplasmin. EMBO J 26, 2823–2831. https://doi.org/10.1038/sj.emboj.7601735

Denholm, B., Skaer, H., 2009. Bringing together components of the fly renal system. Current Opinion in Genetics & Development, Differentation and gene regulation 19, 526–532. https://doi.org/10.1016/j.gde.2009.08.006

Fan, J., Jiang, K., Liu, Y., Jia, J., 2013. Hrs promotes ubiquitination and mediates endosomal trafficking of smoothened in Drosophila hedgehog signaling. PLoS One 8, e79021. https://doi.org/10.1371/journal.pone.0079021

Farnaud, S., Evans, R.W., 2003. Lactoferrin—a multifunctional protein with antimicrobial properties. Molecular Immunology, Innate Mechanisms of Epithelial Host Defence. Spotlight on Antimicrobial Peptides. 40, 395–405. https://doi.org/10.1016/S0161-5890(03)00152-4

Frazer, D.M., Anderson, G.J., 2014. The regulation of iron transport. Biofactors 40, 206–214. https://doi.org/10.1002/biof.1148

Galay, R.L., Umemiya-Shirafuji, R., Mochizuki, M., Fujisaki, K., Tanaka, T., 2015. Iron metabolism in hard ticks (Acari: Ixodidae): the antidote to their toxic diet. Parasitol. Int. 64, 182–189. https://doi.org/10.1016/j.parint.2014.12.005

Geiser, D.L., Winzerling, J.J., 2012. Insect transferrins: Multifunctional proteins. Biochim. Biophys. Acta-Gen. Subj. 1820, 437–451. https://doi.org/10.1016/j.bbagen.2011.07.011

Giansanti, F., Leboffe, L., Pitari, G., Ippoliti, R., Antonini, G., 2012. Physiological roles of ovotransferrin. Biochim. Biophys. Acta 1820, 218–225. https://doi.org/10.1016/j.bbagen.2011.08.004

Gkouvatsos, K., Papanikolaou, G., Pantopoulos, K., 2012. Regulation of iron transport and the role of transferrin. Biochim. Biophys. Acta-Gen. Subj. 1820, 188–202. https://doi.org/10.1016/j.bbagen.2011.10.013

Graveley, B.R., Brooks, A.N., Carlson, J.W., Duff, M.O., Landolin, J.M., Yang, L., Artieri, C.G., van Baren, M.J., Boley, N., Booth, B.W., Brown, J.B., Cherbas, L., Davis, C.A., Dobin, A., Li, R., Lin, W., Malone, J.H., Mattiuzzo, N.R., Miller, D., Sturgill, D., Tuch, B.B., Zaleski, C., Zhang, D., Blanchette, M., Dudoit, S., Eads, B., Green, R.E., Hammonds, A., Jiang, L., Kapranov, P., Langton, L., Perrimon, N., Sandler, J.E., Wan, K.H., Willingham, A., Zhang, Y., Zou, Y., Andrews, J., Bickel, P.J., Brenner, S.E., Brent, M.R., Cherbas, P., Gingeras, T.R., Hoskins, R.A., Kaufman, T.C., Oliver, B., Celniker, S.E., 2011. The developmental transcriptome of Drosophila melanogaster. Nature 471, 473–479. https://doi.org/10.1038/nature09715

Hamill, R.L., Woods, J.C., Cook, B.A., 1991. Congenital Atransferrinemia A Case Report and Review of the Literature. American Journal of Clinical Pathology 96, 215–218. https://doi.org/10.1093/ajcp/96.2.215

Han, O., 2011. Molecular mechanism of intestinal iron absorption. Metallomics 3, 103–109. https://doi.org/10.1039/c0mt00043d

Harizanova, N., Tchorbadjieva, M., Ivanova, P., Dimov, S., Ralchev, K., 2004. Developmental and Organ-Specific Expression of Transferrin in Drosophila Melanogaster. Biotechnology & Biotechnological Equipment 18, 118–121. https://doi.org/10.1080/13102818.2004.10817097

Hattori, M., Komatsu, S., Noda, H., Matsumoto, Y., 2015. Proteome Analysis of Watery Saliva Secreted by Green Rice Leafhopper, Nephotettix cincticeps. PLoS ONE 10, e0123671. https://doi.org/10.1371/journal.pone.0123671

Helmstädter, M., Huber, T.B., Hermle, T., 2017. Using the Drosophila Nephrocyte to Model Podocyte Function and Disease. Front. Pediatr. 5. https://doi.org/10.3389/fped.2017.00262

Hirai, M., Watanabe, D., Chinzei, Y., 2000. A juvenile hormone-repressible transferrin-like protein from the bean bug, Riptortus clavatus: cDNA sequence analysis and protein identification during diapause and vitellogenesis. Arch. Insect Biochem. Physiol. 44, 17–26. https://doi.org/10.1002/(SICI)1520-6327(200005)44:1<17::AID-ARCH3>3.0.CO;2-O

Huebers, H.A., Huebers, E., Finch, C.A., Webb, B.A., Truman, J.W., Riddiford, L.M., Martin, A.W., Massover, W.H., 1988. Iron binding proteins and their roles in the tobacco hornworm, Manduca sexta (L.). J. Comp. Physiol. B, Biochem. Syst. Environ. Physiol. 158, 291–300.

Iatsenko, I., Marra, A., Boquete, J.-P., Peña, J., Lemaitre, B., 2020a. Iron sequestration by transferrin 1 mediates nutritional immunity in Drosophila melanogaster. PNAS 117, 7317–7325. https://doi.org/10.1073/pnas.1914830117

Iatsenko, I., Marra, A., Boquete, J.-P., Peña, J., Lemaitre, B., 2020b. Iron sequestration by transferrin 1 mediates nutritional immunity in Drosophila melanogaster. PNAS 117, 7317–7325. https://doi.org/10.1073/pnas.1914830117

Kim, B.Y., Lee, K.S., Choo, Y.M., Kim, I., Je, Y.H., Woo, S.D., Lee, S.M., Park, H.C., Sohn, H.D., Jin, B.R., 2008. Insect transferrin functions as an antioxidant protein in a beetle larva. Comparative Biochemistry and Physiology Part B: Biochemistry and Molecular Biology 150, 161–169. https://doi.org/10.1016/j.cbpb.2008.02.009

Kosman, D.J., 2020. A holistic view of mammalian (vertebrate) cellular iron uptake. Metallomics 12, 1323–1334. https://doi.org/10.1039/d0mt00065e

Kosman, D.J., 2010. Redox cycling in iron uptake, efflux, and trafficking. J. Biol. Chem. 285, 26729–26735. https://doi.org/10.1074/jbc.R110.113217

Kurama, T., Kurata, S., Natori, S., 1995. Molecular Characterization of an Insect Transferrin and its Selective Incorporation into Eggs During Oogenesis. European Journal of Biochemistry 228, 229–235. https://doi.org/10.1111/j.1432-1033.1995.0229n.x

Lambert, L.A., 2012. Molecular evolution of the transferrin family and associated receptors. Biochim. Biophys. Acta-Gen. Subj. 1820, 244–255. https://doi.org/10.1016/j.bbagen.2011.06.002

Lee, K.S., Kim, B.Y., Kim, H.J., Seo, S.J., Yoon, H.J., Choi, Y.S., Kim, I., Han, Y.S., Je, Y.H., Lee, S.M., Kim, D.H., Sohn, H.D., Jin, B.R., 2006. Transferrin inhibits stress-induced apoptosis in a beetle. Free Radic. Biol. Med. 41, 1151–1161. https://doi.org/10.1016/j.freeradbiomed.2006.07.001

Liu, G., Sanghavi, P., Bollinger, K.E., Perry, L., Marshall, B., Roon, P., Tanaka, T., Nakamura, A., Gonsalvez, G.B., 2015. Efficient Endocytic Uptake and Maturation in Drosophila Oocytes Requires Dynamitin/p50. Genetics 201, 631–649. https://doi.org/10.1534/genetics.115.180018

Mehta, A., Deshpande, A., Bettedi, L., Missirlis, F., 2009. Ferritin accumulation under iron scarcity in Drosophila iron cells. Biochimie 91, 1331–1334. https://doi.org/10.1016/j.biochi.2009.05.003

Mizutani, K., Toyoda, M., Mikami, B., 2012. X-ray structures of transferrins and related proteins. Biochim. Biophys. Acta-Gen. Subj. 1820, 203–211. https://doi.org/10.1016/j.bbagen.2011.08.003

Najera, D.G., Dittmer, N.T., Weber, J.J., Kanost, M.R., Gorman, M.J., 2020. Phylogenetic and sequence analyses of insect transferrins suggest that only transferrin 1 has a role in iron homeostasis. Insect Sci. https://doi.org/10.1111/1744-7917.12783

Nichol, H., Locke, M., 1990. The Localization of Ferritin in Insects. Tissue Cell 22, 767–777. https://doi.org/10.1016/0040-8166(90)90042-8

Pham, D.Q.D., Winzerling, J.J., 2010. Insect ferritins: Typical or atypical? Biochim. Biophys. Acta 1800, 824–833. https://doi.org/10.1016/j.bbagen.2010.03.004

Qu, M., Ma, L., Chen, P., Yang, Q., 2014. Proteomic Analysis of Insect Molting Fluid with a Focus on Enzymes Involved in Chitin Degradation. J. Proteome Res. 13, 2931–2940. https://doi.org/10.1021/pr5000957

Schonbaum, C.P., Perrino, J.J., Mahowald, A.P., 2000. Regulation of the Vitellogenin Receptor during Drosophila melanogaster Oogenesis. MBoC 11, 511–521. https://doi.org/10.1091/mbc.11.2.511

Simmons, L.W., Tan, Y.-F., Millar, A.H., 2013. Sperm and seminal fluid proteomes of the field cricket Teleogryllus oceanicus: identification of novel proteins transferred to females at mating. Insect Mol Biol 22, 115–130. https://doi.org/10.1111/imb.12007

Snelling, E.P., Seymour, R.S., Runicman, S., 2011. Moulting of insect tracheae captured by light and electron-microscopy in the metathoracic femur of a third instar locust *Locusta migratoria.* Journal of Insect Phys. 57, 1312-1316. DOI: 10.1016/j.jinsphys.2011.06.006

Tang, X., Zhou, B., 2013a. Ferritin is the key to dietary iron absorption and tissue iron detoxification in Drosophila melanogaster. Faseb J. 27, 288–298. https://doi.org/10.1096/fj.12-213595

Tang, X., Zhou, B., 2013b. Iron homeostasis in insects: Insights from Drosophila studies. IUBMB Life 65, 863–872. https://doi.org/10.1002/iub.1211

Wagner, C., Isermann, K., Fehrenbach, H., Roeder, T., 2008a. Molecular architecture of the fruit fly's airway epithelial immune system. BMC Genomics 9, 446. https://doi.org/10.1186/1471-2164-9-446

Wagner, C., Isermann, K., Fehrenbach, H., Roeder, T., 2008b. Molecular architecture of the fruit fly's airway epithelial immune system. BMC Genomics 9, 446. https://doi.org/10.1186/1471-2164-9-446

Ward, P.P., Mendoza-Meneses, M., Cunningham, G.A., Conneely, O.M., 2003. Iron status in mice carrying a targeted disruption of lactoferrin. Mol Cell Biol 23, 178–185. https://doi.org/10.1128/MCB.23.1.178-185.2003

Weavers, H., Prieto-Sánchez, S., Grawe, F., Garcia-López, A., Artero, R., Wilsch-Bräuninger, M., Ruiz-Gómez, M., Skaer, H., Denholm, B., 2009. The insect nephrocyte is a podocyte-like cell with a filtration slit diaphragm. Nature 457, 322–326. https://doi.org/10.1038/nature07526

Weber, J.J., Kanost, M.R., Gorman, M.J., 2020a. Iron binding and release properties of transferrin-1 from Drosophila melanogaster and Manduca sexta: Implications for insect iron homeostasis. Insect Biochem Mol Biol 125, 103438. https://doi.org/10.1016/j.ibmb.2020.103438

Weber, J.J., Kashipathy, M.M., Battaile, K.P., Go, E., Desaire, H., Kanost, M.R., Lovell, S., Gorman, M.J., 2020b. Structural insight into the novel iron-coordination and domain

interactions of transferrin-1 from a model insect, Manduca sexta. Protein Sci. https://doi.org/10.1002/pro.3999

Whiten, S.R., Eggleston, H., Adelman, Z.N., 2018. Ironing out the Details: Exploring the Role of Iron and Heme in Blood-Sucking Arthropods. Front. Physiol. 8. https://doi.org/10.3389/fphys.2017.01134

Xiao, G., Liu, Z.-H., Zhao, M., Wang, H.-L., Zhou, B., 2019. Transferrin 1 Functions in Iron Trafficking and Genetically Interacts with Ferritin in Drosophila melanogaster. Cell Reports 26, 748-+. https://doi.org/10.1016/j.celrep.2018.12.053

Xiao, G., Wan, Z., Fan, Q., Tang, X., Zhou, B., 2014. The metal transporter ZIP13 supplies iron into the secretory pathway in Drosophila melanogaster. eLife 3, e03191. https://doi.org/10.7554/eLife.03191

Xue, J., Wang, H.-L., Xiao, G., 2020. Transferrin1 modulates rotenone-induced Parkinson's disease through affecting iron homeostasis in Drosophila melanogaster. Biochemical and Biophysical Research Communications 531, 305–311. https://doi.org/10.1016/j.bbrc.2020.07.025

Yun, E.-Y., Lee, J.-K., Kwon, O.-Y., Hwang, J.-S., Kim, I., Kang, S.-W., Lee, W.-J., Ding, J.L., You, K.-H., Goo, T.-W., 2009. Bombyx mori transferrin: Genomic structure, expression and antimicrobial activity of recombinant protein. Developmental & Comparative Immunology 33, 1064–1069. https://doi.org/10.1016/j.dci.2009.05.008

Yuva-Aydemir, Y., Bauke, A.-C., Klämbt, C., 2011. Spinster controls Dpp signaling during glial migration in the Drosophila eye. J Neurosci 31, 7005–7015. https://doi.org/10.1523/JNEUROSCI.0459-11.2011

Zhang, F., Zhao, Y., Han, Z., 2013. An In Vivo Functional Analysis System for Renal Gene Discovery in Drosophila Pericardial Nephrocytes. JASN 24, 191–197. https://doi.org/10.1681/ASN.2012080769

Zhang, J., Lu, A., Kong, L., Zhang, Q., Ling, E., 2014. Functional Analysis of Insect Molting Fluid Proteins on the Protection and Regulation of Ecdysis. J. Biol. Chem. 289, 35891–35906. https://doi.org/10.1074/jbc.M114.599597

Zhang, L., Gao, J., Gao, X., 2018. Role for Transferrin in Triggering Apoptosis in Helicoverpa armigera Cells Treated with 2-Tridecanone. J. Agric. Food Chem. 66, 11426–11431. https://doi.org/10.1021/acs.jafc.8b02505

Zhou, G., Kohlhepp, P., Geiser, D., Frasquillo, M.D.C., Vazquez-Moreno, L., Winzerling, J.J., 2007. Fate of blood meal iron in mosquitoes. J. Insect Physiol. 53, 1169–1178. https://doi.org/10.1016/j.jinsphys.2007.06.009

Zschätzsch, M., Oliva, C., Langen, M., De Geest, N., Ozel, M.N., Williamson, W.R., Lemon, W.C., Soldano, A., Munck, S., Hiesinger, P.R., Sanchez-Soriano, N., Hassan, B.A., 2014.

Regulation of branching dynamics by axon-intrinsic asymmetries in Tyrosine Kinase Receptor signaling. Elife 3, e01699. https://doi.org/10.7554/eLife.01699

Appendix A - Tsf1 sequence alignment

The following pages of Appendix A contain an amino-acid sequence alignment of two serum transferrin, two lactoferrin, two ovotransferrin and 98 Tsf1 sequences. A full description of how the sequences were collected and analyzed can be found in the Material and Methods of Chapter 2 in the section “Sequence alignment for binding residue determination”. Information (including order, species, and accession number) about each sequence used in the alignment is listed in Chapter 2’s supplementary Table 2-3. The amino acid residues in serum transferrin, lactoferrin and ovotransferrin that coordinate iron or bind the carbonate anion are highlighted in yellow (for iron coordination) or red (for carbonate anion binding). The Tsf1 amino acid residues that are in the same positions in the alignment as the iron and carbonate binding residues are similarly highlighted.

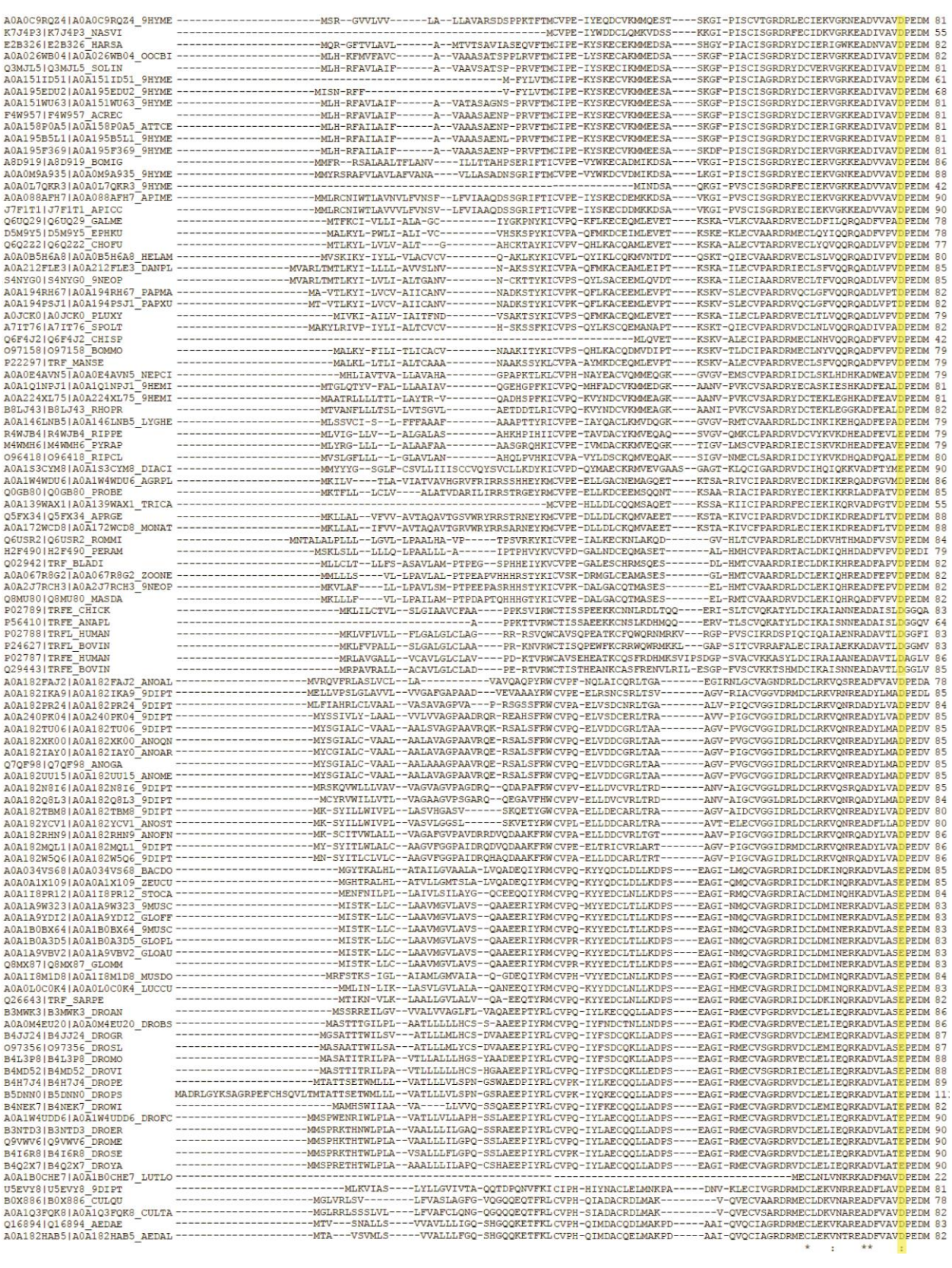

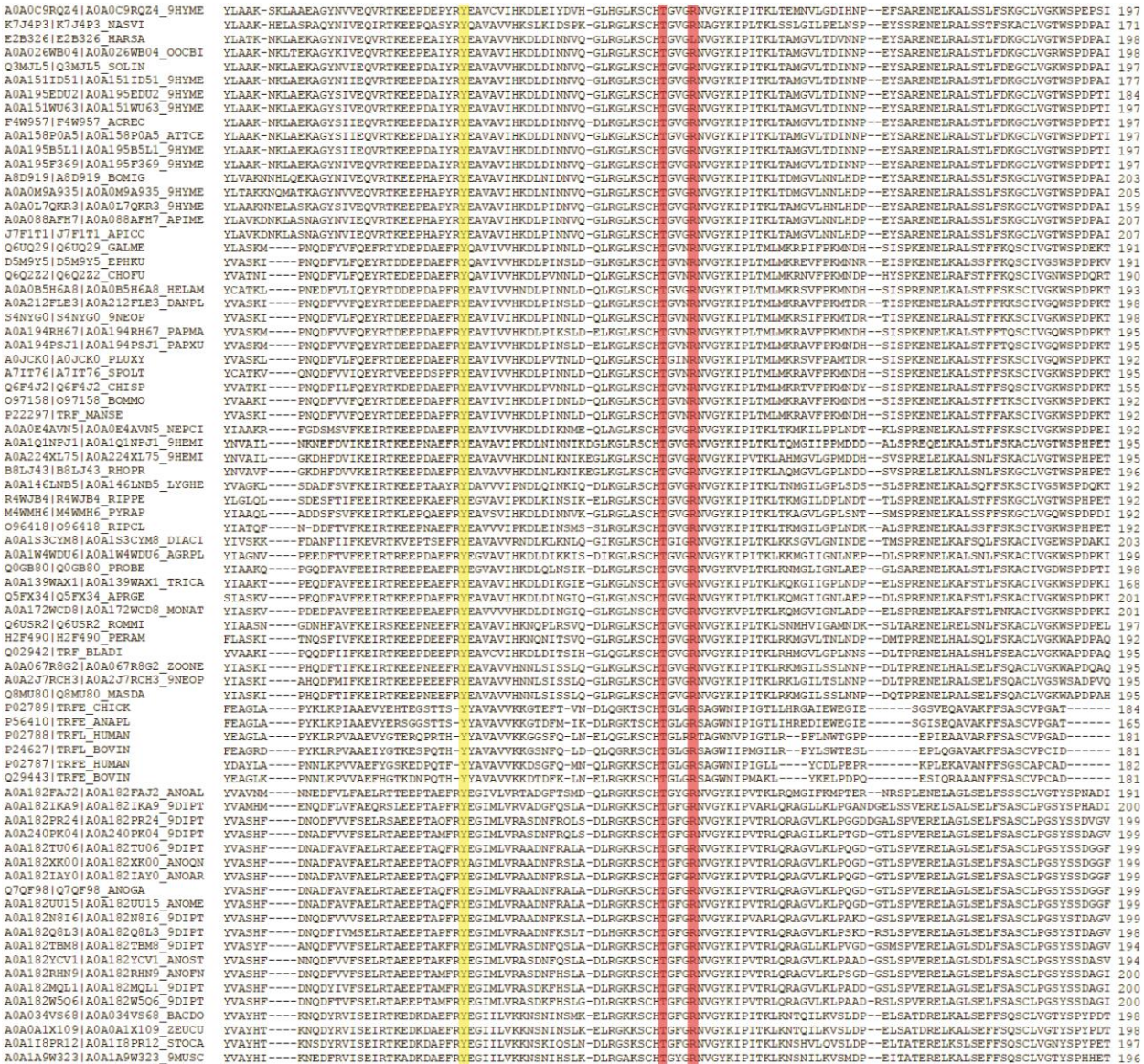

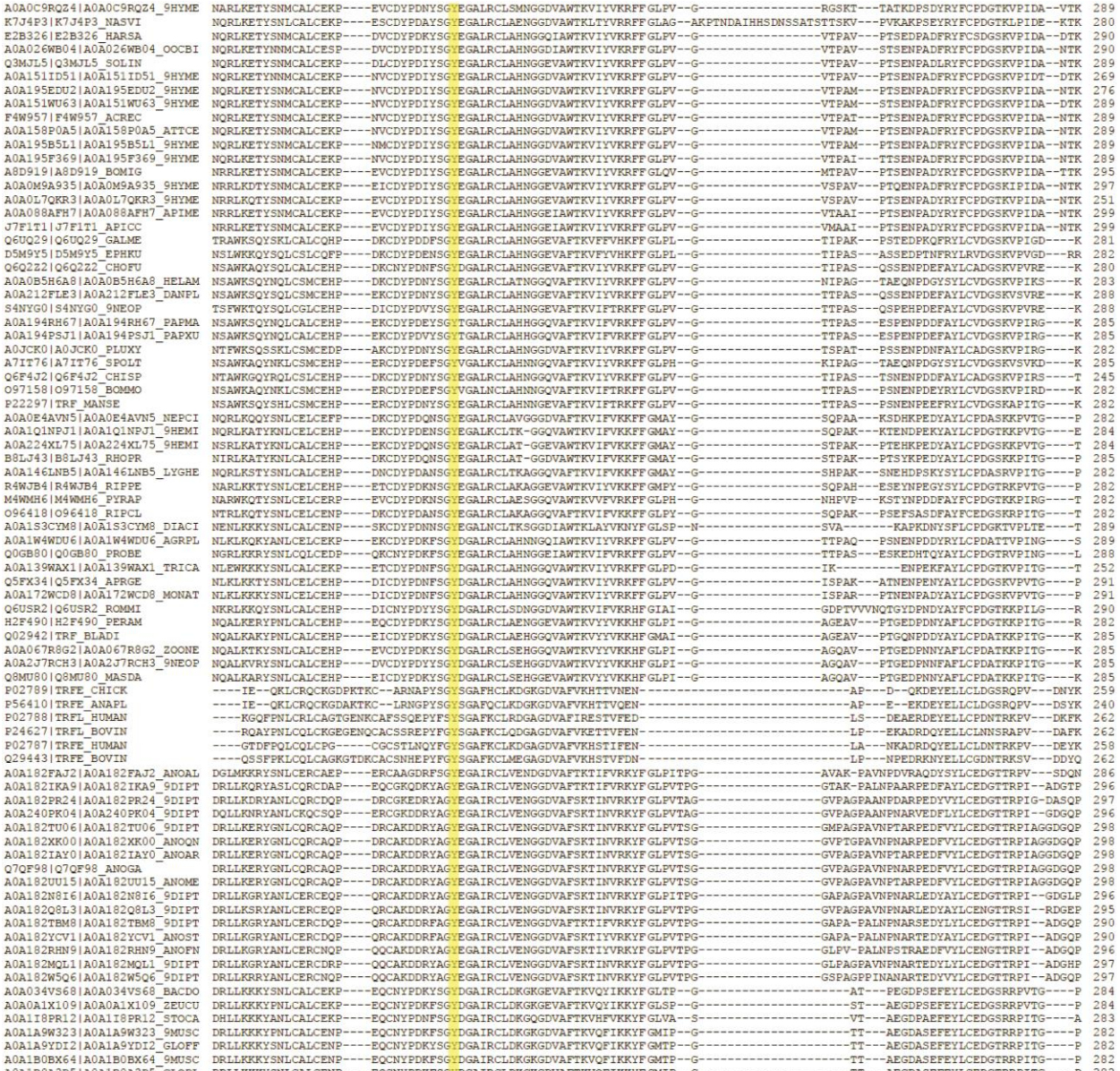

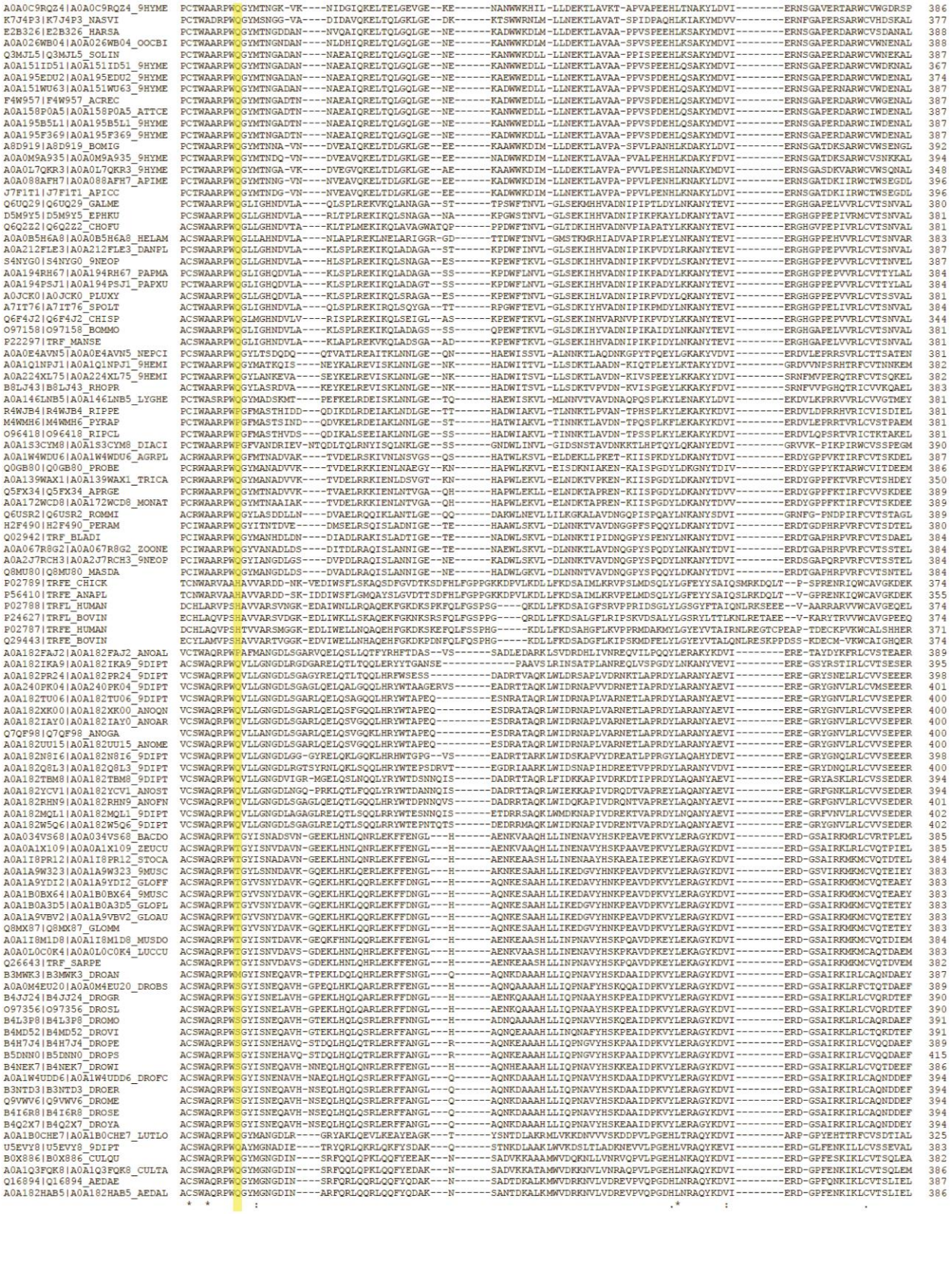

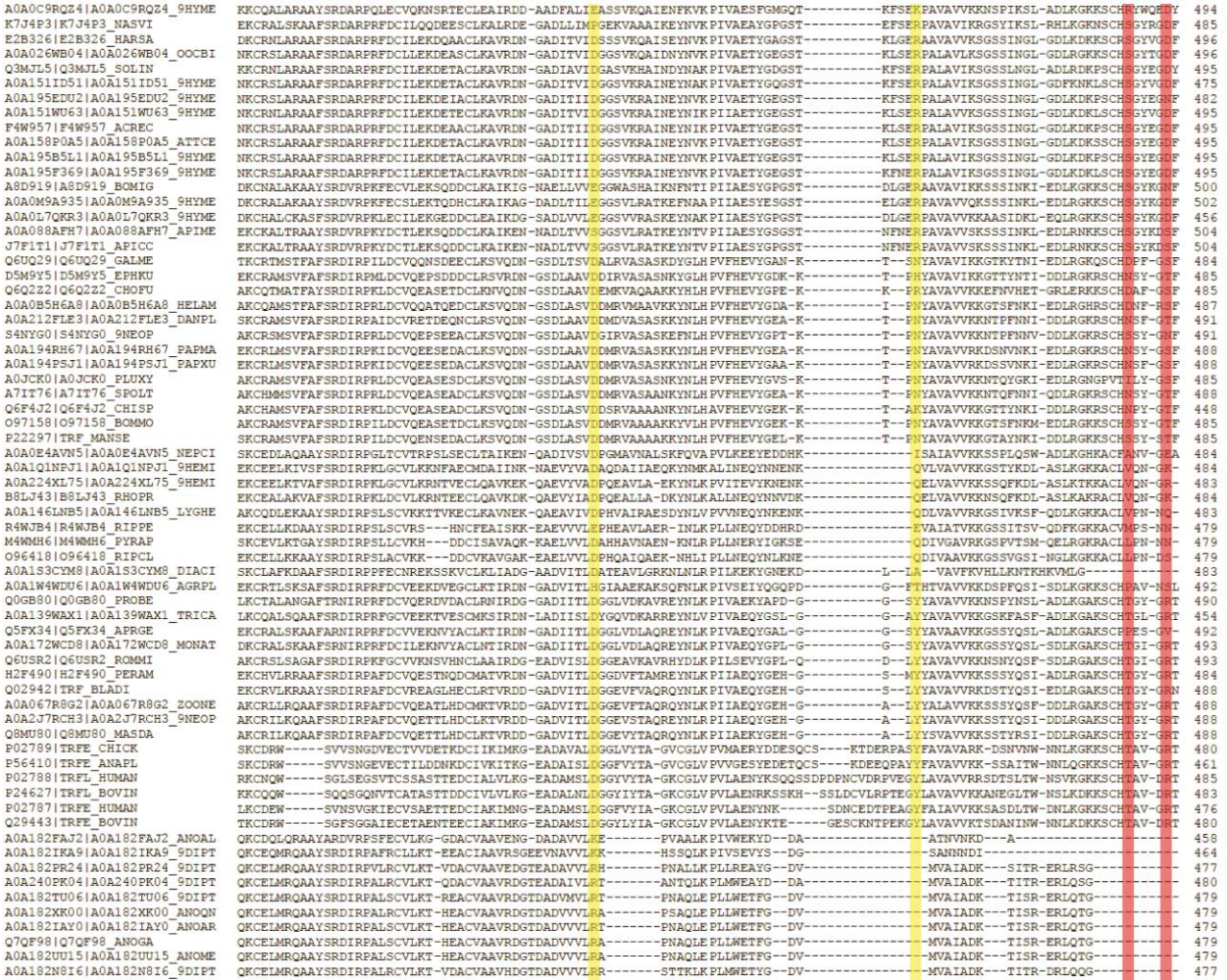

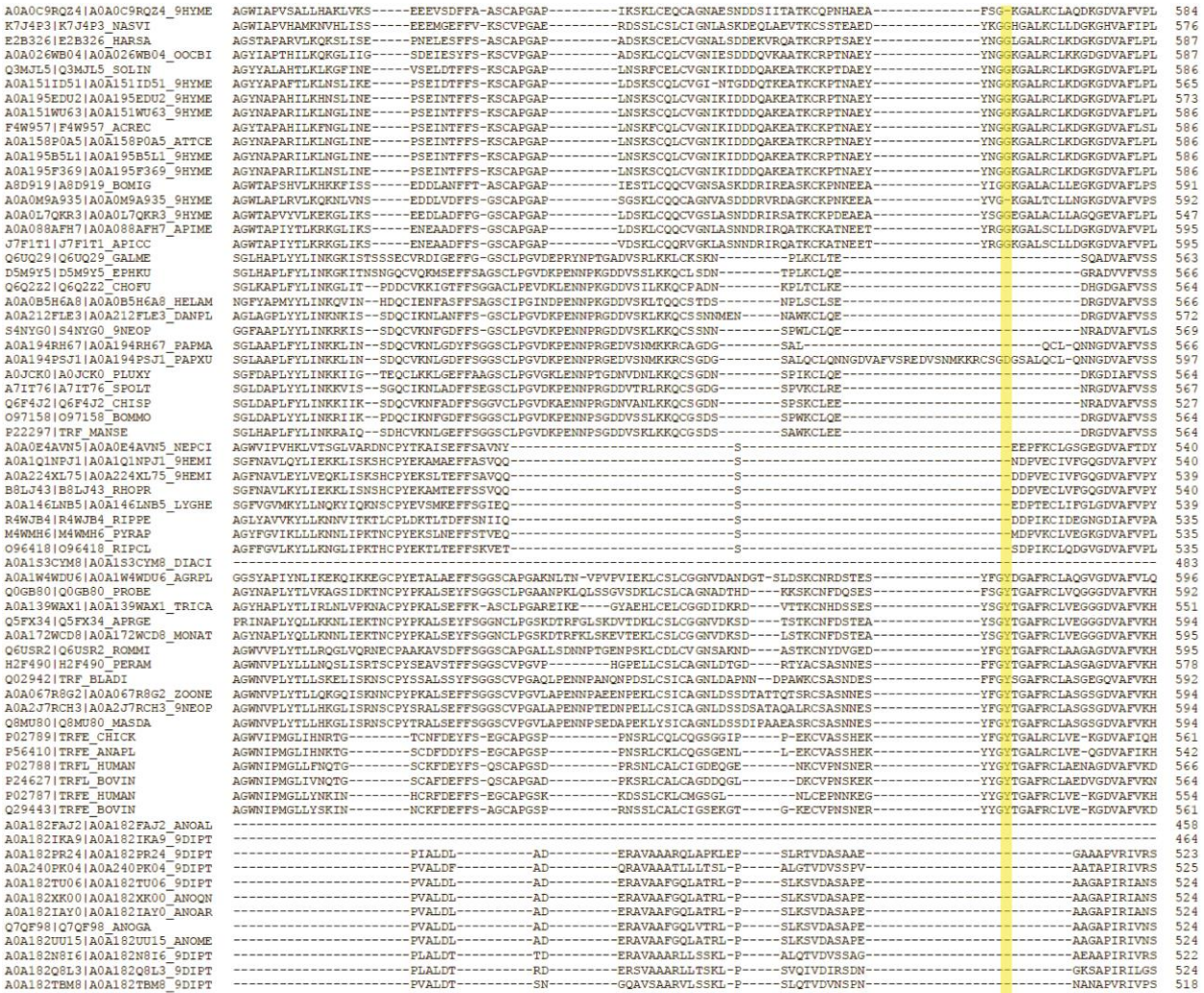

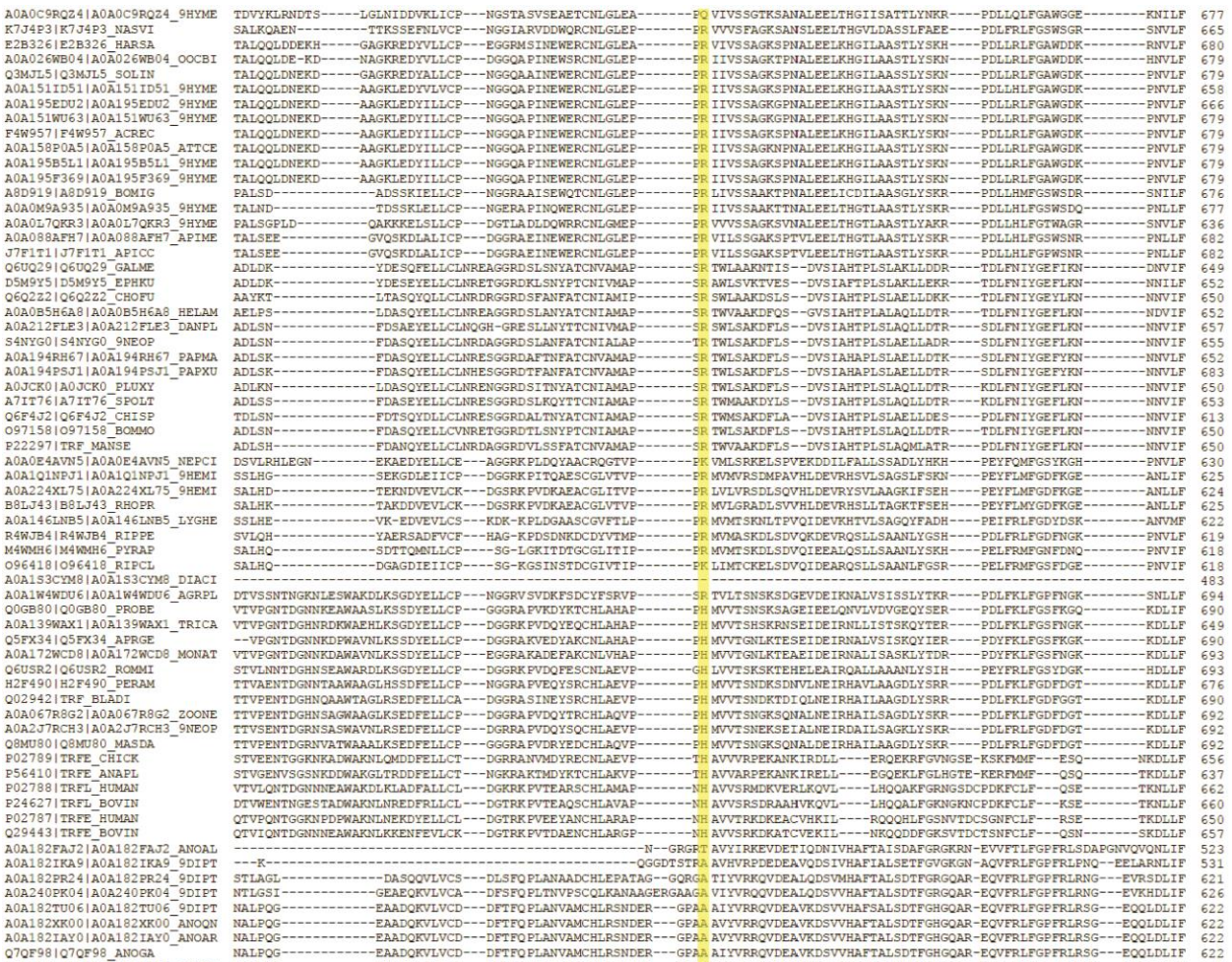

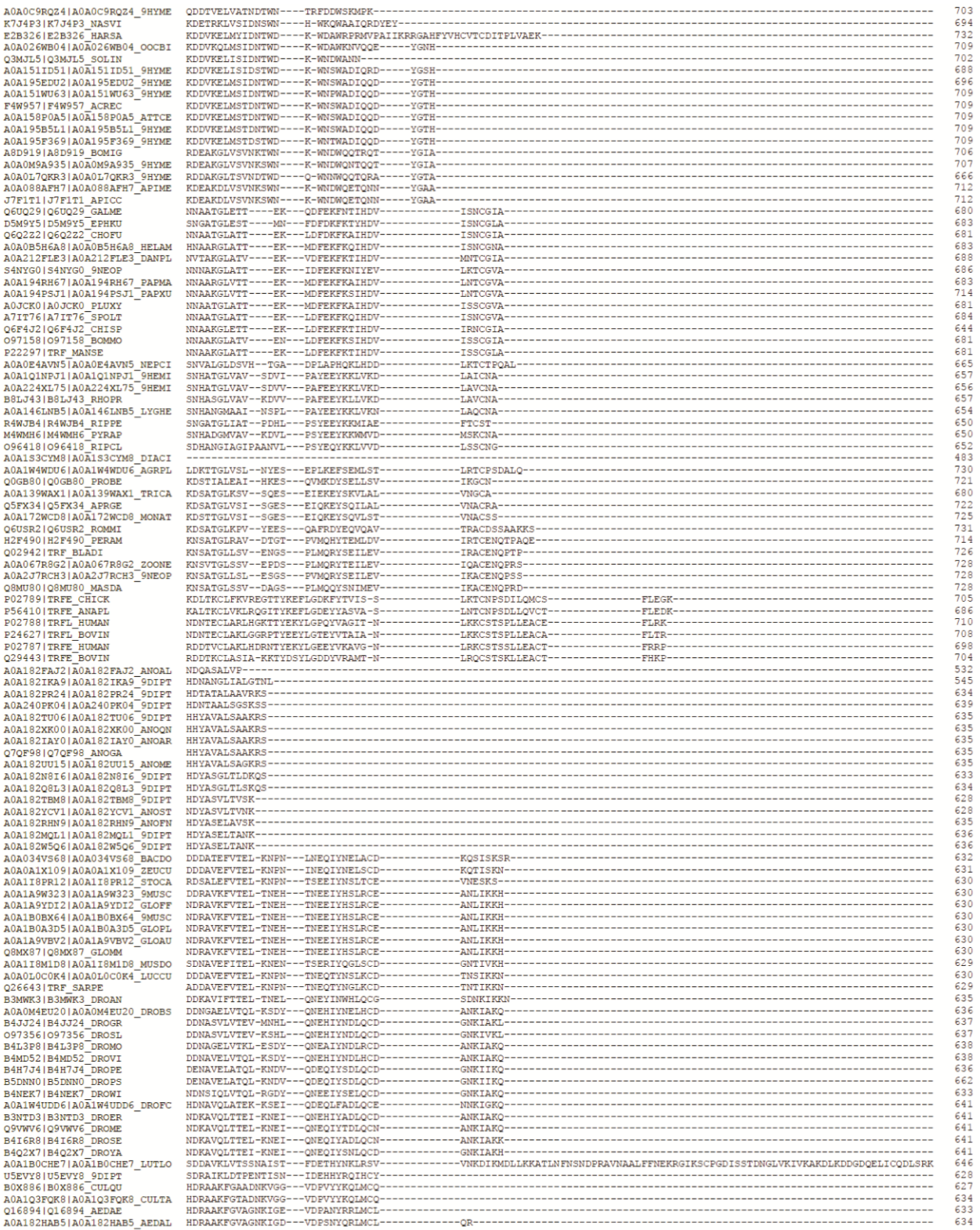

Appendix B - Disruption of the interlobal interaction in MsTsf1

Our analysis of the N-lobe of *Drosophila melanogaster* Tsf1, $DmTsf1_N$, suggested that Fe^{3+} binding in the N-lobe is stabilized by the C-lobe (Weber et al., 2020a), and our structural analysis of MsTsf1 (Weber et al., 2020b) revealed that the N-lobe and C-lobe have substantial interlobal interactions with one another. Taken together, I hypothesized that these interlobal interactions affect the iron binding and iron release mechanisms of MsTsf1. To investigate this hypothesis, I made a triple mutation in MsTsf1, R344G/R376G/R379G, with the aim of disrupting the interlobal interaction between the N- and C-lobe.

Arg344 in MsTsf1 is found in the linker peptide which links the N-lobe and C-lobe, and its side chain has electrostatic interactions with both the C1 and N2 domains (Weber et al., 2020b). Arg376 and Arg379 are located in the C1 domain of the C-lobe, and their side chains form electrostatic interactions with amino acid residues in the N-lobe (Weber et al., 2020b). Amino acid sequence analysis of Tsf1s has shown that all three arginines are highly conserved in Tsf1 sequences. I predicted that mutating these arginines to glycines would disrupt their electrostatic side chain interactions and the interlobal interaction, which would lead to destabilization of the iron binding site. I planned to test this prediction by analyzing the mutant's UV-Vis spectra, affinity for iron, and pH-mediated iron release; however, attempts at removing the iron from protein resulted in precipitate formation. Thus, only the UV-Vis spectra of the holo-protein could be obtained.

Materials and Methods

Site-directed mutagenesis

The QuickChange Multi Site-Directed Mutagenesis Kit (Agilent) was used to mutagenize the MsTsf1+pOET3 plasmid. I used two mutagenic primers in the reaction, one for R344 and one for R376 and R379: 5' TAC ACG GAG GTC ATT GAG GGA GGG CAT GGA G 3' and 5' TTC GCA AGT GGA GAC ATC GGA CCG ATC CTA G 3' (the mutagenic codons are underlined). DNA sequencing verified the correct sequences of the mutant plasmids. The flashBAC Gold system (Oxford Expression Technologies) was used to generate a recombinant baculovirus stock for the R344G/R376G/R379G mutant. (See Chapter 4 Material and Methods for more information on isolation of MsTsf1 cDNA and plasmid preparation.)

R344G/R376G/R379G mutant expression and purification

Recombinant baculovirus was used to infect Sf9 cells at 2 x 10^6 cells/ml in Sf900III serum free medium, using a multiplicity of infection of 1 pfu/cell. After two days, the culture was centrifuged at 500 × *g*, and the cell pellet was discarded. While stirring, ammonium sulfate was slowly added to the supernatant to obtain 100% saturation, and protein precipitation occurred over a two-day period at 4°C. Floating brown precipitate was collected with a pipet and dialyzed three times against 20 mM Tris, pH 8.3 (4°C). The dialyzed sample was collected, centrifuged at 10,000 × *g*, and applied to a Q-Sepharose Fast Flow column (1.5 x 10 cm). Proteins were eluted from the column with a linear gradient of 0-1 M NaCl in 20 mM Tris, pH 8.3 (4°C). Following SDS-PAGE analysis, fractions containing transferrin were pooled and concentrated with 30 kDa molecular weight cut-off Amicon Ultracel centrifugal filters. The samples were then applied to a HiLoad 16/60 Superdex 200 column (GE Healthcare)

equilibrated in 20 mM Tris, 150 mM NaCl, pH 7.4. Fractions were analyzed by SDS-PAGE and pooled. Protein yield was determined using the Pierce Coomassie Plus (Bradford) Assay Reagent (Thermo Scientific). 6.6 mg of the R344G/R376G/R379G mutant was purified from 1.2 liters of infected Sf9 cells.

Holo-R344G/R376G/R379G mutant preparation and spectral analysis

To ensure the R344G/R376G/R379G mutant was purified in its holo-form, an absorbance spectrum (from 260-700 nm) of at ~ 5 mg/mL in 10 mM HEPES, 20 mM sodium bicarbonate, pH 7.4, was measured, then 0.1 molar equivalent of ferric-nitrilotriacetic acid was added and allowed to equilibrate for 5-10 minutes, and finally a spectrum was collected. We concluded that the R344G/R376G/R379G mutant was saturated after purification because its absorbance spectra (specifically the ligand-to-metal-charge-transfer (LMCT) peak) did not change.

Failed Apo-R344G/R376G/R379G mutant production

Attempts at producing the apo-form of the R344G/R376G/R379G mutant were made by dialyzing purified protein against two exchanges of 1 liter of 0.1 M sodium acetate, 10 mM EDTA, pH 5, and then removing the EDTA by dialysis against two exchanges of 1 liter of 10 mM HEPES, pH 7.4. However, the attempts ended up with large amounts of precipitate forming.

I estimated the pH the protein began to precipitate by dialyzing it at various pH levels. I extensively dialyzed holo-R344G/R376G/R379G (5 mg/ml) against buffers at pH 5.0, 5.5, 6.0, 6.5, 7.0, and 8.0 for a two-day period at room temperature. The mutant precipitated at pH levels below 6.0.

Results and Discussion

The recombinant R344G/R376G/R379G mutant of MsTsf1 was expressed in the Sf9 insect cell line using a baculovirus expression system. The mutant was purified by ammonium sulfate precipitation followed by anion exchange and size exclusion chromatography. The protein was determined to be pure (Figure B-1). The yield of the purified mutant (~5.5 mg/liter) was lower than previously purified forms of MsTsf1, which were in the range of 11 to 25 mg/liter. During trial expressions, the R344G/R376G/R379G mutant also had lower expression levels compared to wild-type MsTsf1 and other MsTsf1 mutants (data not shown). SDS-PAGE analysis during the purification process did not indicate that large amounts of the protein were lost during the purification process. Therefore, my hypothesis is that due to the instability of the R344G/R376G/R379G mutant, it is not produced as effectively or is misfolded and degraded prior to secretion by the Sf9 cells.

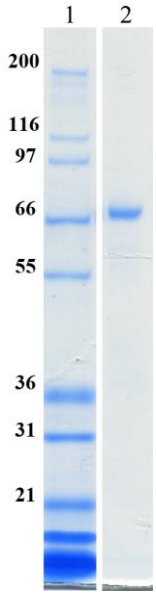

Figure B-1. SDS-PAGE analysis of the purified R344G/R376G/R379G mutant of MsTsf1. The purified R344G/R376G/R379G mutant was analyzed by reducing SDS-PAGE followed by Coomassie staining. Lane 1 is the protein molecular mass standard (masses in kDa are shown to the left) and lane 2 is the purified mutant protein The expected mass was 73 kDa.

Following purification, the R344G/R376G/R379G mutant had an orange color indicating it was bound to iron, similar to previously purified forms of MsTsf1. This color is due to the LMCT peak that arises when iron is bound to the protein. The absorption maximum of the recombinant WT holo-MsTsf1 is 420 nm and was previously determined by generating a difference spectrum (subtracting the apo-spectrum from the holo-spectrum). I estimate the R344G/R376G/R379G mutant's absorption maximum is also 420 nm. Because I could not produce an apo-form of the R344G/R376G/R379G mutant, I had to estimate the absorption maximum of the mutant solely from the UV-Vis spectrum of the holo-form (Figure B-2). The shoulder that appears in the spectra around 420 nm for the R344G/R376G/R379G mutant closely resembles the shoulder of the WT. The spectra of purified Y90F/Y204F, which does not bind iron, is also shown for comparison (Figure B-2). This result indicates that the R344G/R376G/R379G mutant coordinates iron similarly to WT MsTsf1, and supports the results previously found by analyzing $DmTsf1_N$ (Weber et al., 2020a), which also showed the C-lobe and its interlobal contacts with the N-lobe are not essential for iron coordination.

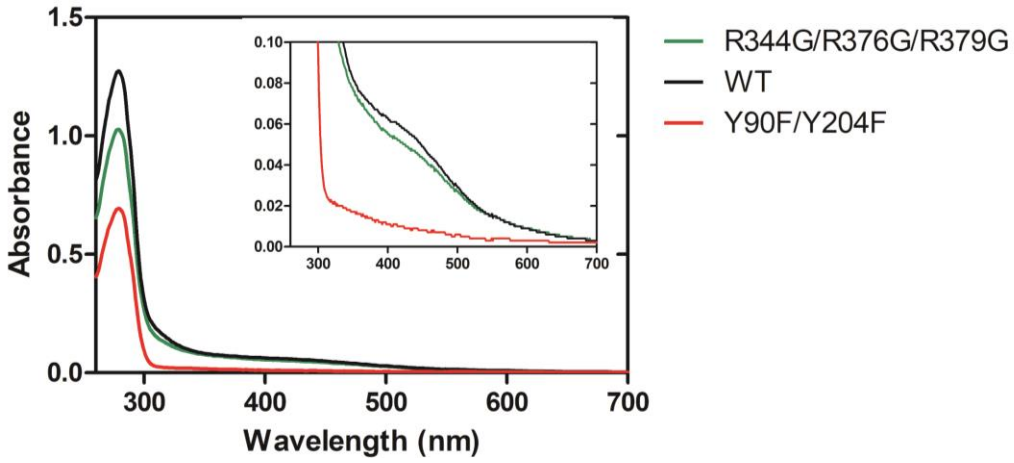

Figure B-2. Absorbance spectra for MsTsf1 WT and mutants.
WT MsTsf1 is indicated by a black line, R344G/R376G/R379G by a green line, and Y90F/Y204F by a red line. Proteins were at approximately 2 mg/mL in 10 mM HEPES, 20 mM sodium bicarbonate, pH 7.4.

Without the apo-form of the mutant, the affinity for iron could not be measured using previously described methods (Weber et al., 2020a). Analysis of the mutant's stability indicated that the protein precipitates at pH levels below 6. It was not clear whether the iron is released from the protein prior to precipitation, which makes it difficult to determine if the disrupted interlobal contacts have a direct role in the release mechanism. Thus, it is difficult to determine from these results what, if any, importance of the interlobal contacts have to the iron binding affinity and iron release mechanism. Nevertheless, the results do indicate that the interlobal contacts are important to the overall stability of the protein.

References

Weber, J.J., Kanost, M.R., Gorman, M.J., 2020a. Iron binding and release properties of transferrin-1 from Drosophila melanogaster and Manduca sexta: Implications for insect iron homeostasis. Insect Biochem Mol Biol 125, 103438. https://doi.org/10.1016/j.ibmb.2020.103438

Weber, J.J., Kashipathy, M.M., Battaile, K.P., Go, E., Desaire, H., Kanost, M.R., Lovell, S., Gorman, M.J., 2020b. Structural insight into the novel iron-coordination and domain interactions of transferrin-1 from a model insect, Manduca sexta. Protein Sci. https://doi.org/10.1002/pro.3999